A critical survey of the methods of observation of dislocations in crystals

Painter, Gerald H.

A CRITICAL SURVEY OF THE METHODS OF OBSERVATION OF DISLOCATIONS IN CRYSTALS.

by

GERALD H. PAINTER, B.Sc.

Submitted in candidature for the degree of Master of Science of the University of Durham.

ACKNOWLEDGMENTS.

The author wishes to thank Dr. W. D. Corner, who suggested the topic, for his continued help and encouragement. His valuable criticisms and suggestions have made an important contribution to the work.

The author is indebted to the organisers and lecturers of the Summer School in Solid State Physics, held at the Cavendish Laboratories, Cambridge, 1959, and to the Ford Foundation for making this most informative course possible. Leave of absence to attend the course was by kind permission of Mr. N. S. T. Benson, Headmaster of Giggleswick School.

He thanks the undermentioned for so generously providing photographs and diagrams to include in the thesis:
Mr. J. Blakely, Dr. W. Bollman, Dr. W. Bontinck, Dr. W. C. Dash, Professor W. Dekeyser, Dr. J. J. Gilman, Dr. P. B. Hirsch, Dr. W. G. Johnston, Dr. A. R. Lang, Dr. D. W. Pashley, Mr. J. Silcox, Dr. M. J. Whelan, and W. Wykeham and Co., Ltd.

Finally, he wishes to express gratitude to the following for their assistance in providing books and reprints of published articles: Dr. V. R. Cosslett, Dr. J. J. Gilman, Dr. W. G. Johnston, Dr. A. R. Lang, Dr. J. B. Newkirk,

Dr. J. Nutting, and the West Riding County Library.

CONTENTS.

CONTENTS. (cont.)

CONTENTS. (cont.)

CONTENTS. (cont.)

PART 1.

GENERAL FEATURES OF DISLOCATIONS.

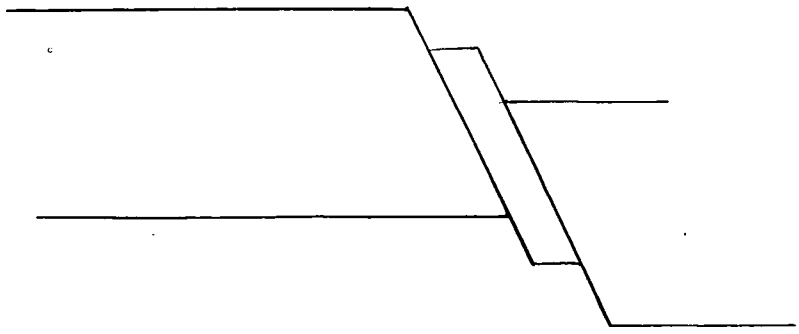

Fig. 1. Slip.

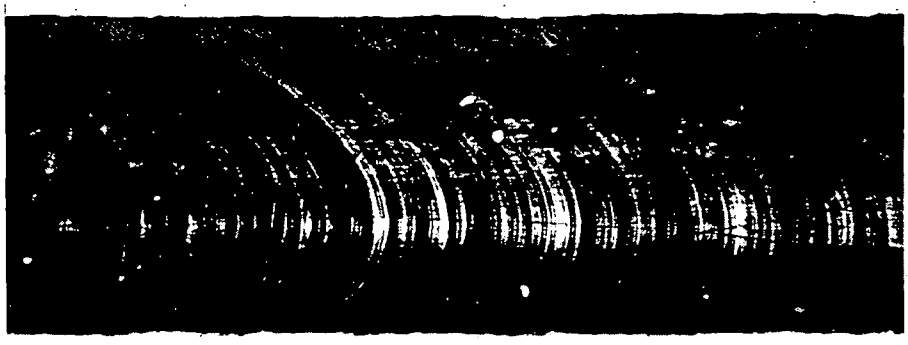

Plate 1. Cadmium single crystal, extended by 40%. (x 40)
(After Andrade, 1950).

1.1 INTRODUCTION TO PLASTIC DEFORMATION.

The strength of a metal is only about a thirteenth of the value to be anticipated from the theory for a perfect crystal. A similar conclusion is reached on considering yield under stress. In general, the region of perfect elasticity is small. The metal does not usually fracture in a brittle manner, but there is a large plastic yield, when the metal toughens, or 'work hardens'. For higher temperatures and maintained stresses, the metal slowly flows or 'creeps'.

These irregularities may at first seem due to the fact that the metal consists of many small crystals. However, tests have been carried out on large single crystals and these diverge even more widely from the anticipations of simple theory.

1.2 SLIP.

Single crystal wires, when extended show a characteristic structure of bands. These are called slip bands. A slip band is the line of intersection of a slip surface with the outer surface of the crystal, Fig. (1) and Plate (1). It is found that slip occurs most easily along certain crystal planes and directions, where the atoms are most closely packed. For example, face centred cubic crystals slip along $[110]$ directions on (111) planes.

When slip takes place, all the atoms in the planes do not slip simultaneously. The slip gradually progresses over the

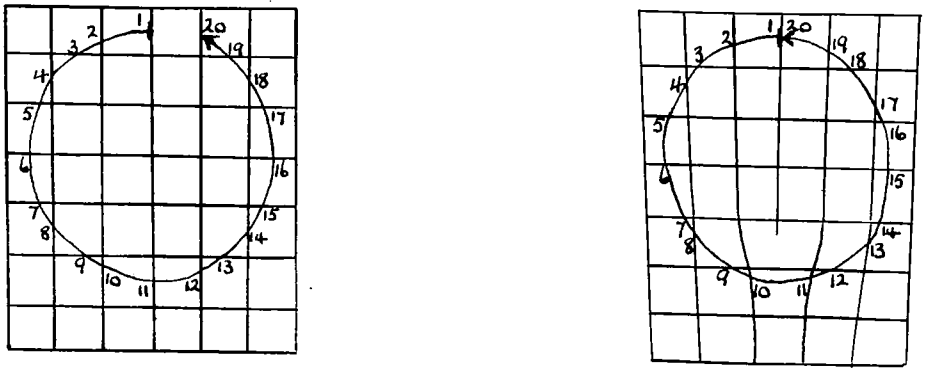

Fig. 2. (a) Ideal Crystal.
(b) Real crystal containing a dislocation.
(After van Bueren, 1957).

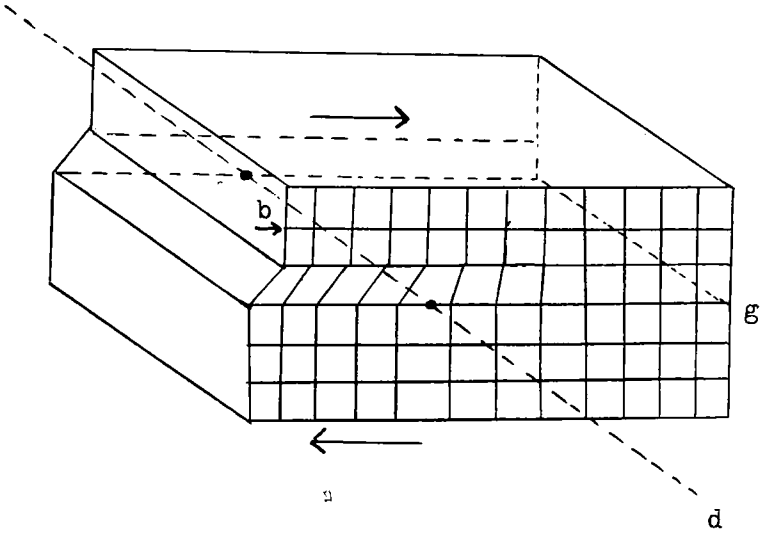

Fig. 3. Perspective diagram of an edge dislocation that has progressed halfway through a crystal. The dotted line d is the dislocation axis; the drawn lines represent atomic planes. The Burgers vector b is perpendicular to the axis. To complete the shear, the dislocation must move along the slip plane g in the direction of b. (After van Bueren, 1957).

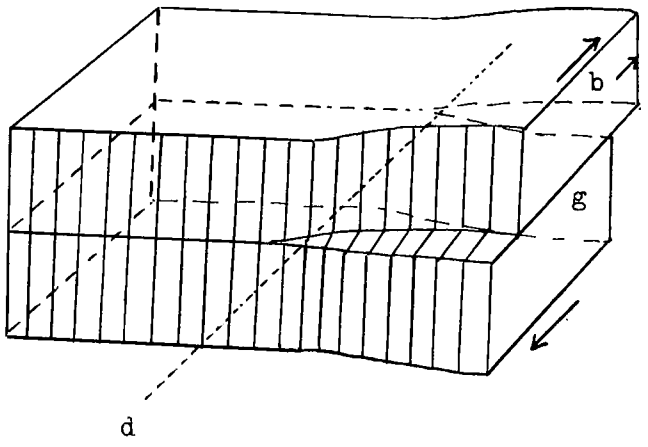

Fig. 4. Perspective diagram of a screw dislocation. The letters have the same meaning as in Fig. 3. To complete slip, the dislocation has to move over the slip plane g perpendicularly to its Burgers vector b.
(Ater van Bueren, 1957).

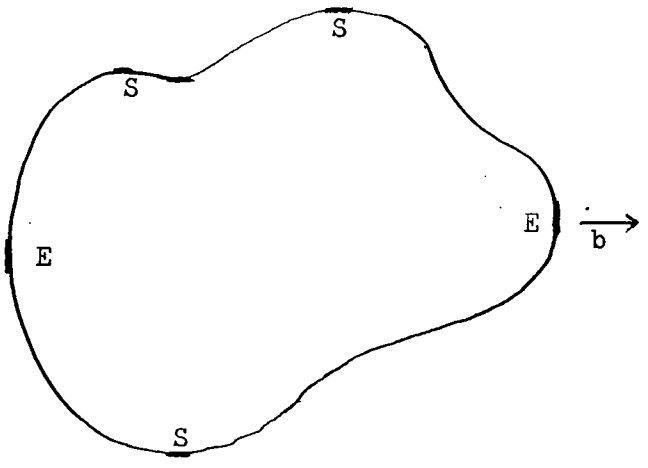

Fig. 5. Closed dislocation loop; b is the Burgers vector, which is constant along the loop. Only the parts E and S are of pure edge and screw character respectively.
(After van Bueren, 1957).

slip plane. The boundary of the slipped region is a dislocation line, and this can move with comparative ease.

1.3 THE BURGERS VECTOR.

In reality ideal crystals do not exist. By comparing actual and ideal crystals one can try to establish a one to one correspondence between the atoms in the two crystals. Regions where the actual crystal resembles the ideal crystal are called 'good' regions. Deformed regions are called 'bad'.

Consider a closed circuit in the actual crystal. If the region enclosed is good then an associated circuit in the ideal crystal will also be closed. If, however, the circuit encloses one or more dislocations in the actual crystal then the associated circuit in the ideal crystal will not be closed, Figs. (2a) and (2b). Such a circuit in the actual crystal is called a Burgers Circuit. The closing failure shown in Fig. (2a) is equal to the Burgers vector of the dislocation.

1.4 EDGE AND SCREW DISLOCATIONS.

There are two basic types of dislocations, the edge dislocation with its Burgers vector perpendicular to its axis, and the screw dislocation with its Burgers vector parallel to its axis. Other types of dislocation may be considered to be a mixture of the two. See Figs. (3), (4), and (5).

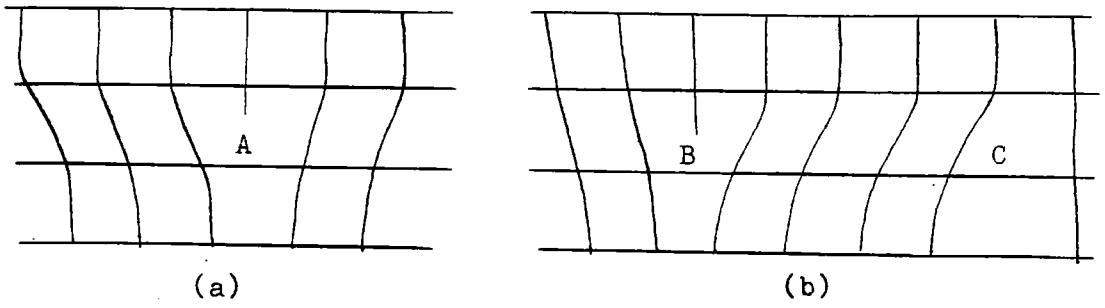

Fig. 6. (a) An edge dislocation at A.
(b) Two imperfect dislocations at B and C.

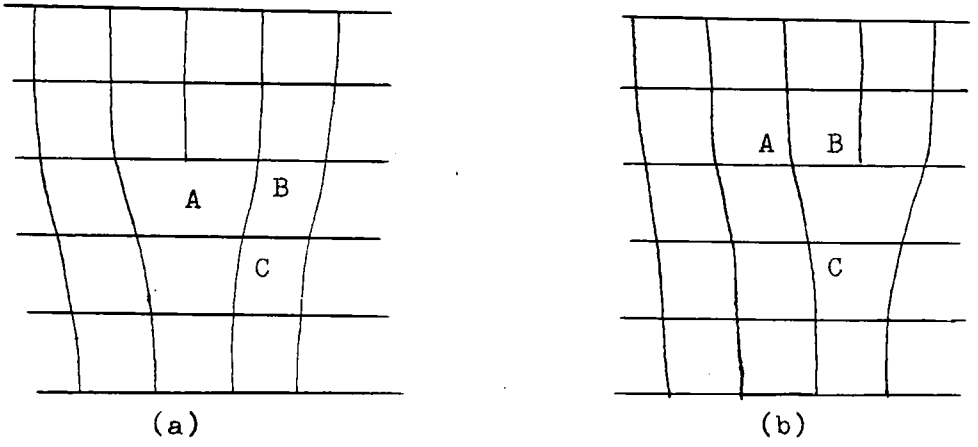

Fig. 7. (a) Edge dislocation at A.
(b) The dislocation moves to B by glide.

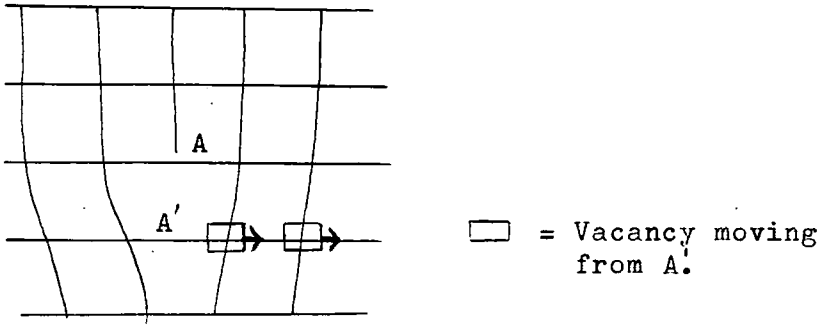

Fig. 8. The climb of a dislocation.

1.5 IMPERFECT DISLOCATIONS.

Dissociation of an edge dislocation (A) into two imperfect dislocations (B and C) is shown in Fig. (6). The two imperfect dislocations are separated by a strip of 'imperfect' material. Stacking faults are found in such regions between partial dislocations.

1.6 MOTION OF DISLOCATIONS.

There are two types of movement of dislocations known as glide and climb.

(a) Glide.

When a dislocation moves parallel to the Burgers vector, the dislocation is said to glide. It moves in the surface containing itself and its Burgers vector, Fig. (7). This surface is called the glide or slip surface of the dislocation.

(b) Climb.

If in Fig. (8) the dislocation is to move from A to A' out of its glide plane, a new row of atoms must be added to the half plane. This is effected either by diffusion or by the movement of vacancies. The latter is most likely but requires long times and high temperatures. At high temperatures both glide and climb are possible giving a dislocation two degrees of freedom. At low temperatures climb is not possible.

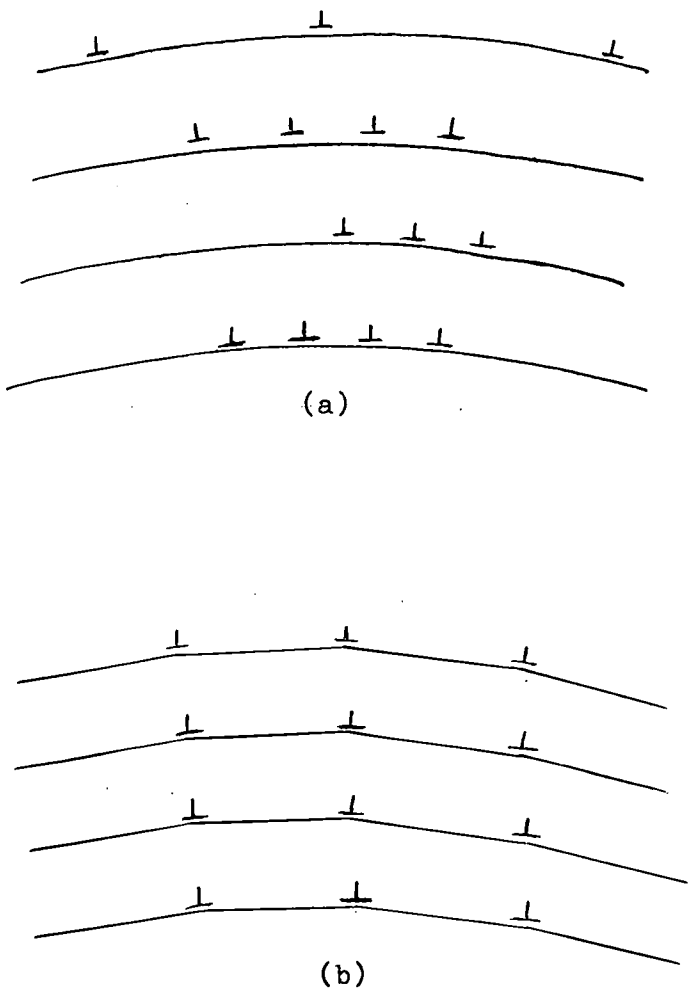

Fig. 9. Showing Polygonization.
(a) Dislocations introduced by bending the crystal.
(b) Stable arrays of dislocations after anneal.

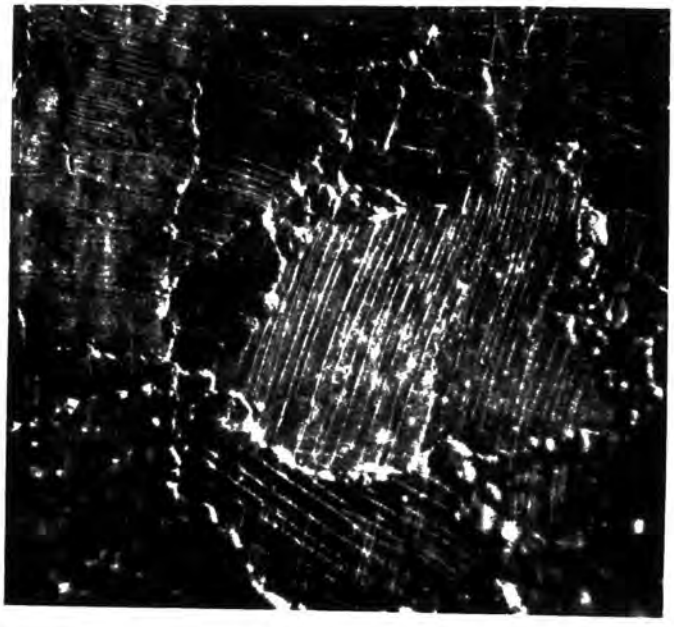

Plate 2. Slip lines in grains of polycrystalline lead. (x 70) (After Andrade, 1950).

1.7 GRAIN BOUNDARIES AND POLYGONIZATION.

Observation of a pure metal shows it to have a polygonal network (Plate 2). The metal consists of small crystals joined together, each differing in orientation from its neighbours. The crystal grains themselves are not exactly perfect in structure and are often built up of smaller units called sub-grains. The sub-grains are separated by boundaries where the orientation of the lattice changes by a very small angle. Sub-boundaries consist of dislocations usually uniformly spaced, (Plate

If a crystal is plastically deformed and annealed, the above sub-grain structure is produced. Dislocations, introduced by bending the crystal Fig. (9a), form stable arrays after anneal as shown in Fig. (9b). This re-arrangement of dislocations is known as polygonization.

1.8 INTERACTION OF DISLOCATIONS.

The density and arrangement of dislocations in a metal strongly influence the properties of the metal. Plastic deformation has been shown to depend upon the movement of dislocations. This is impeded by other dislocations present in the metal, as it is very difficult for dislocations to cross. Point defects such as impurity atoms, vacancies, and interstitials also present opposition, and here, dislocations tend to become pinned.

At high temperatures dislocations move more readily and

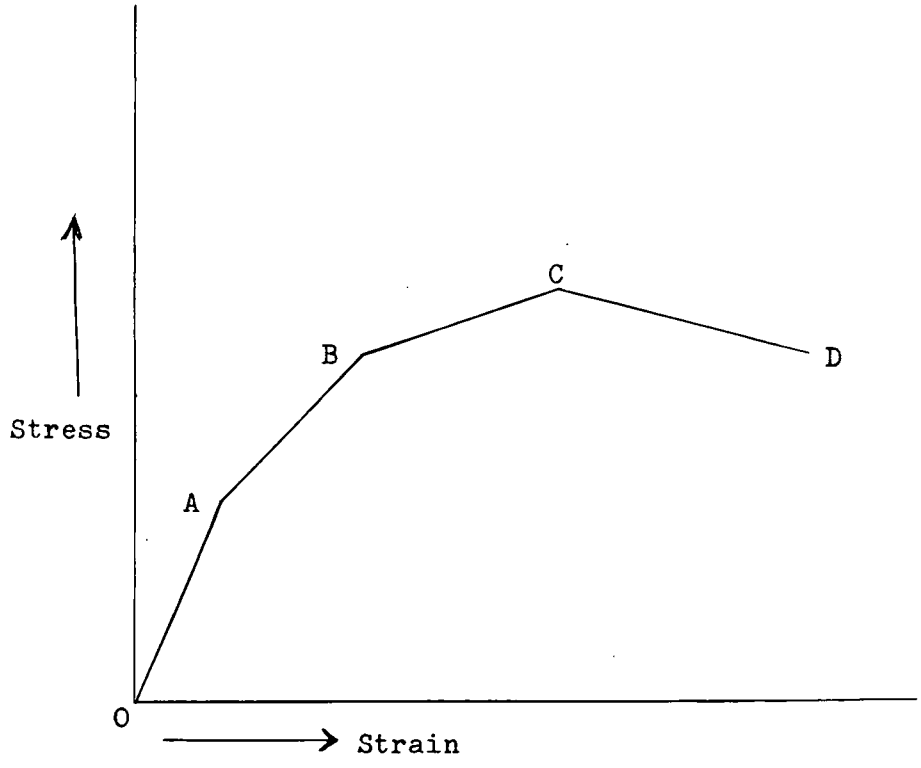

Fig. 10. Stress-strain relationship for a polycrystalline metal.

O to A represents the elastic region.

At A yielding takes place and dislocations begin to move.

A to B is a region of rapid hardening when dislocations become grouped in piled-up arrays.

B to C the rate of hardening is less rapid. Networks are formed.

At C work hardening no longer counter balances the reduction in cross section.

At D the specimen breaks.

annealing takes place, when there is a reduction in the number of dislocations and a relaxation of stress in the specimen.

Work hardening is due to the interaction between dislocations. When a material is plastically deformed the dislocation density increases and hardening occurs. This effect is not due to point defects. When the stress concentration is sufficiently great and dislocations pile up, relaxation can occur in a number of ways. Dislocation networks often form, new loops may be produced, dislocations may cross the barrier of a grain boundary, cracks may be formed, or twinning may result. Fig. (10) indicates, very generally, what happens when a polycrystalline metal is stressed to breaking point.

PART 2.

OUTLINE OF THE HISTORY OF THE OBSERVATION OF DISLOCATIONS.

It was in 1905 that Siedentopf published hand drawn diagrams representing his observations of linear imperfections in rock salt. His ultramicroscope showed the distribution of colloidal sodium in additively coloured and in naturally occurring blue rock salt.

Little experimental work was done in the next 20 years even though Darwin (1914 and 1922) had interpreted the observed intensities of X-ray diffraction maxima assuming a mosaic substructure in inorganic crystals. In the Institute at Halle, Smekel (1929 and 1933) endeavoured to make visible imperfections which he considered determined the structure sensitive physical and chemical properties of crystals. Rexer (1931, 1932a, b) developed a method to make line imperfections and substructures visible in polygonised crystals by additive coloration. This method, slightly modified, was used later by Amelinckx to investigate imperfections in sodium chloride by separation of particles of colloidal sodium.

The first interpreted observations came after 1933 when it was shown by Taylor, Orowan, and Polanyi that the existance of dislocations would explain some of the mechanical properties of metals. They suggested that dislocations are produced during deformation, and that they exert elastic forces on each other resulting in work hardening. The Taylor-Orowan dislocation is now known as the edge dislocation. J. M. Burgers (1939) introduced the screw dislocation. Dislocation theory developed

steadily due, amongst others, to Peierls (1940, Mott (1940). and Nabarro (1947), and at this stage was well ahead of verification by observation.

An interesting way of illustrating many properties of metal crystals was developed by Bragg and Nye (1947) and later work on this was carried out by Bragg and Lomer (1949). In their model each atom is represented by a bubble in a raft of very uniform small bubbles floating on soap solution. These two dimensional models can be used to observe plastic flow, and the movement of individual dislocations. Observations of the behaviour of bubble rafts give a remarkably clear picture of what might happen when dislocations move in crystals.

A simple and very useful means of locating dislocations is by etching; as a result of preferential etching, pits are formed where dislocations reach the surface. This preferential attack may be caused by elastic strain around dislocations which enhances the chemical potential, and by accummulation of impurities at dislocations facilitating chemical attack, Cottrell (1953). Hausser and Scholz (1927) observed preferential action on a single crystal of copper. Since then etching techniques have been developed and although limited to surfaces, nevertheless, valuable information about dislocations has been obtained from them.

There was a great advance in observation when Hedges and Mitchell (1953) developed a method of producing preferential deposition of silver at dislocations in silver bromide. Using

this technique of decoration, dislocations inside crystals at various stages of plastic deformation could at last be clearly seen. Many phenomena predicted by theory were observed.

Amelinckx (1956) decorated dislocations in sodium chloride using additive coloration. These methods have been extended to other crystals and many clear photographs of dislocations published. A combination of etching and decoration techniques by Dash (1956,1957) and others has proved quite effective.

The use of transmission electron microscopy by Hirsch, Horne, and Whelan (1956) has enabled the dislocation structure in metals to be examined. The high resolution, 5A enables dislocation networks and grain boundaries in thin foils of aluminium and stainless steel to be clearly seen. Valuable additional information about surface features and the structure of materials can be gained by using replicas with the electron microscope.

The resolving power of the electron microscope has been further increased to 1A by the indirect method of Moire patterns due to Bassett, Menter, and Pashley (1959).

Lang (1957 and 1959) and Newkirk (1958a and b, and 1959) revealed and studied undecorated individual dislocations in crystals by X-ray diffraction microscopy, and their methods show considerable promise.

A better than 3A resolving power has been attained by Müller (1957) using his field-ion microscope. His method is restricted to the study of tungsten and rhenium surfaces.

PART 3.

BUBBLE RAFTS.

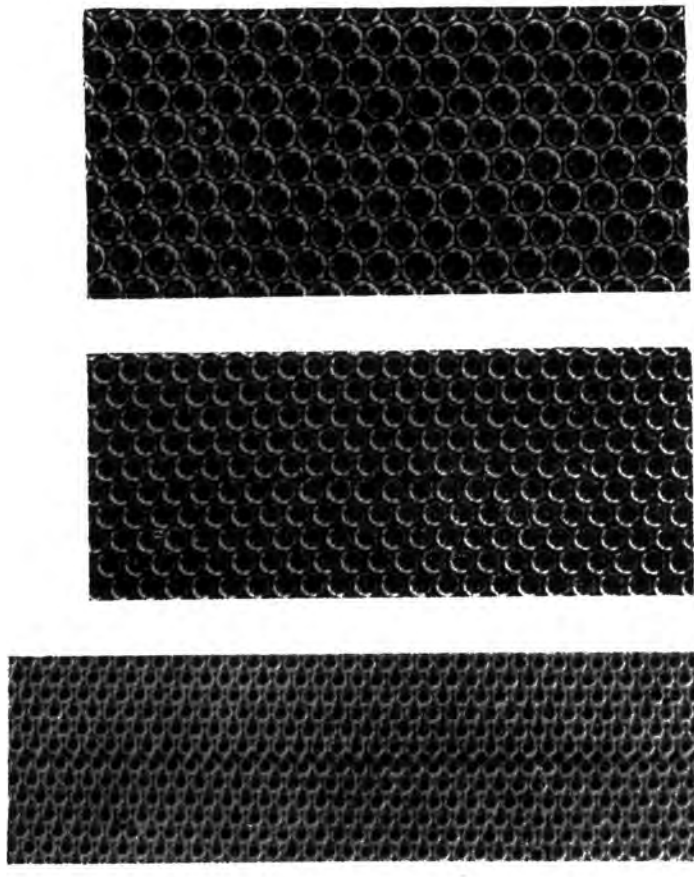

Plate 3. Bubble models.
(a) Closed dislocation. (soft atoms)
(b) Open dislocation. (hard atoms)
(c) Intermediate case.
The atomic interaction in copper corresponds to a bubble size between (b) and (c).
(After Bragg and Nye, 1947).

Bragg and Nye (1947) developed a striking model which illustrated many properties of metal crystals. They constructed rafts of soap bubbles to represent two dimensional crystals. See Plates (3) and (4).

The bubble model is a close packed layer of bubbles of uniform size. The forces acting on the bubbles resemble those on the atoms of a crystal. The attractive force between bubbles is due to the surface tension. The repulsive force acts between bubbles in contact and depends upon the excess pressure inside the bubbles. As this pressure is inversely proportional to the radius of the bubble, the size of the bubbles determines their hardness. The smaller the diameter, the harder the atom represented. Bubbles of diameter about 1.1 or 1.2 mm. resemble copper atoms. Those of diameter 1.9 mm. represent relatively soft, and 0.76 mm. relatively hard atoms.

Observation of bubble rafts to which stress has been applied, shows that some dislocations are initiated near the edge of the raft and some in pairs within the raft. Slip is observed to take place along the close-packed rows of bubbles. The lattice slips by one bubble diameter during the glide of a dislocation, and the core of the dislocation is confined to a few atomic distances. The movements of dislocations in bubble rafts are clearly shown in a 16 mm. film called "Bubble Model of a Metal", made by Bragg and Nye in 1947.

With bubbles of diameter 1.2 mm. resembling copper atoms,

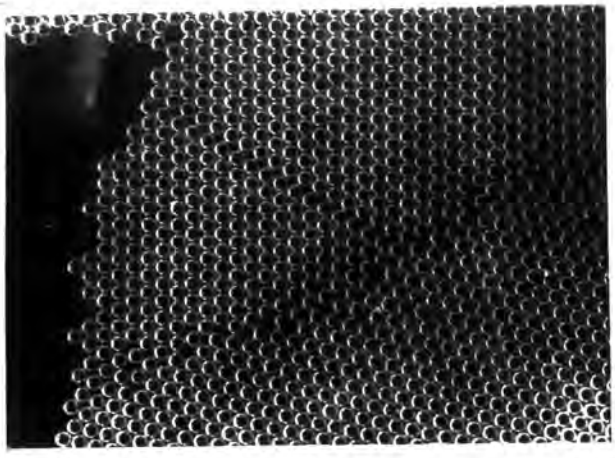

(a) A grain boundary.

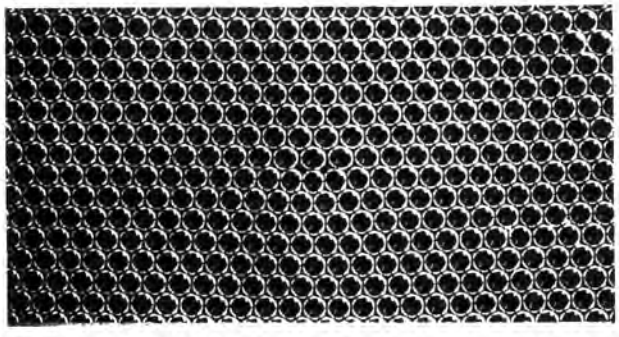

(b) A dislocation.

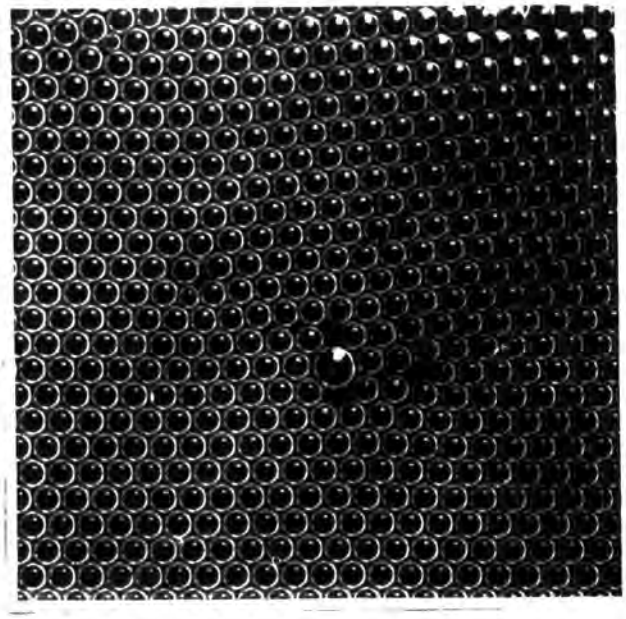

(c) Effect of a larger foreign atom.

Plate 4. Bubble models.
(After Andrade, 1950).

the observed critical shear strain was 3.25 deg. and the corresponding shear strength about $\frac{\mu}{30}$. These values agree with those calculated for a perfect crystal. It must be remembered, however, that the bubble models are two dimensional and even if forces between bubbles are representative of those between atoms, the raft cannot be considered exactly representative of a crystal. In a crystal there are also forces acting between the layers of atoms. Thus caution must be used when comparing the properties of rafts with those of crystals. Nevertheless, rafts do give a useful, but incomplete, picture of what may happen in a crystal which is plastically deformed.

PART 4.

CRYSTAL GROWTH.

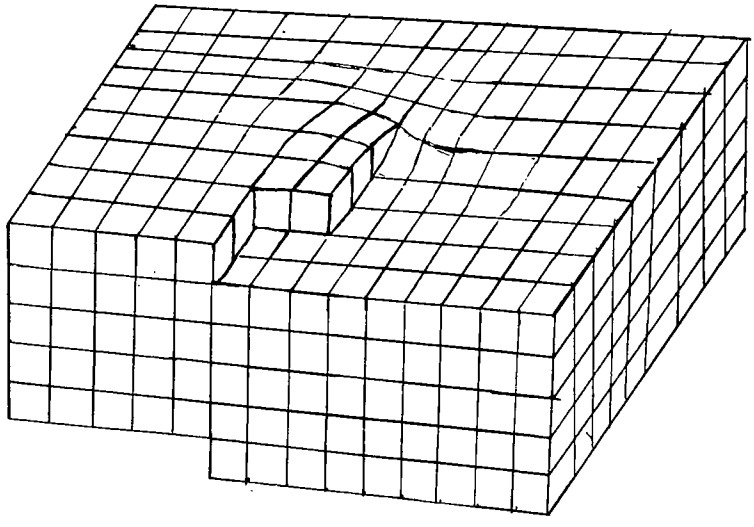

Fig. 11. The end of a screw dislocation. (After Read, 1953).

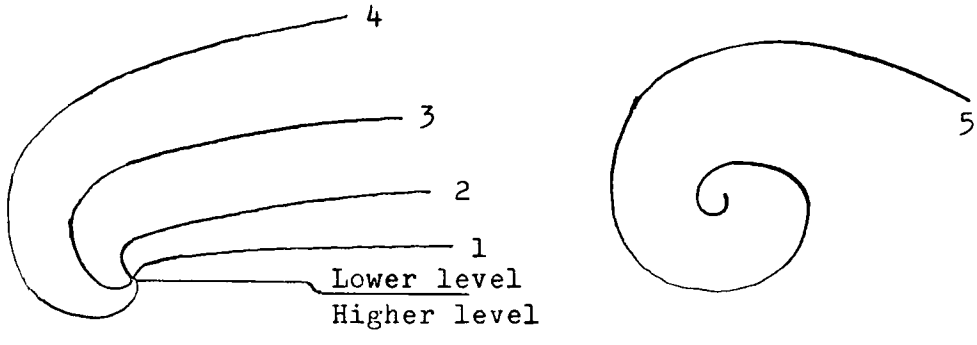

Fig. 12. Stages in the development of a growth spiral. (After Verma, 1953).

4.1 INTRODUCTION.

In his theory of crystal growth Frank (1952) shows that dislocations are necessary to crystal growth. This is especially applicable when large crystals are grown.

Frank (1950 and 1951) predicted that on the surfaces of crystals grown from vapour, when screw dislocations have been instrumental in the growth mechanism, small spiral pyramids should be observed. A screw dislocation emerging on the surface of a crystal provides it with a step, see Fig. (11). This step is self-perpetuating in the sense that when one, two, or any number of layers of atoms have been laid down on the crystal surface, the step remains, see Fig. (12). Hence the steps needed for the growth of a crystal are provided by the screw dislocations. Griffin (1950) observed such a growth structure on beryl crystals using an ordinary metallurgical microscope. The step height was 8 A, these being monomolecular steps with a Burgers vector equal to one lattice parameter.

Before the discovery and development of the electron microscope only optical instruments were available for the study of crystal growth. For this purpose two characteristics of the instrument require consideration, the lateral resolution perpendicular to the direction of observation, and the resolution of depth. The depth resolution needed is of the order of a few Angstrom units and depends upon the surface of the crystal under examination. The lateral resolution is limited by the

wavelength of the light used. Assuming a wavelength of 5000 A the resolving power of the best optical microscope is about 2000 A. Thus any feature with size less than 2000 A will give an image of 2000 A diameter. This means that the complete image is built up of image points of 2000 A diameter and in practice it is difficult to clearly distinguish features closer than 10,000-20,000 A. Consequently to have the spacings of growth features necessary for resolution observation must be made on crystals which are almost perfect.

4.2 TECHNIQUES TO STUDY SURFACE FEATURES.

When studying growth features the technique adopted depends upon whether mere observation of the features is required, or the measurement of actual step heights. The surfaces may be coated with a thin reflecting layer of a metal such as silver, or with an impurity, and then viewed in the metallurgical microscope. Probably the most sensitive method of observation is that using phase contrast microscopy.

To measure step heights less than 500 A the following methods are used:

a. Multiple beam Fizeau interferometry.

b. Internal interference method.

c. Method of metal shadowing.

4.2 (a) DECORATION TECHNIQUES.

The silvering technique involves the thermal evaporation of

silver at low pressure on to the specimen. The surfaces of the crystals must be carefully cleaned before depositing the silver. A layer of silver may be deposited which does not impose any structure of its own and which gives a reflectivity of 80-90%. Surface contours may be clearly seen. As one of the alternatives to silver, aluminium may be used. This is necessary in cases where the silvered surface would be attacked chemically, but the reflectivity is not quite so high.

Another method to give high reflectivity is to use dielectric multilayer films as described by Turnbull and Belk (1952), and Tolansky (1953). If a layer of thickness $\frac{\lambda}{4}$ of say zinc sulphide is deposited on glass, light will be reflected from the air-zinc sulphide surface, and from the zinc sulphide-glass surface. The light reflected at the first interface will undergo a phase change of π on reflection. Thus the path difference between the two reflected beams will be λ, giving reinforcement, and the reflectivity of the surface is effectively increased to about 31%.

The multilayer consists of alternate deposits of dielectric materials, each of thickness $\frac{\lambda}{4}$, of high and low refractive indices with respect to the crystal. Cryolite and zinc sulphide may be used on glass. The refractive indices are 1.36, 2.37, and 1.5 respectively. If a layer of cryolite is put on one of zinc sulphide which rests on glass, this layer of optical thickness $\frac{\lambda}{2}$ causes reflectivity to drop to about 14%. Odd

numbers of layers of dielectric 1. 3, 5, 7, and 9 give reflectivities of 31, 67, 87, 94, and 97% respectively.

The layers of the multilayer films are evaporated onto the substrate in vacuum, which must not be broken. The two dielectric materials are mounted on molybdenum filaments which are used alternately. The thicknesses are controlled to exact values by using their optical reflecting properties, or by a more reliable method involving the use of a photoelectric cell which enables the thickness of maximum reflectivity to be found.

Many other techniques to make steps visible have been found successful. For instance, decoration of growth steps on magnesium, cadmium, and silver by Forty and Frank (1953) is obtained by mounting on 'plasticine' for several hours. The action of the plasticine is a delicately controlled tarnish of the surfaces, and clear step-line patterns are obtained.

Amelinckx (1952) observed spirals on (111) faces of gold crystals obtained by precipitation. Using bright field illumination, photographs were taken slightly off focus as this increases the visibility of small surface steps. Steps of height 7 A were visible. To measure step heights, a small drop of alcohol-water mixture was put on the crystal face. Evaporation is fairly rapid, leaving a thin layer of liquid. Between the interfaces, liquid-crystal and air-liquid, two beam interference fringes of the Fizeau type are formed. This procedure allows only visible interpretations as the fringes

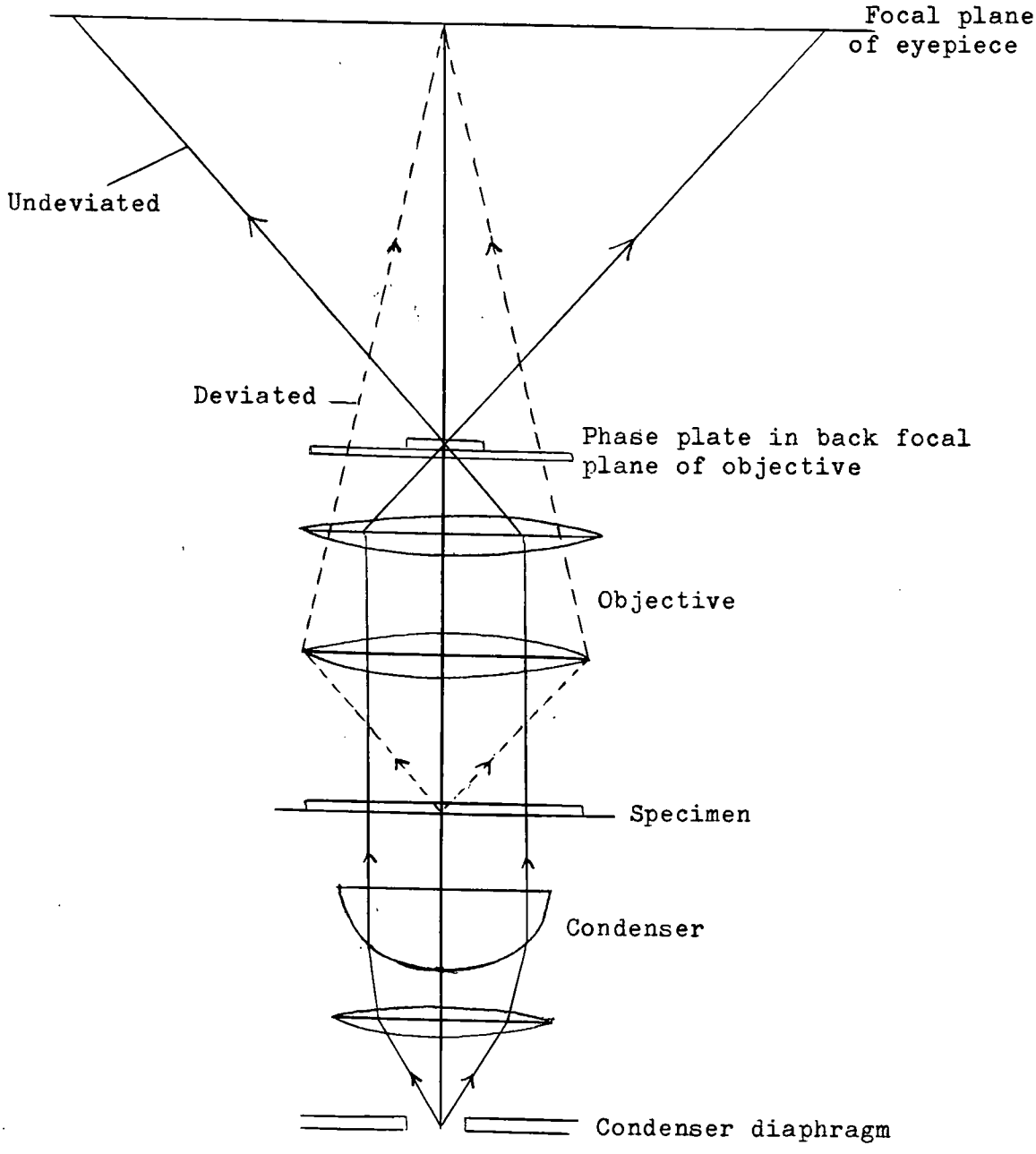

Fig. 13. Ray diagram for a phase-contrast microscope. (After Verma, 1953).

are constantly moving. Verma (1951) adopted a similar technique by breathing lightly on a clean crystal surface.

4.2 (b) THE PHASE-CONTRAST MICROSCOPE.

The novelty of phase-contrast resides in the neat optical device due to Zernike, whereby invisible changes in phase are transformed into changes in amplitude. A full account of the microscope is given by Bennett, Jupnik, Osterburg, and Richards (1951) and Verma (1951). The action of the microscope may be understood by reference to Fig. (13).

Assuming the light from the source to be focussed on the condenser diaphragm which is in the first focal plane of the substage condenser, parallel rays will pass through the object specimen.

Consider a transparent point or particle on the object, situated in homogeneous material of different refractive index. Light emerging from the particle differs slightly in phase from the light from the surrounding material. The incident light passing through the particle is diffracted, the light through the surrounding homogeneous medium continuing undeviated as parallel rays.

On passing through the objective lens, the undeviated rays are brought to a focus in the focal plane of the eyepiece. The rays deviated by the object are spread out over the focal plane of the eyepiece. Thus the image of the surrounding medium is produced by the undeviated wave and the image of the

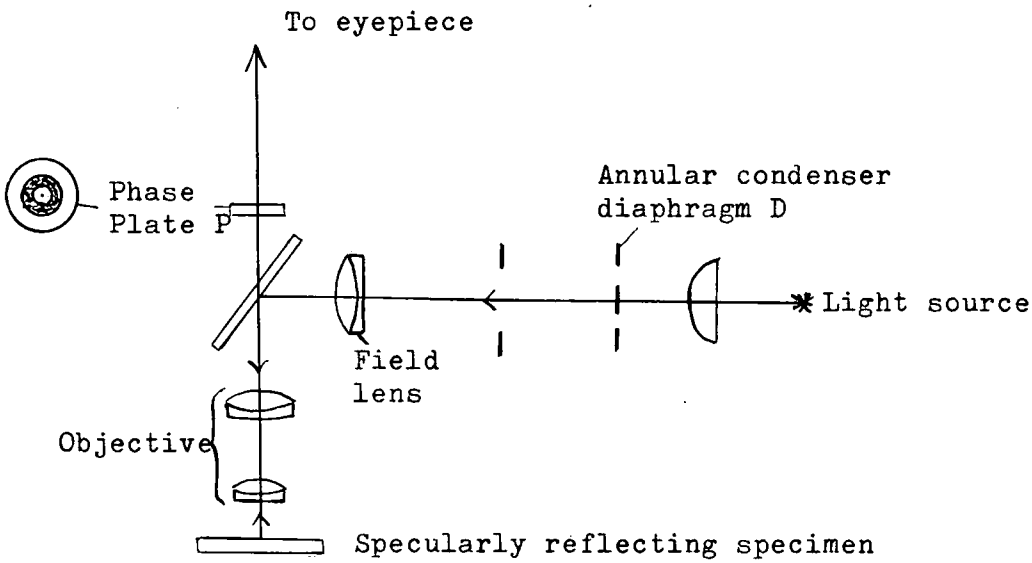

Fig. 14. Optical arrangement of a phase-contrast microscope. (After Verma, 1953).

particle by the deviated wave. Due to the diffraction, these two waves will be out of phase by about $\frac{\pi}{2}$ and where they overlap they will produce interference. If either of these waves undergoes an extra phase change of $\frac{\pi}{2}$ then they will either be in phase or out of phase, the resultant amplitude being either the sum or difference of the amplitudes of the two waves. The image of the particle will be illuminated by light of the resultant amplitude and will appear either brighter or darker than the background.

When regions of greater retardation produce darker parts of the image it is called positive phase-contrast, and when brighter than the background, it is known as negative phase-contrast.

The phase change of $\frac{\pi}{2}$ is produced in the undeviated wave by placing a phase plate in the position shown. This phase plate also contains a layer of absorbing material which reduces the amplitude of the undeviated wave, so that it is approximately equal to that of the deviated wave. This produces better contrast.

An arrangement used by Verma shown in Fig. (14) used the Cooke, Troughton, and Simms phase-contrast equipment for incident illumination. The light from the source was focused onto the annular diaphragm D by the condenser lens. The phase plate P was placed to coincide with the image of the diaphragm. The annular condenser diaphragm and phase plate assisted in obtaining axial symmetry. The resolution was improved, and the depth of

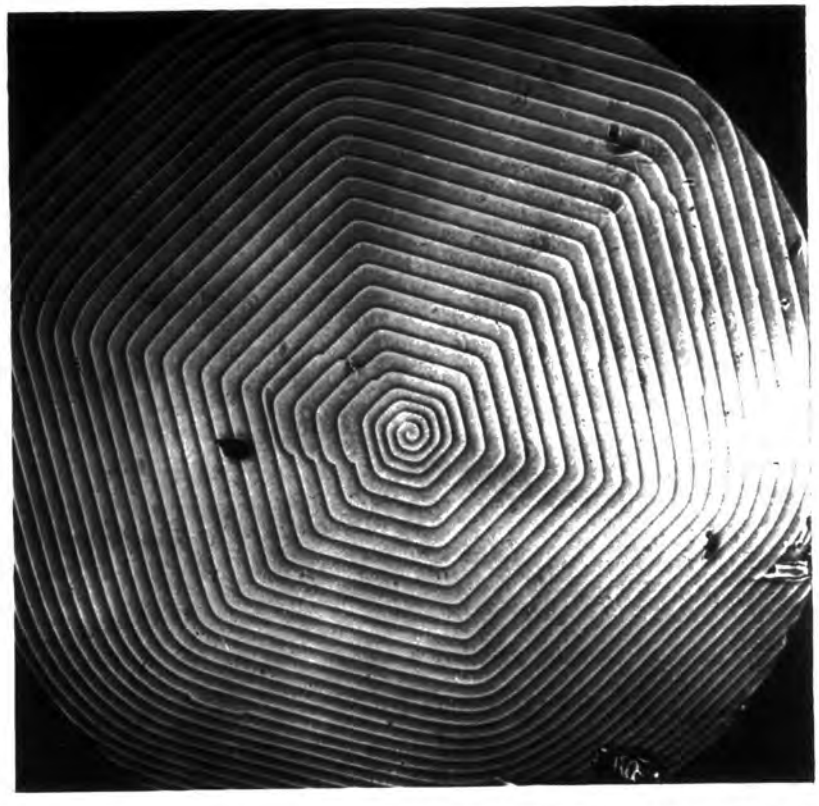

Phrase-contrast micrograph of a hexagonal spiral on SiC crystal with a step height of 165 Å (×90)

Plate 5. (After Verma, 1953).

focus diminished, by using a large objective aperture for the direct, undeviated light.

In phase-contrast microscopy the lateral resolution, at right angles to the direction of observation, is that characteristic of light microscopy, and observations must be made on almost perfect crystal faces. This requirement has restricted the method to a few crystals. Silicon carbide forms suitable crystals, having molecularly flat surfaces and small step heights, see Plate (5). The light from the surface is specularly and coherently reflected, and little is scattered. Steps in the region of 15 A are easily revealed.

4.2 (c) THE MEASUREMENT OF STEP HEIGHTS.

Multiple-beam interferometry has been shown by Tolansky (1948) to be useful for precise measurements of step heights of 100 to 500 A but unsuitable for small crystals with complex surface structure.

The internal interference method described by Forty (1952) is probably the most useful. The crystals are nucleated between a microscope slide and a coverslip, and very thin plane parallel platelets are grown. When examined in reflection with unfiltered mercury light, the microscopic images are coloured by the interference of light reflected from the two surfaces. Thin tablets with no surface structure are a uniform tint. When a plate is seated on a slide, growth takes place only on the top surface. On illuminating such crystals with parallel mercury

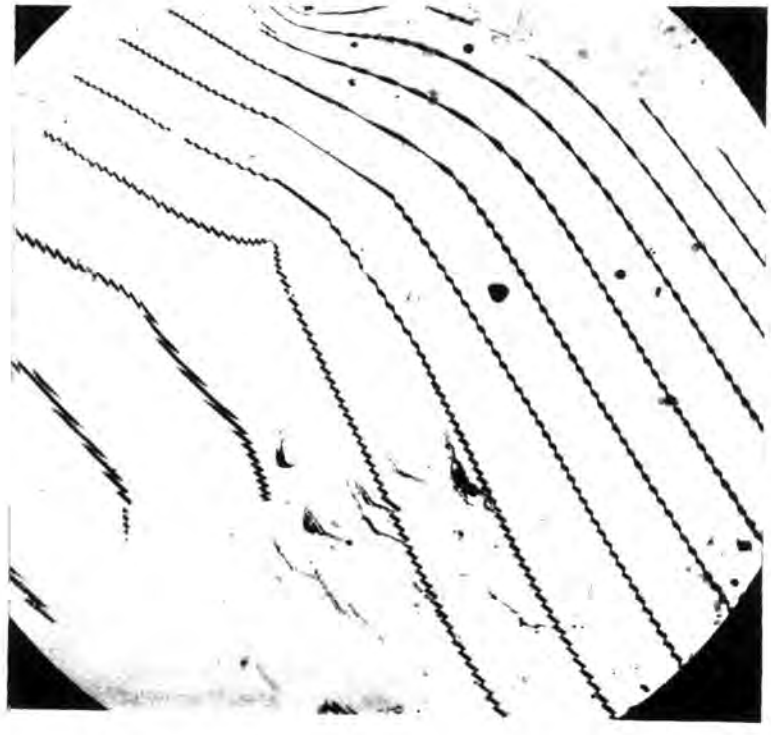

Plate 6. Fizeau fringes showing the shift of the fringes passing over the spiral steps of Plate 5. (After Verma, 1953).

green light of wavelength 5461 A, interference between reflections from the two surfaces shows a uniform shading corresponding to uniform thickness. The growth hills produce maxima and minima of intensity. A 100 A step on Cadmium Iodide crystals can be measured from a growth hill containing only two or three maxima and minima with a probable error of less than 1 A. The results show excellent agreement with the same measured by the Fizeau multiple-beam interferometer, using reflections from the crystal surface and a glass reference flat, as for Plate (6).

The method of internal interference has the following advantages over other techniques. It is a simple, accurate method for measuring steps on a growing crystal with a wide range of applicability. The lower limit is about 50 A, below which steps cannot be counted. There is an upper limit of 1500 A, where the method becomes complex because of ambiguities. These may be avoided by using light of several wavelengths. It is essentially two beam interference interferometry, and the conditions are consequently not so stringent as in multiple-beam interferometry. Strict parallelism is not so essential, and so a high power microscope objective can be used.

The method is used for measurement and observation of the structure of growth hills. The contrast for small steps is high, particularly for areas between maxima and minima, where the variation of intensity with crystal thickness is large. Using cadmium iodide Forty (1952) measured steps as small as

55 A and the contrast was comparable with that due to the phase-contrast microscope. Even smaller steps can be seen clearly on lead iodide crystals.

4.2 (d) METHOD OF METAL SHADOWING.

As this type of observation will be discussed later in connection with electron microscopy, the method will be considered here only very briefly.

It is most suitable for the measurement of large steps between 1000 and 2000 A, and according to Forty (1952) is accurate to within 20 A. Silver, or to give sharper shadows, palladium-gold, is evaporated onto the surface at an angle of 5 degrees of arc. The lengths of the shadows are measured under a microscope using a micrometer screw in the eye-piece, or from a microphotometer trace across a micrograph. The latter is the most accurate as allowance can be made for the none sharpness of the edge of the shadow, and for the superimposed image of the step-line.

The chief advantage of the method over that of interferometry is that step heights are clearly defined without ambiguity.

4.3 OBSERVATION OF SURFACES OF METALS.

Using these optical methods there was no evidence of large dislocations in metal crystals. All observations of crystals of hexagonal metals and silver by Forty and Frank (1953),

appeared to show simple dislocations of one lattice parameter. Metal crystals were grown from their vapours by heating a stock of the metal, usually in the form of tightly packed turnings at temperatures close to the melting point for 12 hours to 10 days. Observation of these by a phase-contrast microscope by Forty (1952) showed perfect plane mirror-like surfaces.

The heights of growth steps on crystals of silver are expected to be about 2 A on the cube and octahedral faces if the growth layers are monolayers of silver atoms. Steps of 20 A are just visible under the phase-contrast microscope. Steps less than 5 A are normally much too small for detection, but for such steps, probably only 5 A high on crystals of the hexagonal metals, resolution is greatly assisted by decoration of the edges of monolayers. An irregular deposit of zinc oxide concentrated along the steps on crystals of zinc, enhances the appearance of growth patterns which can then be observed under the ordinary metallurgical microscope.

4.4 MOVEMENT OF DISLOCATIONS.

Apart from the fact that growth spirals mark the points where screw dislocations meet the surface, they provided some of the earliest evidence of movement of dislocations due to small shears. Slip lines on growth spirals indicating dislocation movement were seen on crystals of silver and on n-paraffin by Dawson and Anderson (1953), and Forty and Frank (1953). Other

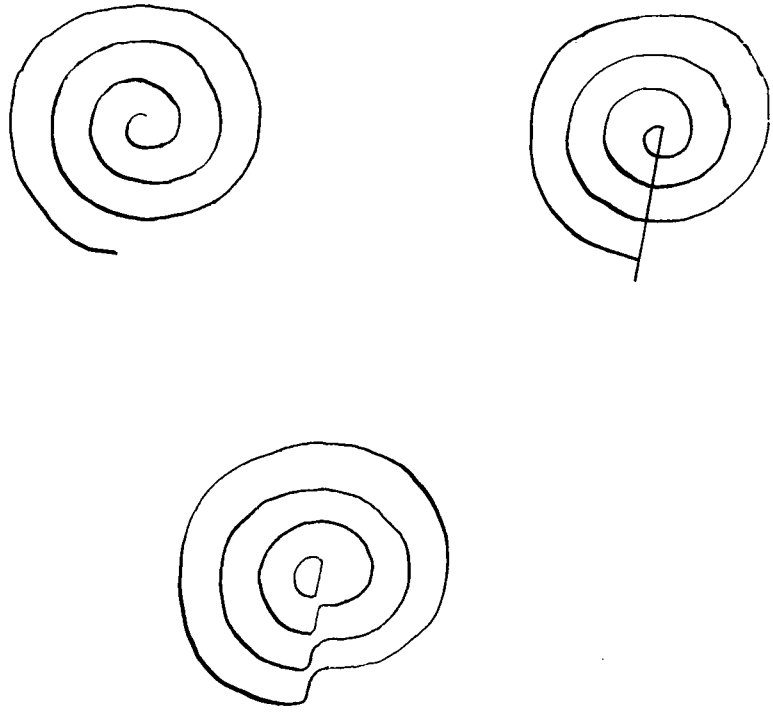

Fig. 15. The movement of a dislocation.

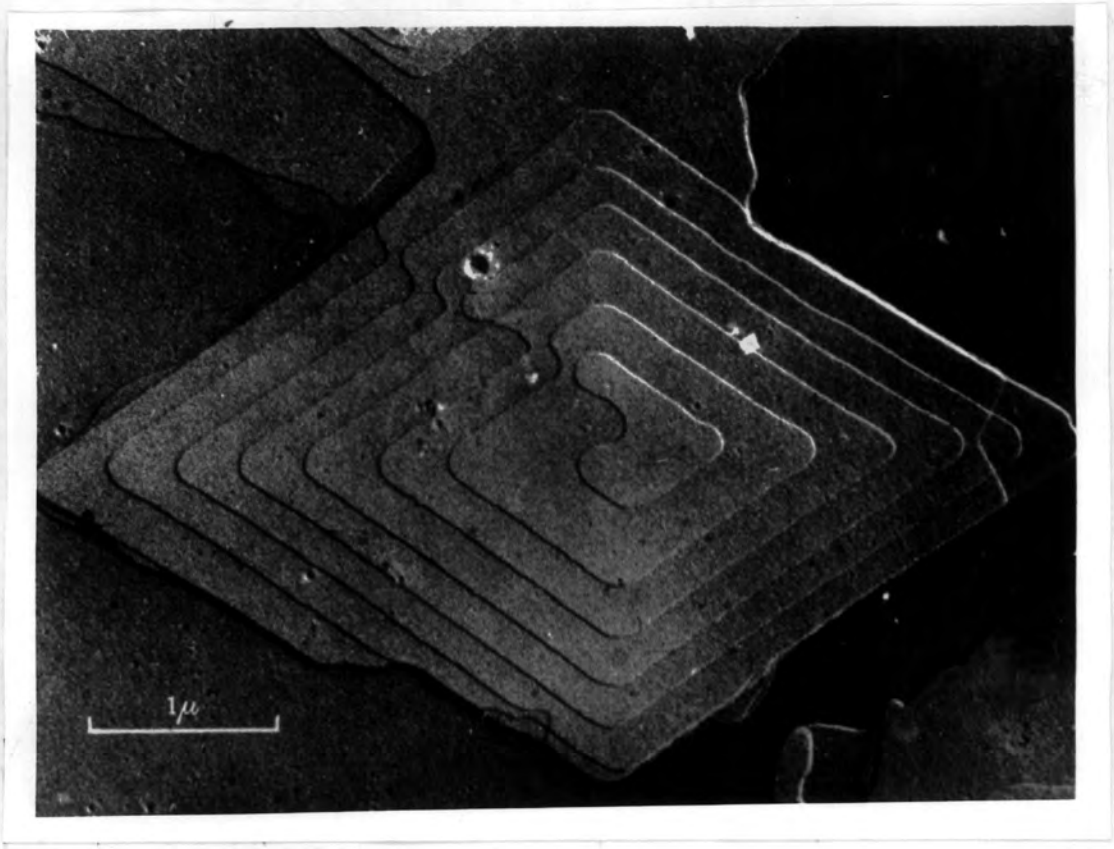

Plate 7. Electron micrograph showing a single crystal of n-nonatriacontane shadowed with nickel-palladium, showing a growth pyramid consisting of closed loops but without visible evidence of a dislocation. The dislocation is considered to have moved in its own glide plane to the edge of the crystal, (corresponding to Fig. 15).
(After Anderson and Dawson, 1953).

similar studies show the movement of dislocations, and that when they move they raise a unit slip step in the surface.

Forty and Frank (1953) found that the direction of these slip lines, i.e. the trace of the intersection of the glide plane on the free surface of the crystal, was observed to be parallel to the edges of the crystal surface on the octahedral faces and therefore represents the slip in the easy glide plane (111). See Plate (7).

4.5 THE CREATION OF DISLOCATIONS USING AN INDENTOR.

An interesting experiment by Korndorffer, Rahbek, and Sultan (1952) threw light on the creation of dislocations. They investigated the effect of mechanical deformation on the growth of cadmium iodide crystals from solution. A crystal growing as a flat plate was selected and a photograph taken. The crystals were seen to spread laterally without growing in thickness at all. An indentor - a clean glass rod drawn out to a fine point - was allowed to make slight contact with the crystal. No growth was observed for a few seconds. Then the 'dead' crystal began to grow rapidly, increasing both in extension and thickness, and on some of these crystals spiral steps could be clearly resolved. The stresses produced by the indentor created dislocations, altering the growth properties of the crystals. They observed the initiation of growth on the crystal faces at points remote from the points where it was indented, and that certain curved,

unstable edges quickly transformed into straight edges in accordance with the symmetry of the face.

4.6 CONCLUSION.

Although the study of crystal growth yielded useful information about dislocations which at the time helped to establish the existance of dislocations and their movement, as a means of observing dislocations it is very limited. Steps less than 20 A could not be seen without decorating techniques, and until undecorated steps could be detected, other methods to observe metal crystals had to be found.

PART 5.

ETCHING TECHNIQUES.

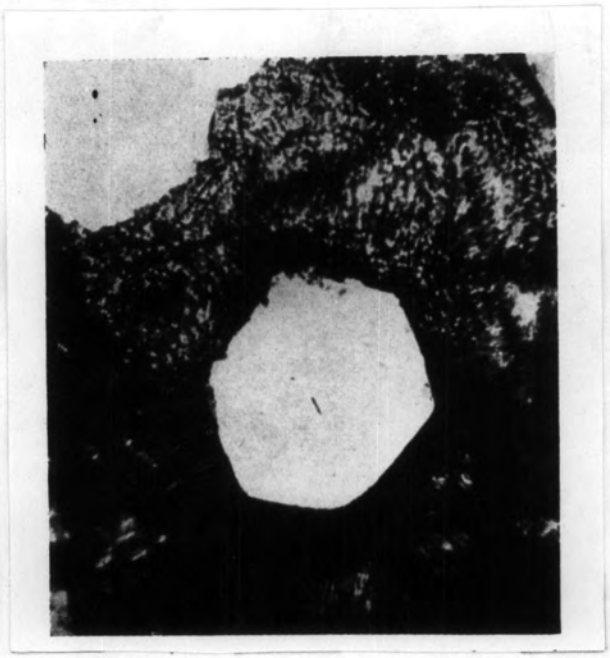

Plate 8. Hexagonal hole on SiC crystal due to prolonged etching.
(After Horn, 1952).

5.1 INTRODUCTION.

A crystal when placed in its unsaturated solution will dissolve, resulting in a general retreat of the growth fronts. A similar effect is seen when a crystal is placed in an etching medium. Etch figures are produced. The shape, arrangement, and density of these figures, produced both naturally and artificially, have been studied for many years. They are minute depressions or pits. A survey of these may be found in the book by Honess (1927).

Etching does not take place uniformly over the surfaces of a crystal. Solutions often attack particular crystal surfaces more rapidly at points where dislocations emerge than elsewhere. Preferential chemical action is due to elastic strain around the dislocation and the accumulation of impurities along dislocation lines.

The rate of etching is known to be increased by strain energy. This was illustrated by Lacombe and Yannaquis (1947) who found that large angle grain boundaries in aluminium etch rapidly and appear as grooves on the surface, whereas twin boundaries of lower energy did not etch so well.

Before other means of observation of dislocations had been developed, it was difficult to say whether every etch pit was produced at a dislocation, or whether every dislocation was etched. Horn (1952) observed etch figures due to the rapid chemical dissolution of growth spirals on silicon carbide. Each spiral

from an independent screw dislocation gave an etch pit. Prolonged rapid dissolution resulted in a hole through the crystal at the site of the screw dislocation. This was also shown to be the case by Horn, Kasper, and Fullam (1952) using crystals of aluminium boride formed in an aluminium melt, and recovered by dissolving away the melt with strong acid. It was shown, by using acids of different strengths that the dissolution must be rapid, otherwise a general disintegration of the crystal results.

Silicon carbide was treated by Horn in a fused alkali carbonate mixture at 1000 deg. C. for 2 minutes in air. This first of all removed the growth spirals, and where the centre of each spiral had been, appeared a very fine pit. These pits enlarged and deepened on further treatment. After prolonged etching, the hole, which was round, became hexagonal. Other etch pits not corresponding to spirals were also produced, see Plate (8).

Vogel, Pfann, Corey, and Thomas (1953) found evidence of dislocation structure of small angle boundaries in germanium. The boundary appeared as a row of tiny pits, relatively evenly spaced, the spacing being about a micron. This agrees with the spacing calculated from the measured difference in orientation of grains.

5.2 THE IMPORTANCE OF IMPURITIES.

Lacombe and Beaujard (1948) observed polygonised grain

boundaries in pure aluminium crystals. They used an etchant consisting of aqua regia and hydrofluoric acid which attacks an electro polished surface. This technique was used by Forty and Frank (1953) on super-pure aluminium. They showed that dislocations alone do not suffice to produce etch pits. Traces of impurities in the metal were shown to play a part. These collected at dislocations giving rise to preferential chemical action.

Young (1958) carried out experiments to reveal dislocations in copper by etch pits, and studied polygonization in very pure copper. He demonstrated that dislocations may be revealed as etch pits in copper doped with a small amount of tellurium. The correspondence between the pits and edge dislocations was found to be 100%. Climb occurred at 500 deg. C. and there was complete polygonization after annealing for 2 hours at 1000 deg. C. The progress of the polygonization was followed with back reflection X-ray diffraction. The X-ray spots were distinctly split after annealing.

To find if the impurity tellurium played any part in the climb of dislocations giving the polygonization, Young considered samples of nominally 99.999% copper. There is no known way to etch such pure copper. The specimens were bent and annealed at various temperatures and the progress of polygonization followed with X-rays. Two of the three samples polygonised, but the one that did not was probably the purest sample. He concluded

from this that if impurity is necessary for polygonization, very little is required. There was no evidence that the ease of polygonization was proportional to the amount of impurity present.

5.3 DISLOCATIONS IN LITHIUM FLUORIDE CRYSTALS.

5.3 (a) INTRODUCTION.

This section will be devoted to the work on lithium fluoride crystals by Gilman and Johnston (1956 and 1959). Etch pitting has yielded much information which they suggest may be characteristic of other impure and nonperfect crystals, both of metals and non-metals. They considered the behaviour of individual dislocations and interpreted macroscopic behaviour in terms of these.

Lithium fluoride is particularly suitable due to its properties. The crystals, grown to a high degree of perfection from the melt, have the simple rock salt structure. They can be cleaved with little resulting distortion, and, although hard enough to be handled, are slightly plastic at room temperature.

5.3 (b) ETCHES.

Gilman and Johnston used two different etches. Etch "A" attacks all dislocations equally and gives pits on (110) faces. Etch "W" attacks fresh dislocations more rapidly than annealed ones, and so makes it possible to distinguish the two types. There is a difference in orientation of the pits produced by the two etches. This is illustrated in Fig. (16) where pit (1) is

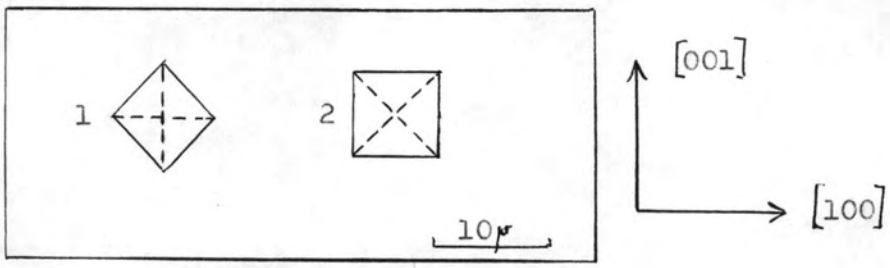

Fig. 16. (1) Pit produced by etch 'A'.
(2) Pit due to etch 'W'.

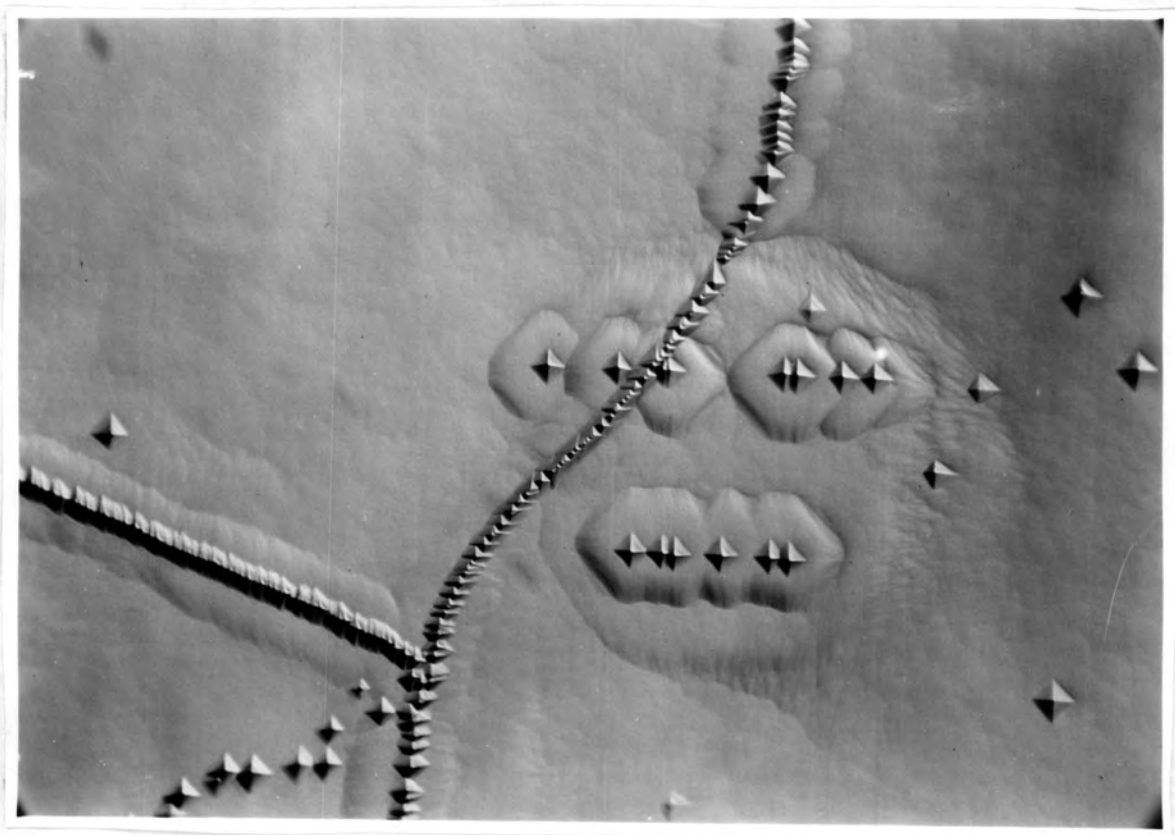

Plate 9a. Action of etch 'A'.
(After Gilman and Johnston, 1957).

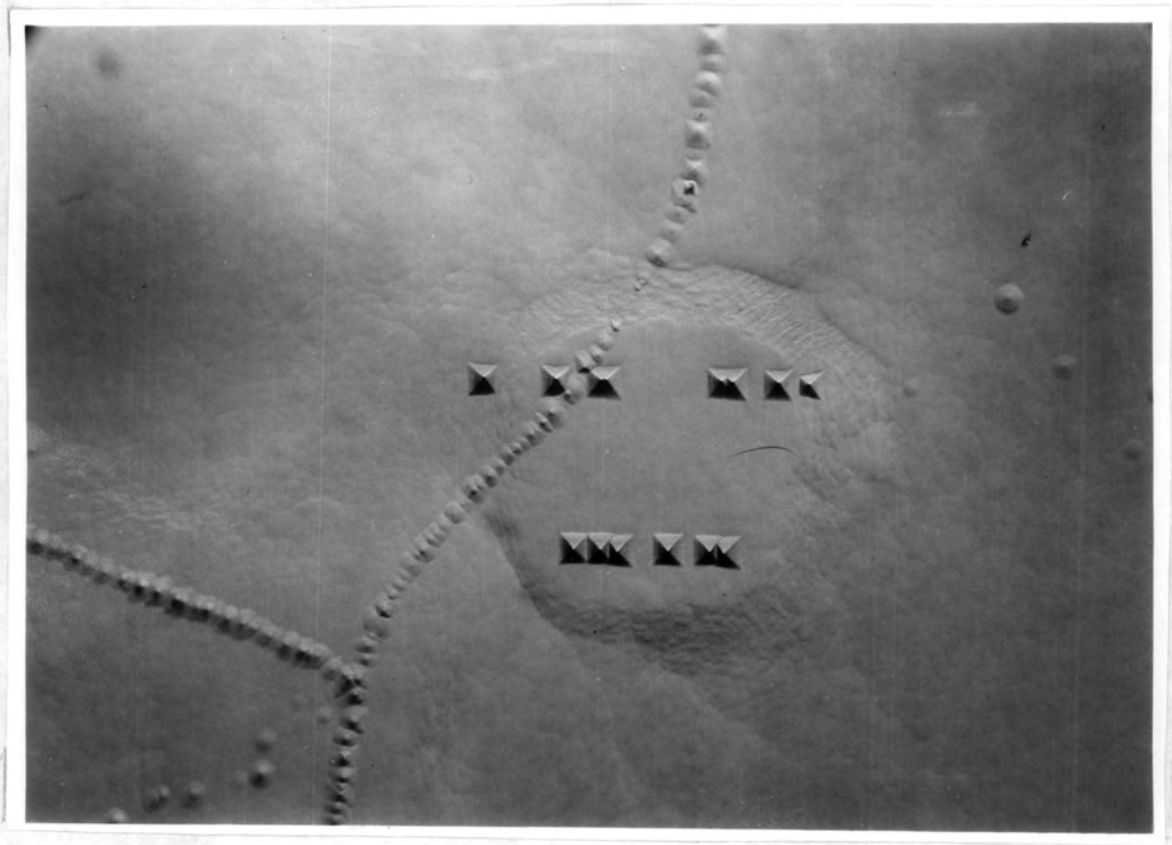

Plate 9b. Action of etch 'W' on the same field. Crystal polished between etchings.
(After Gilman and Johnston, 1957).

due to etch "A", and (2) is due to etch "W". See Plates (9a and b).

Etch "A" consists of equal parts of concentrated hydrofluoric acid and glacial acetic acid, plus one percent volume of concentrated hydrofluoric acid saturated with ferric fluoride. After a 30 to 60 second etch, the crystal is rinsed in absolute alcohol, and then in anhydrous ether. The shape of the pits and the rate of etching depend on the ferric ion concentration. This etch produces a square-based pyramidal pit. The base edges of the pit lie parallel to [110] directions. Dislocations making angles as small as 10 deg. with the (100) face are etched.

Etch "W" is a dilute aqueous solution of ferric fluoride or ferric chloride (1.5×10^{-4} molar). If the ferric ion concentration is low, a two minute etch in this reagent produces large shallow pits, less disinct than those due to etch "A". At the correct ferric ion concentration, a two minute etch produces sharply defined square pyramidal pits about 10μ in size, with basal edges parallel to the [100] directions. After etch "W" the crystal is rinsed in alcohol, and then in ether.

5.3 (c) EFFICIENCY IN REVEALING DISLOCATIONS.

As with all etching methods, the important question is that of how representative the etch pits are of the dislocations. From the results obtained by Gilman and Johnston, it is clear that the pits are formed at dislocations, but only direct observation of the dislocations in crystals can determine whether every dislocation is etched.

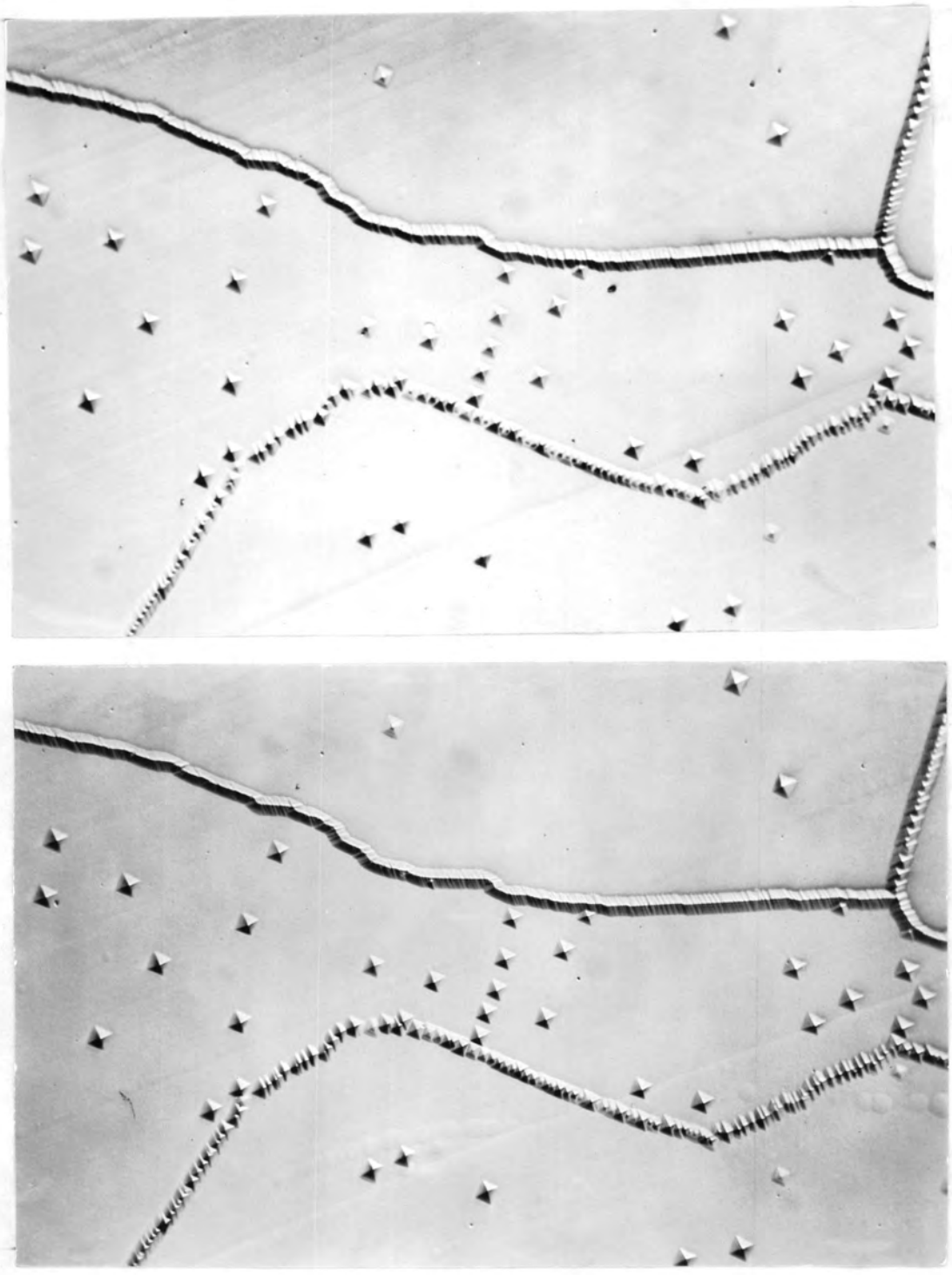

Plate 10. (a) and (b) Etch pits on matched opposite sides of cleavage crack in an 'as-grown' crystal. Etch 'A'.
(After Gilman and Johnston, 1957).

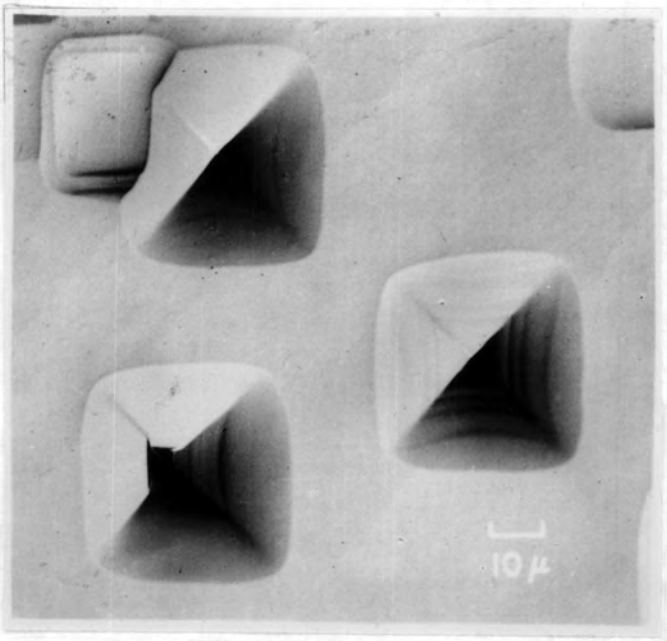

Plate 11. Comparison of etch pits produced at edge and screw dislocations by Etch 'A'. Lower left pit is at screw dislocation. The other pits are at edge dislocations. (After Gilman and Johnston, 1957).

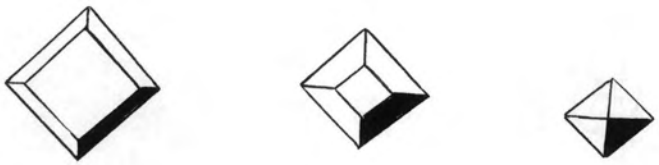

Fig. 17. The change in the shape of the etch pits due to a moving dislocation, using etch 'A'.
(After Gilman and Johnston, 1957).

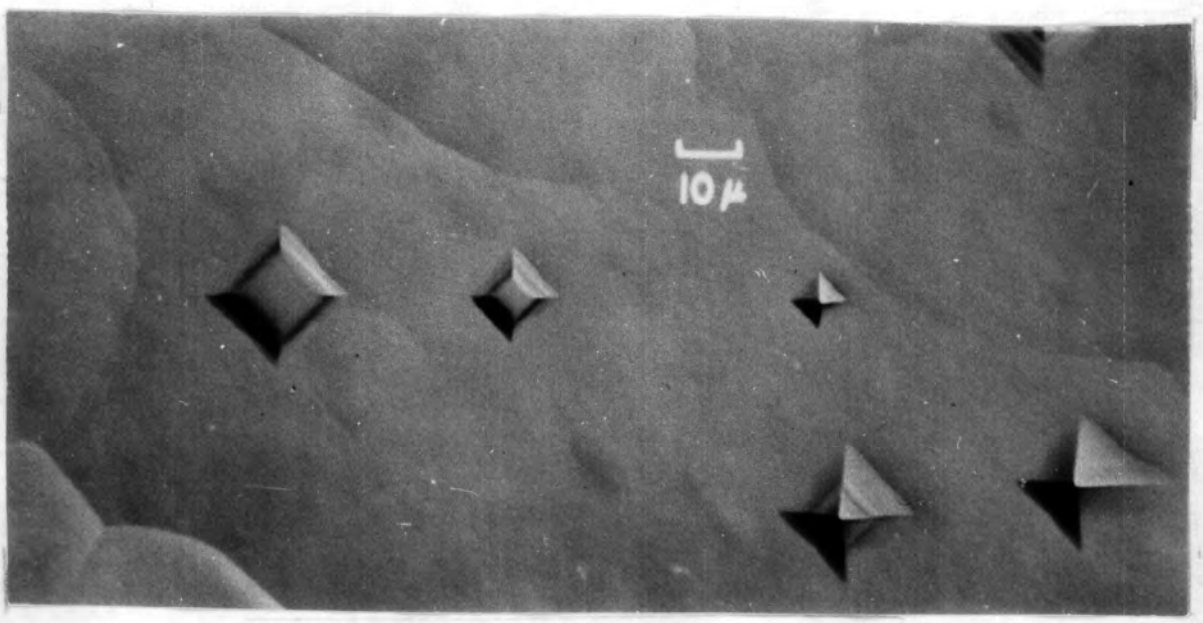

Plate 12. Effect of dislocation motion on etch-pit shapes. Etch 'A'.
(After Gilman and Johnston, 1957).

Gilman and Johnston presented the following circumstantial evidence suggesting that all dislocations are revealed:

1. The patterns of pits on matched cleavage faces are almost identical, see Plates (10a and b).
2. Several other kinds of defects are revealed by etching, but the pits are quite differently shaped from those due to dislocations. The fact that these other defects are etched would suggest that one could expect all dislocations to be etched.
3. The dislocations are attacked uniformly in spite of the fact that the ingrown dislocations may have various Burgers vectors, and lie in various planes.
4. Both edge and screw orientations of (110) $[1\bar{1}0]$ dislocations are etched, and at nearly the same rate. They are distinguishable by the symmetry of the pits produced. The edge dislocations produce symmetric pits; those due to screw dislocations are asymmetric, see Plate (11).
5. The angle the dislocation line makes with the (100) surface can be estimated from the asymmetry of its etch pits.
6. When a dislocation moves away from the position of a pit, subsequent etching causes the pit to lose its pyramidal shape and it becomes flat-bottomed. This indicates that the presence and shape of the pit depends upon the dislocation, Fig. (17), and Plate (12).
7. The dislocation density estimated from the diffraction of

Reflection	Theoretical Intensities		Measured Intensities	
	Good	Bad	Good	Bad
002	39.8	288	17.05	226.7
004	8.35	29	3.53	27.7
006	2.43	4.5	0.33	4.8
008	1.32	1.7	-	0.88
010	1.51	1.4	-	0.44

Fig. 18. Table showing the comparison between theoretical and measured intensities from 'good' and 'bad' crystals of lithium fluoride.
(After Gilman and Johnston, 1957).

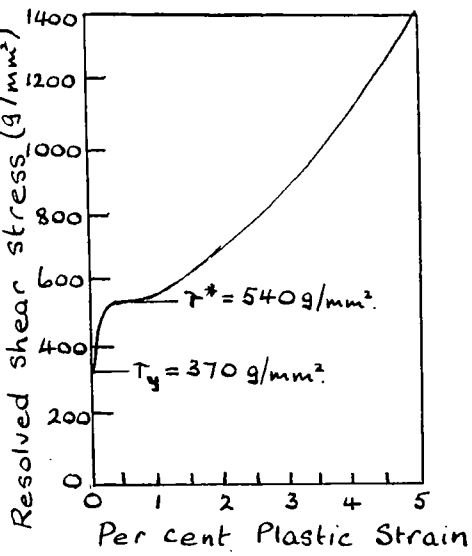

Fig. 19.

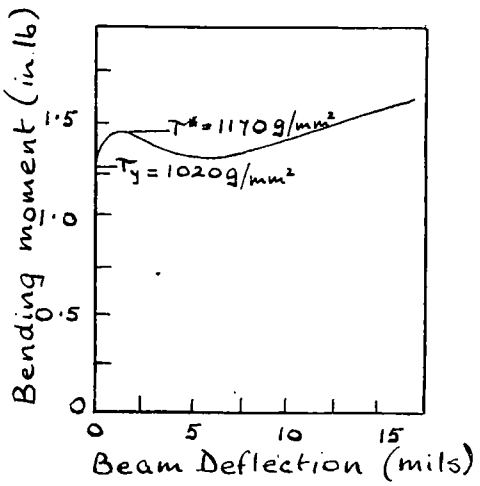

Fig. 20.

Fig. 19. and Fig. 20. Comparison of the results of compression and bending tests carried out on specimens from the same crystal. The strain rate in each case was 3×10^{-5}/sec. (After Gilman and Johnston, 1957).

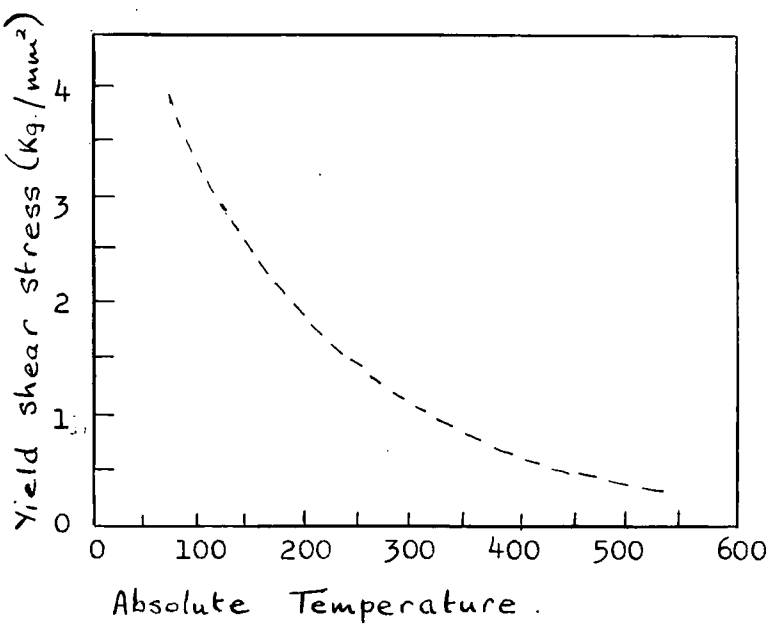

Fig. 21. The temperature dependence of the yield stress. Maximum strain rate 2×10^{-5}/sec. (After Gilman and Johnston, 1957).

X-rays by lithium fluoride crystals agrees with that gained from a study of etch pits.

This is important evidence of the ability of etch pits to locate dislocations as X-ray diffraction is quite independent of the etching method. By making Laue photographs for good and bad crystals, much greater X-ray extinction is found to occur in the good crystal. The results obtained by Gilman and Johnston are given in Fig. (18). The theoretical values were determined using results indicated by etch pit density.

5.3 (d) THE MACROSCOPIC BEHAVIOUR OF LITHIUM FLUORIDE CRYSTALS WHEN PLASTICALLY DEFORMED.

Fig. (19) shows the effect of compression on a lithium fluoride crystal. We are concerned here with T_y, the yield stress, and T^*, the critical resolved shear stress. At the former, dislocations begin to move, and at the latter, large scale glide takes place. The values of these stresses depends upon several factors and this will be discussed in more detail in section 5.3 (j).

The results of bend tests are shown on Fig. (20).

Figs. (19) and (20) represent tests carried out on specimens from the same crystal. It is important also to use specimens of the same shape to compare results, as strain is proportional to the beam depth.

The temperature dependence of the yield stress is shown in Fig. (21). Changing the strain rate has little effect upon

EFFECTS OF THE STATE OF THE SURFACE ON STRESS-STRAIN CURVES.

(After Gilman and Johnston, 1957).

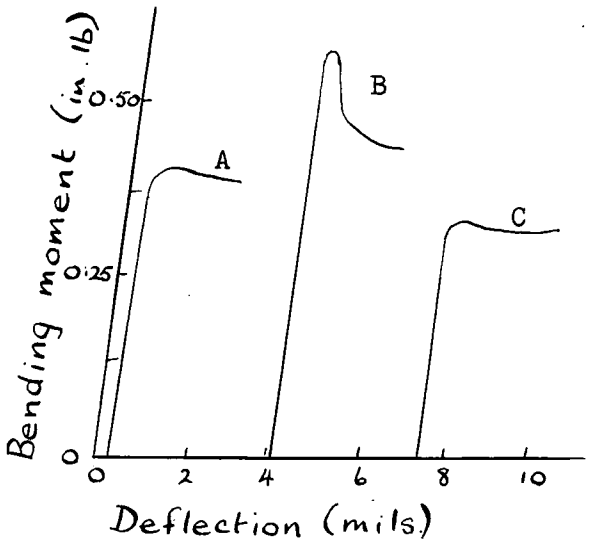

Fig. 22. A - as cleaved
B - chemically polished
C - polished and sprinkled with carborundum

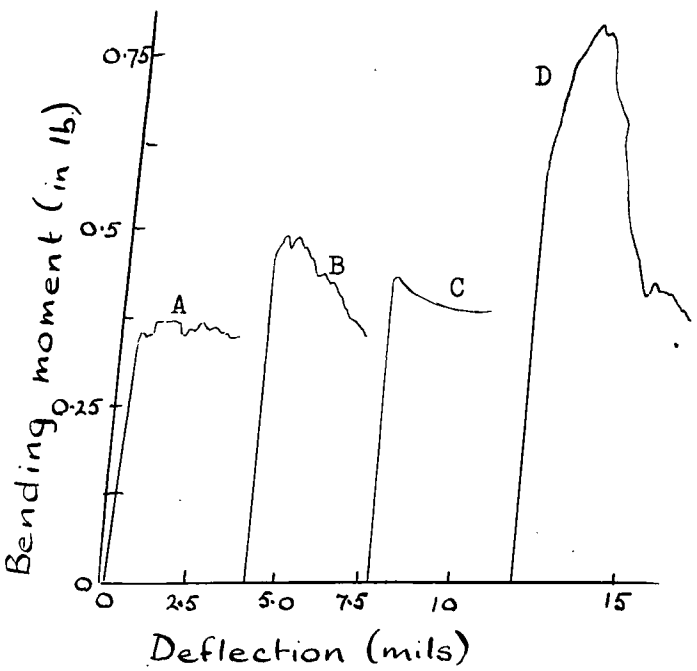

Fig. 23. Curve A and B
400 deg. C.
64 hour anneal

Curves C and D
600 deg. C.
64 hour anneal

A - as annealed
B - polished
C - as annealed
D - polished

EFFECTS OF THE STATE OF THE SURFACE ON STRESS-STRAIN CURVES.

(After Gilman and Johnston, 1957).

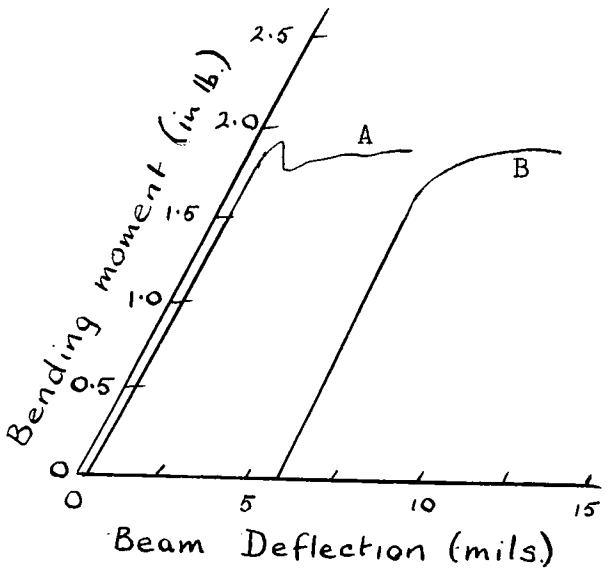

Fig. 24. Tests at -196 deg. C.
A - polished
B - polished and sprinkled with carborundum

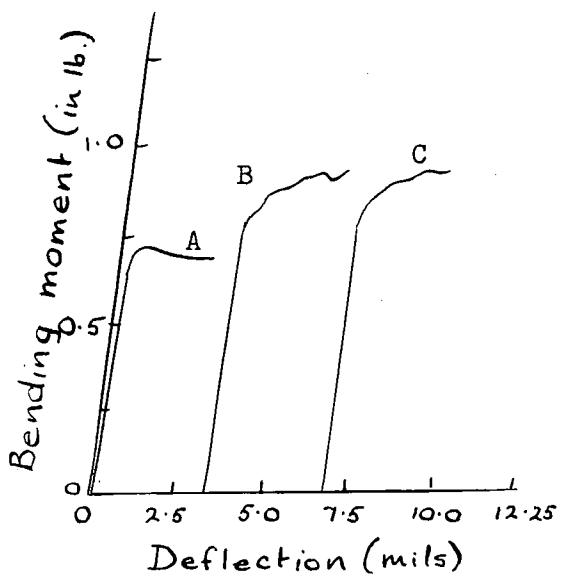

Fig. 25. A - cleaved
B - 15 minute etch
C - 60 minute etch

the macroscopic behaviour.

5.3 (e) EFFECT OF THE STATE OF THE SURFACE ON MACROSCOPIC BEHAVIOUR.

Stress-strain curves are very sensitive to the state of the surface of the crystal. This is well illustrated by Figs. (22), (23), (24), and (25) in which are shown the effects in the stress-strain curve of various surface treatments.

Specimens with surface defects bend more easily and uniformly than those where the defects have been removed. The defects on cleaved crystals are cleavage steps; on those sprinkled with carborundum, dislocations are produced where the carborundum touches the surface, (see section 5.3 f). Heating causes evaporation pits.

The condition of the surface influences the number of glide bands present after a given amount of total strain. In general, after a given amount of strain, etched or polished crystals have fewer glide bands, and more strain per band than those with originally defective surfaces.

5.3 (f) THE NUCLEATION OF DISLOCATIONS.

The dislocations originally present in as-grown crystals of lithium fluoride have little effect on the plastic behaviour. They appear to be pinned by impurities; see section 5.3 (j). This is important, and has a considerable bearing on the conclusions reached on Gilman and Johnston's work.

Dislocations were produced by:

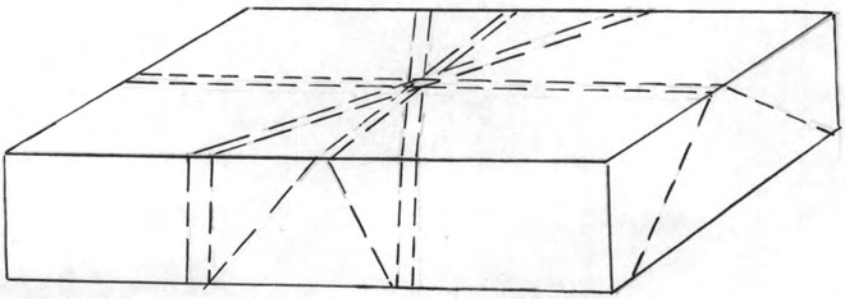

Fig. 26. The six glide planes of rosettes. (After Gilman and Johnston, 1957).

Plate 13. Rosettes due to rolling ¼ inch steel ball across the surface of a lithium fluoride crystal. (After Gilman and Johnston, 1957).

1. Nucleation at crack tips.
2. Contacting balls with the surface.
3. Quenching from high temperatures.
4. Plastic bending.

1. When a crack is made to travel slowly, and to stop in a crystal, many dislocations are produced at the crack tip. The dislocations form as loops ahead of the crack tip, and do not come from Frank-Read sources. They are not considered to be dependent upon originally present dislocations.

2. Small hard particles, e.g. 100 mesh carborundum, brought lightly into contact with the surface of lithium fluoride crystals, produce rosettes as in Plate (13). Fig. (26) shows the six glide planes of the rosettes.

Gilman and Johnston calculated that to nucleate such groups of dislocations would require a very great stress concentration, if one used the conventional theory of dislocation nucleation.

3. By controlling the rate of cooling of a lithium fluoride crystal, Gilman and Johnston produced various densities of dislocations. If heated slowly, and cooled slowly, very few dislocations are produced. By quenching from 600 deg. C., up to 6×10^7 dislocations/cm.^{2} can be introduced into a crystal, which originally had 10^5 dislocations/cm.^{2}

Many of the dislocations are in the form of small loops due to the collapse of vacancies, or to thermal stresses.

If the former were the case, loops formed on cooling from 400 deg. C., which have diameters about 3×10^{-4} cm., would require about 2×10^{8} vacancies. In the time available these would have to be drawn from a volume of 5.3×10^{-12} cm.^{3} and this volume could only contribute 9×10^{3} vacancies. Hence it was concluded that the loops are not due to collapsed vacancy platelets. A calculation of the thermal stresses shows they could be responsible for the formation of the loops.

4. Before plastic bending of the specimens, the surface is removed by chemical polishing to a depth of at least 50μ. Specimens cooled to -196 deg. C. were bent at a maximum strain rate of about 2×10^{-5} /sec. They were then slowly raised to room temperature, etched, and examined. A control specimen was not bent, but otherwise was treated in exactly the same way.

Many glide bands were seen in the bent crystal, and sometimes in small groups of an even number of pits, due to dislocation half loops. No connection was seen between these half loops, and pre-existing dislocations or other defects.

5.3 (g) THE EXPANSION AND MULTIPLICATION OF DISLOCATION HALF-LOOPS.

The specimens were prepared by producing rosettes, and then removing the surface until only the deepest dislocation loops

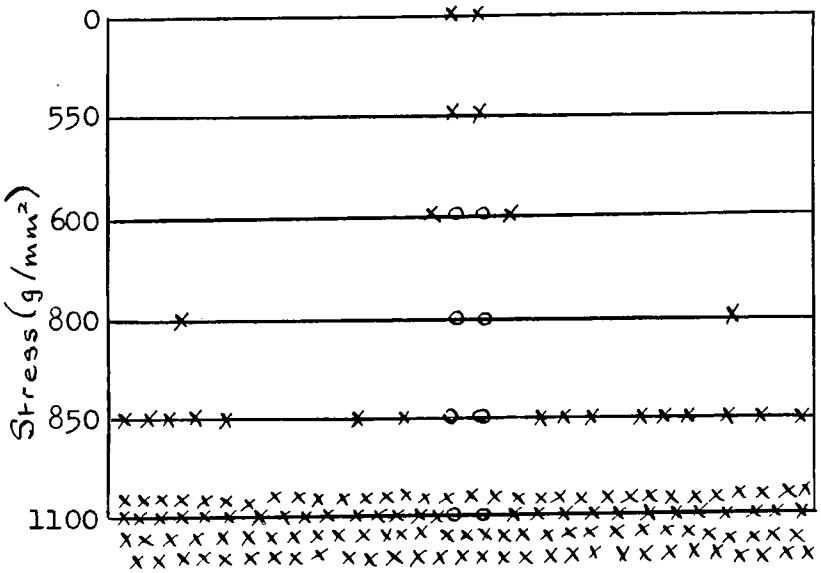

Fig. 27. Drawing of the growth of a glide band from a dislocation half loop. The crosses mark the positions of dislocations, and the circles show the vacated positions of the original half loop. Strain rate about 2×10^{-5}/sec. (After Gilman and Johnston, 1957).

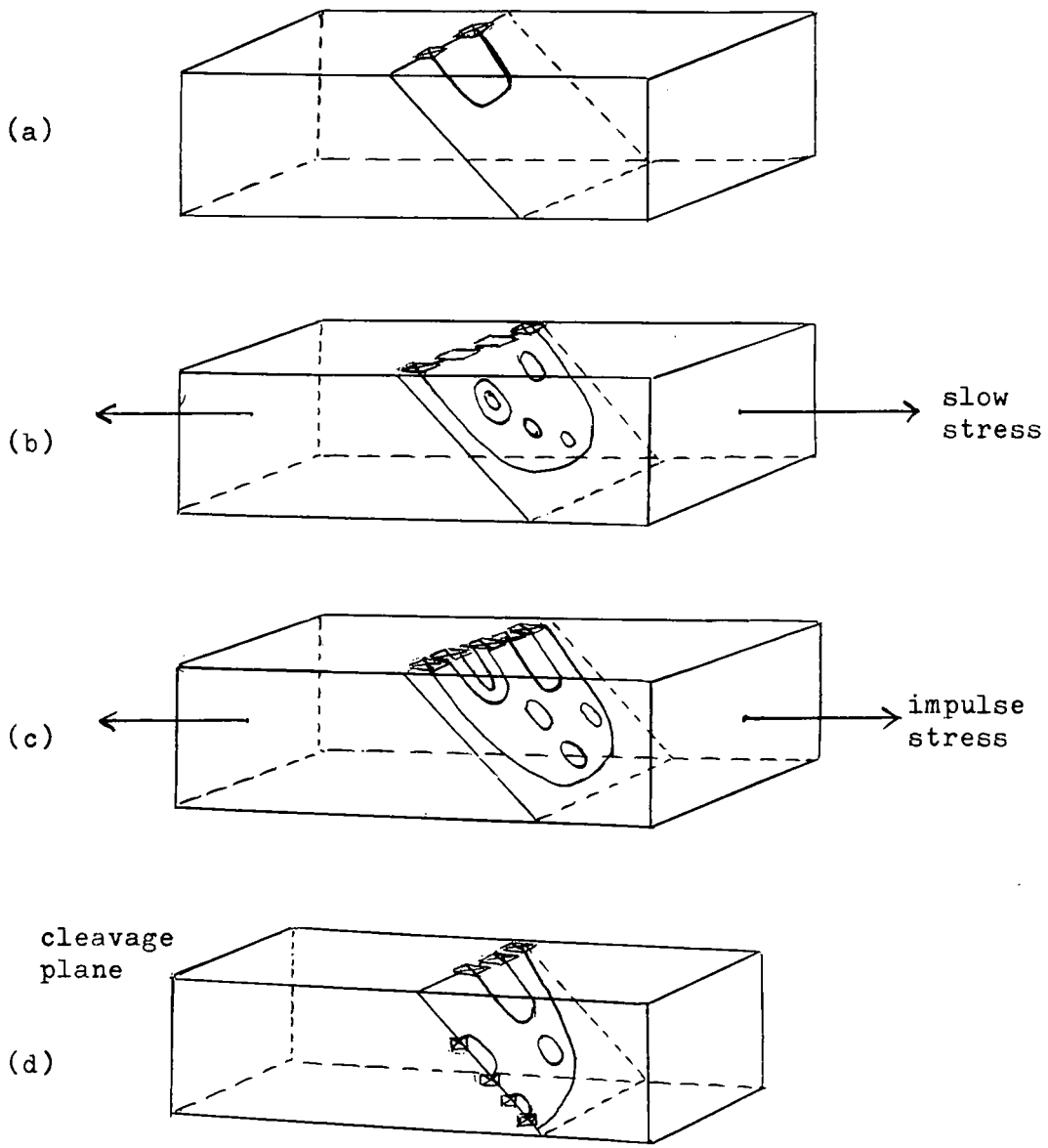

Fig. 28. Sequence of growth of dislocation half loops.
(a) Original half loop.
(b) Expanded half loop under slow stress. New loops created inside the expanded half loop.
(c) Impulse stress expands new loops and they reach the surface of the crystal.
(d) Crystal cleaved perpendicular to the original surface. Etching shows loops not previously detected. (After Gilman and Johnston, 1957).

remained.

The sequence of the growth of a glide band from a dislocation half loop due to a strain rate of 2×10^{-5} /sec. is shown in Fig. (27). The stress is increased from zero to 1100 gm./mm^2.

Careful investigation of multiplication of half loops has shown that as a half loop expands, new loops are formed as shown in Fig. (28). The specimens were cleaved at right angles to the original surface.

These new dislocations do not come from a single source, and are not necessarily coplanar. On applying a stress impulse, the new loops tend to extend to the surface. On collapsing the half loops, and then applying strain again, new half loops appeared on the sites of the previous ones, only if the previous half loops were larger than 50μ wide. This so called 'Memory effect' is due to the dislocation loops left behind inside the crystal by the original half loop.

5.3 (h) THE MEASUREMENT OF DISLOCATION VELOCITY IN LITHIUM FLUORIDE.

By tracing the movement of individual dislocations by repeated etching, and knowing the distance travelled and the time of duration of the stress pulse required to move the dislocation, the average velocity of the dislocation was found.

The specimens used by Gilman and Johnston were approximately 2 x 6 x 35 mm., and dislocations were observed on the tension side of the crystal.

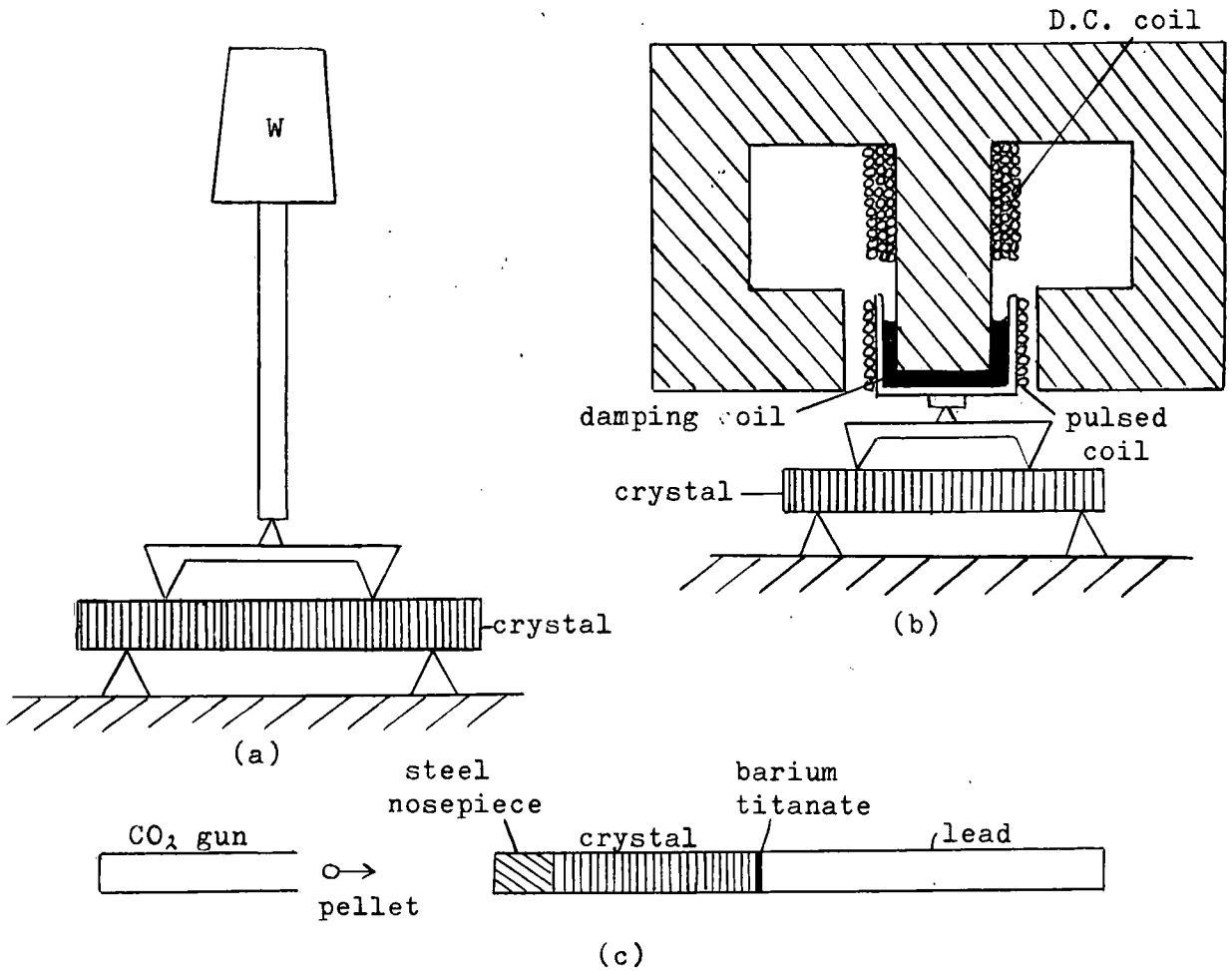

Fig. 29. Apparatus for applying stress pulses.
(a) Four-point bending jig with dead weight load.
(b) Four-point bending jig loaded with pulsed coil in magnet gap.
(c) High speed pellet strikes steel nosepiece and sends short stress pulse through crystal. (After Gilman and Johnston, 1959).

Stress pulses are applied so that the dislocation moves a measurable distance greater than 1μ. Care must be taken not to prolong the pulse as the dislocations may move out of the crystal. The stress pulses last from 10^{-6} seconds to 10^{5} seconds, and are applied using the following three methods:

1. For stresses lasting from 5 to 10^{5} seconds a dead weight load is applied to a four point bending jig, see Fit. (29a).

2. For pulses lasting from 5 seconds down to several milliseconds, a magnetic pulsing machine replaces the dead weight in (a), see Fig. (29b).

   This pulser consists of a large electro-magnet similar to that used in a moving coil loud speaker with a small oil damped coil mounted in the annular gap. The small coil rests on the four point jig so that on passing a square current pulse through the coil, a stress pulse is transmitted to the specimen. A resistance strain gauge calibrated by dead weight loading is used to measure the magnitude of the pulse. Fig. (30) shows the form of the pulse.

3. Pulses of very short duration, down to 1μ second are attained by high speed impact. A steel nose-piece is attached to the crystal to protect it. Ball-bearing spheres $\frac{1}{16}$ inch diameter are fired at the nose-piece. The pulses from the impact travel through the nose-piece, the specimen, a barium titanate transducer, and into a long lead absorber, see Fig. (29c). These are glued together and suspended from a ballistic

Fig. 30. Shape of stress pulse from magnetic loading. (After Gilman and Johnston, 1959).

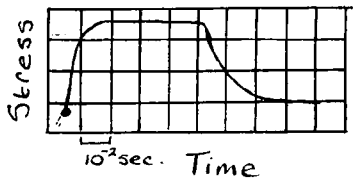

Fig. 31. Shape of pulse from high-speed pellet. (After Gilman and Johnston, 1959).

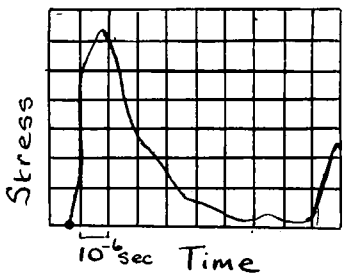

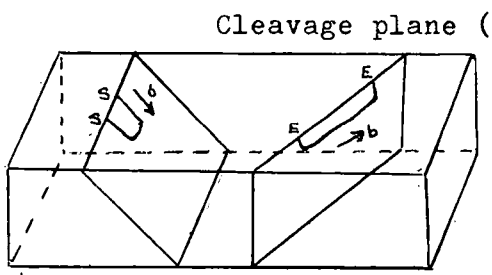

Glide plane (110)

Glide direction [110]

SS = screw component

EE = edge component

Fig. 32. Two dislocation loops that break the surface of a cleaved crystal. (After Gilman and Johnston, 1959).

pendulum, enabling the momentum gained on impact to be calculated.

The shape of the stress pulse is obtained from the barium titanate transducer. In Fig. (31) is shown a typical waveform consisting of the main pulse and a small reflected pulse.

The estimated errors in measurement of dislocation velocities ranged from a few percent for slow movements, to about a factor of 2 at the fastest velocities.

5.3 (i) PREPARATION OF THE LITHIUM FLUORIDE CRYSTALS FOR VELOCITY MEASUREMENTS.

The lithium fluoride crystals were carefully prepared and polished. A ball bearing was rolled to and fro across the crystal. Rosettes were formed. The crystal was then chemically polished to remove a 10 to 15 μ layer. Only the deepest dislocation loops remained. They were of the type shown in Fig. (32) and were suitable for velocity measurements.

5.3 (j) FACTORS INFLUENCING THE VELOCITY OF DISLOCATIONS.

Gilman and Johnston measured the dependence of dislocation velocity on :

a. Stress, Fig. (33).

b. Hardness, Fig. (34).

c. Temperature, Fig. (35).

d. Neutron irradiation, Fig. (36).

The effect of stress on dislocation density and consequently upon dislocation velocity in lithium fluoride is interesting.

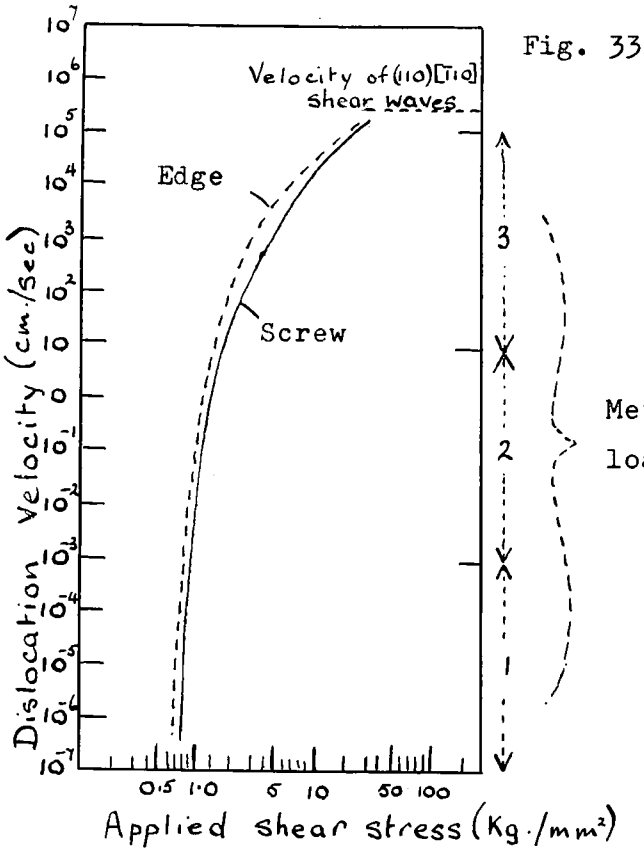

Fig. 33. Graph for an as-grown lithium fluoride crystal. The velocity of the edge dislocation is approx. 50 x that of the screw dislocation. (After Gilman and Johnston, 1959).

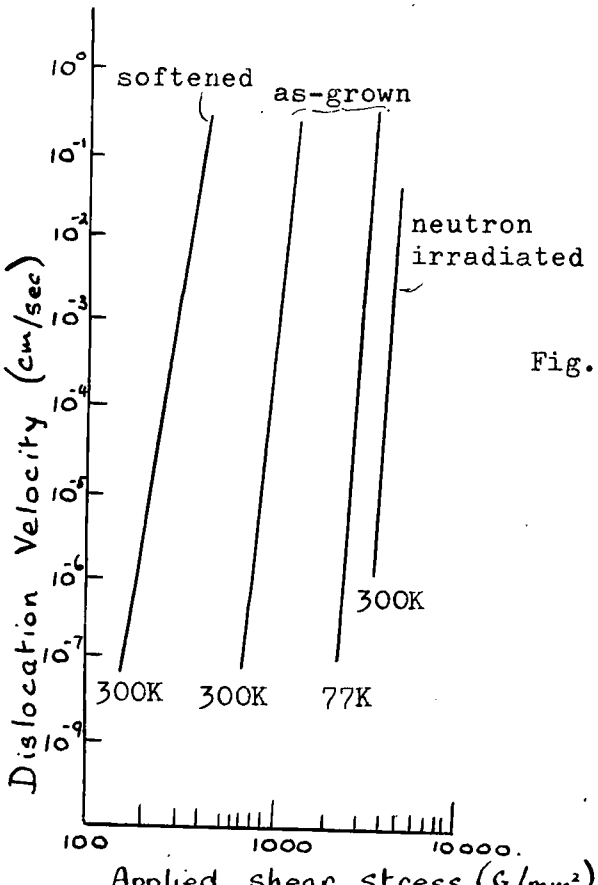

Fig. 34. Velocity of screw components of dislocation loops against applied shear stress for crystals of different hardness. (After Gilman and Johnston, 1959).

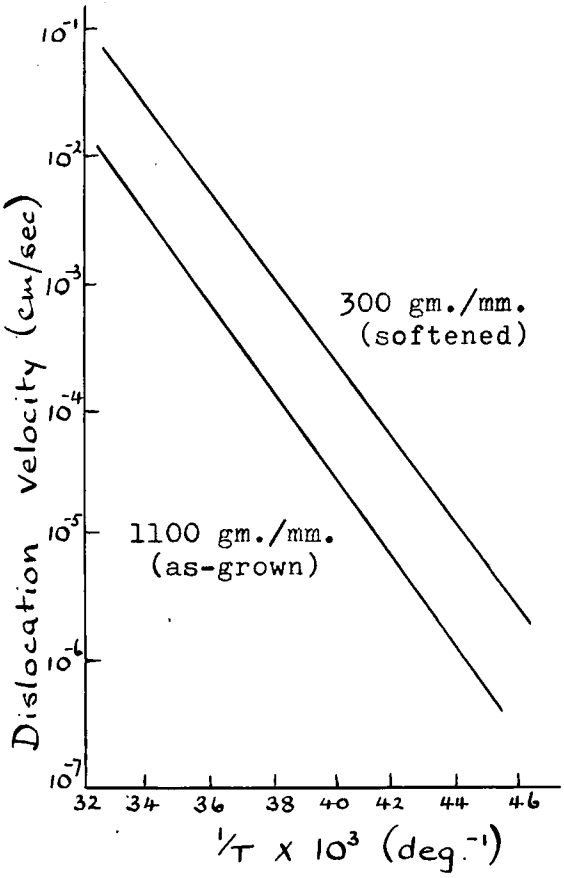

Fig. 35. The dependence of dislocation velocity on temperature. (After Gilman and Johnston, 1959).

Fig. 36. Effect of neutron irradiation on velocity of edge components of dislocation loops. (After Gilman and Johnston, 1959).

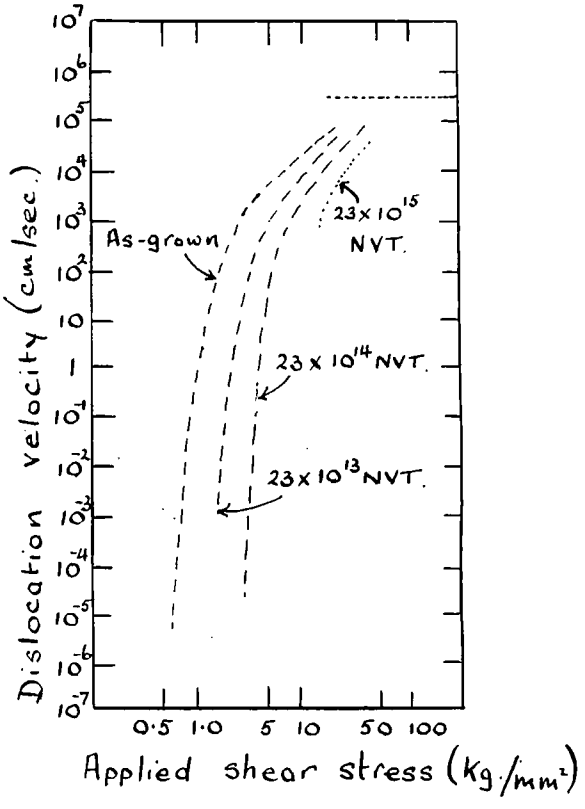

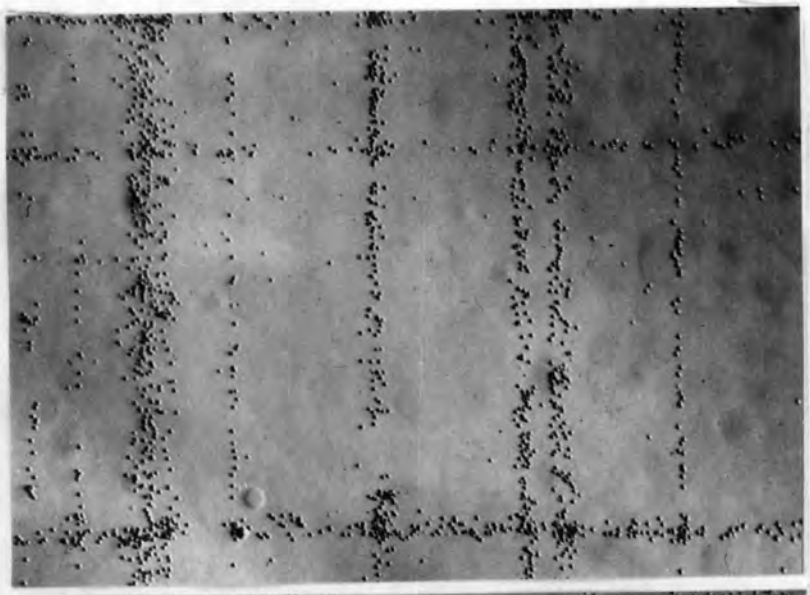

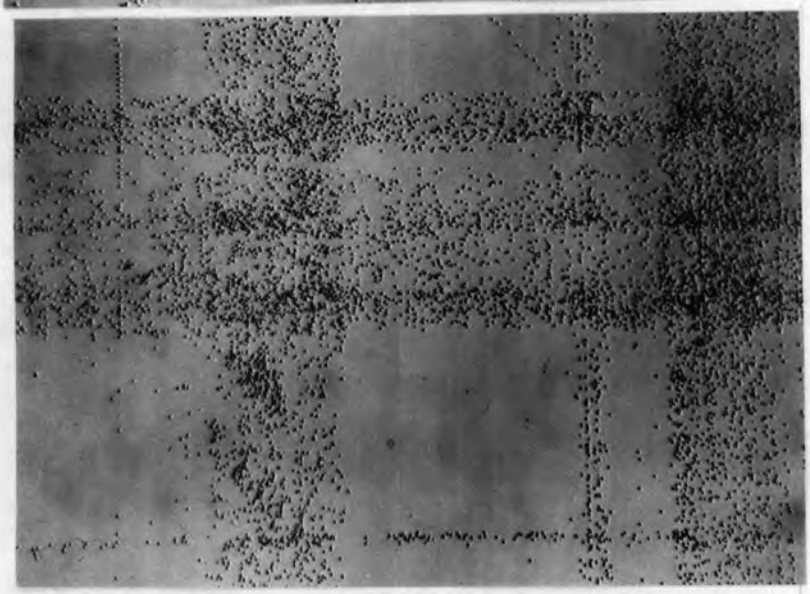

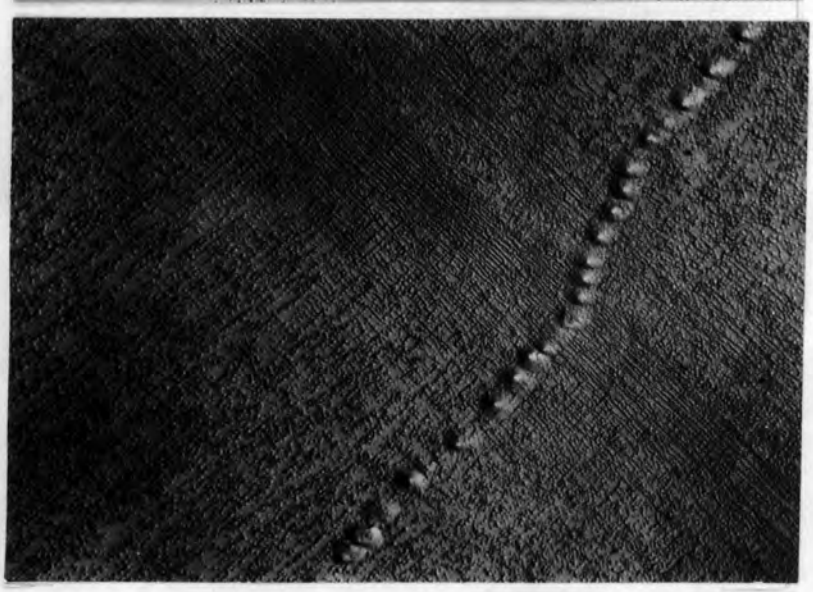

Plate 14. Lateral growth of glide bands in a lithium fluoride crystal.

(a) 0.03% compression.

(b) 0.9% compression.

(c) 8.0% compression.

(After Gilman and Johnston, 1959).

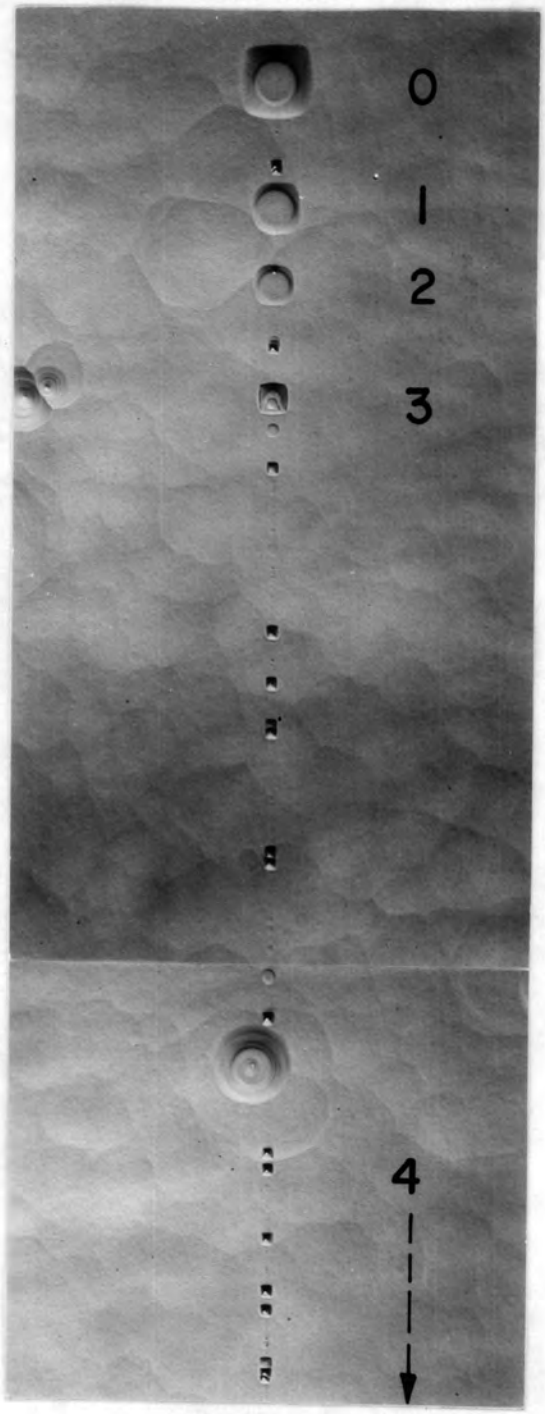

Plate 15. Effect of stress on dislocation multiplication. Starting at 0 the dislocation was moved three times by 10 sec. stress pulses at 1540 g/mm. No multiplication occurred. A final 10 sec. pulse at 1680 g/mm.^{2} caused profuse multiplication, and the original dislocation moved out of the picture. The crystal was etched after each stress pulse. (After Gilman and Johnston, 1957).

The density changes from zero to 10^4 loops/cm.^{2} as the stress is increased. When the applied stress is sufficiently high to cause dislocation motion, profuse dislocation nucleation and multiplication occur, Fig. (28).

If a crystal is compressed, it is possible to expand loops to 0.5 mm. without multiplication, but at .03% compression rows of etch pits are seen with spacing about 2μ. The density within the rows is about 10^7/cm.^{2} When the compression is increased to 0.9% a broadening of the rows of pits occurs, more etch pits appearing alongside existing ones. A compression of 8% gives a complete covering of the surface with etch pits to a density of 10^7/cm.^{2}, see Plates (14) and (15).

Impurities have an expected influence on dislocation movement. They produce two quite distinct effects, static pinning, and dynamic resistance to dislocation movement. The former affects the stress to move a dislocation which has been pinned by impurities; the latter, the stress to move a fresh dislocation through a crystal containing impurities.

Variation in the impurity content of the crystals influences the hardness, which depends upon the stress to move a dislocation. Different heat treatments also produce variations in hardness. Crystals cooled very slowly from 250 deg. C. to room temperature are hard, and crystals of the same purity cooled rapidly through the same range are relatively soft. The hardness has been found to differ by a factor of five.

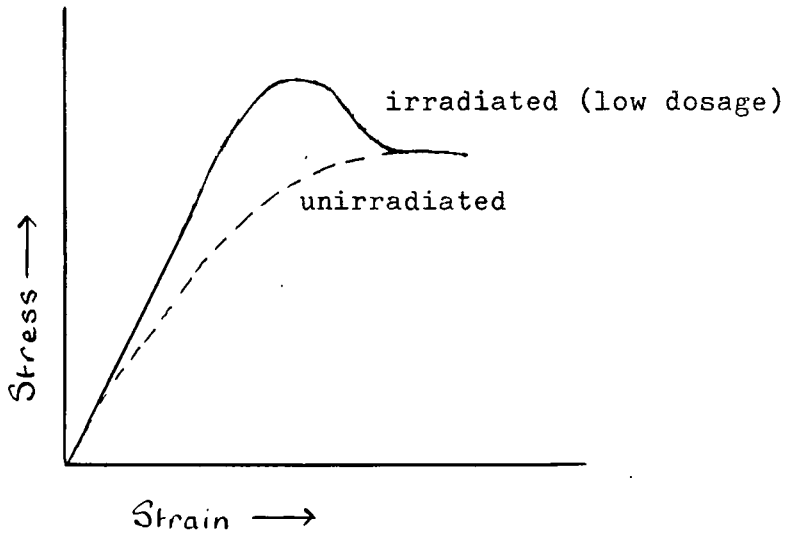

Fig. 37. Graph showing the static pinning of dislocations by low dose of irradiation.

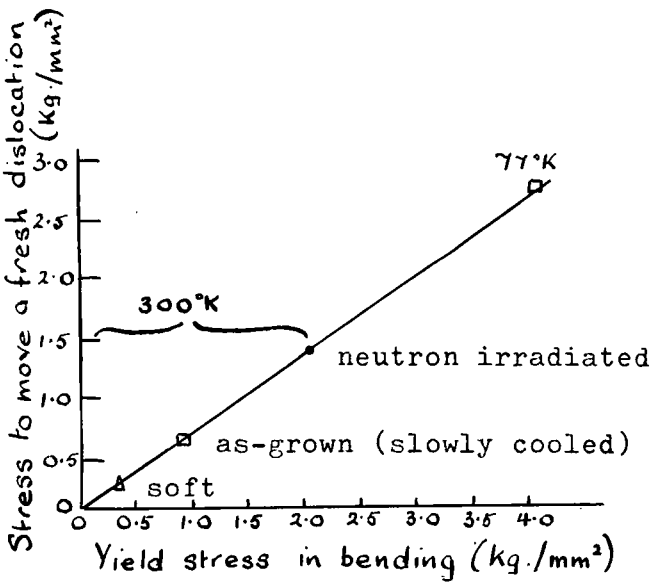

Fig. 38. The relationship between the stress to move a fresh dislocation, and the crystal strength. (After Gilman and Johnston, 1959).

Gilman and Johnston consider this to mean that the dynamic resistance due to impurities is greater when the impurity atoms have precipitated than when they are in the form of scattered atoms.

Hardness is found to be very sensitive to the rate of cooling from 200 deg. C. to 100 deg. C. This implies that a precipitation of impurities is occurring at below 200 deg. C.

Irradiation of lithium fluoride crystals has two effects, depending upon the dose, i.e. the product of the time in the reactor and the neutron flux.

1. Static pinning due to low doses makes dislocations harder to move initially, but when they break away they are as easily moved as before irradiation, see Fig. (37). The pinning here is considered due to point defects.

2. Considerable irradiation produces dynamic resistance, making it difficult to move all dislocations, including those put in before and after irradiation. This is effective at high and low stresses and indicates a lattice friction due to something put in by the radiation. Optical studies reveal the presence of colour centres composed of multiple point defects. See Fig. (38).

The origin and growth of glide bands appear to be independent of the existing dislocations, and the state of pinning and geometrical arrangement of those dislocations do not affect the yield stress. The initial yield stress is determined by the

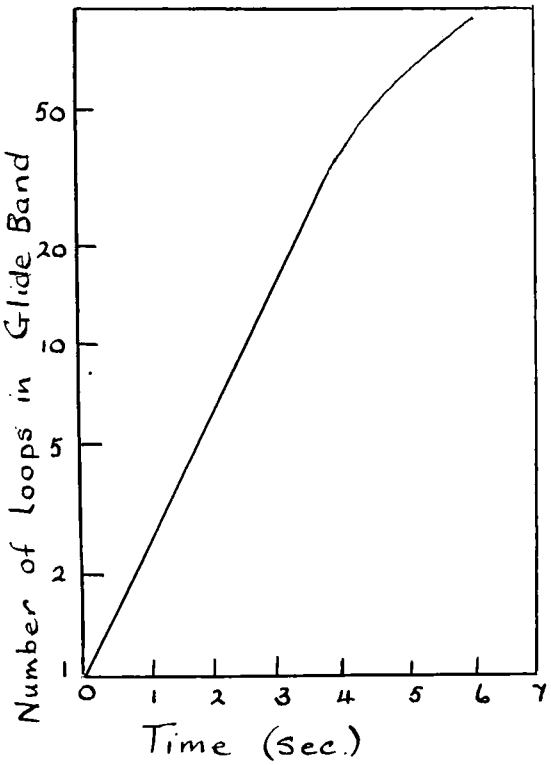

Fig. 41. Growth of glide bands from a single loop, shown as a function of time. Applied stress = 1640g/mm. (After Gilman and Johnston, 1959).

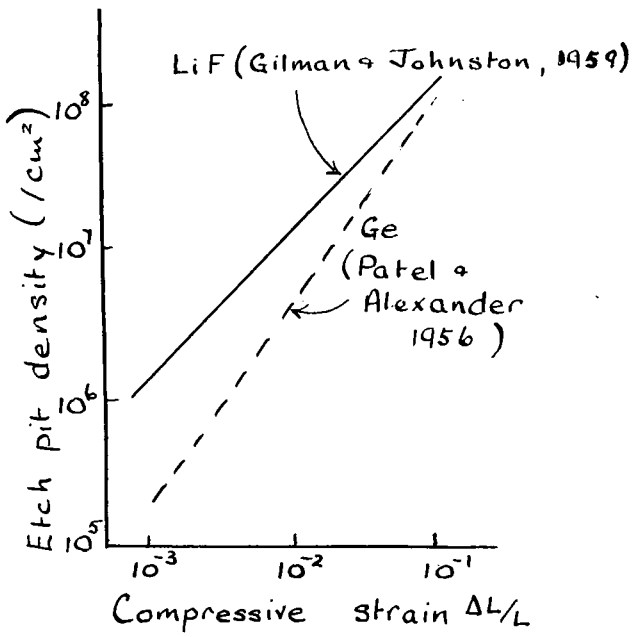

Fig. 42. Graphs showing the similarity in change of etch pit density with compressive strain for lithium fluoride and germanium.

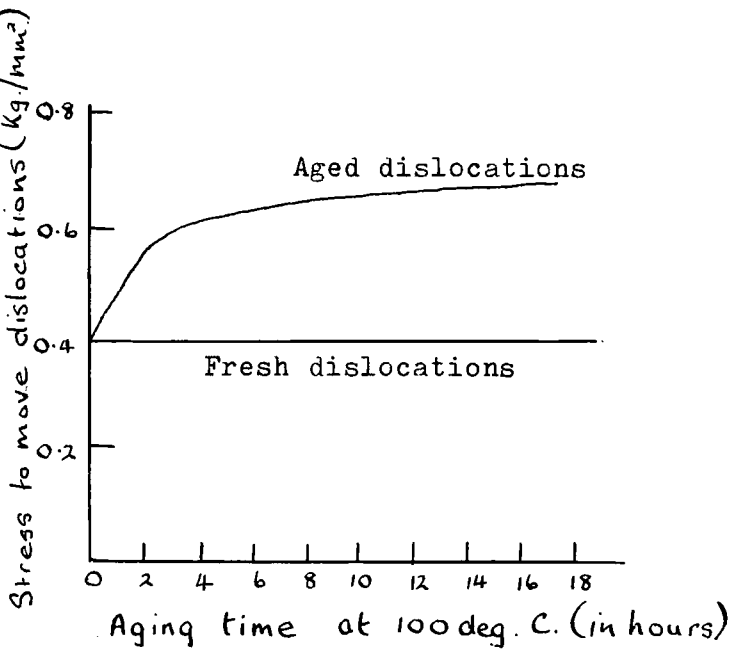

Fig. 39. Dislocation pinning by low-temperature aging.
(After Gilman and Johnston, 1959).

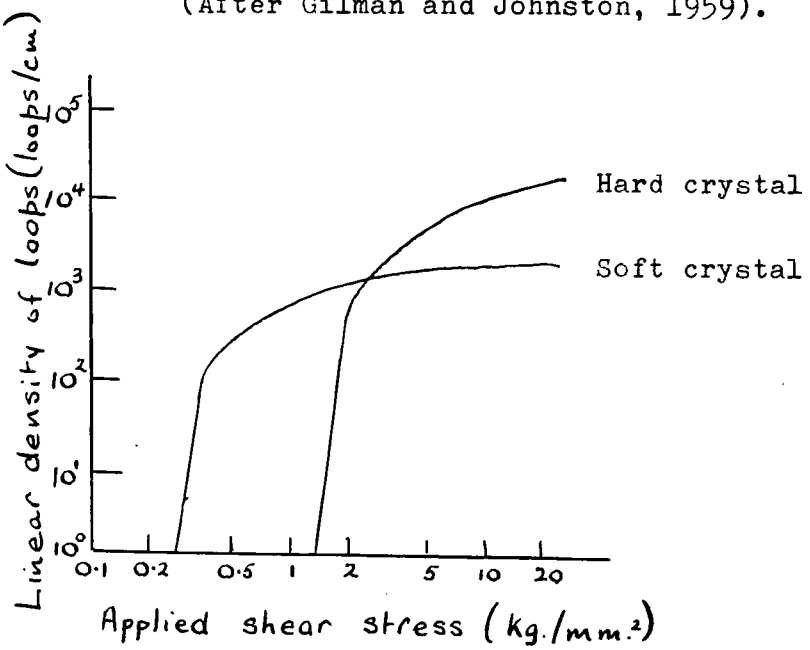

Fig. 40. Graph for screw components of loops of diameter about 0.5 mm.
(After Gilman and Johnston, 1959).

resistance to motion encountered by a glide dislocation in an otherwise dislocation-free region of the crystal, see Fig. (39). Even after a small amount of plastic dformation (0.1 to 1% strain), the flow stress of lithium fluoride can be understood in terms of the numbers of glide dislocations and their mobility in a dislocation-free crystal. At large strains work hardening occurs, and the effect on the motion of glide dislocations of the many other dislocations in the crystal, is indicated.

A real understanding of the mechanism of multiplication and interaction in work hardening has not yet been attained.

5.3 (k) SUMMARY.

The following is a summary of the more important results of observations by Johnston and Gilman.

1. Grown-in dislocations do not move in lithium fluoride and so Frank-Read sources are not responsible for multiplication nor for yield.
2. Dislocations can be nucleated in dislocation-free crystals at low stress, see Fig. (40).
3. The multiplication mechanism and the broadening of slip bands is not understood, but the rate depends upon the applied stress and the dislocation velocity.
4. The bulk strength of crystals is determined by the stress required to move a fresh dislocation.

Plate 16

~~Fig. 1~~

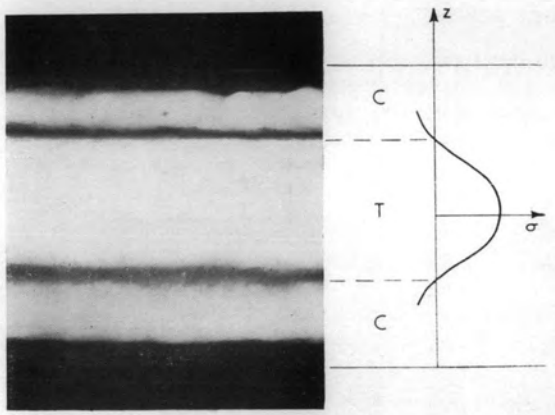

(*a*) ×13 (*b*)

Bar of silver chloride plastically deformed in tension; load released. (*a*) photoelastic pattern, (*b*) distribution of longitudinal stress σ.

Plate 17

~~Fig. 3~~

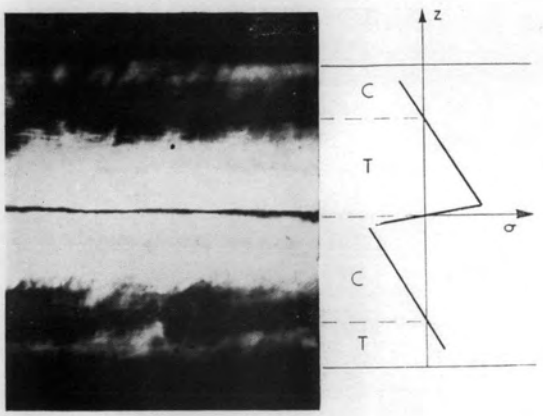

(*a*) ×11 (*b*)

Bar plastically bent; external couples removed. (*a*) photoelastic pattern, (*b*) stress distribution.

Photographs taken with crossed nicols, at 45° to the extinction directions. T=tension, C=compression.

Plates 16, 17, and 18. (After Nye, Spence, and Sprackling, 1957).

5.3 (1) CONSIDERATION OF THE RESULTS AND DEDUCTIONS MADE BY GILMAN AND JOHNSTON.

The observed behaviour of dislocations in lithium fluoride differs in many respects from the more prevalent views of dislocation behaviour. Dislocation loops are formed at low stresses with no obvious sources. It is assumed that sources are present, but are not detected by the methods used.

Gilman and Johnston suggest that their results for lithium fluoride can be extended to apply to other crystals. Preliminary investigations indicate that magnesium oxide and calcium fluoride deform in a similar manner, but it cannot be concluded that all crystals behave in the same way. Probably it is only true for fairly impure crystals. There must be small particles on which nucleation can occur, and it has been shown that precipitates are the determining factor regarding the stress to move dislocations.

Work done by Nye, Spence, and Sprackling (1957) supports the condemnation of the generalizations by Johnston and Gilman.

Nye et al used the photoelastic effect to study the plastic deformation of single crystal bars of silver chloride in tension and bending. They found that in tension the plastic deformation is greatest near the surfaces. In bending, the plastic deformation is found to propagate longitudinally along the bar rather than transversely. The distribution of the birefringence resulting from the stress was interpreted in terms of a simple

dislocation model. They found that the ratio of the stress necessary to propagate dislocations to the stress needed to generate them is less than 0.6.

When a crystal is not fully annealed the dislocations in it produce long range elastic strains. In transparent cubic crystals such strains are visible as distributions of birefringence produced by the photo-elastic effect.

Schmid and Boas in Germany, and Olinemov and Schekinkoo in Russia had employed polarised light and birefringence in sodium chloride to study plastic deformation, but this was done before the acceptance of the idea of dislocations.

The photo-elastic pattern shown in Plate (16) is of a fully annealed crystal which has been plastically extended, and the load removed. The two dark lines parallel to the length of the specimen are the neutral lines of zero longitudinal stress. The extinction angle is nearly the same at all points of any one specimen, as the path differences are less than a quarter of a wavelength. The neutral lines are clearly visible in a circular polariscope.

The sign of the birefringence effect is such that the outer parts of the bar are in compression while the inner core is in tension. So during plastic extension the outer layers have plastically deformed more than the inner core, as when the load is removed the outer part is thrown into compression. This leads to the assumption that more dislocation sources are active at,

or near, the surface than in the interior.

A similar specimen was bent elastically by applying equal and opposite couples to the ends so that the upper surface was convex. The normal linear variation of stress is shown in Plate (18a) and the birefringence disappeared when the couples were removed.

When the bar is bent into the plastic range the pattern obtained is shown in Plate (18d) and the distribution of birefringence and stress shown in Plate (18e). The change in pattern when going from elastic to plastic deformation is shown in Plate (18c). The length of the transition region is rather less than the width of the specimen.

If, after plastic bending the couples are removed, the pattern changes to Plate (17a) and the corresponding stress distribution to Plate (17b). This shows three neutral planes. The sign of the residual stress in these bending experiments indicate that more plastic deformation has taken place near the surface than in the interior.

In the partially plastic bar, equilibrium considerations show that the maximum stress σ_m in the elastic part must be $\frac{3}{2}$ times the uniform stress in the plastic part. Nye and his collaborators also concluded that slip starts from the surface and works inwards. This is not in agreement with Gilman and Johnston's results for lithium fluoride.

5.4 (a) THERMAL ETCHING.

Thermal etching techniques can be employed to reveal dislocations in many metals and alloys. At high temperatures atomic movements take place to establish a mechanical balance between the dislocation line tension and the surface tension. Pits are thus formed at the points of emergence of dislocations, Frank (1951). Machlin (1957) revealed dislocations in silver using this technique, see Plate (19).

Electropolished silver is immersed in a dynamic flow of argon containing 10 mole % of oxygen at 600 deg. C. for five to ten minutes, and then cooled to room temperature in purified argon. The shape of the depression gives information about the dislocation, Pits are formed at stationary dislocations, and grooves, where dislocations have moved slowly during the etching treatment.

Pits at screw dislocations are several times smaller and shallower than at edge dislocations.

Dislocations that move rapidly during treatment cannot be detected, apart from the vacated pits. These pits are distinguished by having a flat bottom.

The presence of oxygen during thermal etching reduces the surface tension of the metal, and deeper depressions result. Under suitable conditions an oxide particle will form at the bottom of each depression, clearly marking its position.

5.4 (b) THE APPLICATION OF THERMAL ETCHING.

The thermal etching technique may be applied to most metals

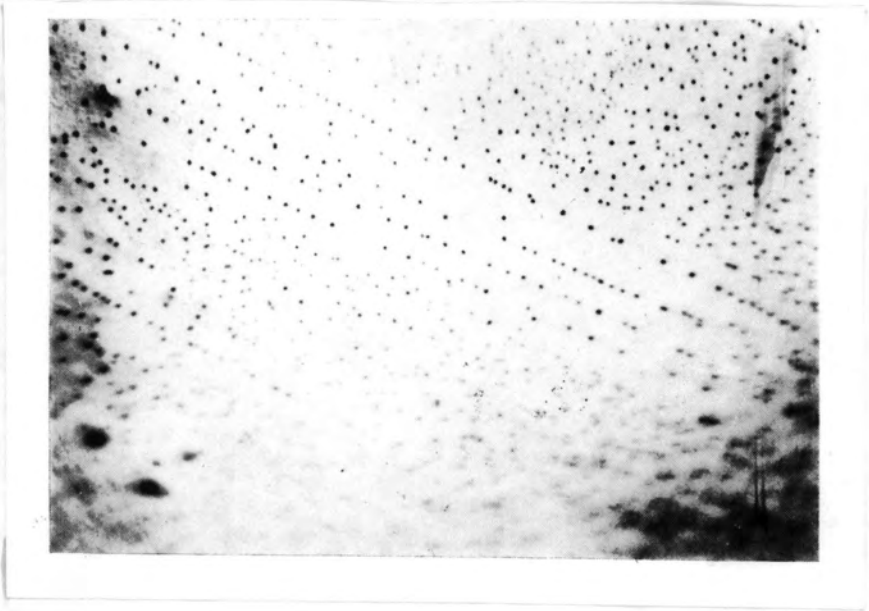

Plate 19. Polygonization revealed by thermal etching of silver single crystal which had been subjected to 3.4% strain at 500 deg. C. Ideal simple glide orientation. Slip direction parallel to paper, normal to rows of pits. (x 650)
(After Machlin, 1957).

Plate 20. A specimen of polycrystalline nickel annealed for 3 hours at 1100 deg. C. under very low pressure. (After J. M. Blakely, unpublished).

and alloys, except for some metals having high vapour pressure at high temperatures, such as zinc, cadmium, magnesium, and their alloys.

The method is particularly useful to study creep at the high temperatures used, see Plate (20).

5.4 (c) CONCLUSIONS.

Chemical etching is effective over a greater temperature range, especially when a reliable reagent has been found for the particular metal.

Gilman and Johnston working with lithium fluoride produced interesting results, especially in connection with dislocation movements, but generalizations from their results appear to be unsound.

Thermal etching is restricted to observations of conditions at higher temperatures, and has been applied successfully to the study of creep in metals.

PART 6.

THE DECORATION OF DISLOCATIONS IN CRYSTALS.

6.1 GENERAL INTRODUCTION.

These methods allow the direct microscopic observation of dislocation lines in transparent crystals. This is made possible by the production of visible patterns along the lines.

Linear imperfections were seen in sodium chloride by Siedentopf in 1905, and reproduced as a series of hand drawn diagrams. Probably the first person to see decorated dislocations in an intentionally deformed and annealed crystal was Rexer, (1931, 1932a, and 1932b) at Halle. About the same time Edner (1932), also at Halle, observed lines in crystals of sodium chloride containing barium chloride. Unfortunately, these observations preceded the development of a theory adequate for their understanding.

The first interpreted observations followed the rapid development of the theory of dislocations when in 1953 at Bristol, Hedges and Mitchell investigated the nature and distribution of the internal photographic latent image in silver bromide crystals. They found that the substructure of strained crystals of silver bromide, which had been lightly annealed, could be made visible by exposing them at room temperature to light with a wavelength close to that of the absorbtion edge.

The networks and distributions of dislocations were seen due to the silver which separated out along dislocation lines. Their observations agreed with many theoretical predictions. They recognised tilt sub-boundaries formed by arrays of parallel

edge dislocations, see Burgers (1939), and Read and Shockley (1950), and twist boundaries formed by crossed grids of screw dislocations later discussed theoretically by Frank, (1955).

Considerable developments have taken place in methods of decoration, and work at Bristol, Ghent, and the G.E.C. Research Laboratories, Schenectady, will be discussed.

6.2 THE DECORATION OF DISLOCATIONS IN CRYSTALS OF SILVER HALIDES.

6.2 (a) INTRODUCTION.

At Bristol observations were made on silver bromide and silver chloride. The great advantage of methods using silver halides is that the crystals do not have to be annealed at a higher temperature before dislocations are decorated. The dislocations are fixed in position and made visible by exposure to light while the stress is still applied to them.

It is possible using these ionic crystals to observe both the probable behaviour of dislocations on incipient slip bands at a definite stage during plastic deformation, and the arrangements of dislocations in the polygonized crystals which result from the annealing of strained specimens. The results of annealing at various temperatures have been studied, and the deformation structures are modified by annealing.

Either bright or dark field illumination may be used, and dislocations are made visible to a depth of at least 30μ.

6.2 (b) THE PREPARATION OF THE SPECIMENS.

Progress in this field has depended very much on ability to grow large single crystals. Great care is taken in the preparation of the thin sheets of silver halide material for experiment, see Clark and Mitchell (1956).

Metallic silver is very impure compared with recrystallized silver nitrate, and silver oxide must be eliminated as it adheres to glass. Cationic impurities are removed from the silver nitrate by special methods, and careful recrystallization using a temperature gradient. Anionic impurities are removed from the constant boiling point mixtures of the hydrogen halides by chemical methods, and by fractional distillation.

When the oxide has gone, heat is applied. A stream of dry hydrogen halide, in nitrogen as a carrier gas, is passed through the melt for about one hour. Particles of silica on the surface are then removed from the molten silver halide by filtration through fine glass capillaries. If not removed, the silica gives rise to randomly distributed etch pits and fog specks, which have no connection with the decorated dislocation lines. Fractional distillation in high vacuum breaks down silver oxide and silver sulphide and removes volatile impurities such as cuprous and mercury halides, and polyvalent cationic impurities. Traces of cuprous chloride and mercurous chloride are still present and these are removed by vacuum melting.

The molten halide is then run through a vacuum melting stage

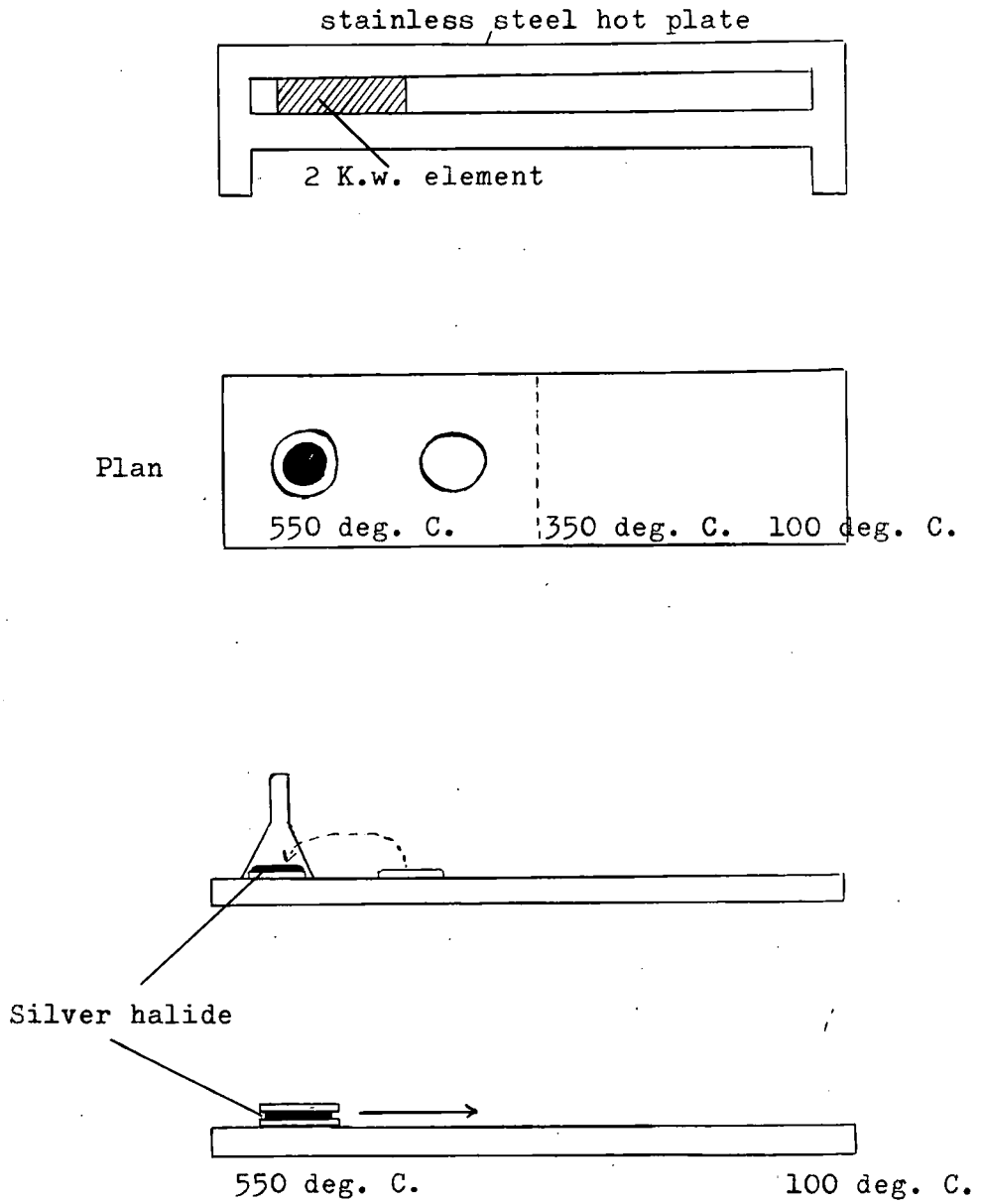

Fig. 43. Conversion of globules into thin sheets.

at 450 to 500 deg. C., and at a pressure of 10^{-6} mm. of mercury, for at least 8 hours. Bromine is admitted to destroy silver nuclei and nitrogen over the silver halide keeps out oxygen. Small globules are transferred onto a plate, and immediately recrystallise.

Silver chloride is easier to purify than silver bromide.

The next stage is to convert the silver halide globules into thin sheets. The globule is placed on glass rods resting on a pyrex disc which in turn rests on a hot plate. It is flamed with an oxy-coal gas torch to burn away unwanted particles. The disc is covered with a funnel to protect it from oxygen as the globule melts, and once melted the funnel is quickly removed, and another pyrex disc placed on the top. The sandwich is then slowly displaced along the hot plate down the temperature gradient until the disc of silver halide crystallizes. On placing the sandwich in distilled water, the plates immediately separate. Care must be taken not to scratch the crystal surface. The thickness of the crystal is determined by the spacing of the glass discs. The crystal is then placed on a pyrex plate and cut into sections using a stiff backed razor blade. It cuts quite easily, in a very similar manner to lead. The crystals are heavily strained when cooling, the halide having a coeffieient of expansion much higher than that of pyrex.

The crystal surfaces are always close to (100) planes. To grow (111) orientation crystals a glass wedge is used, see Fig. (44).

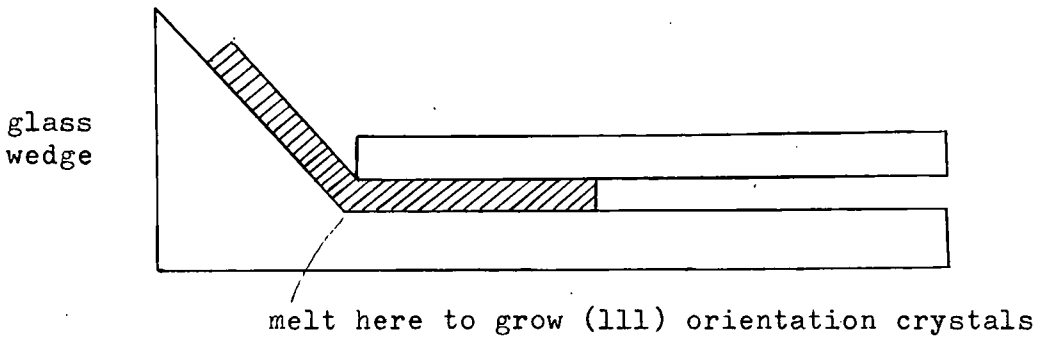

Fig. 44. The arrangement to grow (111) orientation crystals.

Finally the crystal is annealed in an atmosphere of halogen at temperatures between 200 and 400 deg. C. for periods up to twelve hours.

A 4% solution of potassium cyanide is used to dissolve away the surface of the crystal, removing the surface which was in contact with the glass plate and leaving a smooth crystal surface, showing no facets. The crystals may then be exposed to produce photolytic silver, or exposed and developed.

6.2 (c) THE DECORATION OF THE DISLOCATIONS.

The surfaces of crystals may be exposed while covered with a thin film of a halogen acceptor. This is usually formed between the crystal surface and a microscopic cover glass. With acceptors such as 1 phenyl - 3 - pyrazolidinone, discrete specks of silver are produced at the points of emergence of dislocations through the surfaces of the crystals. This method makes possible good resolution at high magnification, and is particularly useful for studying the properties of closely spaced dislocations.

The fishnet structure and distributions of dislocations may be revealed to a depth of about 30 μ in strained and lightly annealed crystals of silver bromide and silver chloride by exposing them to light with a wavelength in the longwave edge of the absorbtion band of the crystal. Silver separates out along the dislocation lines, and it may be observed with bright or dark field illumination. See Plates (21) and (22).

A combination of the above two methods is very useful, but

(*a*)

(*b*)

(*a*) Tilt subboundary with the axis of tilt inclined at an angle to the surface of the crystal. The crystal was exposed under a dilute solution of phenyl pyrazolidinone and the points of emergence of the dislocations through the surface have been made visible by the separation of specks of silver. (*b*) Same field as (*a*), but 20 μ below the surface.

Plate 21. (After Mitchell, 1957).

Three grain boundaries intersect in the left-hand part of the field. The upper grain shows a series of tilt subboundaries with the axis of tilt nearly parallel to the surface of the specimen. The lower grain has a three-dimensional network of dislocations

Plate 22. (After Mitchell, 1957).

the former does often give a greater surface density of dislocations than would be indicated by the internal separation of silver. Doubt is therefore cast on the ability of the latter method to decorate all dislocations.

It has not been possible to make the dislocations in large single crystals of the purest silver bromide visible by the separation of photolytic silver in a reliable way. Unless the crystal is plastically deformed very little silver separates in them during exposure. Etching methods on these large single crystals have also been unreliable.

As it is impossible to detect any difference in hardness and other plastic properties between the large and the thin crystals of silver bromide, it must be assumed that mobile dislocations are present in both types of crystal, and that those in the thin crystals have modified properties which permit their decoration with colloidal silver, but which, in the purest crystals do not impede their displacement during plastic deformation.

More recently Jones and Mitchell (1957) described methods which show a correspondence between etch pits and the points of emergence of dislocations which have been decorated by the separation of silver along the lines. The silver chloride, silver chloro-bromide, and silver bromide sheets are grown from the melt by the method described by Clark and Mitchell (1956).

The crystals are deformed by elongation and indentation with hemispherical glass indentors, and then etched and exposed to

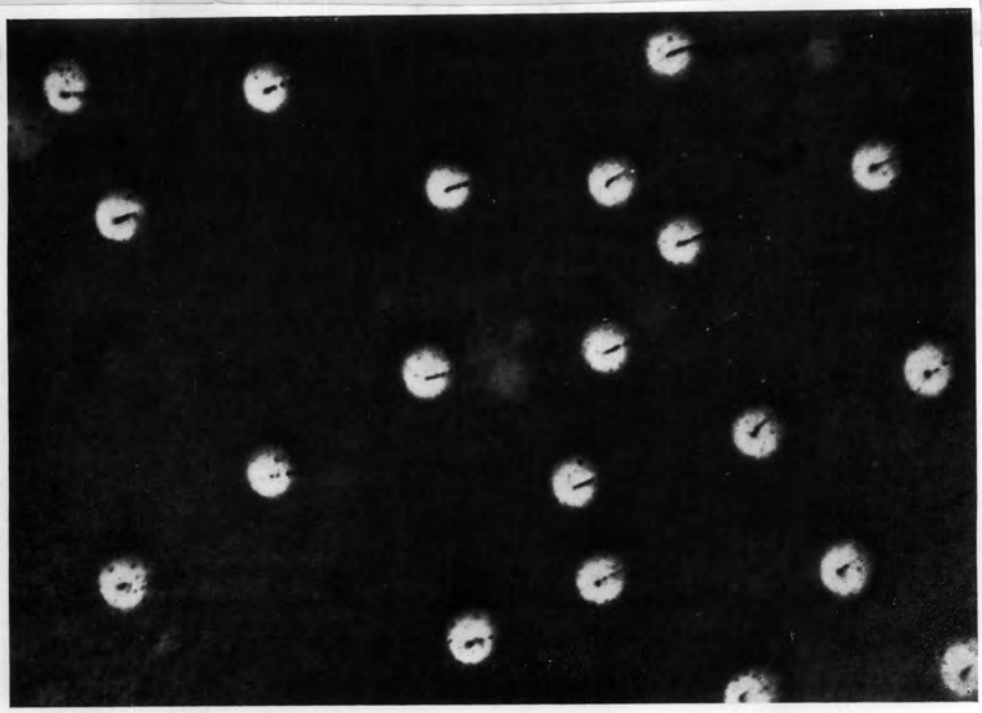

Dislocations forming elements of a coarse three dimensional network (see Hedges and Mitchell 1953, fig. 3) made visible in a crystal of silver chloride both by etching and by the internal separation of silver resulting from the subsequent exposure to light. This establishes the correspondence between etch pits and dislocation lines. (×2500)

Plate 23. (After Jones and Mitchell, 1957).

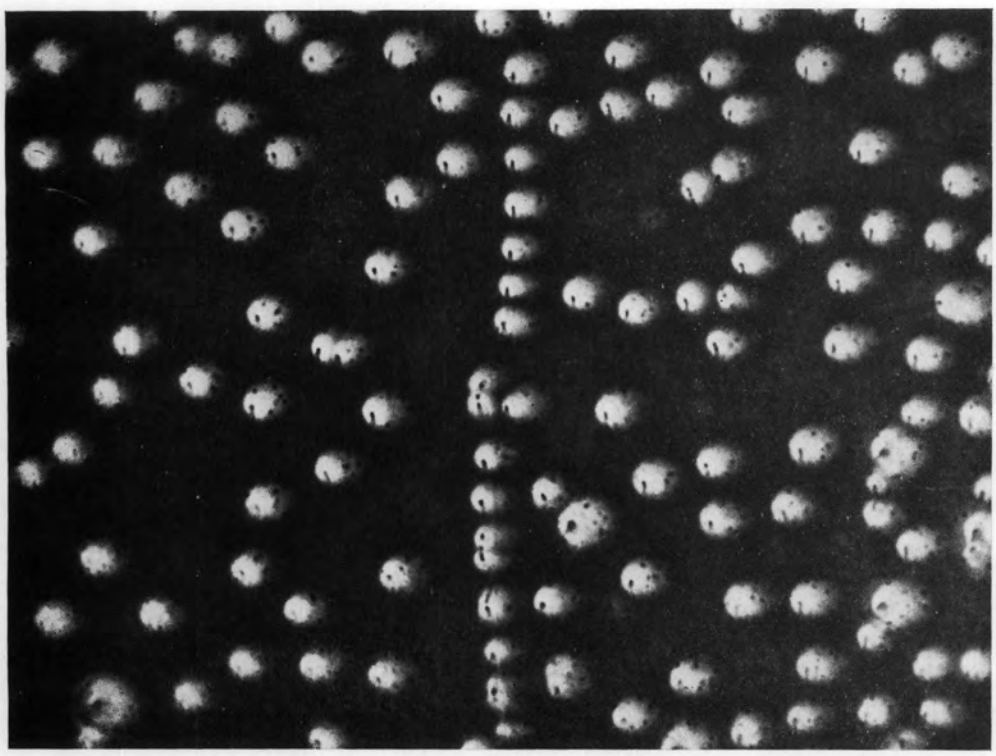

A wall of dislocations in an annealed crystal of silver chloride. (×2500)

Plate 24. (After Jones and Mitchell, 1957).

reveal the dislocations. A 3 to 5 N solution of sodium thiosulphate is the most reliable etchant. The crystal must be in the etchant for a very short time and is then transferred immediately into water. A solution of 0.1 N sodium thiosulphate is then used to shape the etch pits and develop facets. Silver chloride etches better than silver bromide. The pits formed on the former are smaller in area, but about the same depth. After they have been thoroughly washed and dried, the etched crystals are exposed to the unfiltered radiation from a 250 watt high pressure mercury vapour lamp for 30 seconds at a distance of about 30 cm. from the lamp. Silver separates to a depth of about 40μ. Below this depth recombination takes place. See Plates (23,24).

The correspondence between the two methods appears to depend upon the properties of individual crystals. It is complete in many crystals but absent in others. The dislocations which appear during plastic deformation at room temperature give smaller etch pits and print out to a smaller extent than those which are already in annealed specimens. To show this a specimen is etched, deformed with a hemispherical indentor, and then re-etched.

The most sensitive conditions for the study of the behaviour of dislocations during the deformation of silver chloride occur when the crystals have surfaces almost parallel to (001) planes. The apparently small numbers of grown-in dislocations in such crystals are made just visible by etching. The small shallow pits corresponding with dislocations on slip bands produced by

deformation can easily be resolved using the phase-contrast microscope.

Jones and Mitchell found their experiments indicated that the dislocations in annealed crystals which give rise to deep etch pits, and along which visible amounts of silver separate rapidly during exposure, do not play an important role during the early stages of plastic deformation. Their mobility is affected by the segregation of impurities, or of vacancies, but it has been shown that dislocations appear within the elements of the sub-structures as in the experiments of Gilman and Johnston on lithium fluoride.

The great advantage of the method of decoration of dislocations in silver halides with photolytic silver is that it does not depend on the introduction of foreign substances, or upon thermal treatments at elevated temperatures. The dislocation formations are likely to be modified to a smaller extent by this process than those in the alkali halide crystals discussed later. The decoration is almost continuous, and discrete particles of photolytic silver cannot usually be resolved.

An important disadvantage is that it is never possible to decorate dislocations at a depth greater than 40μ below the surface.

6.2 (d) THE NATURE AND FORMATION OF THE PHOTOGRAPHIC LATENT IMAGE.

Mitchell and Mott (1957) outlined the mechanism by which the latent image is formed in the following steps:

1. The formation of the 'pre-image speck'. This is a silver 'atom' probably adsorbed at a kink site terminated by a silver ion. It is formed by the co-operation of one electron and one interstitial silver ion. The pre-image speck has a life time of 1 to 10^{-5} seconds.

2. The formation of the 'sub-image'; a neutral pair of silver atoms adsorbed at a kink site. This involves the utilization of a second photoelectron and a second interstitial silver ion. The sub-image has a life time of days and can be developed.

3. The formation of the stable latent image. This utilizes a further electron and two interstitial silver ions, and gives in equilibrium a positively charged group of four silver atoms Ag_4+. This is the minimum stable image, and from this point onwards any further growth of the silver speck will be by the Gurney and Mott mechanism (1939).

Silver bromide was known to be a photoconductor at the temperature of liquid air, and it was assumed to be so at room temperature, so that each quantum of light absorbed released one electron and a positive hole. If sufficiently mobile, the electron will easily be trapped by colloidal silver or by sensitivity specks. This would then be neutralized by the movement to the speck of interstitial silver ions, so causing the silver particle to grow. It is considered that as silver in in contact with silver halides carries a positive charge, this may be regarded as attracting photoelectrons rather than a

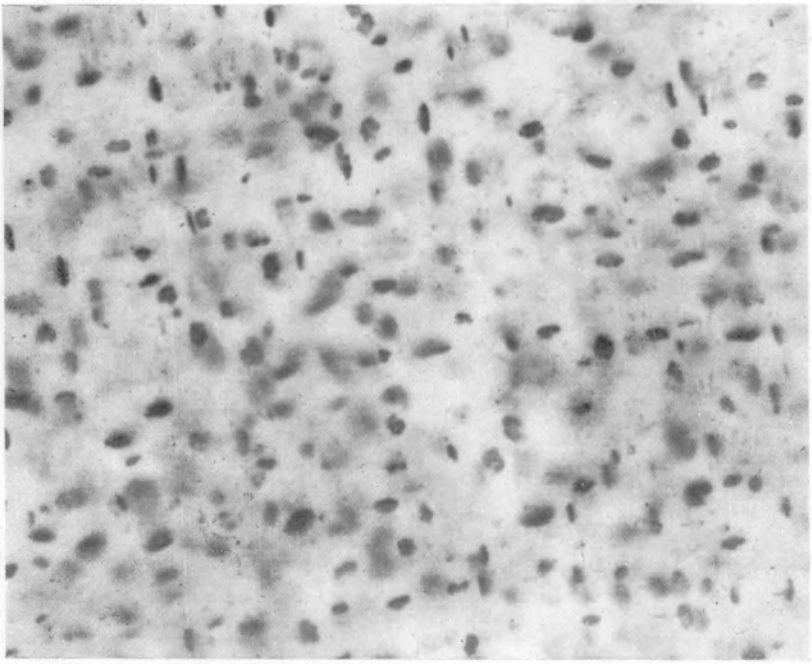

Platelets of gold produced by exposing and heating a silver chloride crystal containing 0·05 mol% aurous chloride. (×875.)

Plate 25. (After Bartlett and Mitchell, 1958).

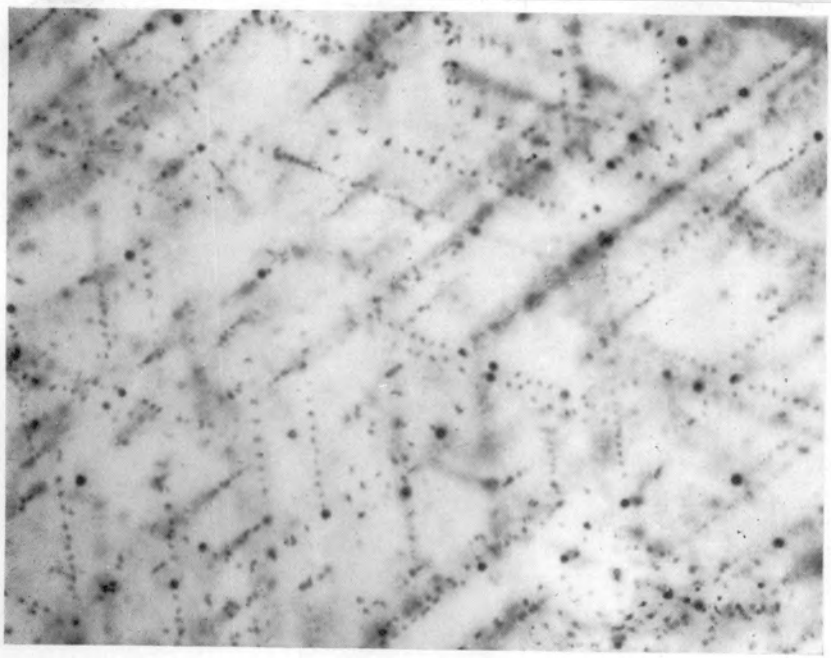

Particles of gold with associated systems of decorated prismatic dislocations in a silver chloride crystal. The photomicrograph is taken in a (111) plane. (×875.)

Plate 26. (After Bartlett and Mitchell, 1958).

negatively charged speck attracting interstitial cations as is suggested by the Gurney-Mott model. Positive holes cannot move to positively charged silver specks in equilibrium with silver halide, and this explains why stable centres do not act as centres of recombination of electrons and holes, as surface traps and dislocations do in germanium.

6.2 (e) THE DECORATION OF DISLOCATIONS IN SILVER CHLORIDE WITH GOLD.

It is possible to decorate silver chloride crystals to a much greater depth if platelets of gold are used, Bartlett and Mitchell (1958). See Plates (25) and (26).

Sheet crystals of thickness 200 to 400μ are sensitized by heating them together with gold wire and cupric chloride in an atomosphere of chlorine in sealed tubes at 350 deg. C. for eight to twelve hours. After straining and exposure to light from a mercury vapour lamp, the crystals are heated for a few minutes at a temperature between 140 and 160 deg. C. Nuclei of gold are produced along dislocation lines and during the final heating, grow in size until they are visible in the microscope. The dislocations are decorated throughout the volume of the crystals.

6.2 (f) THE MECHANISM OF DECORATION USING GOLD.

When crystals of silver chloride are cooled, the Schottky defects present at temperatures near the melting point aggregate to form small dislocation loops and internal cavities. Nuclei consisting of groups of silver and gold atoms are formed on the

surfaces of internal cavities, and along dislocation lines when the crystals are exposed to light, with a wavelength beyond the absorbtion edge of silver chloride. The nuclei absorb gold or silver ions and become positively charged when they exceed a certain size, the compensating negative charge being provided by vacant silver ion lattice sites. When the crystals are heated to a temperature between 140 and 160 deg. C. electrons are transferred from the full band, producing positive holes, to the low lying acceptor levels in the forbidden band associated with the positively charged nuclei. Their positive charge is restored by the adsorption of further cations and further vacant silver ion lattice sites are created. The positive holes and vacant silver ion lattice sites diffuse to the surface of the crystals where chlorine escapes. Copper chloride assists in the transfer and liberation of chlorine molecules from the surface during the heat treatment, see Mitchell (1957). The decoration consists of systems of regularly spaced fine precipitates extending along the [110] directions passing through the central particles.

Although it is impossible to resolve the structure of these fine precipitates, there is a close analogy between these systems and the systems of positive prismatic dislocations which form during cooling around glass spheres imbedded in the silver chloride crystals as described by Jones and Mitchell (1958).

6.2 (g) THE PRODUCTION AND DECORATION OF PRISMATIC DISLOCATIONS.

Prismatic dislocations had been predicted by theory. Seitz

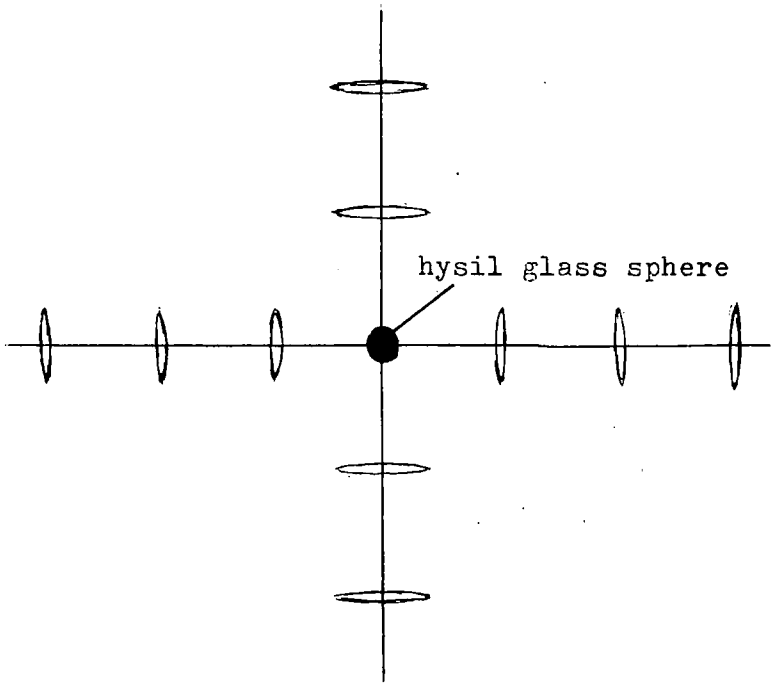

Fig. 45. Prismatic dislocations around a hysil glass sphere (looking along the 100 axis).

Fig. 46. Disc of atoms giving prismatic dislocation.

(1950) first proposed the mechanism of prismatic punching and prismatic dislocations in thallous halide crystals. Nye (1949) established that silver chloride deforms by pencil glide with a [110] slip vector, so that prismatic punching is a possible mode of deformation.

Jones and Mitchell (1958) used silver chloride crystals with (100) planes parallel to the surface. The crystals were annealed so as to be free from dislocations. Hysil glass spheres, diameter about 3μ, introduced into a globule of silver chloride were found to remain fairly close to the surface. The coefficient of cubical expansion of hysil glass is 34×10^{-7} whereas that for the silver halide is 340×10^{-7} per degree C. If there is a state of equilibrium at 454 deg. C., cooling introduces compressive strains around the spheres. This strain is relaxed by discs of atoms being displaced along the [110] directions, see Figs. (45) and (46). These circular loops of edge dislocations are prismatic dislocations.

Harvey and Mitchell (1958) have observed systems of prismatic dislocations formed in the same way during the cooling of crystals of sodium chloride containing aurous chloride. Specks of gold provide the central particles. The positive nature of the prismatic dislocations has been established by observing the inclinations in known stress fields, see Jones and Mitchell (1958).

Parasuis and Mitchell (1959) have also observed systems of prismatic dislocations extending along all twelve [110] directions radiating from particles of photolytic silver formed during the

exposure of crystals of silver chloride containing 0.1 mol. % of cuprous chloride. They have concluded that the space for the separation of silver is made available at the interface between a silver particle and the silver halide by the formation of positive prismatic dislocations, which glide away from the interface along slip cylinders with the twelve [110] directions as axes.

These groups of independent observations provide evidence for a previously unrecognised phenomenon in precipitation reactions in the solid state. It is believed that the formation of prismatic dislocations may prove of importance for the understanding of precipitation hardening. Bartlett and Mitchell (1958) observed that the systems of closely spaced prismatic dislocations, which result from mutual interactions when there is a high density of precipitate particles, present an effective barrier to the glide motion of dislocations. The strain associated with a particle of a precipitate has been observed to be transmitted to distances many times the radius of the particle by the mutual repulsion of the prismatic dislocations.

6.3 THE DECORATION OF DISLOCATIONS IN ALKALI HALIDES.

6.3 (a) INTRODUCTION.

Amelinckx (1956) used additive coloration by means of sodium metal to decorate dislocations in transparent sodium chloride crystals. This is a modification of the method used by Rexer (1932).

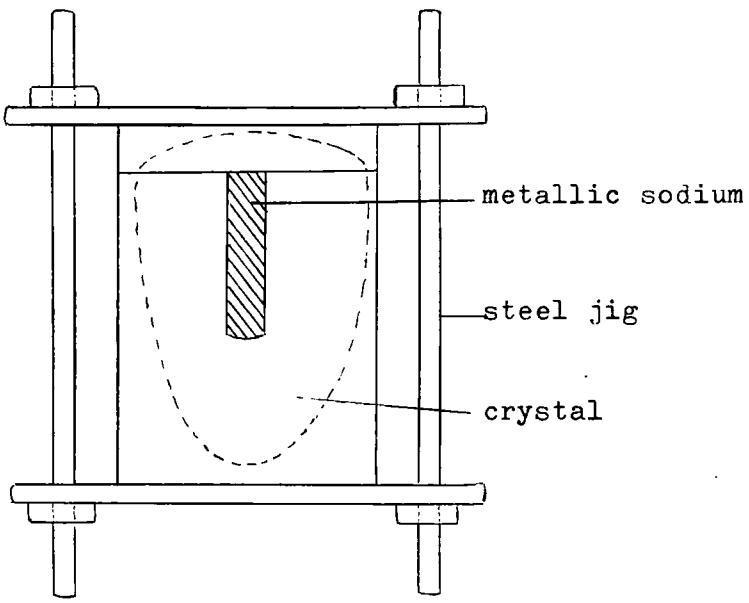

Fig. 47. Specimen in holder.

Work by Van der Vorst, Dekeyser, and Bontinck will also be discussed.

6.3 (b) THE METHODS OF DECORATION.

Amelinckx enclosed a stock of metallic sodium in a cavity made in the crystal. The cavity was closed in the initially cleaved-off part to ensure an exact fit and maximum tightness. The crystal was held firmly in a steel jig, see Fig. (47). It was then heated to about 750 deg. C. until a coloured diffusion zone developed. When using 'pure' sodium chloride the crystal was cooled to room temperature in about 15 minutes to obtain decoration by means of colloidal particles. The crystals were blue in transmission, the decoration being best near to the sodium stock. When crystals which contain a small amount (0.01 - 0.001%) of silver are used, the cooling can be at a much slower rate. In this case the colour of the diffusion zone can vary from yellow to ruby red.

A method by Van der Vorst and Dekeyser (1956) uses sodium chloride heavily doped in silver chloride (1% to 3% addition to the melt), and annealed in a stream of hydrogen at a temperature between 600 and 700 deg. C. for about twelve hours. This gives decoration immediately under the surface, the depth of the region decorated depending upon the annealing time. Annealing in sodium vapour also gives decoration in such heavily doped crystals.

It is probable that these methods apply to all the alkali halides. Bontinck and Dekeyser (1956) used the above methods to

decorate dislocation lines in natural and synthetic calcium fluoride.

The formation of visible diffusion zones, and visible specks, depends upon the impurities present. In pure crystals the decoration is shown to be due to the colloidal sodium by observing the crystals dissolving in water. The particles dissolve and hydrogen is given off. When crystals containing silver are used, the needle shaped precipitates are probably metallic silver. They dissolve in nitric acid.

6.3 (c) THE MECHANISM OF DECORATION.

The diffusion of the excess sodium is considered likely to take place as F-centre diffusion. At high temperatures during additive colouring, the sodium vacancies diffuse to the sodium stock and die. The halogen vacancies, not so mobile, stay in the crystal in the neighbourhood of the dislocations. The sodium stock endeavours to send in Cl.-vacancies. Some of these will be converted into F-centres by capturing electrons sent in by the sodium metal every time a sodium vacancy dies, maintaining an equal number of vacancies of both kinds as well as charge equilibrium. Thus, so long as the temperature is high enough to ionize sodium, F-centres are formed at the expense of Cl.-vacancies. At the same time F-centres will die and become halogen vacancies by loss of their electrons, or by going to a dislocation line. At a given pressure of sodium vapour a given concentration of F-centres is in equilibrium. This condition may be frozen in by very

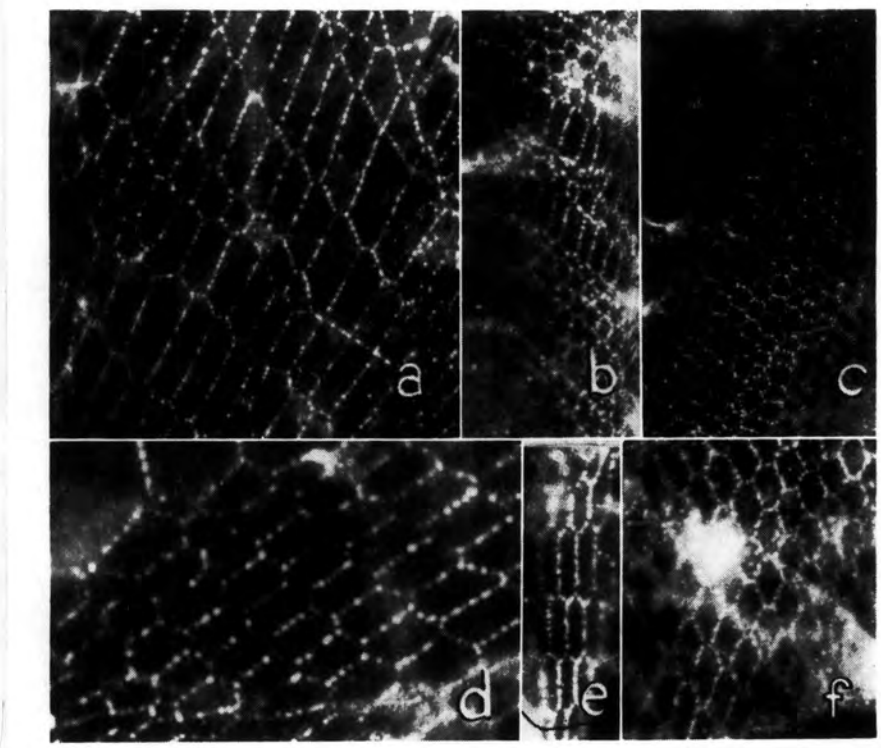

Plate 27. Hexagonal networks exhibiting differently shaped meshes:
(a) x 600 (b) x 700 (c) x 600
(d) x 760 (e) x 550 (f) x 600
(After Amelinckx, 1957).

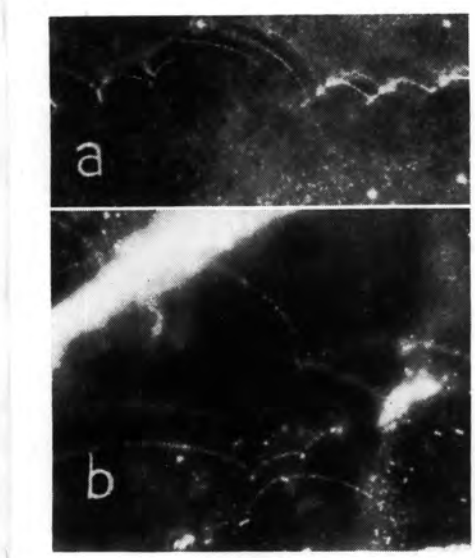

Plate 28. (a) Pinning of dislocations at stationary dislocations of the networks. (x 500)

(b) Pinning of dislocations at precipitates. (x 500)
(After Amelinckx, 1957).

rapid quenching.

The condensation of F-centres and vacancies during cooling, resulting in the formation of a sodium speck on a dislocation line, is due to the attraction of F-centres to dislocations. This supposes that there is a sufficient number of jogs in the dislocation line so that the F-centres and vacancies can always be absorbed. Coulomb and Friedel (1957) have estimated that this is not the case in a rapid quench. It is possible that elastic interaction with vacancies is more pronounced than for F-centres, and the first stage in the precipitation is probably the formation of cavities. Condensation of F-centres at these cavities will make them increase in size, resulting in the formation of sodium specks.

6.3 (d) THE OBSERVATION OF THE DECORATED DISLOCATIONS.

The arrangements of the particles were observed by Amelinckx using ultramicroscopic illumination.

Thin slices cleaved from the treated crystals were used. They were further reduced in thickness to about $\frac{1}{5}$ mm. by dissolving in water. This reduction is necessary, as otherwise, light reflected from particles not in focus reduces the contrast.

The specimen was embedded in a liquid with the same refractive index as sodium chloride to avoid scattering by surface irregularities.

The patterns of specks were photographed at different depths so that the patterns slightly overlapped. The inclination of a

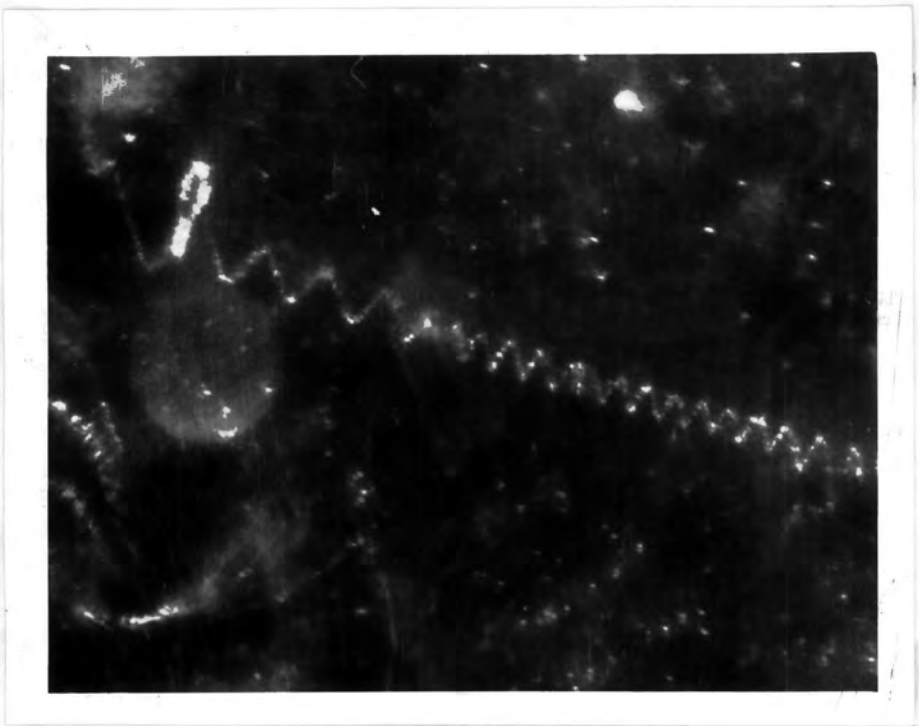

Plate 29. The decoration of dislocations in a synthetic calcium fluoride crystal, showing a helix with variable radius and pitch.
(After Bontinck, 1956).

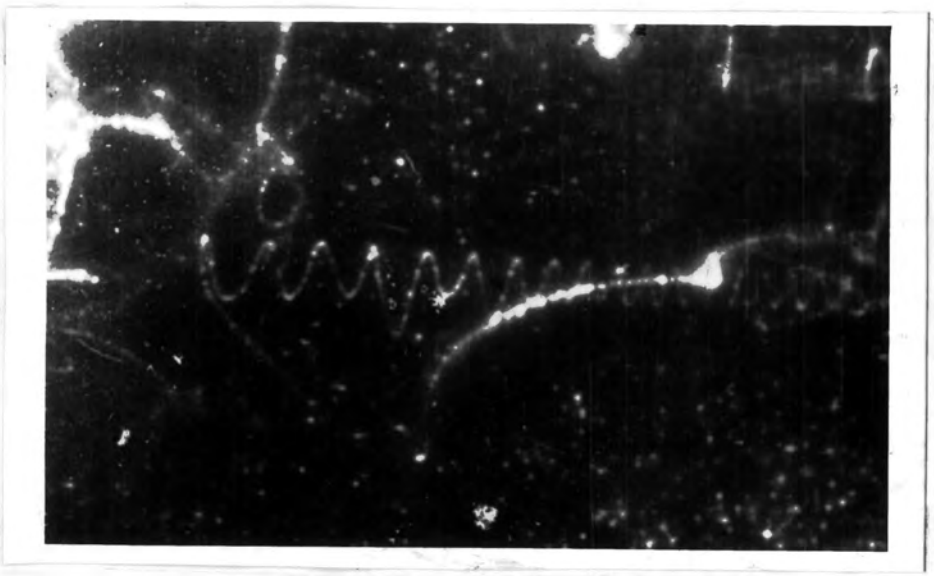

Plate 30. A helix with two windings of a larger radius in a calcium fluoride crystal. A single closed dislocation line can be observed.
(After Bontinck, 1956).

network with regard to the plane of observation, i.e. the (001) cleavage plane, was estimated from the "in focus" width, see Amelinckx (1956). The shapes of the dislocation networks, clearly decorated, agreed with those predicted by theory. All types of dislocation and distribution have been observed, see Plates (27-30).

Relatively high angle boundaries (1 deg. to 2 deg.) are decorated by a thick sheet of particles. The ones studied, revealing this, were those perpendicular to the plane of observation, and they were marked by a ribbon of particles which remained on the same spot no matter where the position of focus was in the crystal. These boundaries were always straight, apart from jogging, and by optical geometry were shown to have mainly tilt character.

Dislocation pinning by precipitates, and the bulging of dislocation lines between pinned points, can be clearly seen.

If the phase-contrast microscope is used with a dark background, the precipitates appear white.

6.3 (e) LUMINESCENCE OF DECORATED DISLOCATIONS.

The luminescence of phosphors is known to be affected by deformation. Van der Vorst and Dekeyser (1956) carried out experiments with single crystals of rock salt, with silver chloride added, to show a relationship between luminescence and dislocations.

When irradiated with X-rays or ultra violet light, emmission bands were produced.

They observed networks similar to those seen by Amelinckx

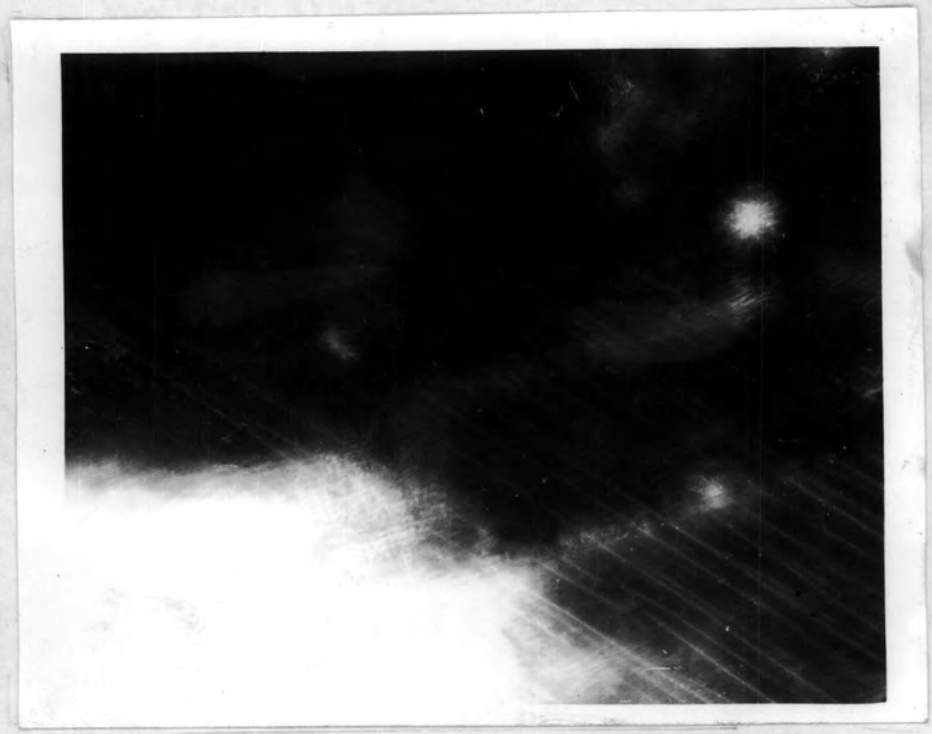

Plate 31. Ultramicroscopic observation of decorated walls of dislocations in a single crystal of rock salt. (After Van der Vorst and Dekeyser, 1956).

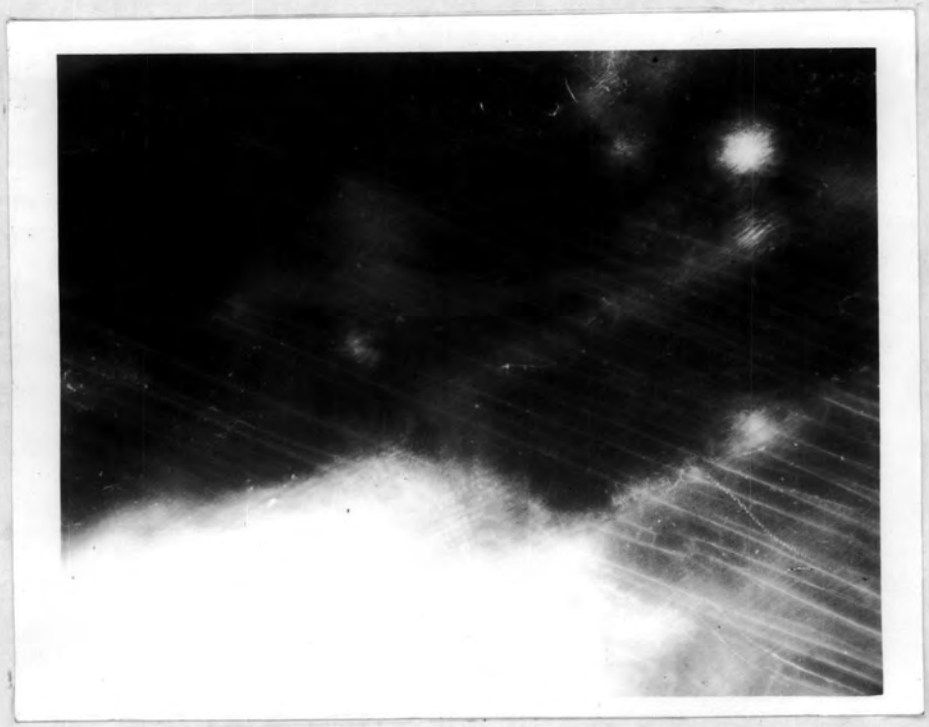

Plate 32. Luminescence photograph of the dislocation walls shown in Plate 31.
(After Van der Vorst and Dekeyser, 1956).

(1956) in additively coloured rocksalt.

The samples were deformed, annealed in air at various temperatures ranging from 300 deg. C. to 700 deg. C., and after cooling reannealed in hydrogen. A thin metallic layer covered the surface of the crystals, and this layer was found to increase with time and temperature. The decoration was by specks of colloidal silver, and only took place close to the surface. The inside of the crystal remained optically empty.

When the crystal was irradiated with X-rays, the decorated lines were seen as brighter lines in a blue haze. By means of long exposure times of twelve to twenty four hours, it was possible to photograph dislocation walls, see Plate (32). The above method has advantages over the Rexer method; it is easier to use and can be applied to smaller specimens, and at lower temperatures.

6.3 (f) CONSIDERATION OF THE VALUE OF OBSERVATIONS.

The patterns observed are remarkably clear and of great value in establishing the configurations possible, but from the point of view of studying the results of strain, there are serious limitations. All methods entail heating to temperatures above 600 deg. C., and at these temperatures dislocations can climb and move quickly. If the decoration process requires participation of the Schottky disorder, then decoration and climb are inseperable. It is possible to illustrate quench hardening very successfully. It would be interesting to know how much of the dislocation structure could be attributed to the presence of the excess sodium.

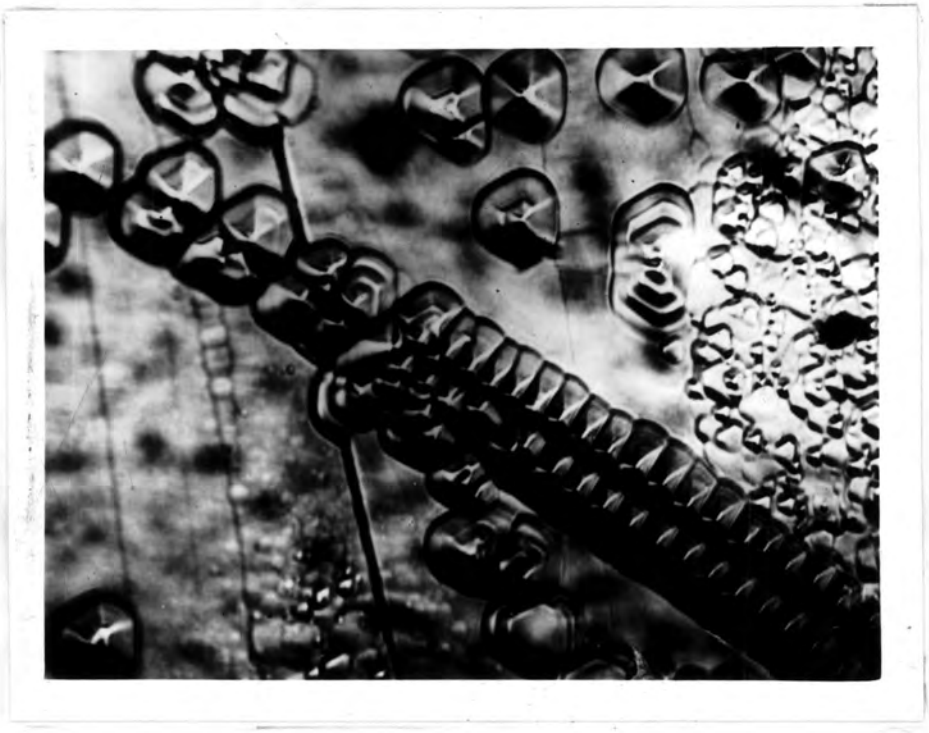

Plate 33. A calcium fluoride crystal, annealed at a high temperature, cleaved and etched. Concentrated sulphuric acid was the etchant. The double rows of etch pits parallel to the [110] direction indicate emergence points of a helical dislocation.
(After Bontinck, 1956).

In lithium fluoride the dislocation density has been found by Johnston (1957) to be considerably increased by addition of excess lithium, and the presence of large precipitates produces prismatic dislocations. The cooling down and precipitation causes stresses, so that the networks are not necessarily in equilibrium.

Photographs taken of dislocations in sodium chloride must be taken soon after decoration as the surface of these crystals is affected by condensation. Replicas of the surfaces can of course be made, if it is desirable to study surface features. Plate (33) shows the surface of an etched calcium fluoride crystal.

6.4 THE OBSERVATION OF DISLOCATIONS IN SILICON.

6.4 (a) INTRODUCTION.

The properties of silicon are ideally suited for a study of dislocations introduced by plastic deformation. Crystals of high purity and perfection can be readily grown, and dislocations in silicon may be revealed by etch pits, or by copper decoration, or a combination of the two. Dash (1956, 1957) decorated dislocations in silicon using the latter method.

6.4 (b) PREPARATION OF THE SPECIMENS.

Single crystals were grown by drawing from the melt contained in a quartz crucible. The density of dislocations in these crystals varies from $10/cm.^2$ to $10^4/cm.^2$

Bars with area of cross section about 10 $mm.^2$ were slightly deformed by twisting about a [111] axis or by bending. They were then etched in a mixture of nitric, hydrofluoric, and acetic acids

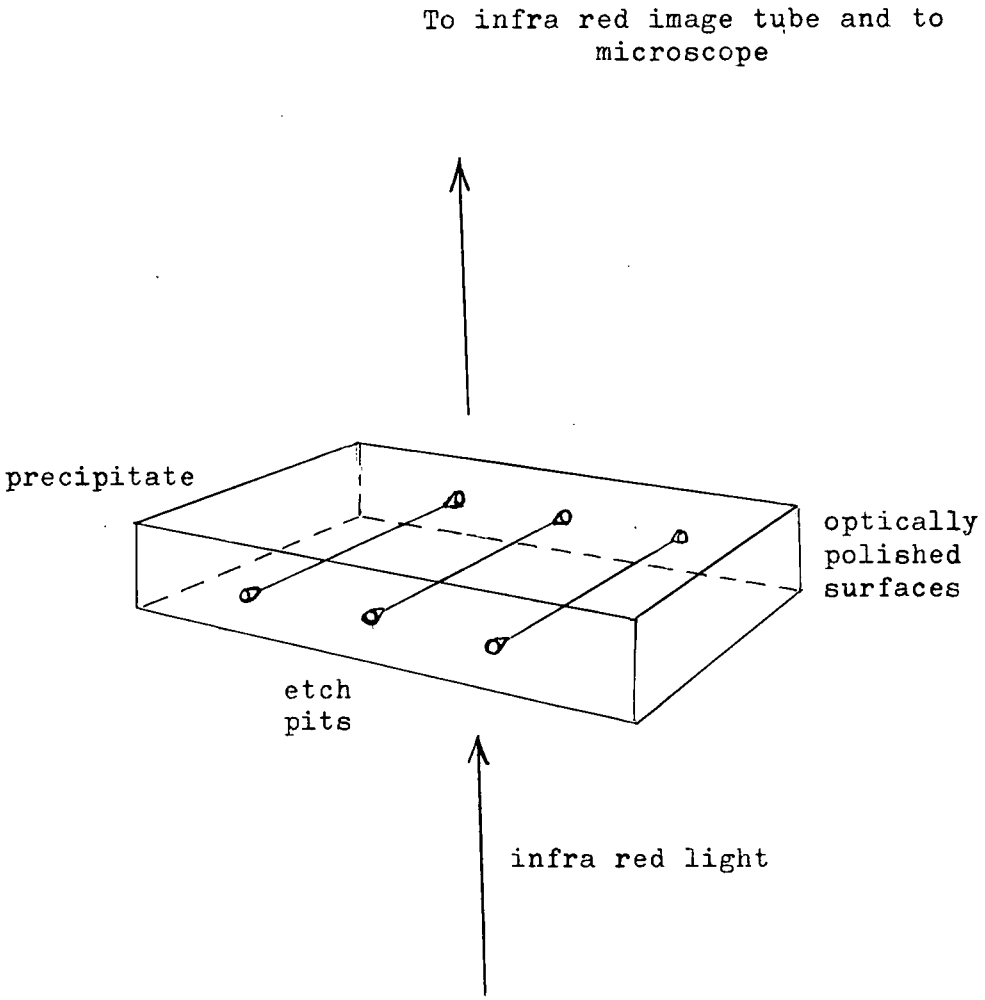

Fig. 48. Arrangement to observe decorated dislocations in silicon.

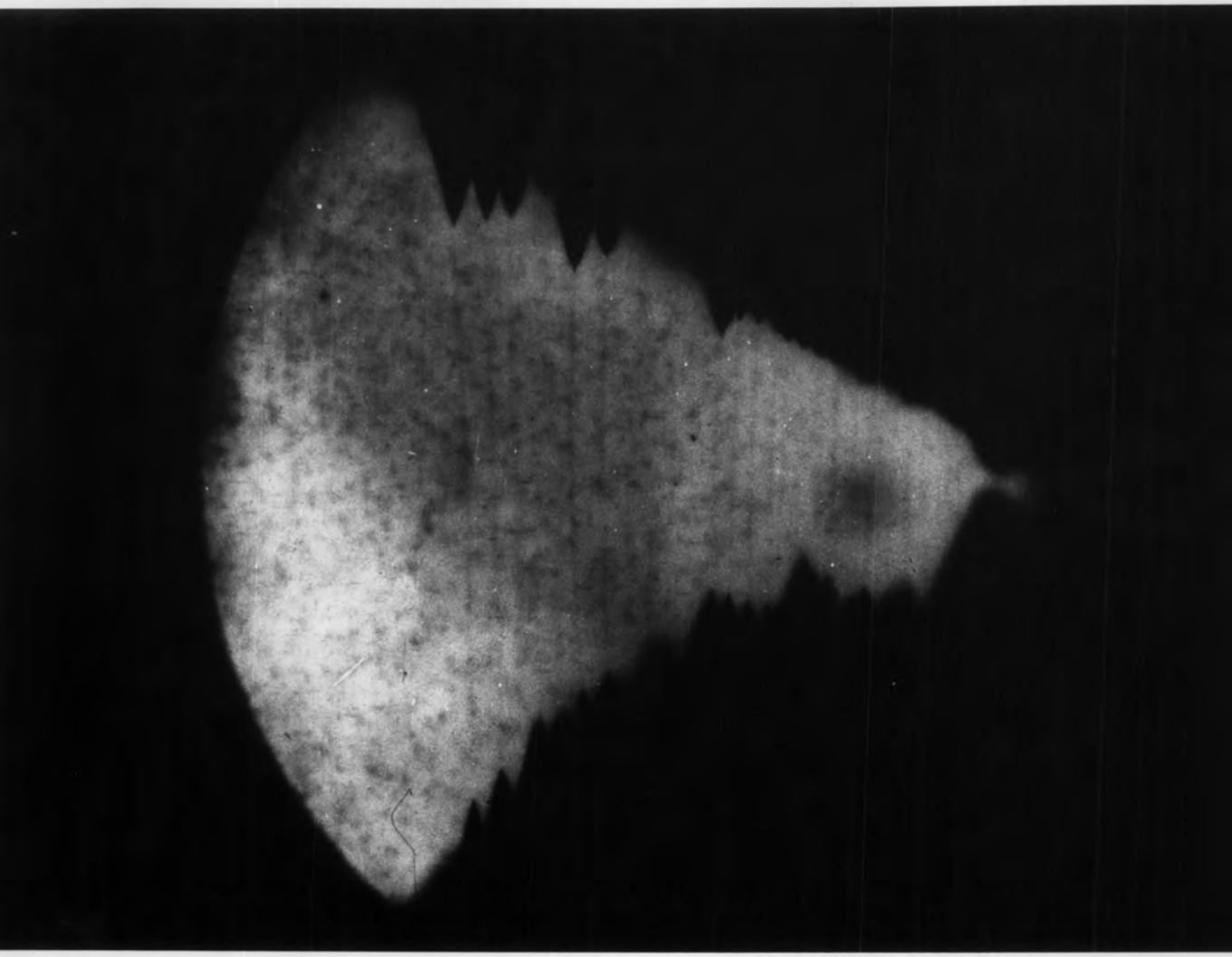

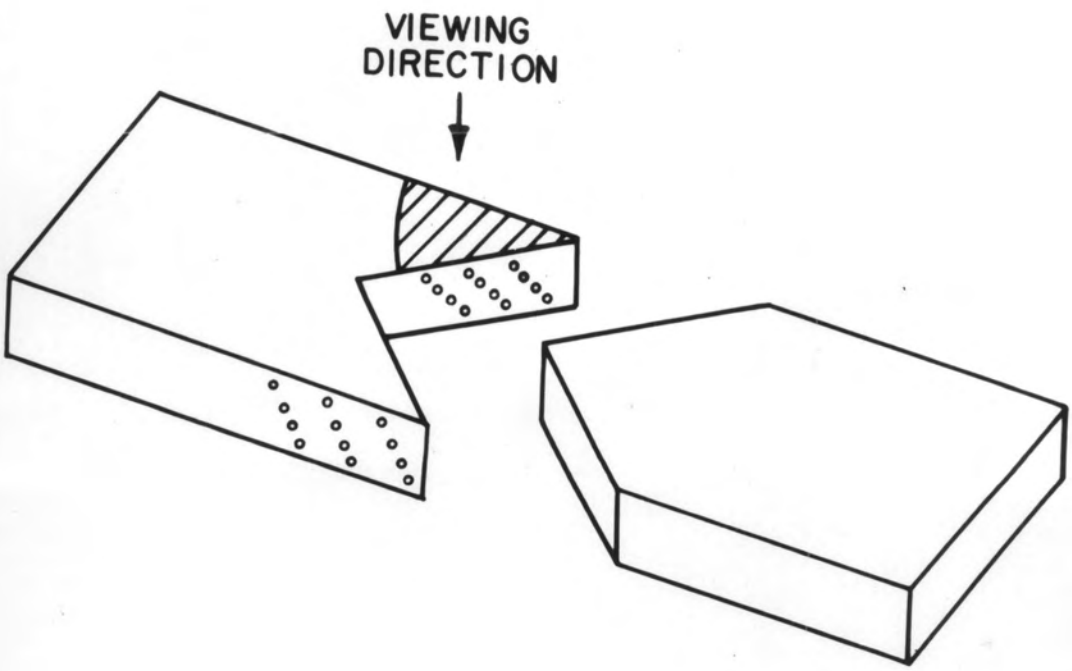
VIEWING
DIRECTION

Plate 34a and b. Decorated dislocations joining etch pits on opposite sides of a wedge-shaped specimen.
(After Dash, 1957).

producing deep etch pits. The bars were cut into 1 mm. thick slices parallel to (111) planes, and the cut surfaces optically polished. A drop of copper nitrate solution with about 10^{-7} to 10^{-6} atom fraction of copper was dried on the edge of each slice. They were then heated to about 900 deg. C. for thirty minutes, and then cooled rapidly to room temperature.

6.4 (c) TECHNIQUE OF OBSERVATION.

Dash examined infra-red light transmitted by the specimens using an infra-red image tube in the position of the eyepiece in the Leitz Panphot microscope. This enabled the precipitates formed to be directly observed, and photographs to be taken with infra-red sensitive plates. His experimental arrangement is shown in Fig. (48).

6.4 (d) OBSERVATION OF THE DECORATED DISLOCATIONS.

Deep etch pits were seen joined by dislocations decorated clearly with copper. Plate (34a) shows a wedge shaped portion of the bar bent about the [001] axis and viewed along the axis of bending. The dislocations are generally straight lines in the [110] directions.

In Plate (35a) the viewing direction is [111] and the bar deformed by twisting. A series of dislocation half loops is seen, all parts lying in [110] directions. The sections approximately parallel to the edge of the sample are screws, the inclined sections are composite edge and screw. Plate(35b) shows the pits as they appear on the (112) surface.

There is a wide variation in decoration from sample to sample, and in the relative amounts of decoration on the screws and composites. This is in the form of precipitate particles. Sometimes the screws are not decorated at all. The form of the precipitate is found to depend upon the initial concentration of copper on the surface, and the cooling rate. Rapid cooling of samples saturated with copper results in uniform decoration. Slow cooling of samples with 10^{-7} to 10^{-6} atom fraction of copper results in preferential precipitation on the composites. Also, patchy decoration is sometimes observed without apparent reason.

As was the case with experiments on sodium chloride, the heat treatment required to decorate the dislocations can be expected to modify the dislocation arrangement.

To avoid such modification, Dash (1958) used an etching method. He cut the specimen exposing a surface parallel to a (111) plane. After chemically polishing the surface with a solution of one part hydrofluoric acid and three parts nitric acid, it was etched three to four minutes in a solution consisting of one part hydrofluoric, three parts nitric, and six parts glacial acetic acid.

The etch patterns produced consist of pits and channels in the surface, which join pits. The channels are due to preferential etching of cores of dislocations which are almost parallel to the surface, and along [110] directions. On high magnification, trails behind moving dislocations are seen to

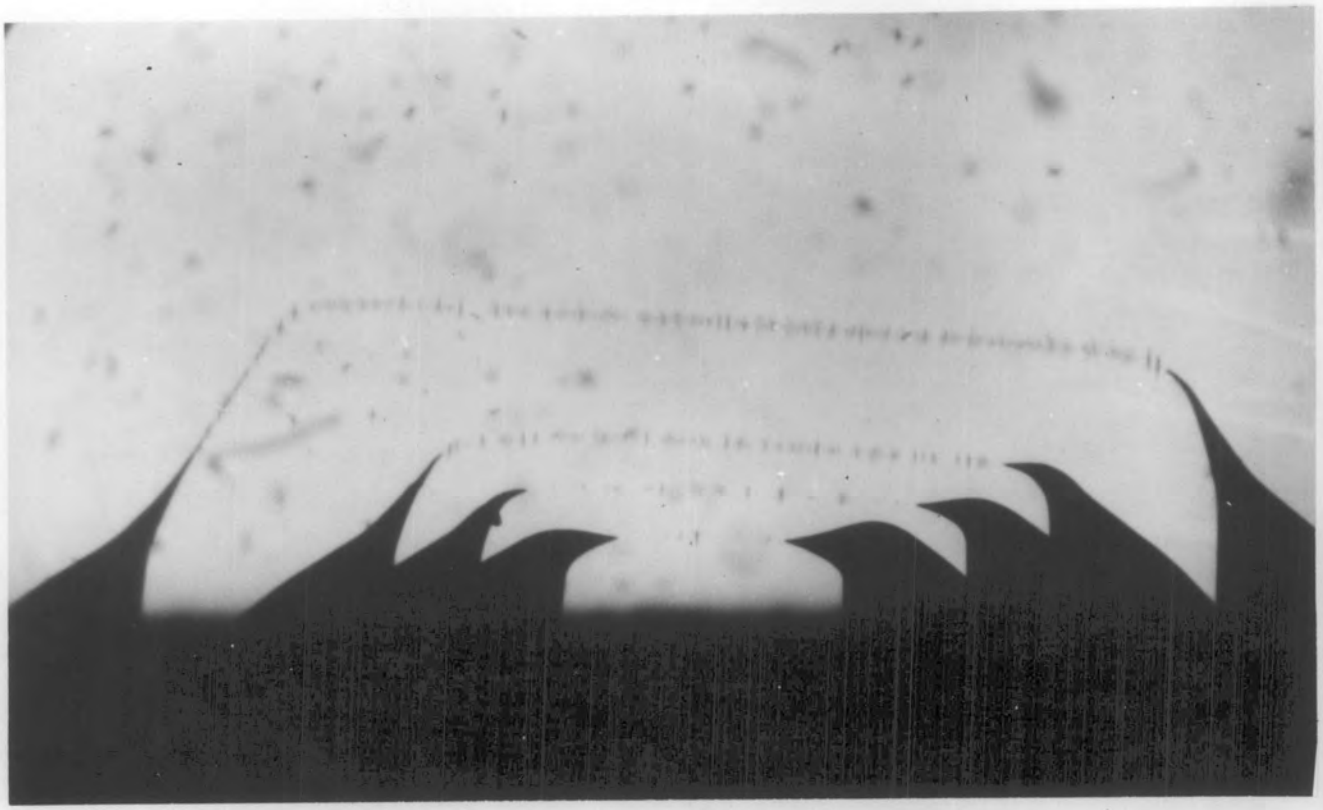

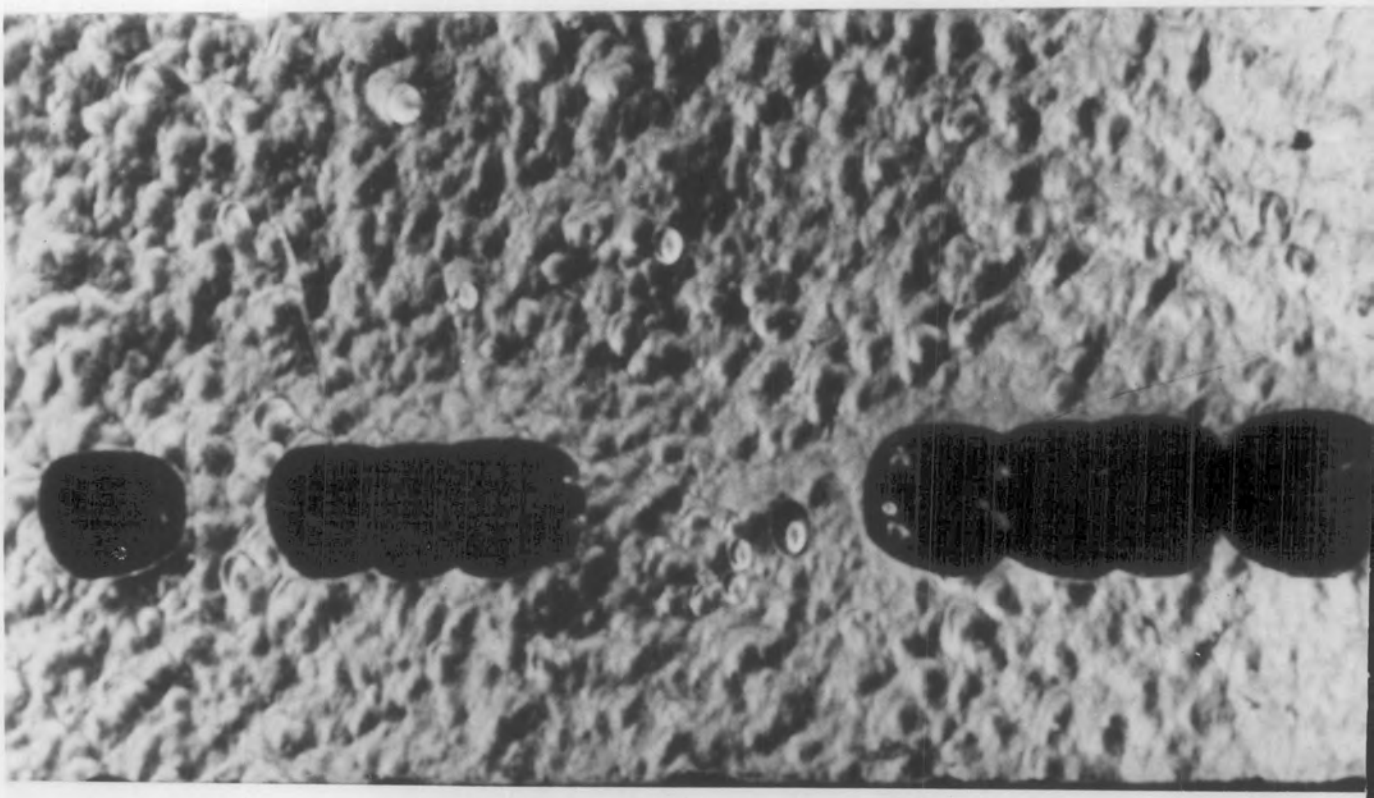

Plate 35a Etch pits and dislocation loops entering from a (112) surface of a silicon crystal.
b Pits at the (112) surface.
(After Dash, 1957).

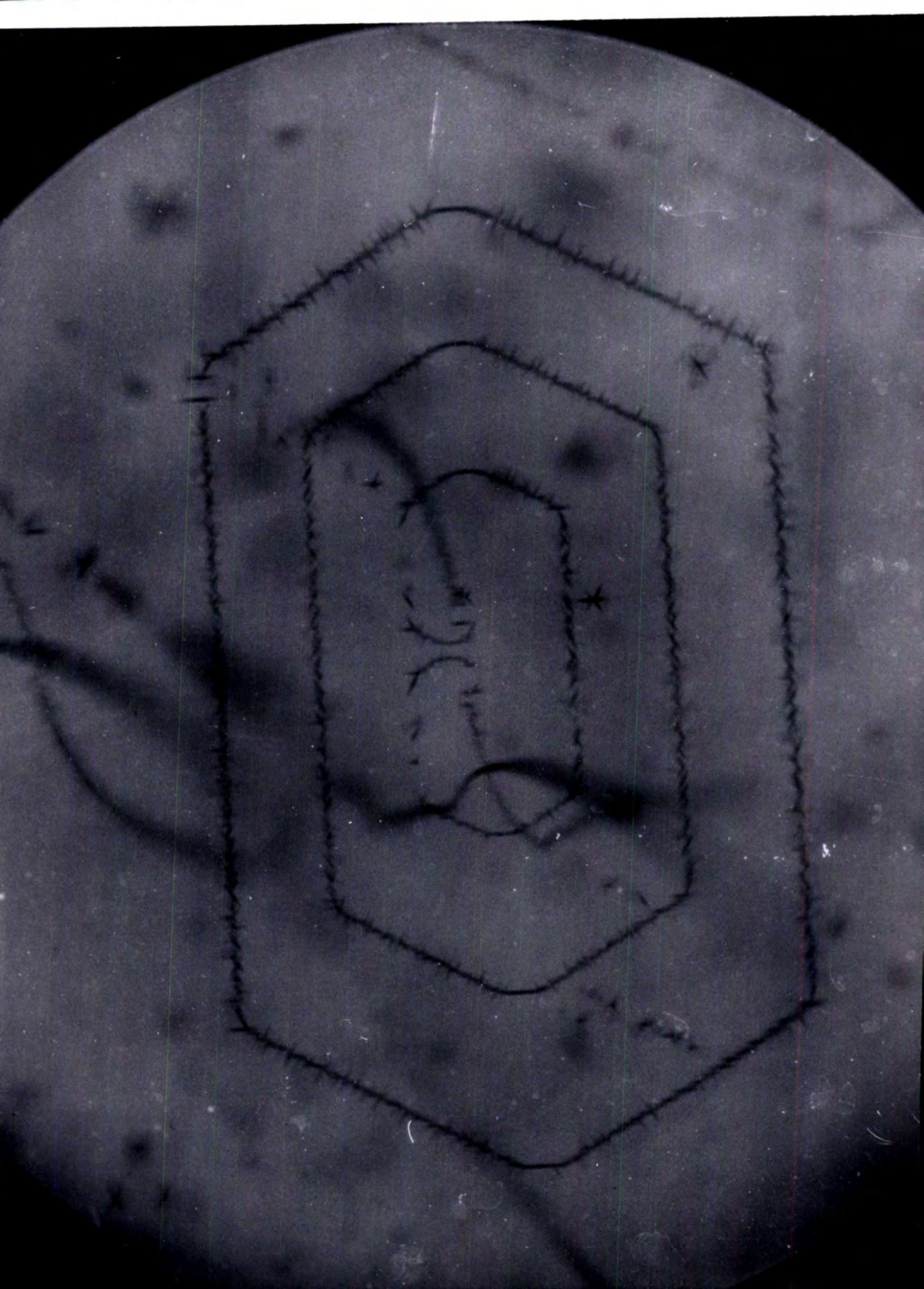

Plate 36. Loop multiplication by a symmetrical Frank-Read source.
(After Dash, 1957).

extend from cusps. In some cases the streamers are very densely concentrated, and as a result a portion of the moving dislocation is retarded. Often zig-zag and segmented trails are found.

The dislocations in Plate (35) appear to have no grown-in dislocations to act as a source. The source may have been removed by the etching process, but when etching is not used, still no sources are visible.

Many interior sources have been seen in deforming imperfect crystals. Frank-Read sources have frequently been found, see Plate (36).

At temperatures of about 1100 deg. C. configurations of curved dislocation lines, entirely different from the patterns at lower temperatures, are observed. Dash considers it probable that at high temperatures dislocations move so freely that they can eliminate the anchoring necessary for Frank-Read sources.

The trails probably arise from nonconservative motion of jogs, causing the injection of vacancies or interstitials into the crystal. Trails from a screw dislocation are mainly along [110] directions. They are sometimes zig-zag and segmented, suggesting alternate gliding and climbing. It is possible to see the trails due to the aggregation of vacancies, or interstitials, into platelets which are then etched or decorated. An alternative explanation is that vacancies formed by jog motion act as nucleation sites for impurities.

Patel (1958) studied dislocations quantitatively in single

crystals of silicon by the etch pit method. Using magnifications up to 750 times on an area 6 x 6 cm., the etch pit density before deformation was 10^4/sq. cm. The average etch pit density after deformation was found to be several times the calculated value. Patel compared his values for the dislocation density due to bending with the calculated values as predicted by Cahn's formula. The formula gives the dislocation density ρ, introduced by bending, to be equal to $(rb)^{-1}$ where r is the radius of curvature of the neutral axis, and b is the average component of the Burgers vector parallel to the neutral plane.

Patel (1958) explained that this equation applies only when the macroscopic internal stress, averaged over large numbers of dislocations, vanishes. Samples annealed after deformation fulfil this condition, as after annealing dislocations arrange themselves in a minimum energy configuration.

Dislocations of opposite signs can exist on the same slip plane in silicon, since appreciable plastic flow does not take place at room temperature. It is expected that on annealing at high temperatures the dislocations are mobile enough to enable dislocations of the opposite sign to annihalate each other.

PART 7.

THE USE OF TRANSMISSION ELECTRON MICROSCOPY

TO OBSERVE DISLOCATION LINES.

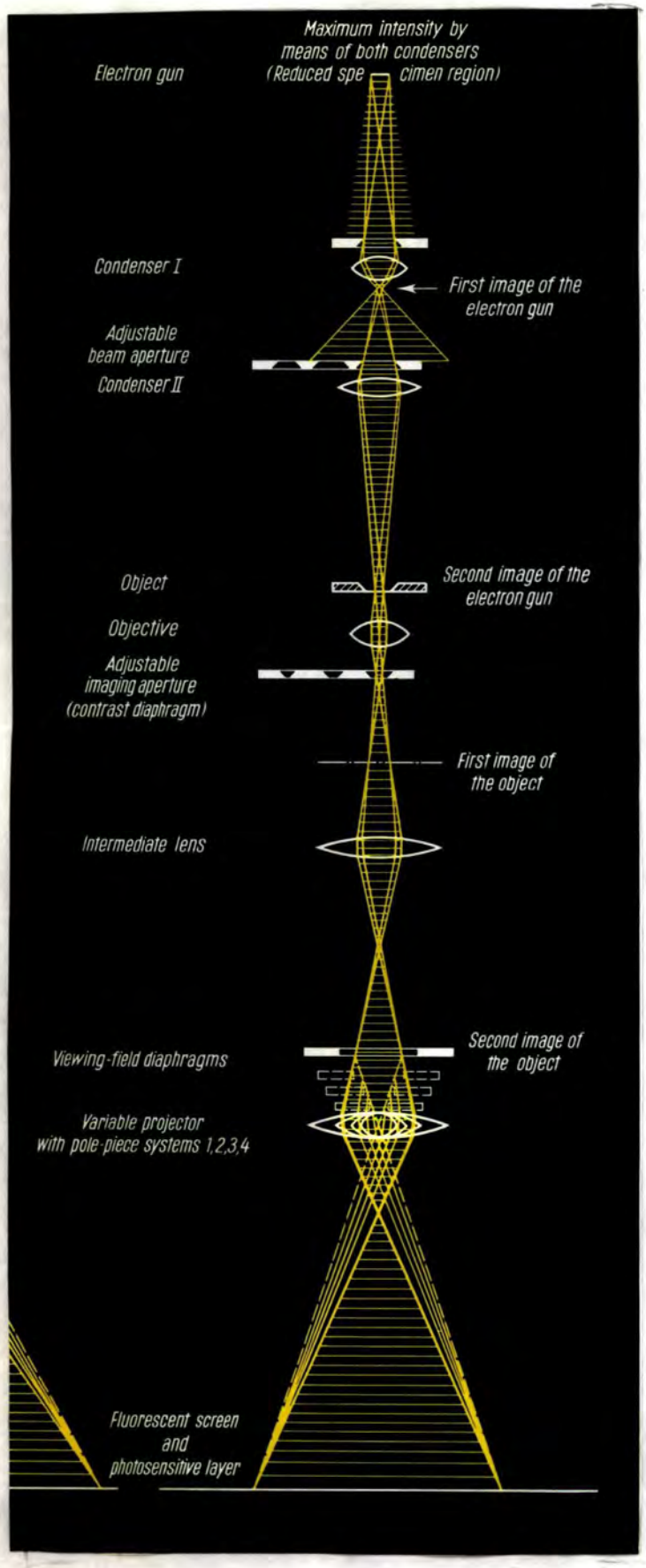

Fig. 49. Triple-stage magnification with objective, intermediate lens, and projector up to approx. 160,000 x, maximum intensity by means of both condensers. (After Siemens 'Elmiskop I').

7.1 INTRODUCTION.

Crystal imperfections are of particular interest in the study of metals. They are of great practical importance.

The methods considered so far only make it possible to infer what may happen in metals. The existance of dislocations in metals has been revealed in a very direct manner by the transmission electron microscopy technique, due to Hirsch, Horne, and Whelan (1956).

It has proved possible to identify dislocations, and to follow their movement under stress by means of a cine-camera.

The microscope can be used to produce electron diffraction patterns from which the crystallographic orientations can be determined.

7.2 THE ELECTRON MICROSCOPE.

At the time of writing, the Seimens Elmiskop is probably the electron microscope in most general use. This has a theoretical resolving power of 3 A and a practical one of 5 A. There is also the Metro-Vickers E. M. 6. capable of a resolving power of 5 A, and the complex new Phillips electron microscope.

Practical resolution is generally reduced by aberrations and scattering to about 20 to 30 A. Spherical aberration presents the outstanding problem.

The specimen used is from 50 A to 5000 A thick, and as the depth of field is about 7000 A the bulk of the foil is in focus

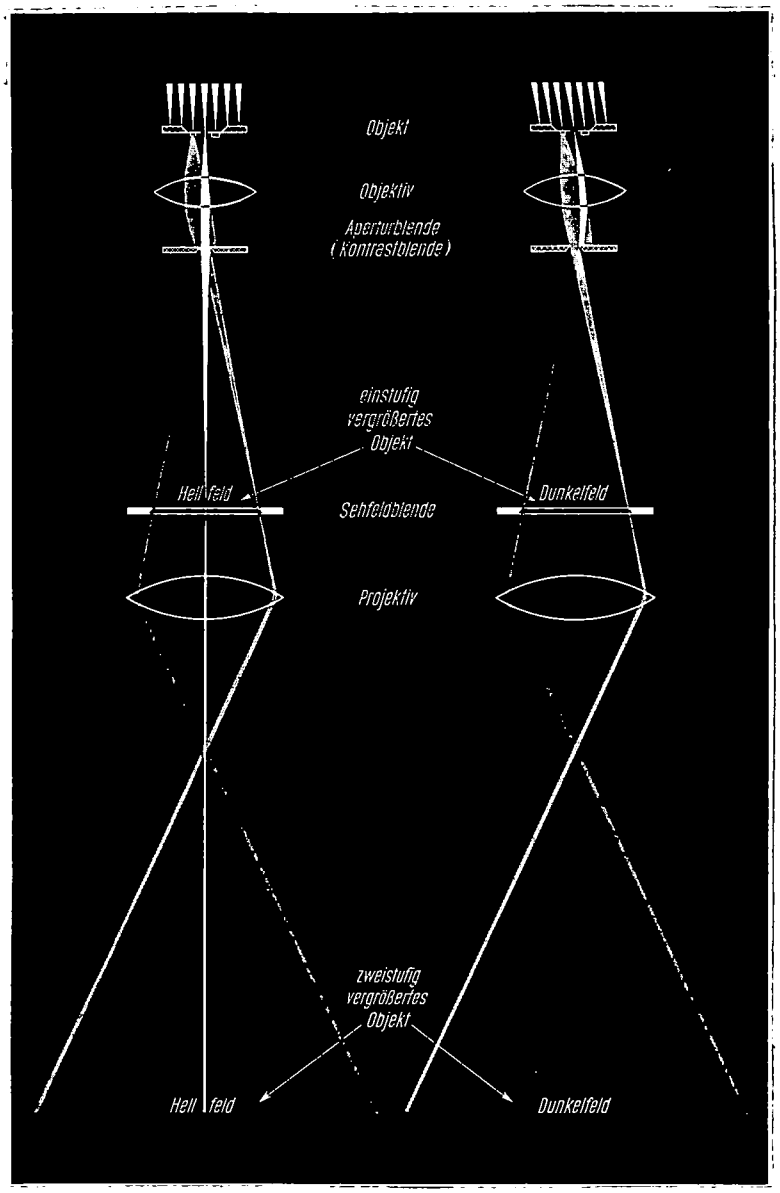

Fig. 50. Bright and dark field images.
(After Siemens 'Elmiskop I').

at the same time. This large depth of focus is useful in that photographic plates may be placed below the plane of the viewing screen, and when photographing the latter acts as a shutter.

The image formation is shown in the Fig. (49). The illuminating electron beam is diffracted by the crystalline object to produce a diffraction pattern in the back focal plane of the objective lens. The recombination of the Bragg reflections to form an image is prevented by the spherical aberration of the object lens. The image, formed essentially by the direct beam and the low angle scattering, is called a bright field image. The contrast is produced by the differences in diffracted intensity from various parts of the specimen. The Bragg reflections are prevented from contributing to the final image by means of an aperture placed behind the objective lens. This method of contrast is known as "Bragg contrast". See Fig. (50).

7.3 ELECTRON DIFFRACTION.

It is often necessary to correlate detail on the electron micrograph with crystallographic orientations; to achieve this electron diffraction patterns of selected areas of the micrograph are required. The back focal plane of the objective lens in which the diffraction pattern is formed is focused onto the screen by reducing the strength of the intermediate lens. By inserting the appropriate aperture, diffraction patterns can be obtained from areas of $\frac{1}{3}$, $\frac{2}{3}$, or $\frac{4}{3}$ micron diameter.

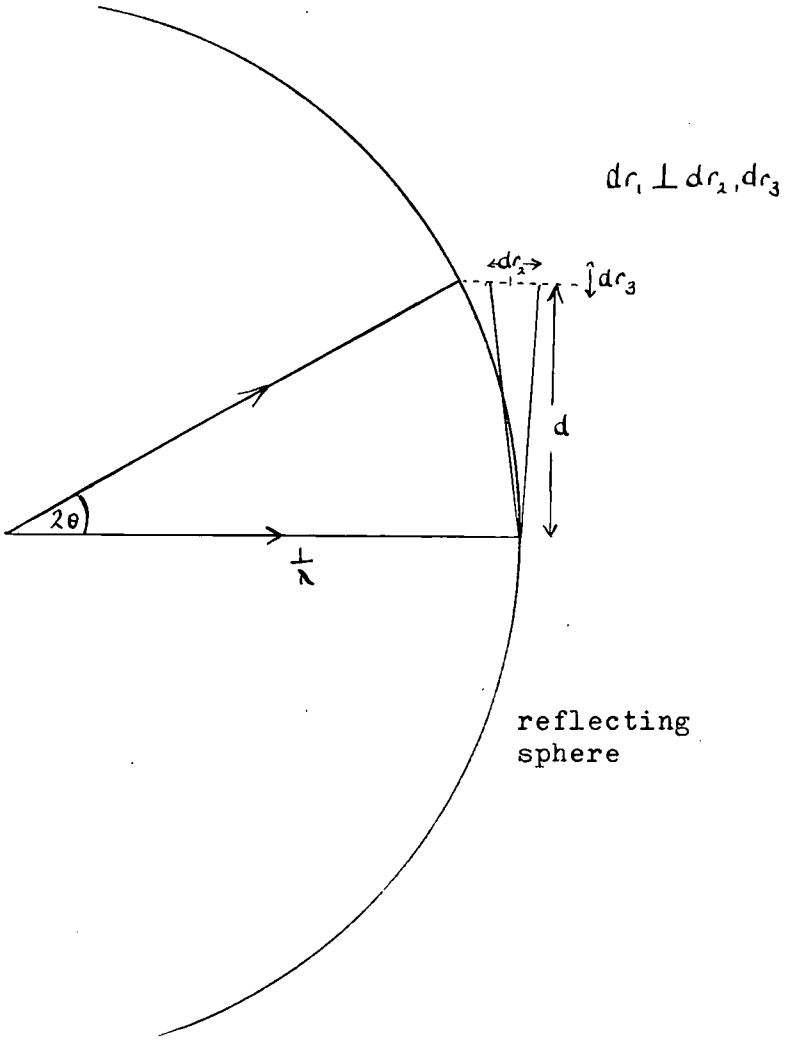

Fig. 51. The reflecting sphere construction.

To interpret these diffraction patterns, consider the reciprocal lattice and reflecting sphere construction, see Fig. (51).

If the electron beam is close to a prominent zone axis of the crystal then the diffraction pattern will be the projection of a prominent zone in the reciprocal lattice. The number of spots appearing on the electron diffraction patterns of single crystal regions of a metal foil decrease as the size of the aperture is decreased. This implies that the area selected consists of regions which are bent with respect to each other. Many micrographs show extinction contours, see Plate (37). These occur when the foil is buckled or bent, and are caused by the strong scattering of the electron beam into Bragg reflections.

The wavelength of the electrons is 0.04 A, and the radius of the reflecting sphere, which is equal to the reciprocal of the wavelength, is very large. Even so, the above shows that it is not sufficient to consider all the spots on the electron diffraction pattern are due to the intersection of the reflecting sphere, considered essentially as a plane, with the reciprocal lattice points which have a finite size dr_1, dr_2, and dr_3. The reciprocal lattice and the reflecting sphere construction gives the direction of diffracted waves. The reciprocal lattice of a F.C.C. structure is B.C. and several prominent zones are recognisable by inspection of the diffraction patterns, see Fig. (52).

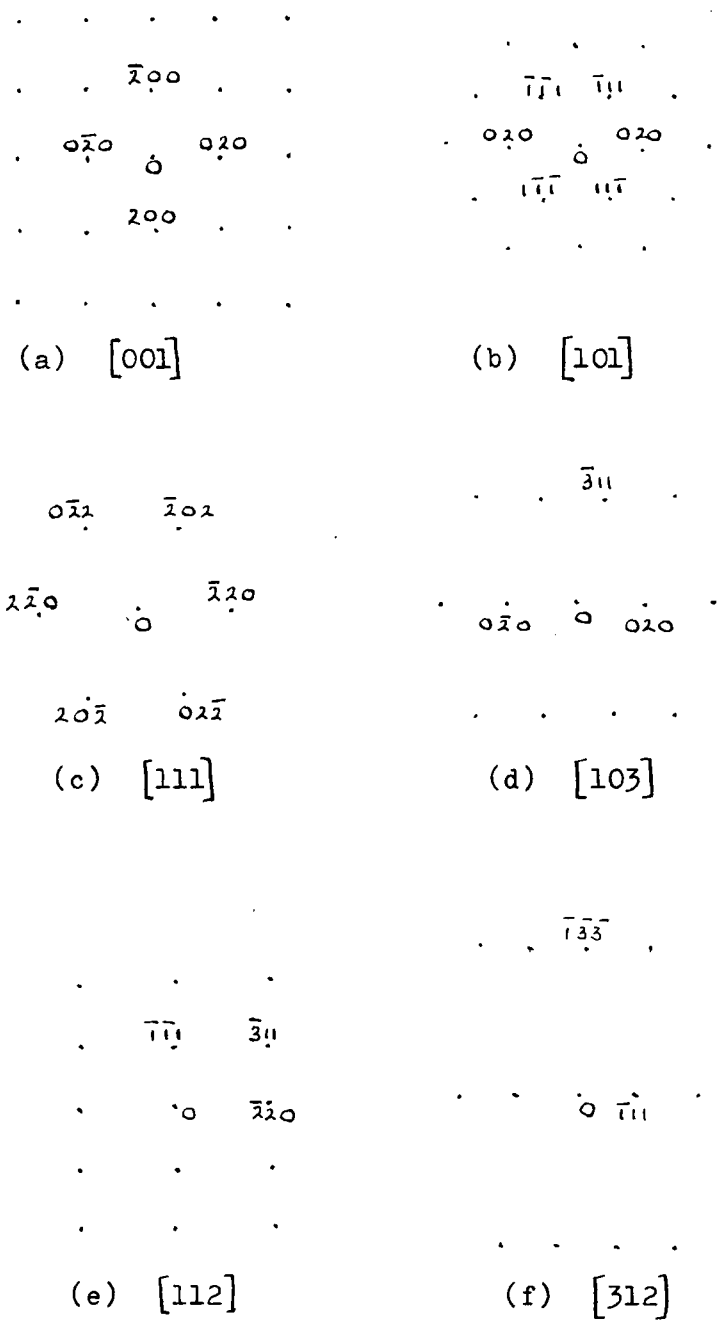

Fig. 52. Electron diffraction patterns.

The metal foils are mounted approximately perpendicular to the incident beam. The crystallographic direction of the electron beam and the foil normal will thus coincide, enabling the normal to the foil to be determined. The data required for the micrographs may be determined graphically, using a stereogram, and a great circle perpendicular to this normal is the plane of the foil.

Due to the great depth of focus the area observed will remain in focus if the foil normal deviates as much as 7 deg. from the beam direction.

The misorientation occurring across sub-grain boundaries, and within grains, can be determined by the splitting of the spots on the diffraction pattern. The method is limited to differences in orientations of greater than ½ deg. by the resolution obtained on the micrograph plate.

7.4 THE PREPARATION OF THIN FOILS FOR THE TRANSMISSION ELECTRON MICROSCOPE.

It was thought from work on biological specimens that the ideal specimen size was 100 to 200 A thick. The apparent impossibility of this retarded development until in 1945 it was found that foils of thickness 200 to 2000 A could be used with success.

The design and construction of electron microscopes is far in advance of techniques of preparing specimens. These are

three methods used for preparing metals for examination, namely (a) Deposition, (b) Deformation, and (c) Dissolution.

(a) Both electrolysis and deposition of evaporated metal produce foils which unfortunately are not representative of bulk material, for example dislocation density is found to be very high. Great care must therefore be exercised in how results are interpreted. Generally speaking, the results are unsatisfactory.

(b) The deformation method involves beating sheets of metal, such as gold or platinum, between sheets of leather. This produces very deformed specimens which prove unsatisfactory for bulk material examination. It is possible to cut thin metal slices using a microtome, and a diamond knife. As the arm rotates it expands due to heating and thin slices are cut off the specimen. These drop into water. The slices are about 200 A thick, and this method can be used for alloys as the relative position of particles remains unchanged.

(c) The dissolution method is the most important. A suitable acid is used to thin down the specimen. One must use pure metals or single phase alloys, provided of course a suitable etching reagent is obtained. The method cannot be used for multiphase alloys.

Thinning by electrolytic polishing was started by Heidenreich (1949), and continued by Castaing (1954). They studied aluminium and aluminium-copper alloys. In the latter, a foil about 100 μ

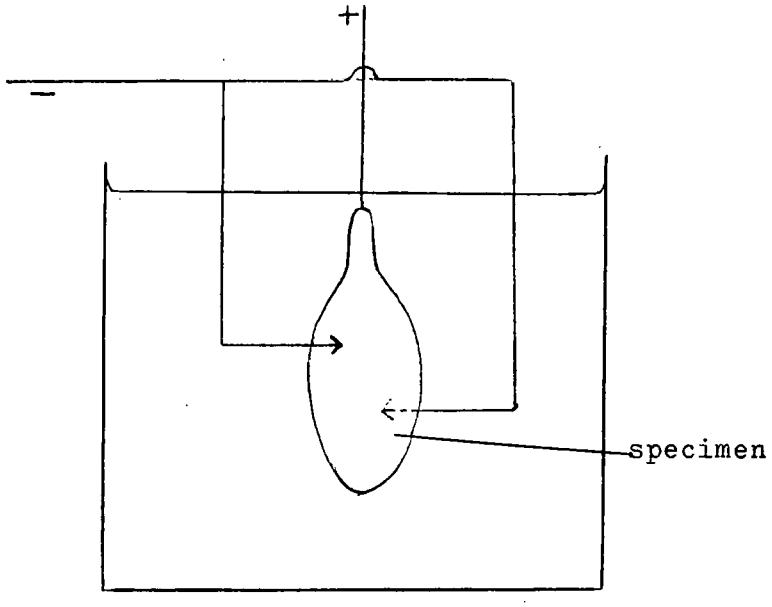

Fig. 53.

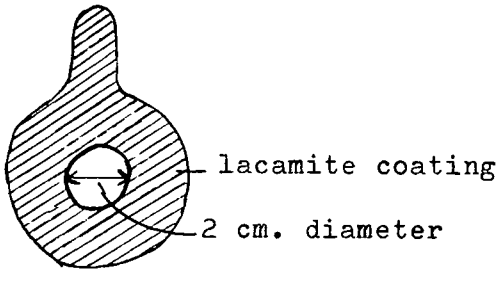

Fig. 54.

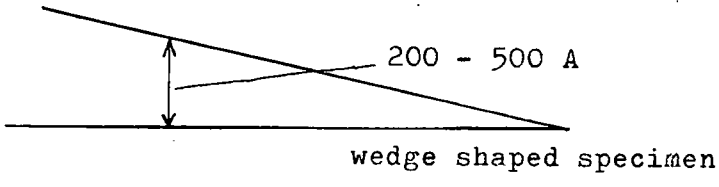

Fig. 55.

thick is cut to shape and insulated with lacamite, except for a small area about 2 cm. diameter. The foil is then polished at 10 v. D.C. in 65% phosphoric acid, 16% chromic acid, 13% sulphuric acid, and 24% water. A current of 0.5 amps./cm.^{2} is used, and the temperature should be 70 deg. C.

The Bollmann technique (see Bollmann, 1956) uses the arrangement shown in Fig. (53). When dealing with F.C.C. chrome 18%, nickel 18% steel, the method uses a disc shaped specimen of 2 cm. diameter, and 0.2 mm. thick. This acts as the anode. The points are adjusted to be about 1 mm. from the specimen, and once a hole is produced, this distance is increased to 1 cm. so that a region close to the hole is preferentially attacked. A new hole opens and this is continued until both holes join. In this region are many thin fragments. These tend to be wedge shaped. This is an advantage, as then the most suitable thickness for observation can be found, and also the strain fields are preserved. See Fig. (55).

Another method for beaten aluminium foil is to cut squares of about 2 cm. sides, immerse in 0.5 to 1.0% hydrofluoric acid in water and remove when pinholes appear, usually after about 2 minutes.

7.5 MOUNTING OF THE SPECIMEN.

Having prepared the specimen, it is mounted on a platform which is a grid of woven stainless steel, or copper, or platinum alloy, the mesh being about 200 lines to the inch. Using the

Seimens Elmiskop operating at 80 K.V., the electron beam is focused by the two condenser lenses to a circular spot between 2 and 5μ diameter on the specimen. When the foil is thus heated locally by the intense electron beam, there is a large temperature gradient in the foil. Even so, the rise in temperature of the specimen is little more than 20 deg. C. The gradient produces stresses which cause dislocations to move in the foil.

7.6 CONTRAST IN THE IMAGE.

Individual dislocations are visible on the fluorescent screen as lines, dots, and networks. The high contrast of a single dislocation is due to distortion of the surrounding lattice over a distance of the order of 100 A, which affects the loss of electrons from the imaging beam by diffraction outside the objective aperture.

Most of the contrast in the electron micrographs is due to differences in diffracted intensity from different parts of the specimen. The diffracted beams are prevented from reaching the image by a suitable aperture in the objective lens, and the electrons lost in this way give rise to contrast. It is sometimes advantageous to remove the electrons directly transmitted through the specimen and to form the image by a proportion of the scattered electrons, thus forming a light image on a dark background, called a dark field image. This helps to differentiate between areas of only slightly different contrast, or

scattering power, which would be difficult to distinguish using a bright field.

The dislocations are seen as dark lines or dots. Many of the patterns of dislocations are similar to those observed in silver halides by Mitchell et al., and sodium chloride by Amelinckx, although in this case dislocations are spaced at distances of only 100 A compared with 1μ in inorganic crystals. The dislocation arrangement in a heavily deformed and recovered metal is similar to that in the well-annealed inorganic crystals. The only difference is in the scale of the arrangement.

7.7 EXTINCTION CONTOURS AND INTERFERENCE FRINGES.

Dark extinction contours are often seen, and these are due to bending and buckling of the foil. They are formed where the foil is oriented so that the beam is strongly reflected from a particular set of Bragg planes. On tilting the illumination or the specimen through angles of about 1 deg. or 2 deg., extinction contours move, whereas dislocation lines remain fixed.

Interference fringes are also seen. These are due to the direct beam, and the beam diffracted twice, so that they emerge almost parallel.

7.8 THE CINE CAMERA TECHNIQUE.

Recordings of dislocation movement, and rapid changes, may be taken by cine camera technique.

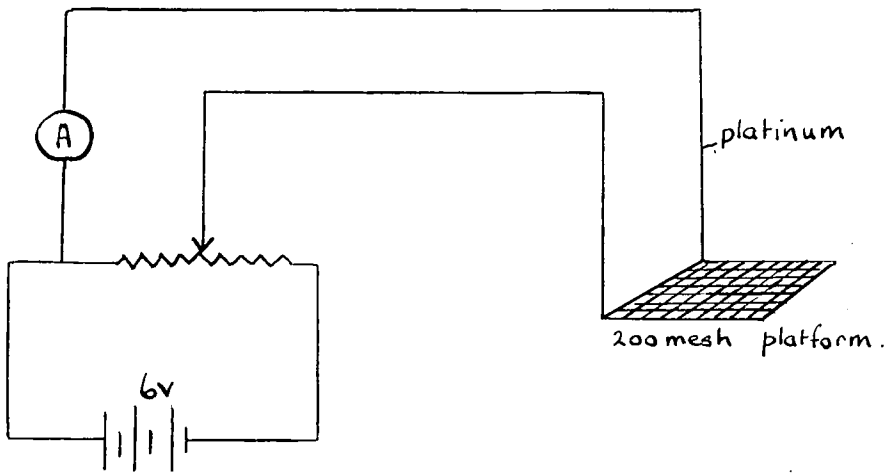

Fig. 56. The high temperature stage.

	Stacking fault energy ergs/cm.^{2}	Ribbon width in Burgers vectors	Seeger's values ergs/cm.^{2}	Ribbon width
Cu	40	8.5	169	2.35
Au	33	7.5	30	7.2
Ag	35	7.2	43	
Ni	95	6.3	410	1.5
Al	200	0.7	230	1.4
Stainless steel	13-20	30		
Brass	8			

Fig. 57. Stacking fault energies.
(After Hirsch (1959), and after Seeger, Berner, and Wolf, 1959).

Using a Kodak cine Special camera with a f/0.95 aperture lens, it is possible to photograph the fluorescent screen from about 12 cm. distance. The Elmiskop produces a sufficiently bright image at x 40,000 magnification to allow external cine photography. High speed 16 mm. film S.G.91, H.P.S. and H.P.3 have been used, but the usual 16 frames per second is not considered fast enough, and many of the rapid movements cannot be closely followed. 100 frames per second are desirable to give a more complete picture.

7.9 THE HIGH TEMPERATURE STAGE.

Whelan designed a high temperature stage to fit into the microscope. This is a specially constructed object holder with leads carrying the heating current through a hole in the side of the objective lens. The stage does not interfere with the normal operation of the microscope, and enables the specimen to attain a temperature up to 1100 deg. C. The heating element dissipates very little heat, about 6 watts at 1000 deg. C. The specimen is quenched simply by turning off the current. The specimen mount consists of two platinum legs, and a piece of 200 mesh stainless steel, which supports the specimen.

The direct current from a 2 volt battery passes through the stainless steel mesh via the platinum legs, thus heating the specimen directly. The end cap of the object holder prevents radiation and evaporation from reaching the pole pieces of the object lens. To calibrate the heating stage a thermocouple

is used, see Fig. (56).

7.10 STACKING FAULT ENERGY.

There is a variation in the dislocation structure from metal to metal, which is found to correlate with the stacking fault energy of the metal, and therefore with the ribbon width of the extended dislocations. If a dislocation, say on the (110) plane splits up into two partial dislocations on the (211) and (121) planes, a stacking fault is formed between them. This was predicted by Heidenreich and Shockley, (1948).

The distance apart of the partial dislocations depends upon the stacking fault energy of the material. They are close together if the energy is high, as can be seen in Fig. (57).

Dislocations in metals with low stacking fault energy, such as stainless steel, have large ribbon width; those with high stacking fault energy, such as aluminium, have narrow ribbon width, assuming the shear moduli to be equal. The table of stacking fault energies is rather unsatisfactory, as at the moment it is not known which values are correct.

7.11 DISLOCATION STRUCTURE.

Three processes are important when considering dislocation structures in a metal:

(a) The tendency for thermally activated cross slip to take place in a metal.

(b) The interaction when a dislocation tries to cut through other dislocations.

(c) The climb of edge dislocations.

Seeger (1957), considering the dislocation mechanisms in F.C.C. and H.C.P. crystals, indicates that the cross slip of a screw dislocation will be difficult if the ribbon width of the dislocation is large, since, in order to cross slip, a dislocation must become constricted. This means that cross slip will be less likely with lower stacking fault energy. Cine films of aluminium and stainless steel foils, viewed using the electron microscope, confirm these predictions.

In stainless steel and brass dislocations move along wide, well defined "tram lines". Cross slip is rarely observed. In aluminium the slip traces are narrower and quickly disappear. Aluminium cross slips very readily. Cross slip is seen to some extent in copper and silver.

In all the metal foils the dislocations move with a characteristic jerky motion, due to pinning and unpinning at the surface. There is also repulsion between dislocations evident as they 'push' one another along.

The ribbon width of a dislocation will also govern the ability of a dislocation to intersect other dislocations, since the dislocation will become constricted during the intersection. One would expect this to be more difficult in low stacking fault energy metals, and this is complicated by the fact that the

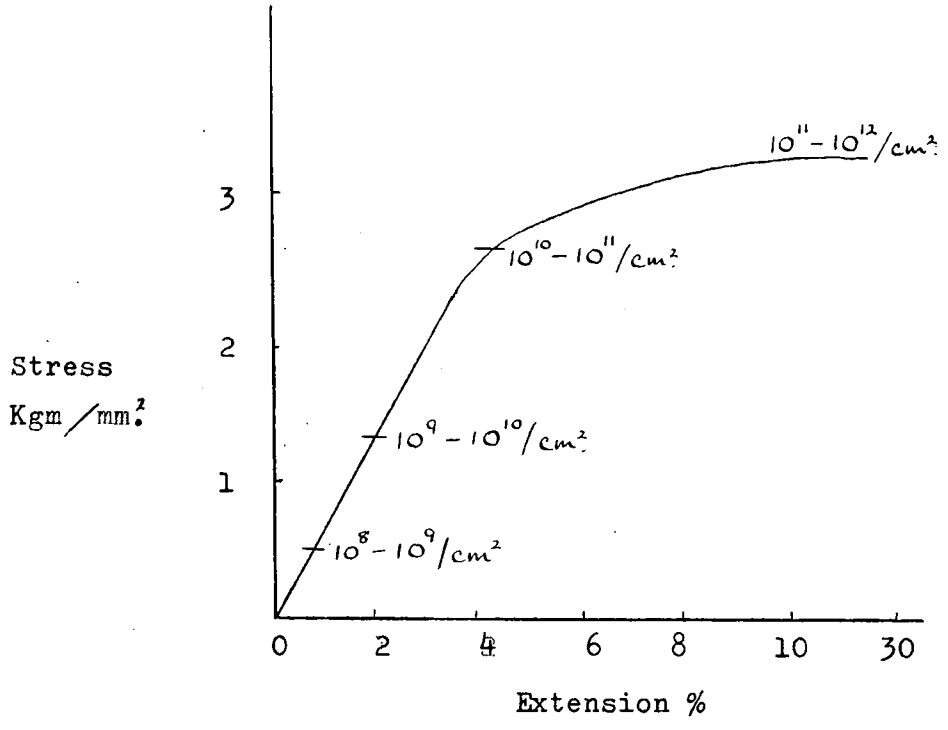

Fig. 58. Stress-extension graph with dislocation densities for stainless steel.

ribbon width depends partly upon the type of dislocation, being larger for the edge type than for the screw. Observations in the electron microscope verify these facts. In stainless steel, where cross slip and intersection of dislocations is difficult, stacking faults pile up, as shown in Plate (47). The dislocations are confined to their slip planes and strongly held up by dislocations on other slip systems that intersect them, see Plate (48). Fig. (58) shows the stress-extension curve for stainless steel with dislocation densities. Networks start to form at about 2% deformation.

In aluminium it is easier to bring dislocations together, giving low energy networks, and high density of dislocations.

If aluminium is rolled or beaten, the substructure becomes very complex, being broken up into mozaic blocks by polygonization, as shown in Plate (37). Dislocation density increases with the applied stress.

As edge dislocations are not hindered by the movement of jogs, it is likely that they are capable of moving further in the lattice than are screw dislocations. Climb involves a diffusion mechanism which is most likely at high temperatures. It is possible that stress activated climb takes place.

7.12 THE USE OF THE THOMSON TETRAHEDRON.

In considering the adding together of dislocations when they intersect, the Thomson Tetrahedron is of considerable value, see

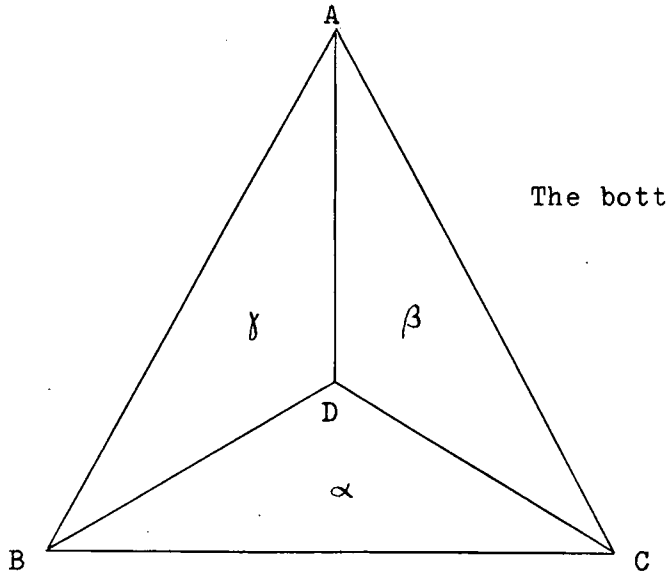

Fig. 59. The Thomson Tetrahedron.

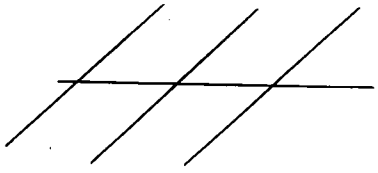

(a)

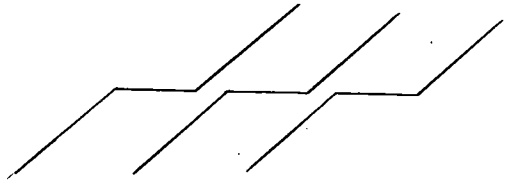

(c) Interaction corresponds to the intersection of slip planes, and represented by edges of tetrahedron.

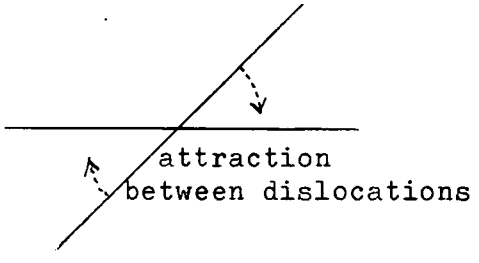

(b)

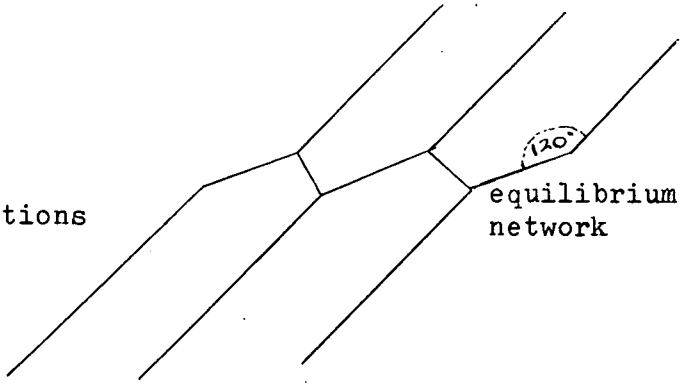

(d)

Fig. 60. Interaction between dislocations.

Fig. (59).

The edges of the tetrahedron represent dislocations and the faces (111) planes, i.e. the planes on which the movement of dislocations is most common in F.C.C. crystals.

If we consider the intersection of dislocations represented by DC in plane α, and CB in plane δ, the resultant will be given by DB in the plane α.

i.e. $\frac{DC}{\alpha} + \frac{CB}{\delta} = \frac{DB}{\alpha}$ See Fig. (60).

Such interactions are important in determining networks.

Possible interactions are:

	Description:
$\frac{DC}{\alpha} + \frac{CB}{\delta} = \frac{DB}{\alpha}$	Glissile in α.
$\frac{DC}{\alpha} + \frac{CA}{\delta} = DA$	Cannot glide at all. Acts as a barrier. (Lomer-Cottrell)
$\frac{DC}{\alpha} + \frac{CD}{\beta} = 0$	Very strong interaction leading to anihalation.
$\frac{DC}{\alpha} + \frac{CA}{\beta} = \frac{DA}{\beta}$	Glissile in β.

It is also possible to consider interactions, taking into account splitting of dislocations,

$DC = D\alpha + \alpha C$.

$CB = C\delta + \delta B$, shown in Fig. (61).

Triangular stacking faults result from dislocation interaction. In this case each node must be sufficiently far away from the other dislocation to avoid long range interaction, see Fig. (62). These are possible in metals of low stacking fault energy.

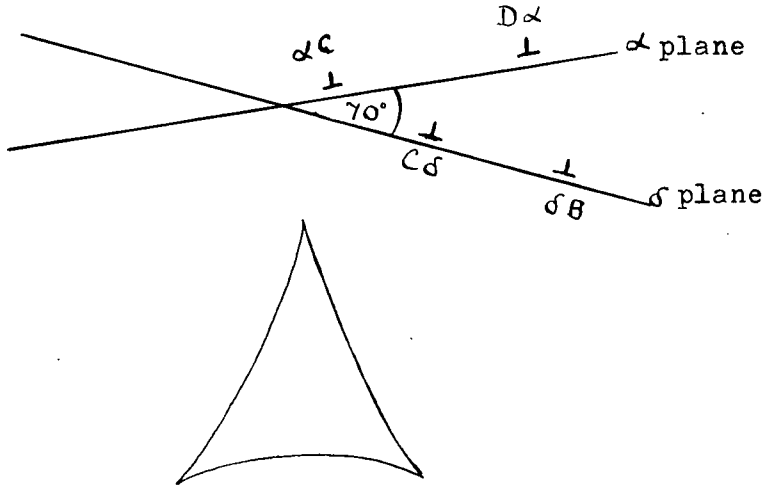

Fig. 61. Interaction and splitting of dislocations.
Fig. 62. Triangular stacking fault.

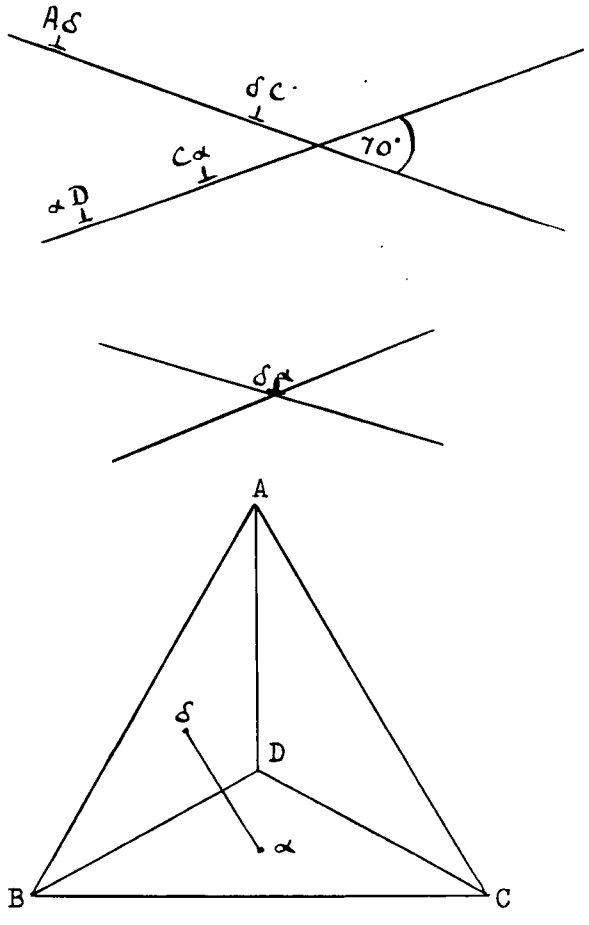

Fig. 63. The formation of a 'stair-rod' dislocation.

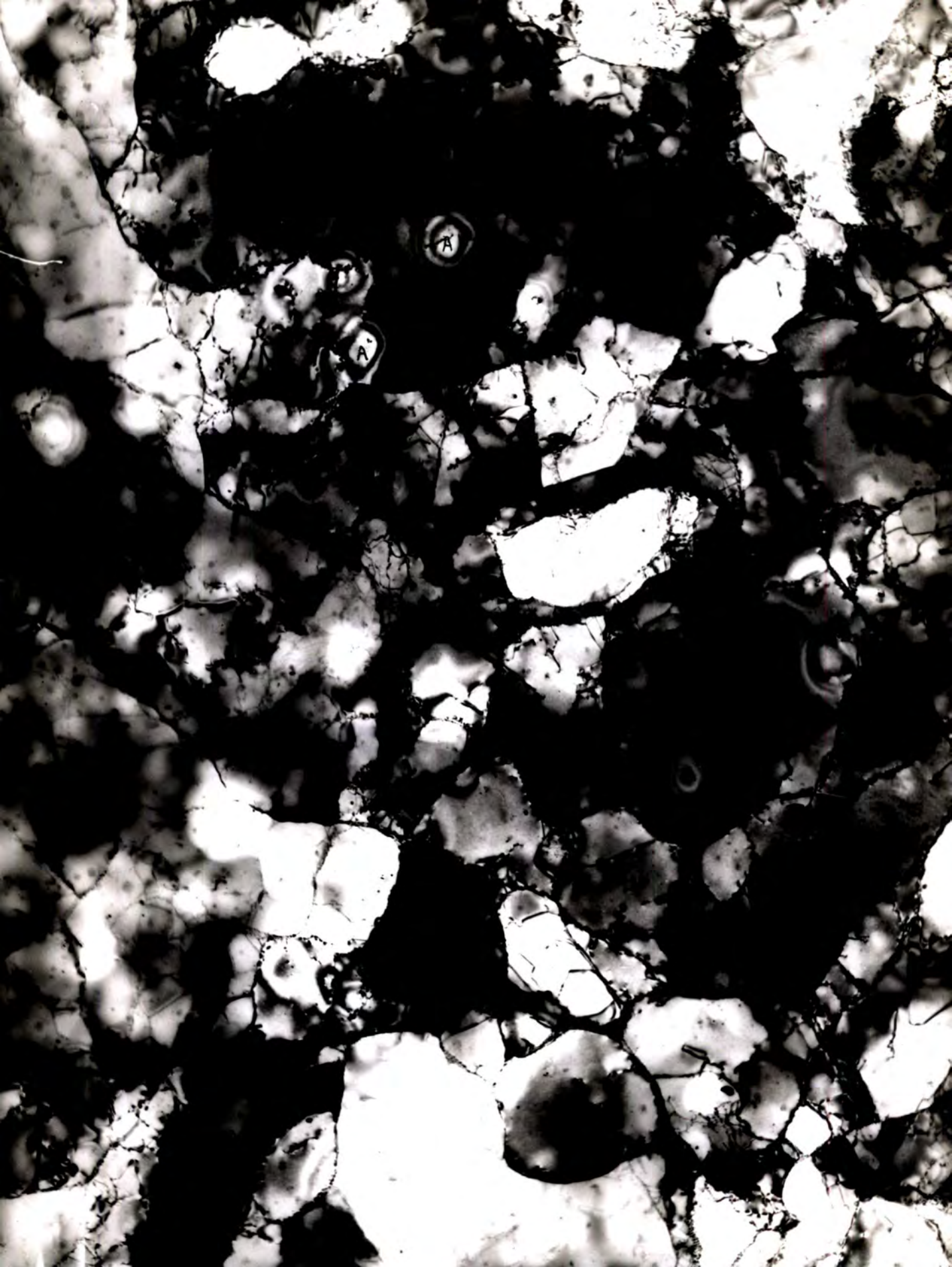
A
A'

Plate 37. Substructure in aluminium annealed at 350 deg. C. after beating at room temperature. (After Hirsch, Horne, and Whelan, 1957).

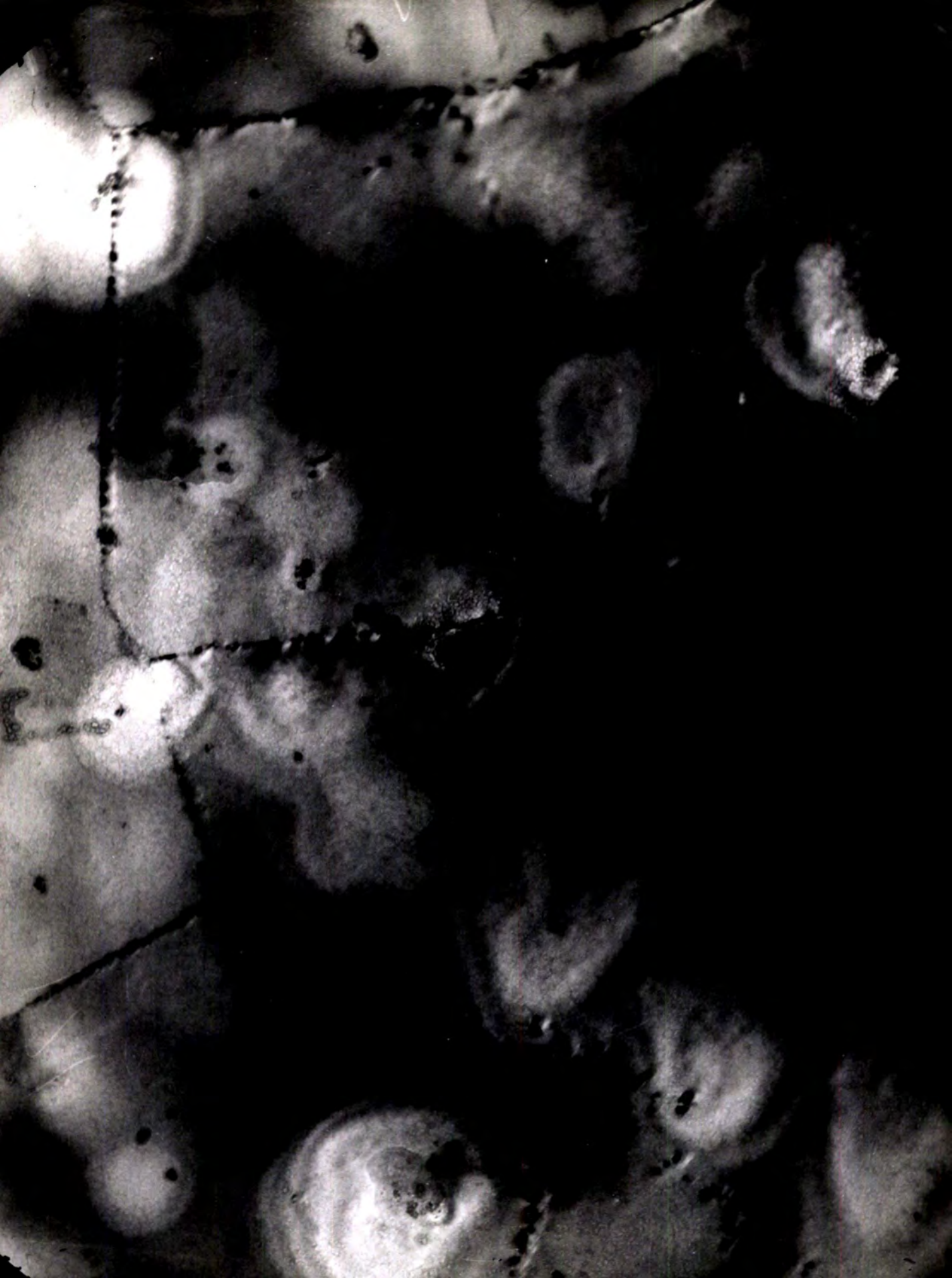

Plate 38. A sub-boundary in aluminium, consisting of uniformly spaced dislocations. (x 132,000) (After Hirsch, Horne, and Whelan, 1957).

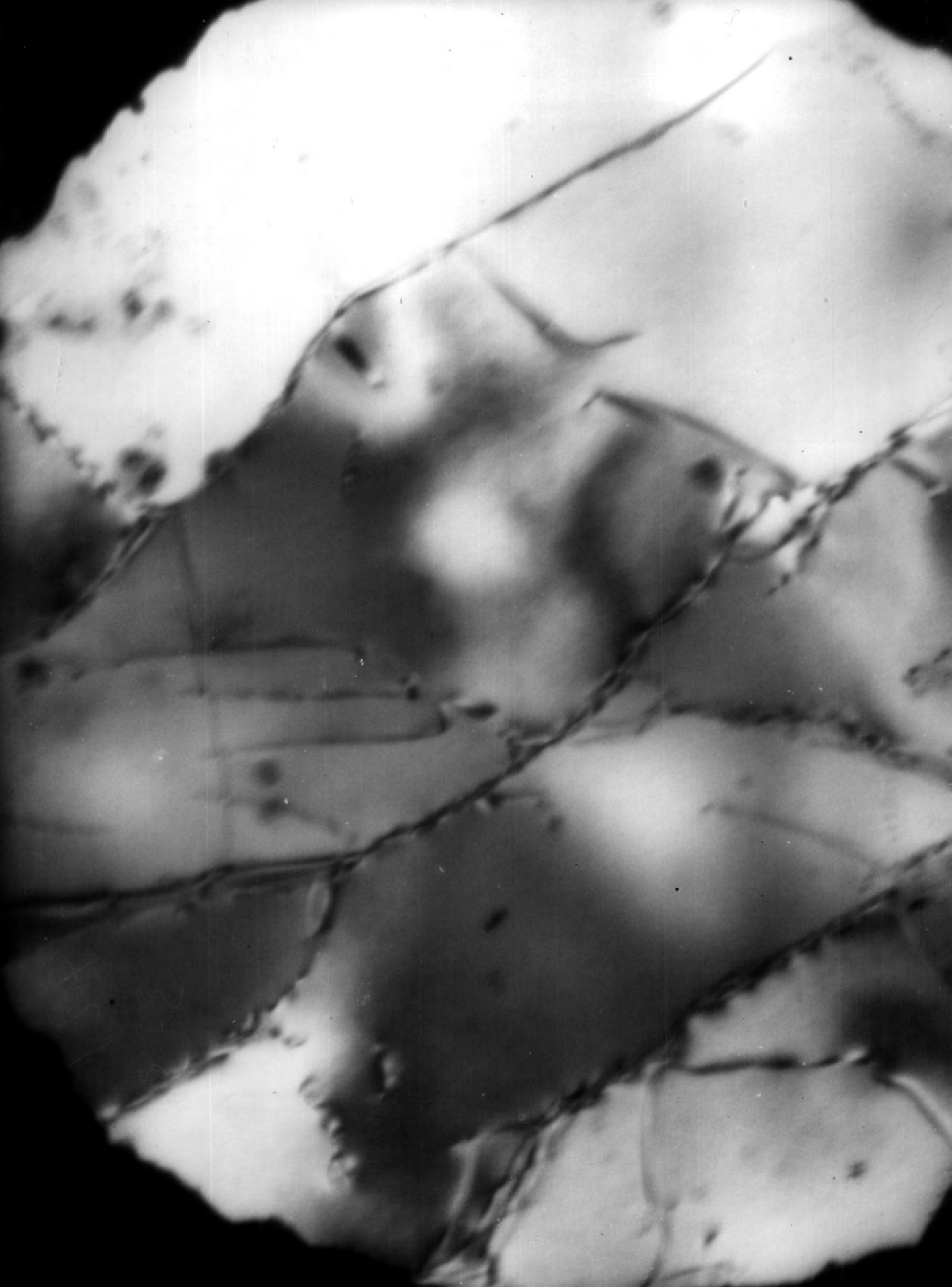

Plate 39. Bright field micrograph showing sub-boundaries and dislocations in aluminium. (x 66,000) (After Hirsch, Horne, and Whelan, 1957).

Plate 40. Dark field micrograph of same area as in Plate 39. (x 66,000)
(After Hirsch, Horne, and Whelan, 1957).

A 'stair-rod' dislocation can result from a Lomer-Cottrell interaction.

e.g. $\frac{CD}{\alpha} + \frac{AC}{\delta} = AD$

$$CD = C\alpha + \alpha D$$

$$AC = A\delta + \delta C$$

Then $\delta C + C\alpha = \delta\alpha$ See Fig. (63).

This is a stair rod dislocation joining one plane to the other.

7.13 THE INTERPRETATION OF OBSERVATIONS AND PHOTOGRAPHS.

Plates (37) to (43) are micrographs obtained using aluminium foils, and Plates (44) to (48) were taken using stainless steel specimens.

Plate (37) shows substructure in aluminium, the average subgrain size being about 1μ, and the average angular misorientation about 1½ deg. Extinction contours may be seen at A. This specimen had been annealed at 350 deg. C. after beating at room temperature. The dislocation density is about 10^{10}/sq. cm. On increasing the magnification the boundaries are seen to be made up of individual dislocations, seen on the micrograph as uniformly spaced lines or dots as in Plate (38). The observed spacings of the dislocations is found to agree with the calculated values expected from the misorientations.

Plates (39) and (40) enable comparison of a bright and a dark field micrograph of the same region. The contrast at dislocations is evident, and this is due to the strong diffraction

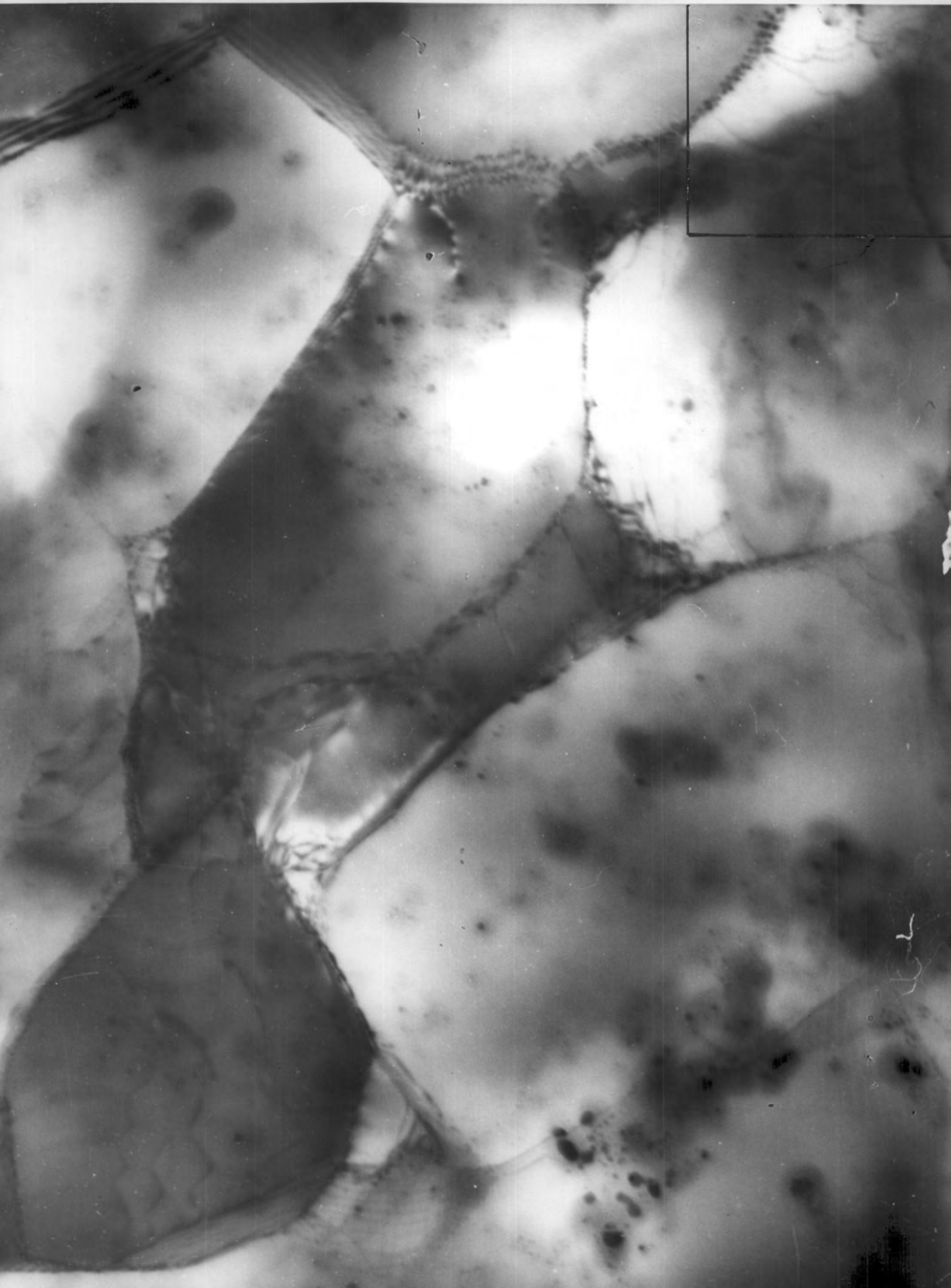

Plate 41. Bowed-out dislocations in aluminium. (x 132,000) (After Hirsch, Horne, and Whelan, 1957).

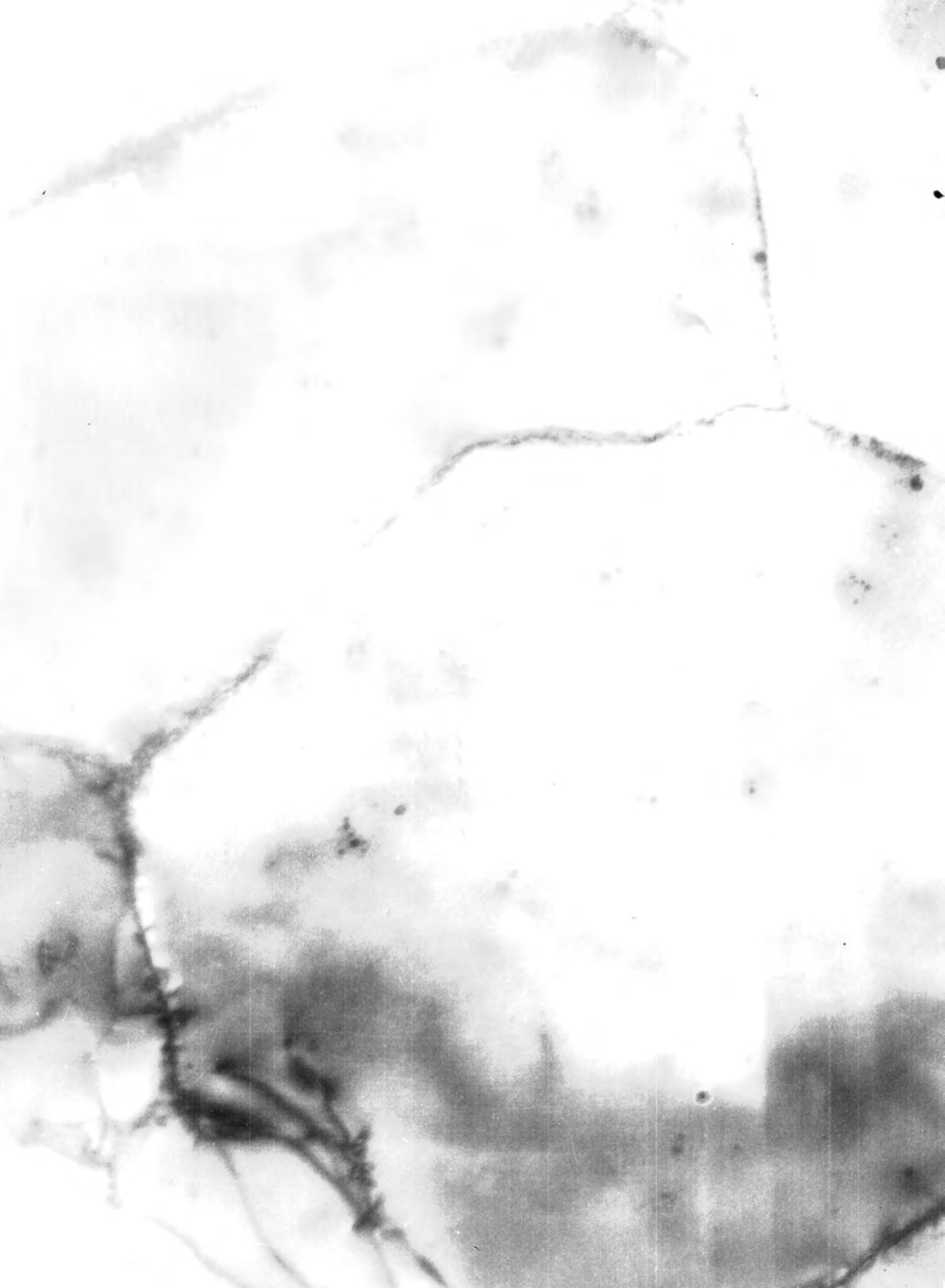

Plate 42. Cross slip in aluminium. (x 132,000)
(After Hirsch, Horne, and Whelan, 1957).

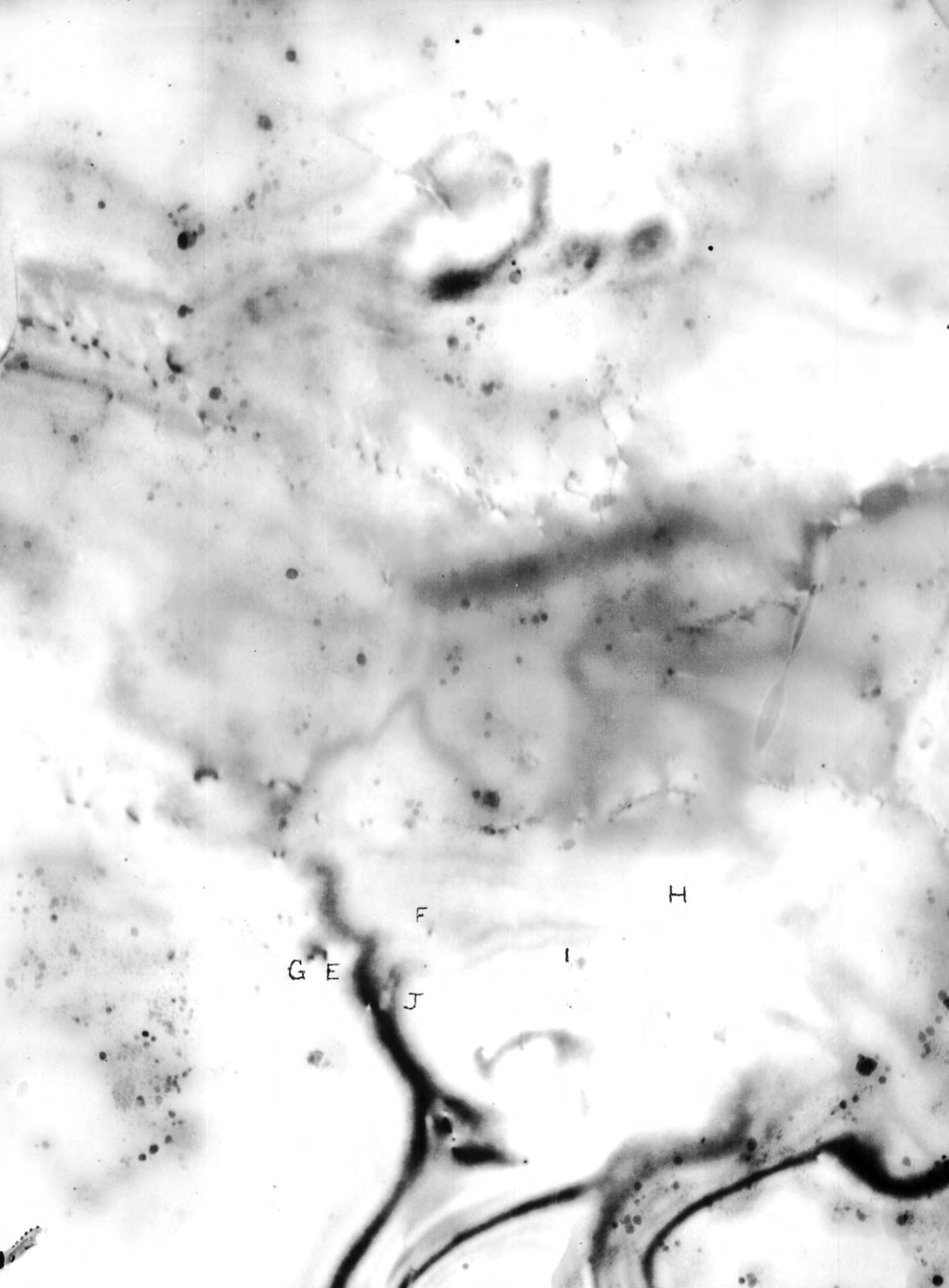
H
F
I
G
E
J

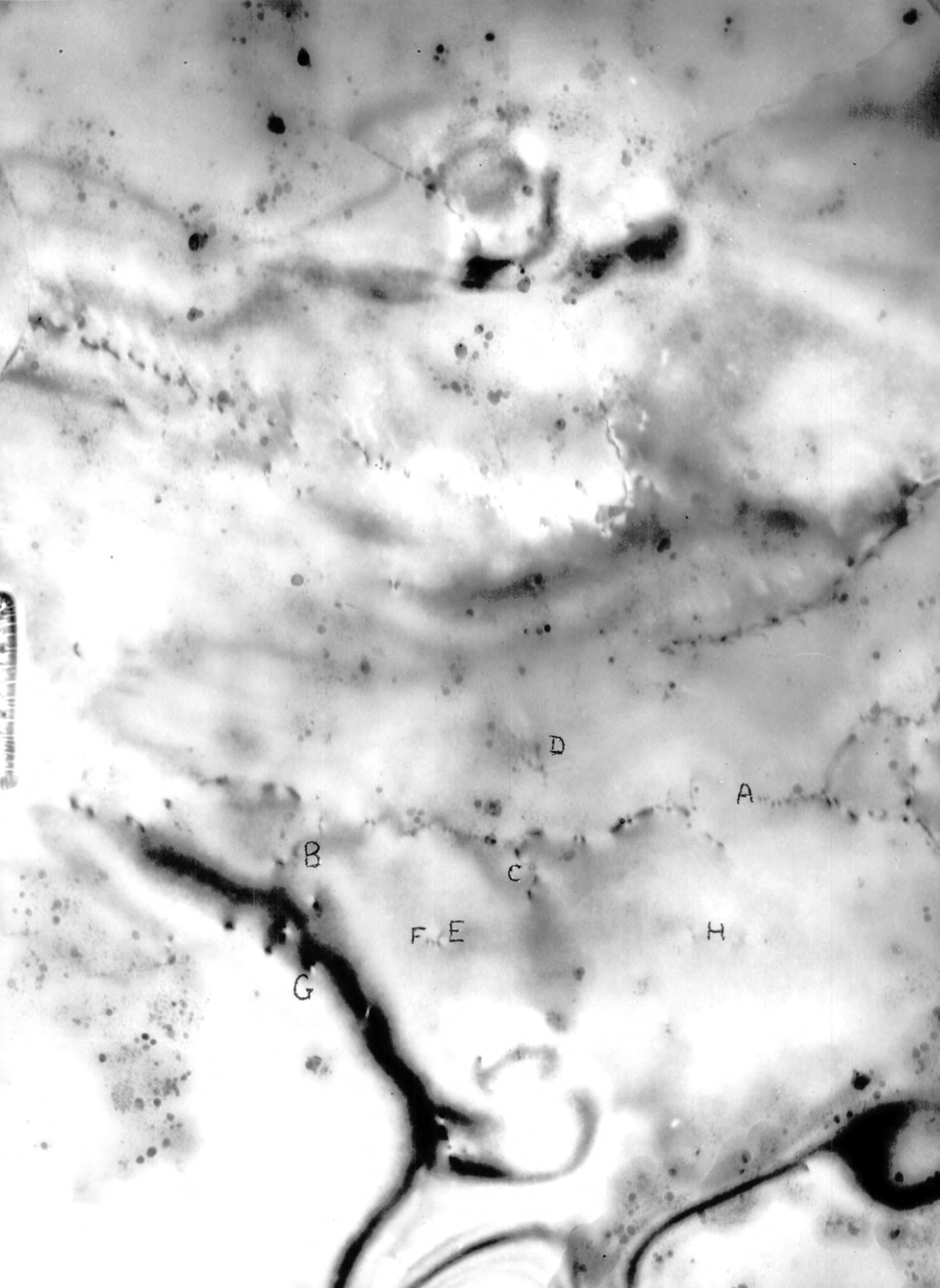
D
A
B
C
F
E
H
G

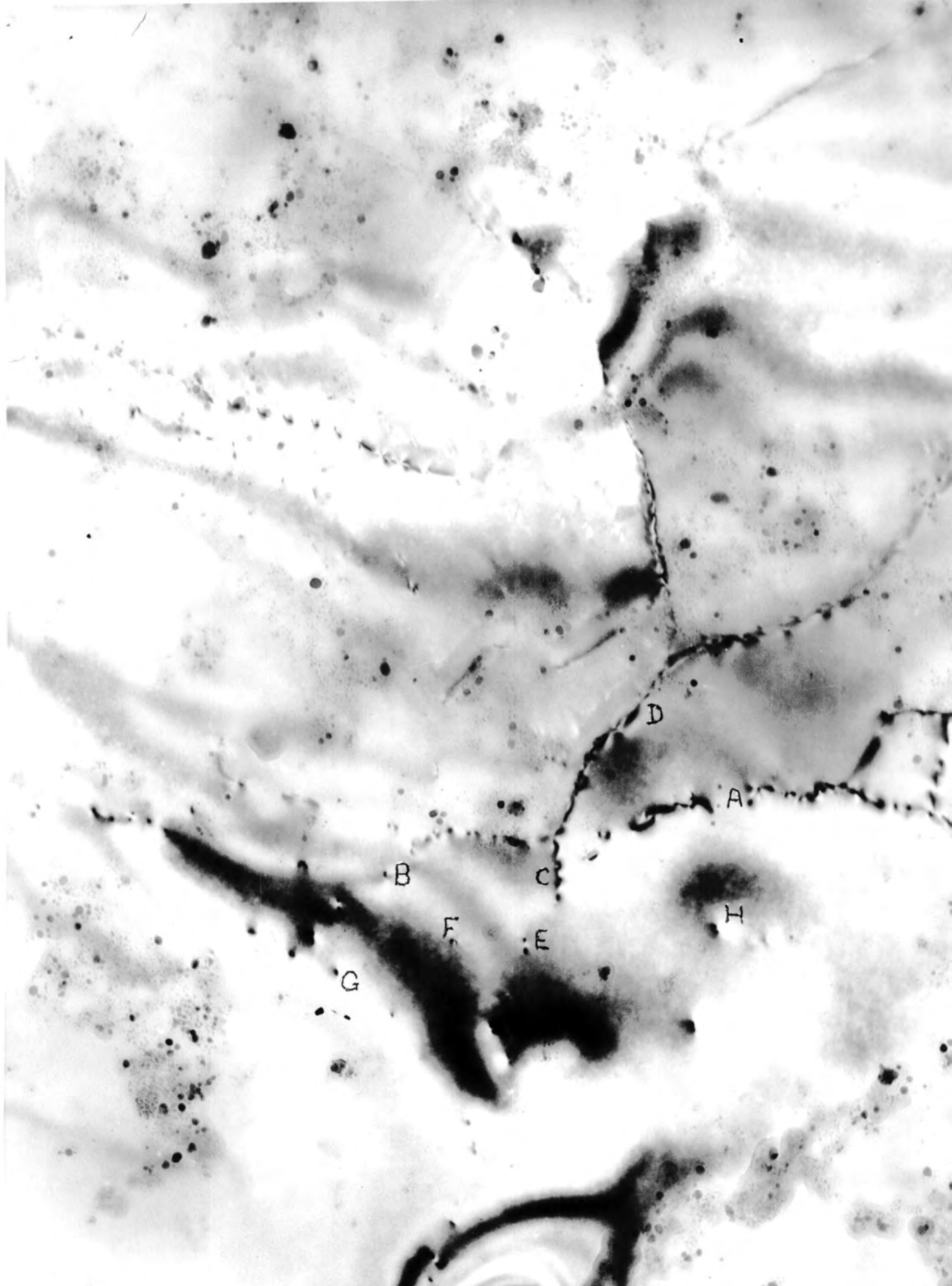
D
A
B
C
H
F
E
G

Plate 43a, b, and c. Sequence showing moving dislocations in aluminium. (x 132,000)
(After Hirsch, Horne, and Whelan, 1957).

of electrons in the neighbourhood of dislocations.

Bowed-out dislocations are shown in Plate (41). This effect is probably due to local strain, and parts being retarded due to pinning.

Plate (42) is an excellent illustration of cross slip by the screw dislocation mechanism. A single dislocation has transferred from one slip plane to another. Mott and Frank predicted this, (see Mott 1951) and, using the transmission electron microscope technique, it has been seen on many occasions. This effect has not been observed in stainless steel, and indeed it is not expected to occur, (see section 7.11).

Slowly moving dislocations are shown in sequence in Plates (43a, b, and c). It is likely that the movement indicated is similar to creep. Individual dislocations are seen within sub-boundaries, and some of these are labelled to show the movement which takes place. A, B, C, and E are dislocations, and D a grain boundary. The latter disappears between Plates (43a and b). Dislocation H has followed the irregular path HIJ.

The Plate (44) shows pile-ups of dislocations in a lightly rolled specimen of stainless steel. In Plate (45) the specimen has been deformed 2-5% by rolling, and the hexagonal network is clearly seen. The dislocations are piled up on a (111) plane. Pile-ups, each consisting of about 25 evenly spaced dislocations, are shown in Plate (46).

Plates (47 a to g) are a sequence of photographs showing

Plate 44. Pile ups in a lightly rolled specimen of stainless steel. (x 3340)
(After Whelan, Hirsch, Horne, and Bolliman, 1957).

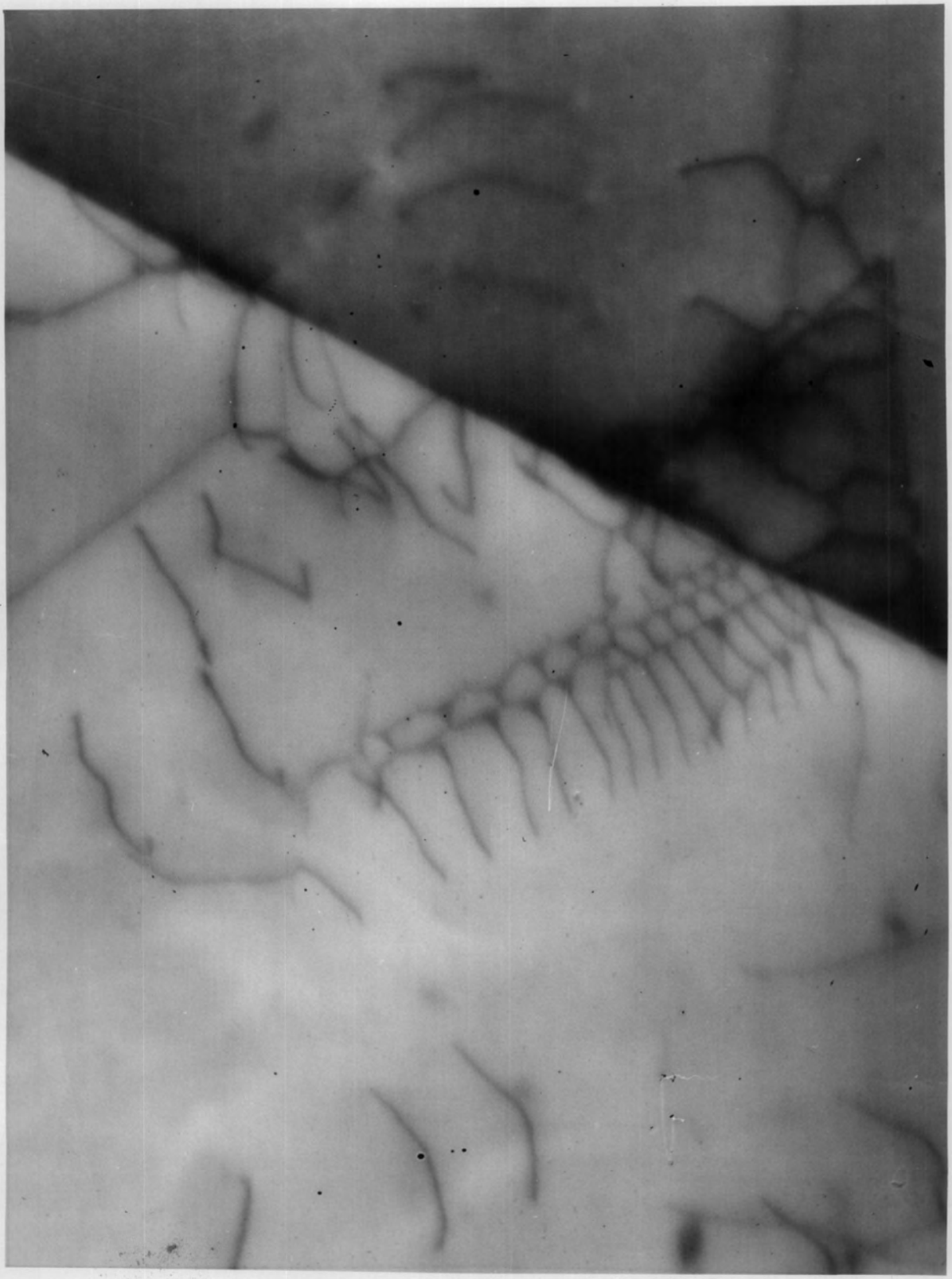

Plate 45. A stainless steel specimen deformed 2.5% by rolling. A hexagonal network and piled up dislocations can be seen.
(After Whelan, Hirsch, Horne, and Bolliman, 1957).


1μ

Plate 46. Pile-ups consisting of regularly spaced dislocations.
(After Whelan, Hirsch, Horne, and Bolliman, 1957).

Fig.6.14

(e)

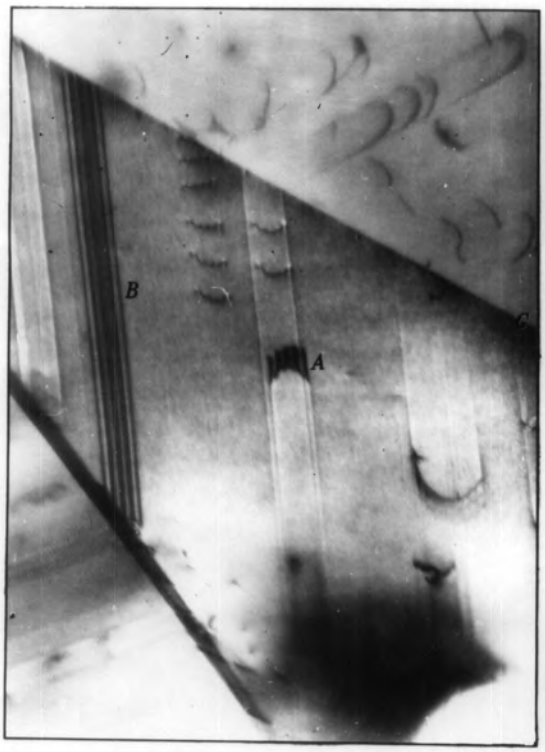

(f)

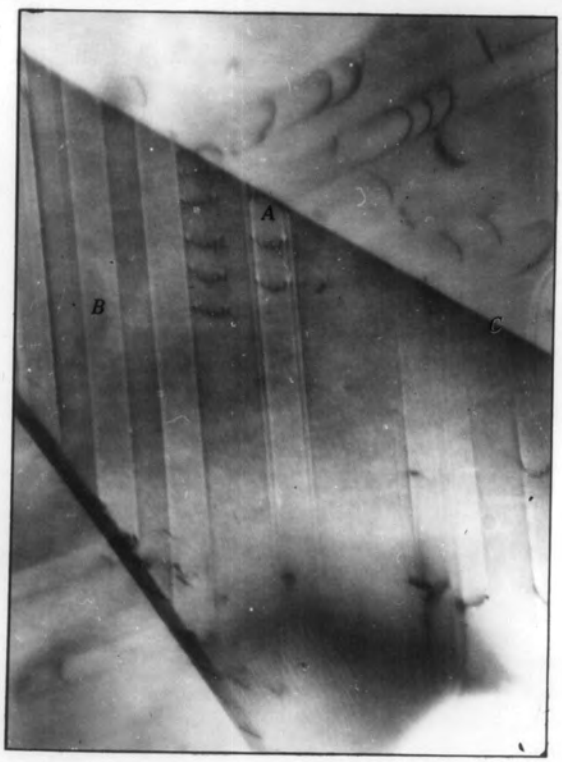

(g)

Fig.6.14

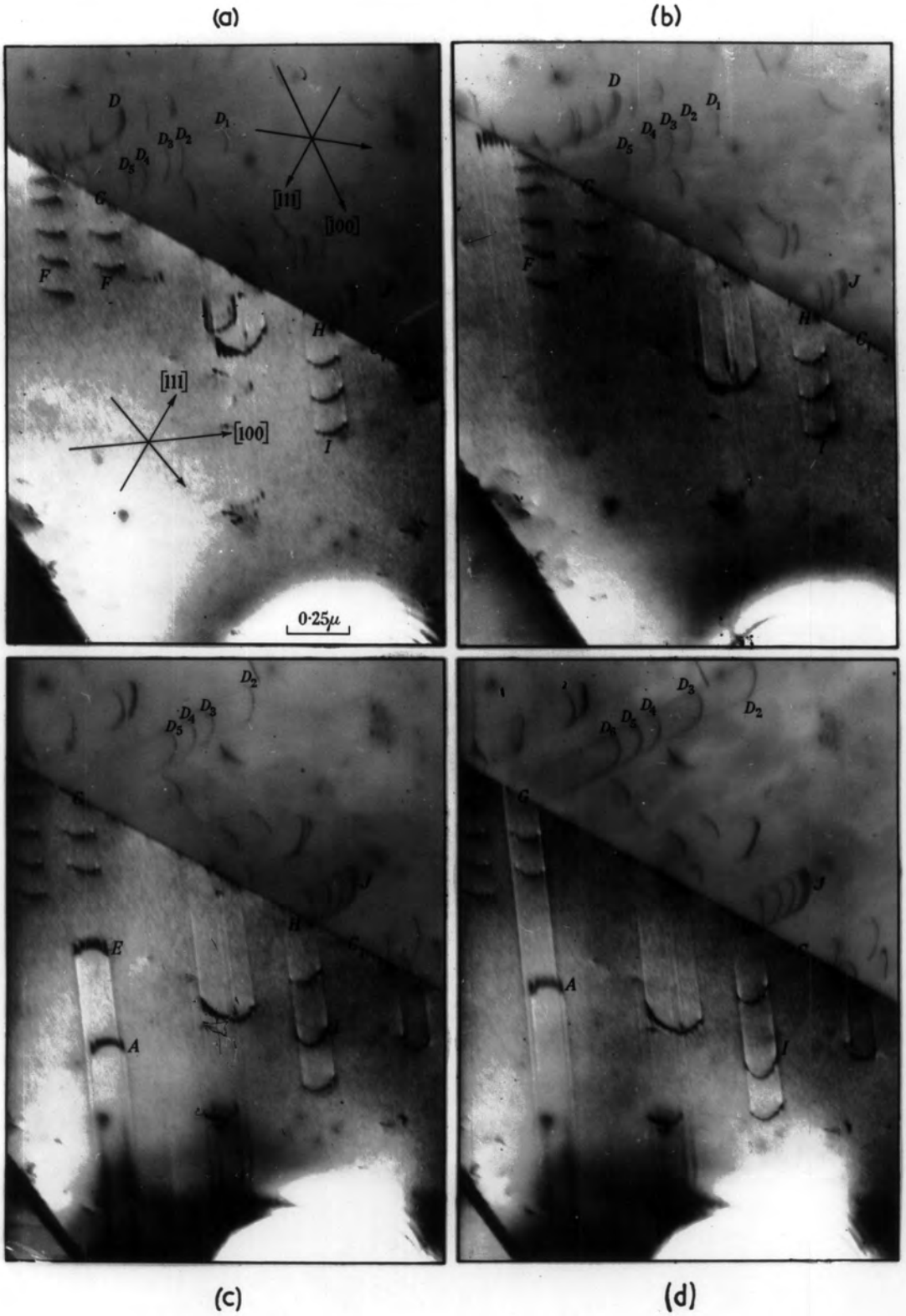

Plate 47. a to g. Sequence of photographs from a region which includes a twin boundary, in stainless steel. Stacking faults between partial dislocations are seen. They are wide at high stresses. The dislocations are moving, and in (g) the stacking faults have been removed by the moving up of the back partials. (After Whelan, Hirsch, Horne, and Bolliman, 1957).

Plate 48 a and b. Sequence of photographs showing the movement of partial dislocations with stacking faults on two systems. Stair rod dislocations may be seen.
(After Whelan, 1959).

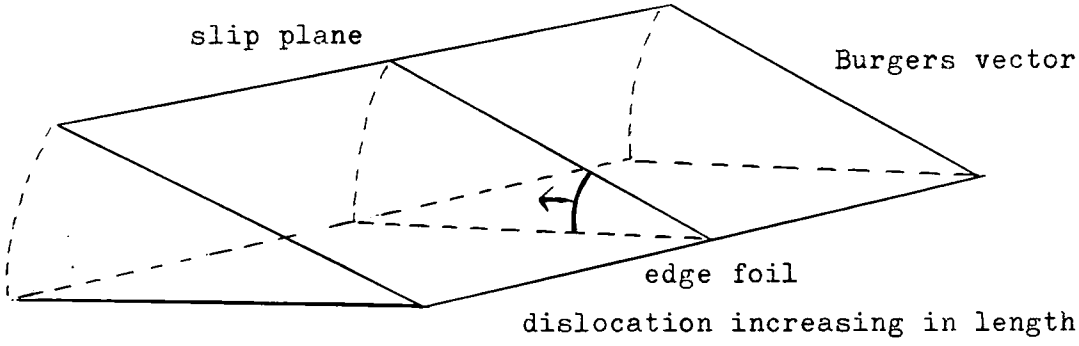

Fig. 64. The nucleation of a dislocation at the edge of a thin foil.
(After Whelan et al, 1957)

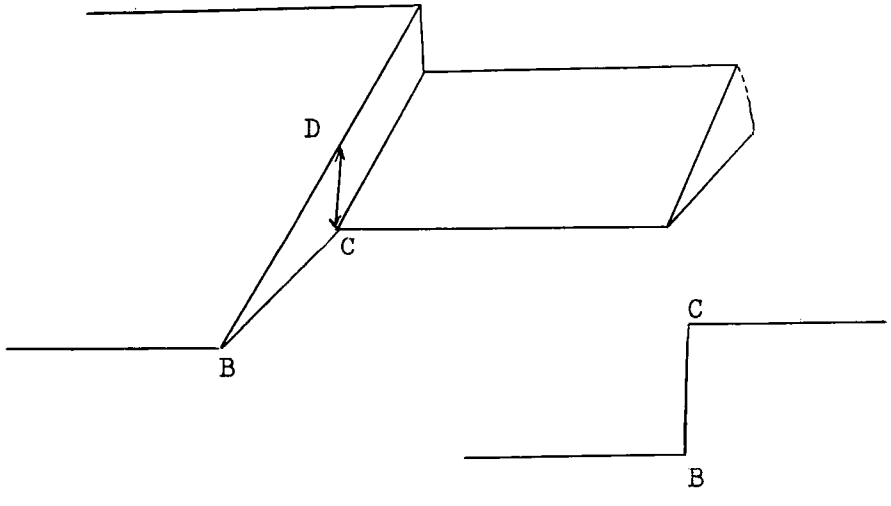

Fig. 65. Steps at the edge of a foil.

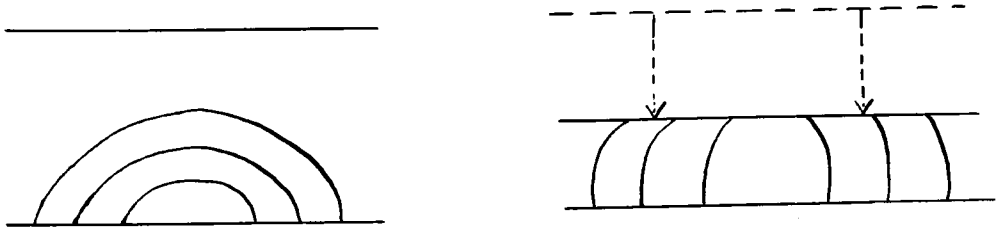

Fig. 66. The effect of thinning down the metal.

dislocations close to a twin boundary. Many of the dislocations are split up into partials with stacking faults. The dislocations are labelled and their movements can be followed. The stacking faults seen in (f) have been removed in (g), due to the back partials moving up.

Finally, in Plates (48a and b), movements of partial dislocations in stainless steel are again shown. In the region are stacking faults on two systems with a stair-rod dislocation at S.

In thin films, under the electron beam, dislocations may be observed running in from the edge of the foil. It has been shown theoretically by Whelan, Hirsch, Horne, and Bollmann (1957) that dislocations are expected to form near the edge. The local stress necessary to nucleate a dislocation at an edge is shown to be only about one seventh that required in bulk material. The general stresses existing in a material are considered to be about one fifth the stress to form a dislocation at the edge.

At the edge of the foil can be seen steps showing displacement normal to slip, see Fig. (65). BC gives a magnified picture of DC. If the angle ϕ is known, the slip step DC can be determined. In tension, the slip is in regular steps, see Fig. (67).

In fatigue, slip alternates in directions, as shown in Fig. (68).

There is the important question of how representative thin

Fig. 67. Steps at the edge of a foil.

Fig. Slip due to fatigue.

foils are of the bulk material from the point of dislocation distribution. If, for instance, there is a piled up group of dislocations, and the metal is thinned down, as in Fig. (66), one would expect some of these dislocations to be attracted to the surface. The lines will be attracted by their mirror image. This group could still be recognised.

According to Hirsch, in practice dislocations parallel to the surface do tend to shorten, but some long dislocations are seen. The pinning effect at the surface helps dislocations to remain in position, and on the whole the thinning down does not have much effect on dislocations.

X-ray data, considered later, agrees with that from electron microscopy.

The relationship between the number of dislocations per unit length of a low-angled boundary, and the angular misorientation of the adjacent subgrains, as determined by electron diffraction, agrees with the theoretical values. The average spacing of such dislocations in stainless steel lies between 100 and 200 A when the angular misorientation is about 1 deg.

7.14 THE USE OF ELECTRON MICROSCOPE OBSERVATIONS TO INVESTIGATE CERTAIN PROPERTIES OF METALS.

Accurate measurements of dislocation density have been made by Bailey (1958) on silver, a metal of intermediate stacking fault energy.

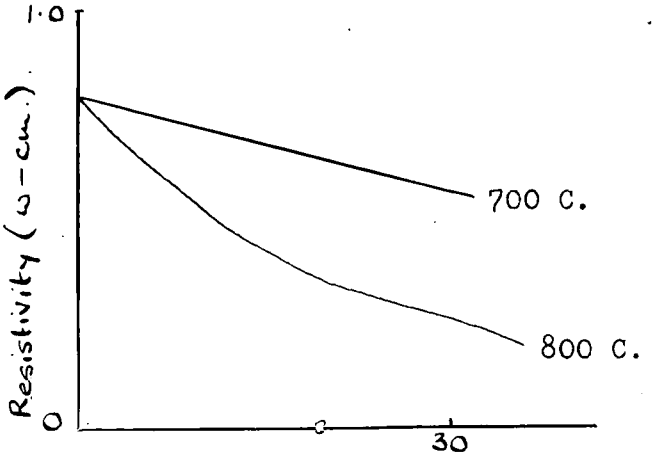

Fig. 69.

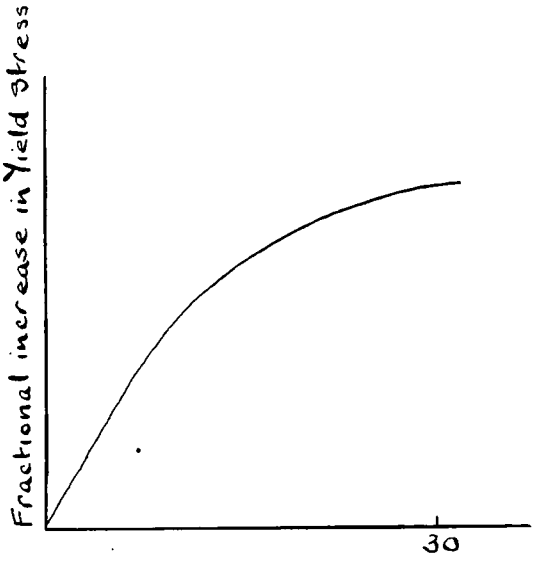

Fig. 70.

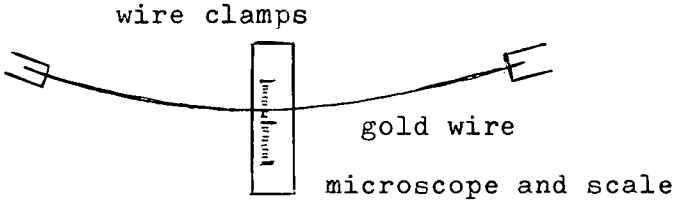

Fig. 71. Method of measuring dimensional changes in a wire.

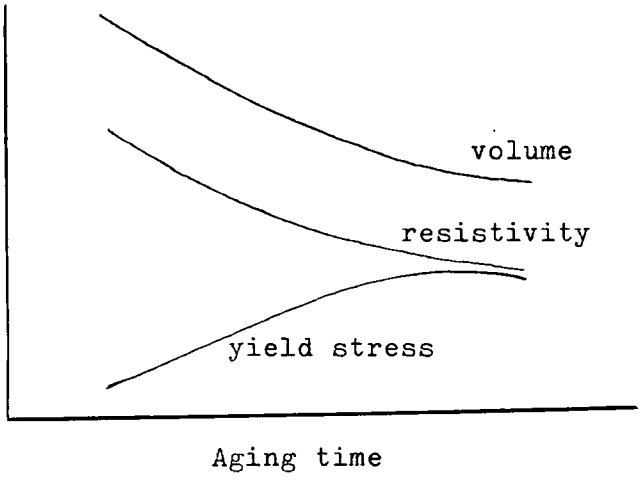

Fig. 72.

Using foils 0.005 inches thick, he measured the total length of dislocation lines in a given area.

Extension %	Dislocation density.
32	$6.8 \times 10^{10}/cm.^2$
21	$5.2 \times 10^{10}/cm.^2$
11	$2.2 \times 10^{10}/cm.^2$

The lengths were worked out knowing their projections and angles of inclination. Slip traces were used to estimate the thickness of the foil.

Bailey compared the values of the energy stored in a cold worked metal with the density of dislocations introduced, and his values agreed remarkably with those predicted by the elastic theory of dislocations, i.e.

Work done on metal	=	Heat released during deformation	+	Stored energy in metal

The energy stored in a cold worked metal is released on annealing at sufficiently high temperatures. Bailey used an isothermal microcalorimeter to measure the rate of release of the stored energy on annealing.

Dealing mainly with pure metals, Hirsch, Silcox, Smallman, and Westmacott (1958), Silcox and Hirsch (1959), and Thomas and Whelan (1959), have studied phenomena when metals are quenched after heat treatment, and also the effects of irradiation. They found vacancies to be the predominant defect. After heating, the metal contains mainly vacancies and a few (about $10^{-7}/cm.^2$)

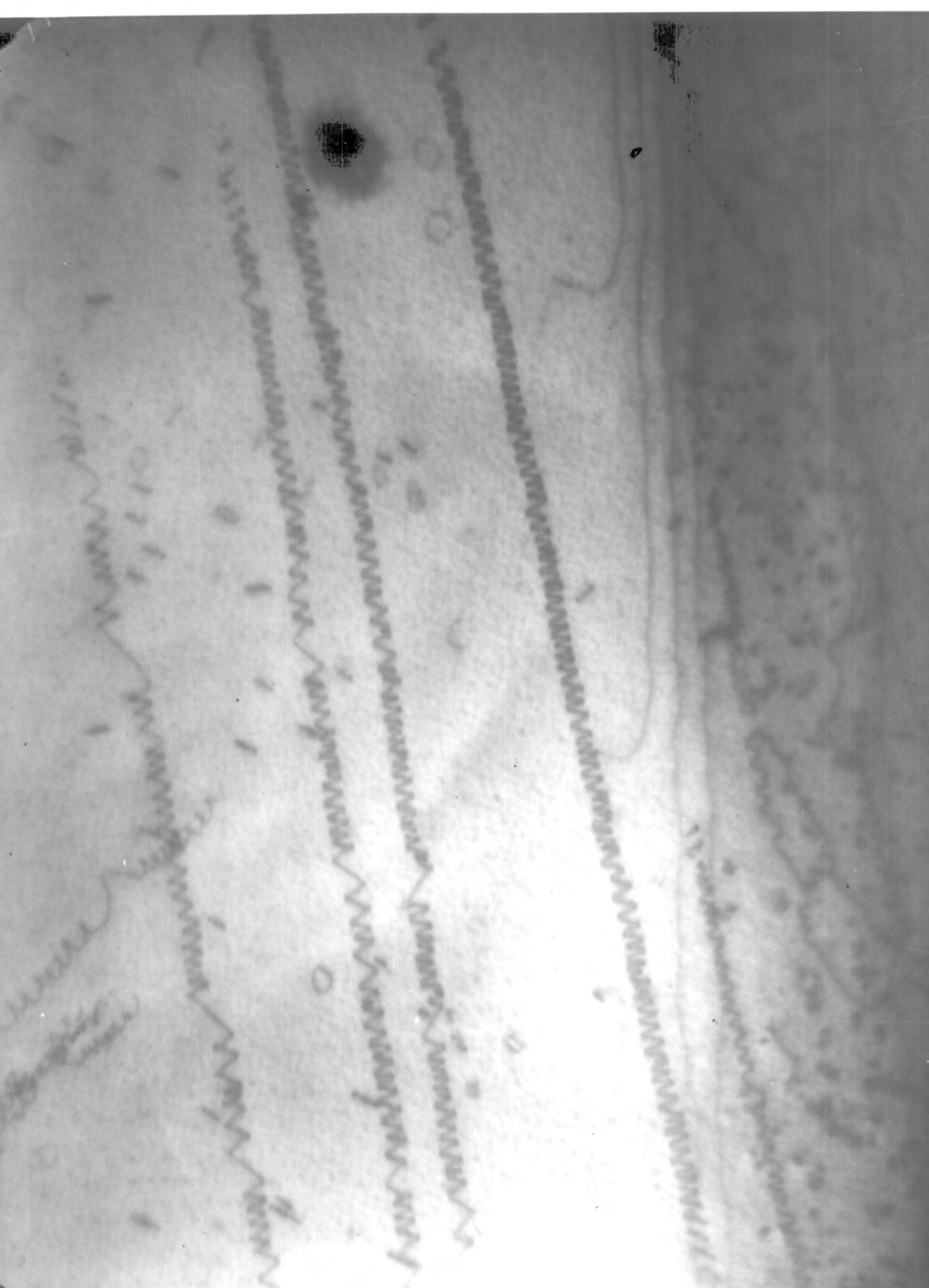

Plate 49. Helical dislocations in aluminium-4% copper quenched from 550 deg. C. (x 60,000) (After Thomas and Whelan, 1959).

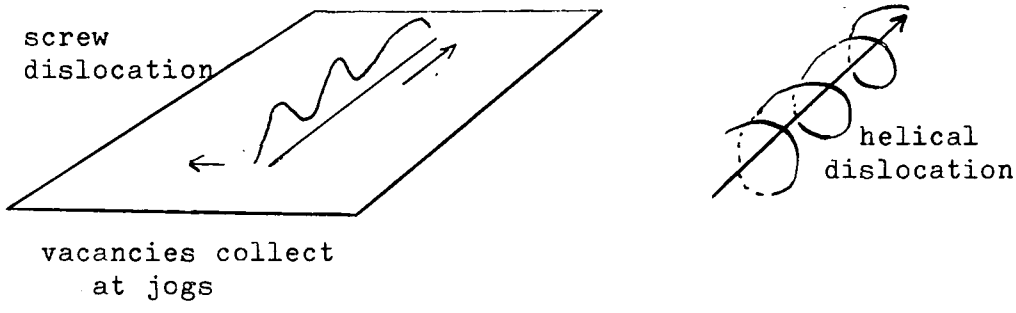

Fig. 73. The development of a helical dislocation.

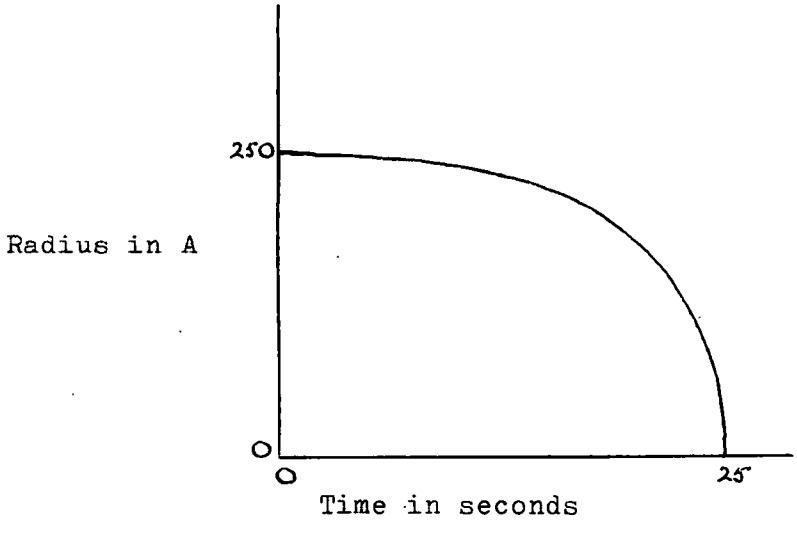

Fig. 74. The shrinking of loops during anneal.

dislocations.

The electrical resistivity ρ of the metal gives an idea of the number of vacancies present,

$$\rho = \rho(T) + \rho(D)$$

$\rho(T)$ is temperature dependent.

$\rho(D)$ is defect dependent.

Vacancies can move around in a metal, and this takes place during heat treatment. Fig. (69) shows how resistivity decays at higher temperatures. Meanwhile the yield stress of the metal increases, Fig. (70). They used gold wire to investigate changes in volume when quenched. Results suggest that vacancies are collapsing and being removed as the temperature falls, see Fig. (72).

There are several possible ways in which vacancies may be removed. The following could act as sinks:

a. Surface.

b. Grain boundaries.

c. Impurity atoms.

d. Dislocation lines,

   1. at jogs,

   2. at screws.

e. Coalesce with other vacancies to give disc shaped, or spherical cavities.

The vacancies trapped at screw dislocation build it up to give a helical dislocation, see Fig. (73) and Plate (49). The disc shaped cavities collapse forming ring dislocations containing

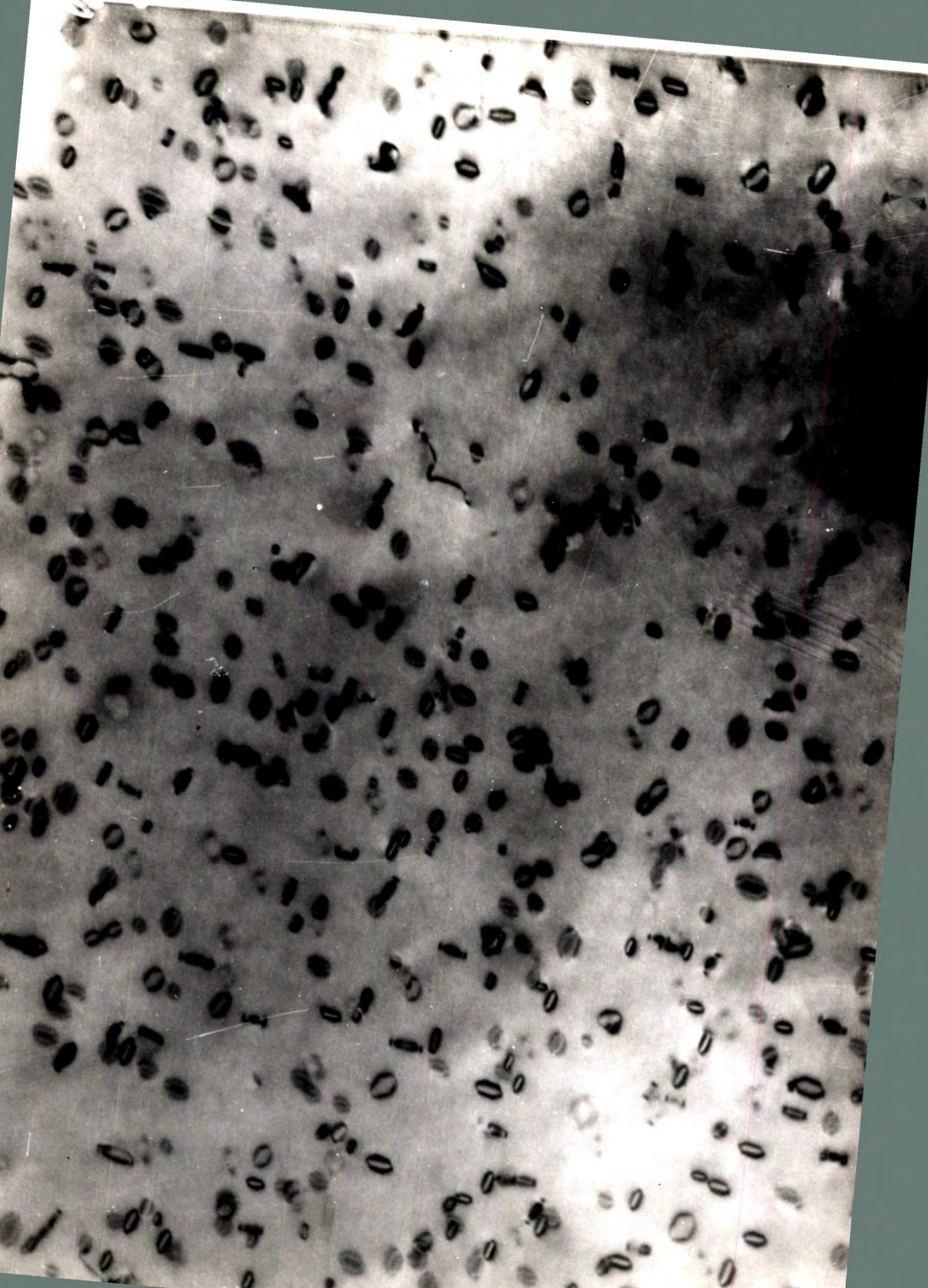

Plate 50. Dislocation loops in aluminium quenched from about 600 deg. C. into iced brine and aged at room temperature. (x 60,000)
(After Silcox, unpublished).

Plate 51. Loops in neutron irradiated copper. The copper was irradiated to 5.6×10^{18} n cm^2. in bulk and then thinned. (x 210,000) (After Silcox and Hirsch, 1959).

stacking faults in their centres. In aluminium a loop is nucleated, but not in gold. If a loop is nucleated, it sweeps away the stacking fault giving a prismatic dislocation.

The concentration of loops is 10^{15}/cc. and their size about 200 A diameter. In a foil about 1000 A thickness, the dislocation density is about 10^{14}/cc. This agrees with resistivity measurements. If the density is 5×10^{14}/cc., and the diameter of the loop 350 A, the vacancy concentration is 6×10^{-5}. Resistivity methods give a vacancy concentration between 8×10^{-5} and 2×10^{-4}.

Experiments with bulk material indicate the loops have a greater diameter, but the dependence of resistivity on concentration of loops due to vacancies, is well established.

Similar loops participate in the mechanism of quench hardening in different metals, see Plate (50), as predicted by Jones and Mitchell (1958) after experiments with the hysil spheres in silver halides.

In neutron irradiated copper loops of 50 A diameter are seen as dots. Increased irradiation enlarges the loops to about 300 A, and also increases the density of the loops, see Plate (51). The effect of irradiation is to make dislocations joggy, and to pin them at various points, hardening the metal. The loops can be annealed out by heating. They shrink rapidly at a rate of about 10 A/sec. for loops of radius 250 A. The loops shrink faster as their radii decrease, see Fig. (74). Also dislocations tend to become smoother, probably due to climb.

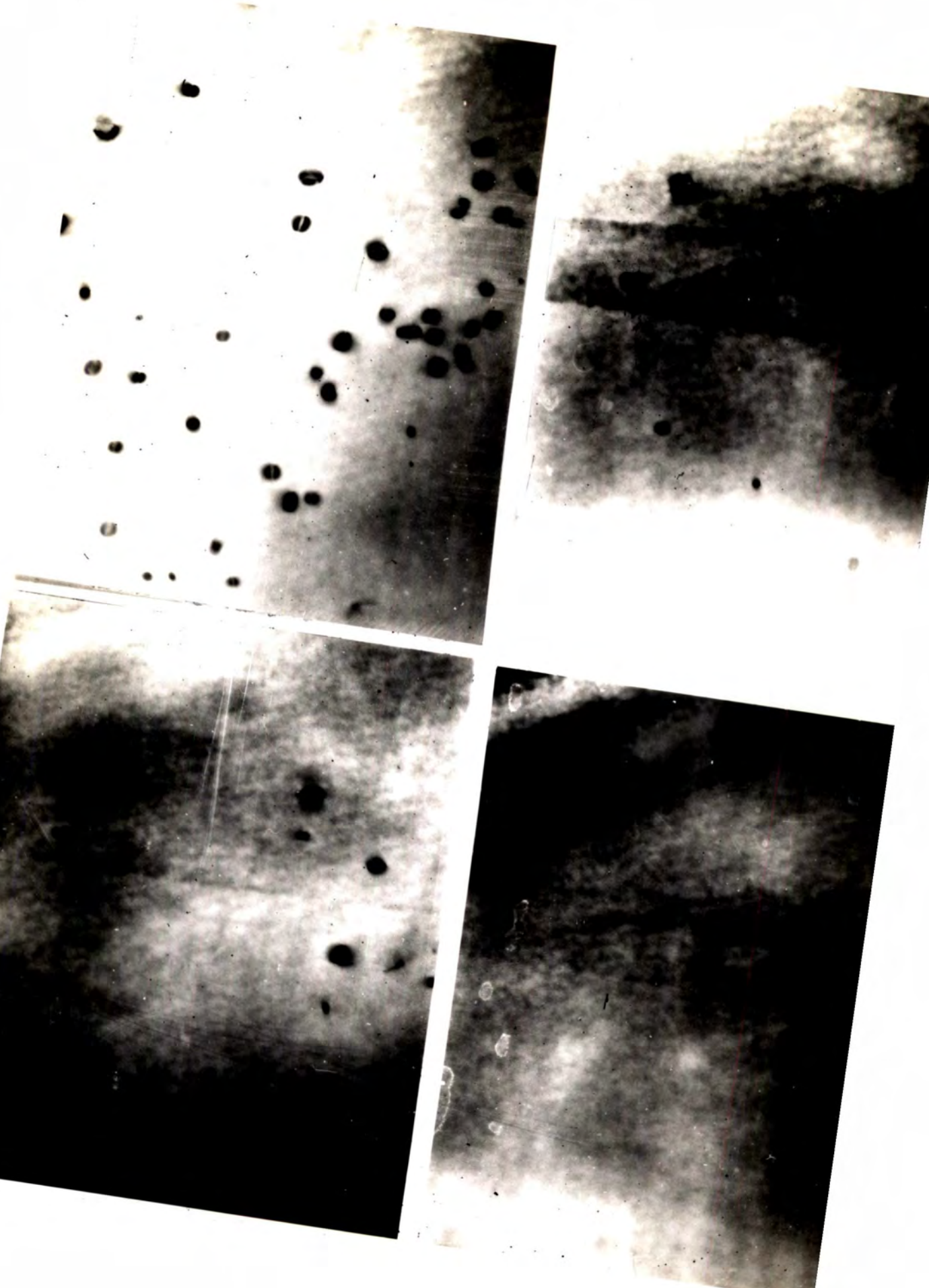

Plate 52. Annealing loops out on the hot stage. The aluminium specimen is at a temperature of about 187 deg. C., and photographs were taken at one minute intervals. (x 60,000)
(After Silcox and Whelan, 1960)

The disappearance of loops is probably the reverse of their formation process, vacancies being given out. The shrinking of loops can be followed using cine sequences as shown in Plate (52).

The observations of thin films agree with theoretical deductions, although it is likely that in bulk material the radii of the loops are greater.

In conclusion one may say that the transmission electron microscope technique is most valuable for checking and amplifying the theory of dislocations. The possibility of filming continuous phenomena at a controlled temperature provides a powerful tool to the study of dislocations, and solid state physics in general. With existing lenses the present resolving power of 5 A could probably be reduced to 2-3 A. The effects of the electron beam on the specimen present the limiting factors. There is displacement of the specimen due to impact of the beam, and due to fluctuations in the electrical supply, and to stray fields. The beam also causes contamination of the specimen due to its thermal effect. Carbon is deposited at the rate of about 1 A per second. It is thought to come from residual material on the inner walls of the microscope. The reduction of these defects to give a resolving power of about 3 A, should enable more structures in metals to be made visible.

PART 8.

THE USE OF MOIRE PATTERNS TO STUDY DISLOCATIONS.

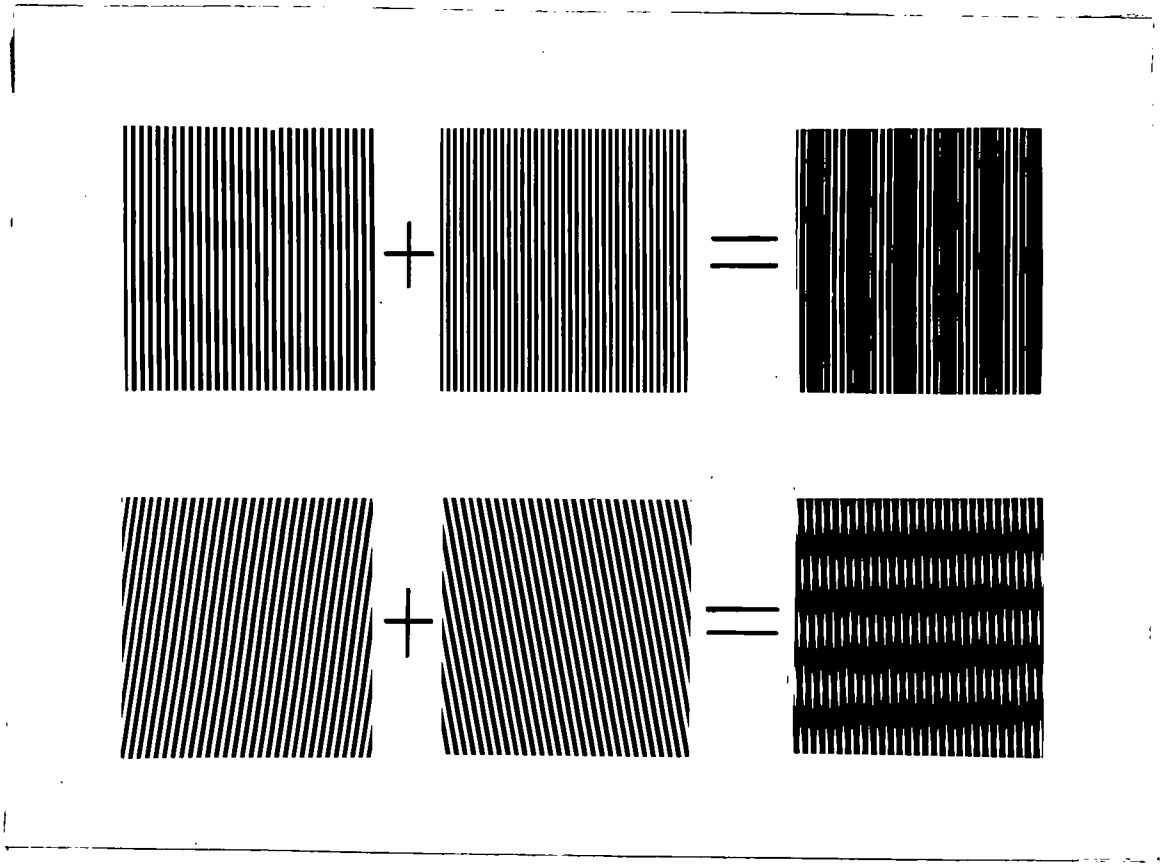

Plate 53. Optical analogue showing the formation of Moire patterns.
(a) With parallel gratings with different spacing.
(b) With like grating and a small relative rotation.
(After Bassett, Menter, and Pashley, 1959).

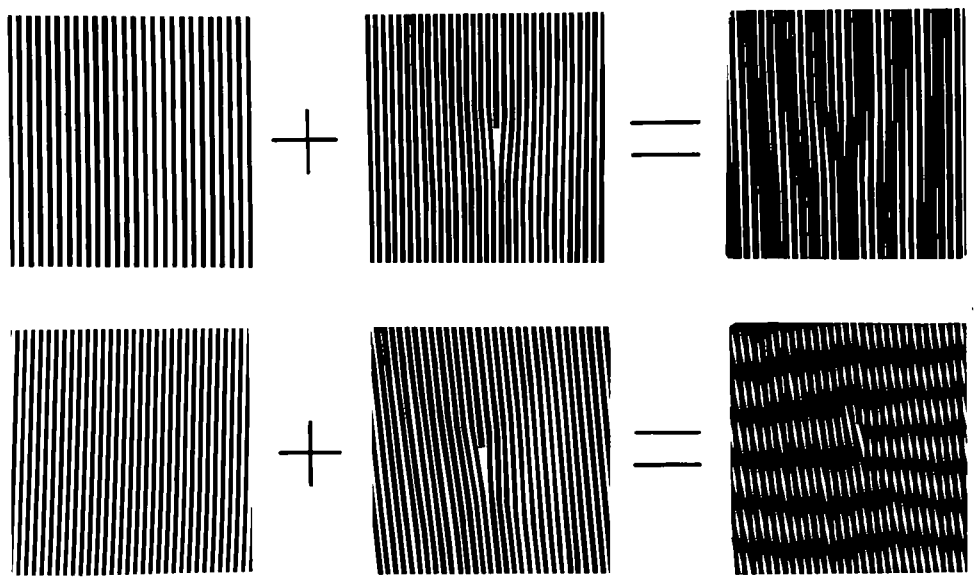

Plate 54. Optical analogues illustrating formation of Moire patterns when one grating contains a dislocation.
(After Pashley, Menter, and Bassett, 1957).

Metal	Crystal Spacings (02$\bar{2}$)	(42$\bar{2}$)	Moire spacings (A) when combined with parallel gold (02$\bar{2}$)	(42$\bar{2}$)	Moire magnification M
Nickel	1.24	0.719	9.2	5.3	7.4
Cobalt	1.26	0.725	9.8	5.7	7.8
Copper	1.28	0.737	11.3	6.5	8.8
Rhodium	1.34	0.773	19.7	11.4	14.7
Palladium	1.37	0.792	29	17	21
Platinum	1.38	0.798	35	20	25

Fig. 75. (After Bassett, Menter, and Pashley, 1958).

8.1 INTRODUCTION.

The resolving power of the electron microscope used for direct observation has been stated to be not less than 5 A. For spacings below this figure an indirect method must be used, by forming Moire patterns between two overlapping crystals. In this way spacings of even less than 1 A may be studied, Bassett, Menter, and Pashley (1958).

The condition is similar to that obtained in optics by Abbe (1837).

8.2 THE PRODUCTION OF MOIRE PATTERNS.

Considering the optical analogue, if we have two slightly differently spaced lattices, and superimpose one on the other, the resultant image is a Moire pattern, see Plate (53).

In Plate (54) five spacings of the first grating have the same width as six spacings in the second grating. The first grating is perfect, the second has an edge dislocation. When placed parallel, the resulting Moire pattern is effectively the magnified image of the dislocated grating. It may have been impossible to resolve the single lattice but possible to observe the dislocation in the Moire pattern.

Moire patterns are formed using the electron microscope by the direct beam and the beam diffracted twice by the two crystals. The two beams emerge not quite parallel.

If the spacing of the gratings is d_1 and d_2 respectively,

then the spacing of the Moire pattern:

$$D = \frac{d_1 d_2}{d_1 - d_2} = M d_2$$

Where M = Moire Magnification

$$= \frac{d_1}{d_1 - d_2}$$ See Fig. (75).

We are considering here the image of the grating with d spacings, by putting the other grating on top of it.

It can be shown that if one crystal is rotated through an angle θ with regard to the other, then the Moire pattern will rotate through an angle ω where

$$\omega = M\theta$$

This indicates that the parallel Moire patterns are very sensitive to lattice distortions, or misalignment of the two lattices.

8.3 THE STUDY OF DISLOCATIONS.

The number of extra half-lines is a measure of the Burgers vector perpendicular to the planes resolved, but there is no direct evidence in such images to allow distinction to be made between the different types of dislocation. Most of the work has been carried out using films about 200 A thick, but results are possible for films ranging in thickness between 50 A and 1000 A.

To use Moire patterns one needs an extensive single crystal film which may be prepared by an evaporation method. The

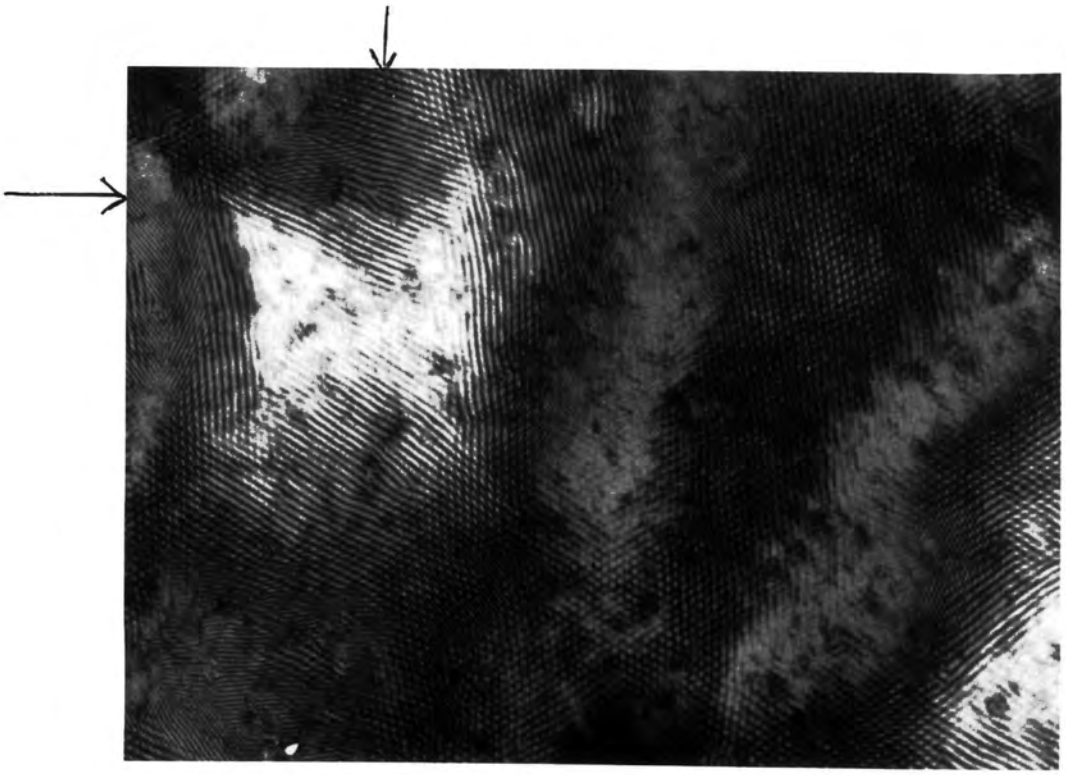

Plate 55. Moire pattern formed by superposition of single crystal films of gold and palladium so that their lattice planes are parallel. A dislocation can be observed near the top left hand corner of the picture. (x 260,000) (After Bassett, Menter, and Pashley, 1958).

	P $[\frac{1}{2}\frac{1}{2}0]$	P_1 $\frac{1}{6}[12\bar{1}]$	P_2 $\frac{1}{6}[211]$
(220)	2	1	1
(202)	1	0	1
(022)	1	$\frac{1}{3}$	$\frac{2}{3}$
$(2\bar{2}0)$	0	$-\frac{1}{3}$	$+\frac{2}{3}$

Fig. 76 a.

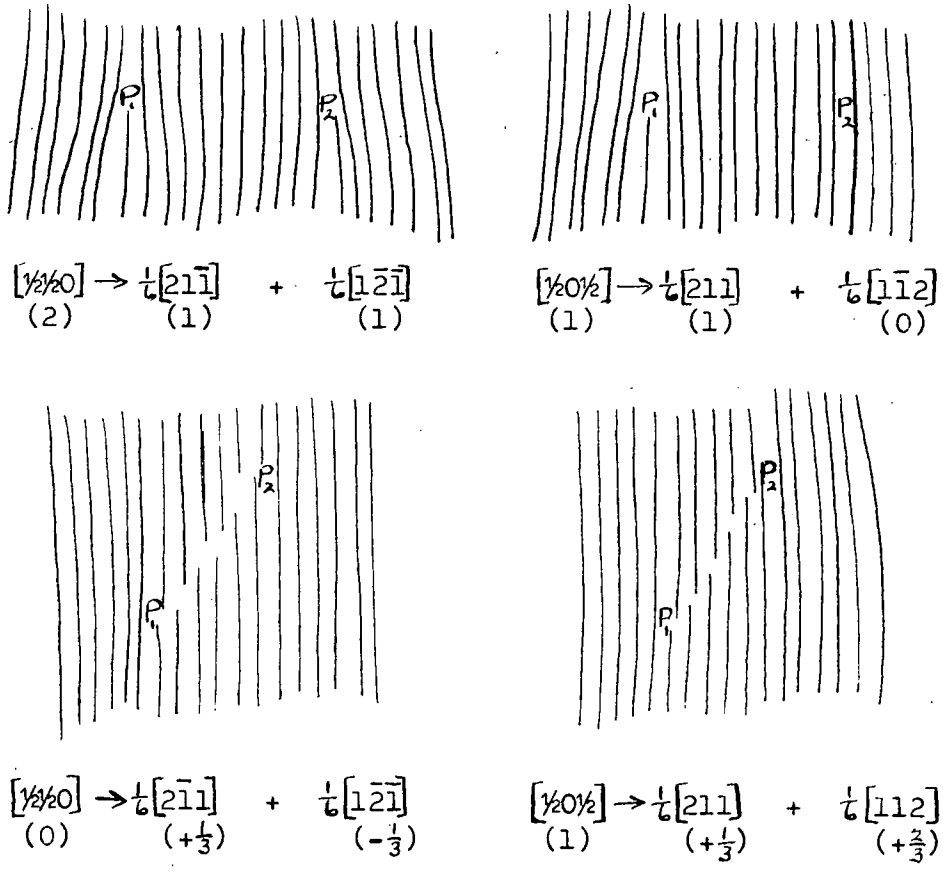

Fig. 76 b. The appearance of partials and their associated stacking faults in the projected image of (220) planes. P_1 and P_2 are the two partials.
(After Bassett, Menter, and Pashley, 1958).

specimens are prepared by two different techniques:

(a) the second crystal is deposited by evaporation onto the first.

(b) the two crystals are prepared separately, and then superimposed.

The second method is preferred as it gives a more regularly spaced pattern.

To detect a dislocation the following conditions are required:

(a) the dislocation line must pass through one film only.

(b) the Burgers vector of the dislocation line must have a component perpendicular to the lattice planes, which give rise to the patterns.

Plate (55) shows a Moire pattern formed by the superposition of single crystal films of gold and palladium. Their lattice planes are parallel.

If a dislocation in the F.C.C. system is split into two partial dislocations, the separation of the two partials depends upon the stacking fault energy. According to Seeger (1955), the equilibrium separations are 35 A for copper, 7 A for aluminium, 18 A for nickel, and 160 A for cobalt.

When the separation is less than one Moire pattern spacing, it is not distinguishable from an unsplit dislocation.

The number of half-lines due to partial dislocations is given in Fig. (76). Here the reaction $[\frac{1}{2}\ \frac{1}{2}\ 0] \rightarrow \frac{1}{6}[121] + \frac{1}{6}[211]$, relating the Burgers vectors of the complete dislocation to the Burgers vectors of the two partial dislocations in the F.C.C.,

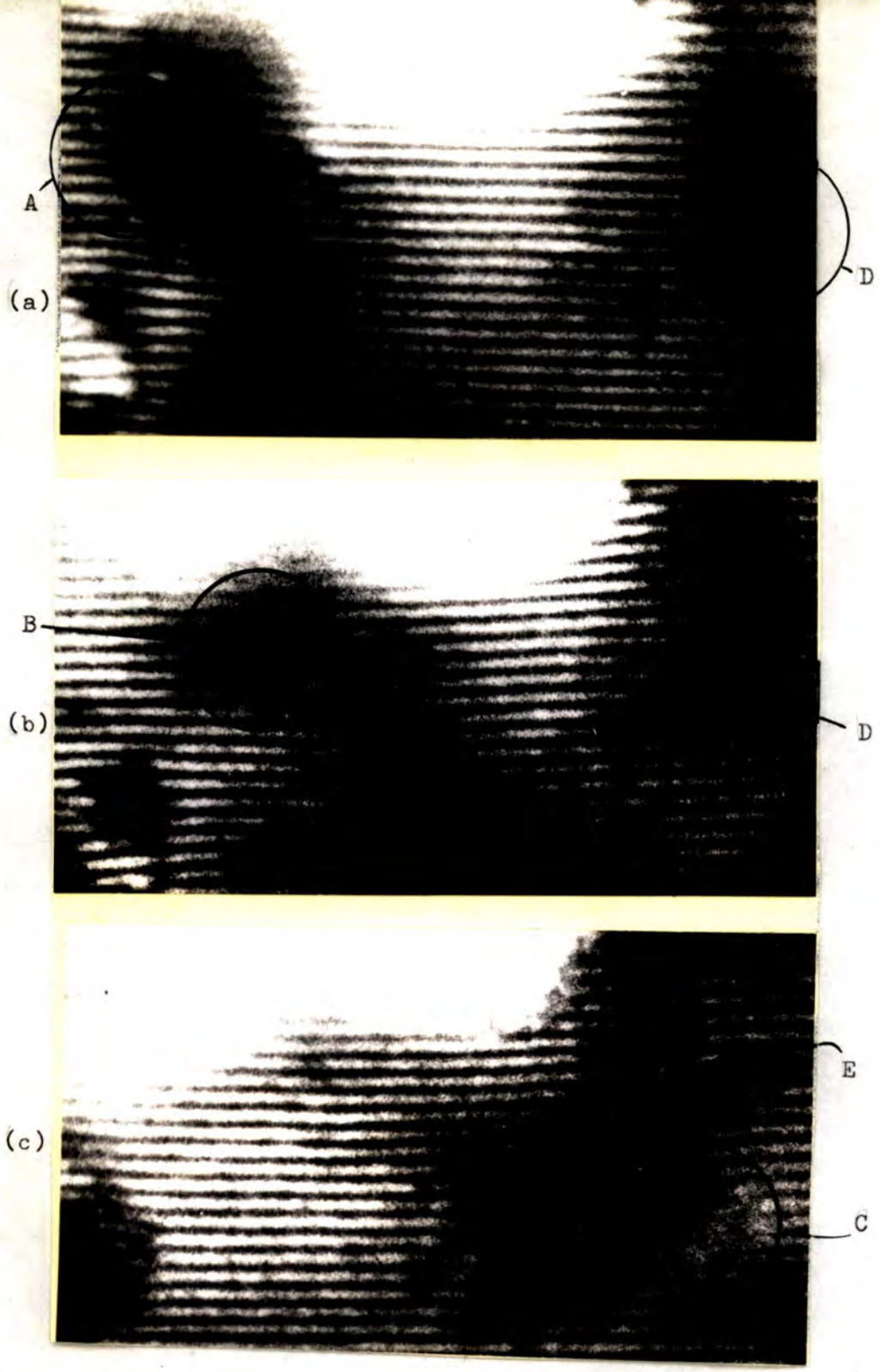

Plate 56. Sequence showing the movement of a dislocation. Films of gold and palladium were used. The dislocation A in (a) has moved to B in (b) and then to C in (c). This has been accompanied by dislocation D in (a) moving to E. (x 1.800,000)
(After Bassett, Menter, and Pashley, 1958).

is considered, see Heidenreich and Shockley (1948). The appearance of the partials is shown in Fig. (76).

Movement of dislocations has been seen during observation of Moire patterns. This is probably due to the localized heating caused by the electron beam.

It has not proved possible to record movements by means of cine techniques, as, due to the high magnifications required to produce the patterns, there is not sufficiently high intensity. Photographs have been taken in sequence, Plate (56), but rapid movements escape unobserved, (see Bassett, Menter, and Pashley, 1958).

8.4 CONCLUSION.

Moire patterns are clearly of value due to the high resolving power obtained, for the detection and estimation of the density of dislocations. They also tell us much about the Burgers vector of a dislocation.

One disadvantage of the method is the possibly undesirable influence due to the interface between the two sections. Also, it is not easy to distinguish between types of imperfections. For instance, large aggregates of vacancies could be mistaken for dislocations close together.

Consequently great care must be used in the interpretation of observations.

PART 9.

THE USE OF REPLICA TECHNIQUES IN THE STUDY OF METAL SPECIMENS WITH THE ELECTRON MICROSCOPE.

9.1 INTRODUCTION.

Objects too thick to be studied by transmission electron microscopy can be examined by replication.

Replica techniques have two main applications in the study of metals. The first of these is in the high resolution study of the surface topography including slip lines, cleavage steps, etch pits, and other detail. The second application is in the use of the replica to extract particles of second phase from the matrix. Such particles may be examined directly in the microscope, and by subsidiary techniques such as electron diffraction, and by X-ray methods.

To be suitable for electron microscopy, a replica must meet certain rather exacting requirements. It must be transparent to the electron beam, it must be structureless so that any structure seen is that of the specimen surface from which it is taken, and it must be able to withstand the electron beam and the necessary handling.

9.2 TYPES OF REPLICA.

The following types of replicas are commonly used:

(a) Plastic replicas.

(b) Plastic-carbon replicas.

(c) Direct carbon or silicon monoxide replicas.

(d) Oxide replicas.

(e) Triple replicas.

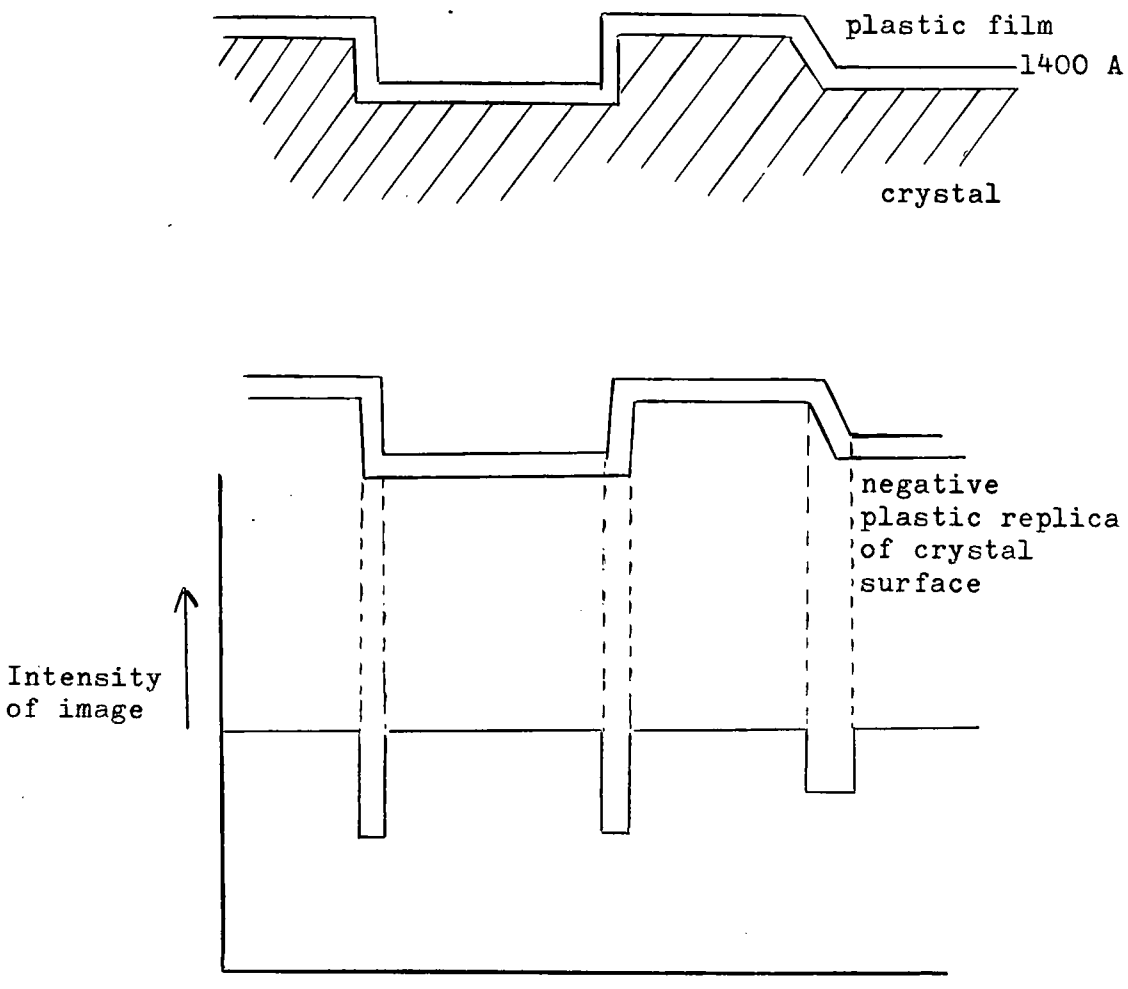

Fig. 77. The plastic replica.

(a) Plastic Replicas.

This is a single stage process, producing a negative replica. It is prepared by flowing a solution (e.g. formvar dissolved in dioxane) over the surface of the specimen. The thickness of the film is determined by the concentration of the solution, but in deciding the thickness a compromise has to be made. The replica must not be too thin, as it is then easily damaged when stripping, but must be made as thin as possible to give the best contrast when viewed in the electron microscope. The thickness used is about 1400 A.

As this replica is difficult to strip off the specimen surface, a backing layer is often used to protect the plastic. This backing is dissolved off before viewing in the electron microscope.

The surface contours of the metal are thus reproduced as differences in thickness of the film, which produce the image by virtue of the differential electron transmission, see Fig. (77).

It is possible to take successive replicas up to about 10 with only slight loss of detail. This is an important advantage.

The replicas are not mechanically strong and are easily strained, producing strain lines. The plastic tends to disintegrate under the electron beam, and if water is present in the replicas fogging results. Air bubbles produce spots.

The method is simple and does not damage the surface of the specimen.

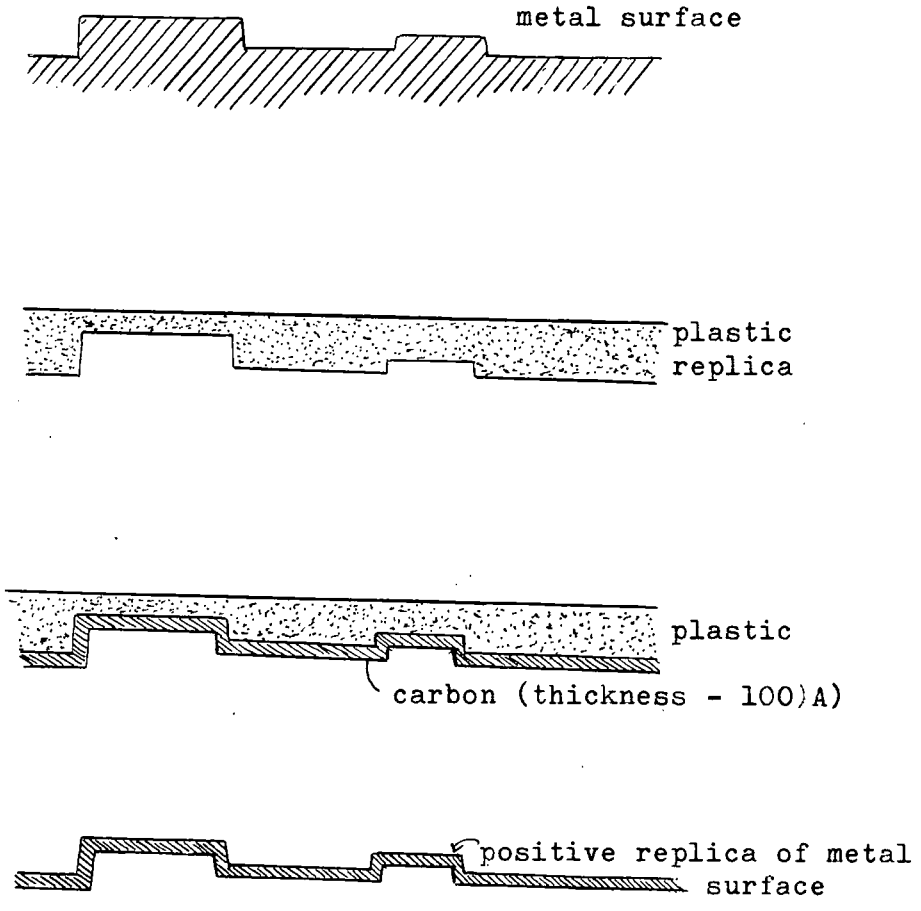

Fig. 78. Plastic-carbon replica.

The resolving power is limited by the size of the molecules in the film, and due to scattering of electrons by the film. It is in the region of 200 A.

(b) Plastic-carbon Replicas.

These are obtained by means of a two stage process and are positive replicas. A thick plastic replica produced as described in (a) is replicated with carbon. The plastic is then dissolved, leaving a positive carbon replica of the specimen surface.

The method does not damage the specimen surface, and it is possible to get a resolving power of about 50 A. The films are very stable in the electron beam.

The disadvantages are that it is more difficult to see pits and steps than with the direct replica, and being a two-stage method, it takes a longer time to produce. See Fig. (78).

(c) Direct Replicas.

This involves the evaporation of carbon or silicon monoxide directly onto the surface of the specimen. Greater resolving power is obtained, but the specimen surface is destroyed on stripping off the replica. The carbon replica method was devised by Bradley, (1954).

The carbon exhibits very little self-structure at the resolutions used. It has been used to study the tempering of steel, and gives a resolving power of about 15 A. The steel is etched in 5% Nital, and then carbon evaporated from an arc for 2 seconds. This gives a 200 A thick film which is stripped in

5% Nital. The carbon films are quite strong and easy to handle. Bradley has used films as thin as 25 A.

Slip steps on α brass can be clearly seen using this type of replica. The brass is polished in 67% orthophosphoric acid, deformed 30% to 40%, and the carbon film evaporated onto it. The replica is stripped in 10% hydrochloric acid, 30% nitric acid.

The carbon film is also used in the extraction replica method of Nutting and Smith (1956) to study the arrangement of precipitated material in a metal surface.

(d) Oxide Replicas.

Oxide replicas have been used successfully for aluminium and aluminium alloys. A thin surface layer of the specimen is converted to oxide anodically, and the oxide layer used as the electron microscope replica. The film must be of uniform thickness as this controls the density of the image.

Contrast and resolution are very good. The films are mechanically strong, easy to handle, and not affected by the electron beam.

The disadvantage is similar to the direct replica method as the surface of the specimen is destroyed on stripping the oxide replica. See Keller and Geisler (1947).

(e) Triple Replicas.

If a material will not etch, or if etching is undesirable, special methods must be employed.

One method is to prepare a plastic replica of the specimen

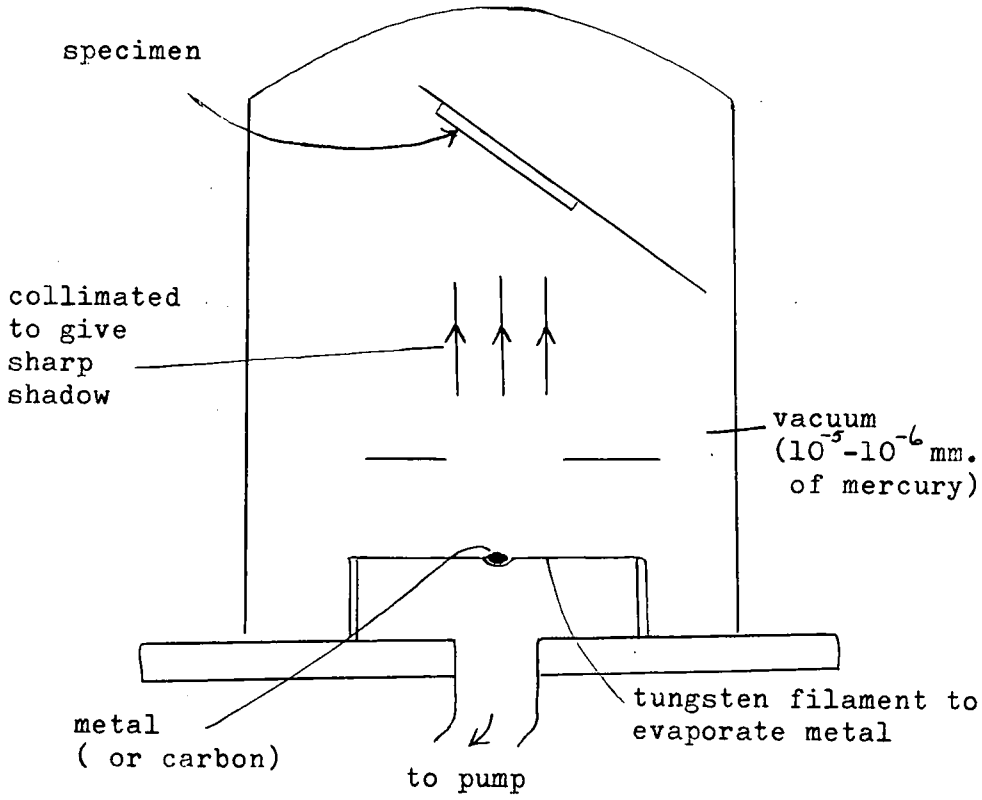

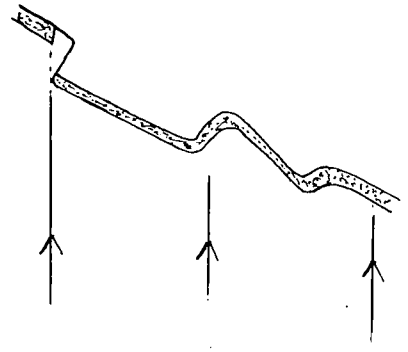

Fig. 79. Shadow casting apparatus.

surface, and then evaporate a thin layer of aluminium onto the plastic replica. Following this, an oxide replica is made from the aluminium film.

Another method would be to evaporate a thin film of aluminium directly onto the specimen surface. This must be a continuous thin layer about 10 A thick. A carbon film is evaporated on top of the aluminium, and the aluminium then dissolved away. Some detail is obscured by the intervening aluminium film.

9.3 SHADOWING.

For the coarser structures, the methods considered provide fairly satisfactory information. For all types of structure, however, shadowing assists in detecting detail. See Figs. (79), (80).

This is usually accomplished by stripping the replica from the specimen, then placing this replica in a vacuum chamber, evacuated by a mercury pump, and evaporating carbon onto the replica. The replica is tilted at an angle to the source of the evaporating metal so that the vapour, travelling in straight lines, is deposited on the contours of the replica at an oblique angle. When viewed, the shadowing indicates the geometry of the surface as it would appear when obliquely illuminated, and so gives a three dimensional effect. If the length of shadow and the angle of illumination are measured, the step heights may be estimated. Shadow-casting at an angle of 45 deg. is found to be successful in producing short shadows which do not obscure too many of the

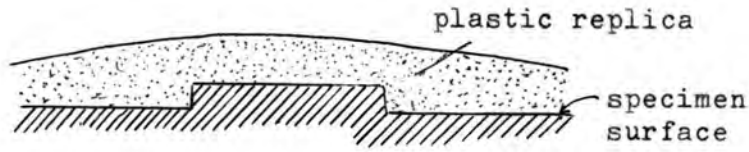

replica stripped from specimen

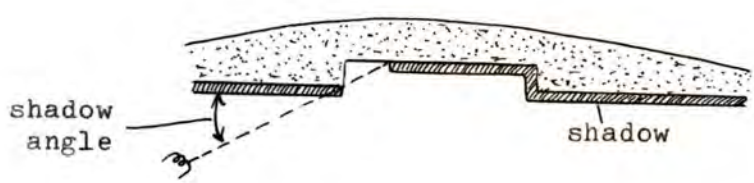

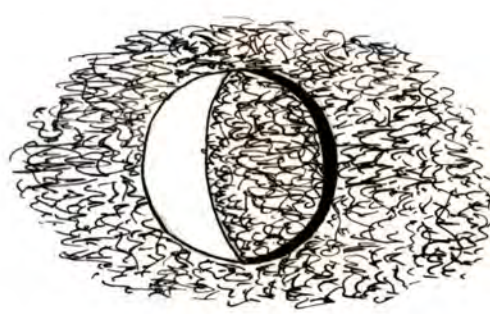

Fig. 80. Shadowing.
(After Teague, 1953).

structural features, and is much easier to interpret.

Shadowing can be applied to all the methods considered, and is useful up to a point, but it does obscure some detail.

9.4 THE METHODS OF PREPARATION OF THE SPECIMENS.

The surface is first of all polished to reveal the true structure of the material. Electropolishing has proved successful in many cases, but it does sometimes give a contour pattern characteristic, not of the metal, but of the particular electrolytic polishing treatment. Mechanical polishing is not satisfactory as one cannot eliminate a thin surface layer of flowed metal.

For the best results with oxide replicas, chemical polishing is employed. A very successful method is called the Alcoa R5 Bright Dip, patented by the Aluminium Company of America. This involves firstly grinding, and polishing the specimen, and then dipping for between two and three minutes. This produces an excellent polish, and reveals many fine microstructural lines.

After polishing, the aluminium specimen is deformed. It is then etched to determine the surface orientation. Etch pits appear on (100) planes. These, as well as giving the orientation, can be used to measure slip distances.

The metal surface is next oxidized under controlled conditions. Films of between 200 A and 400 A thickness are ideal. They are cut to size for the electron microscope specimen holder.

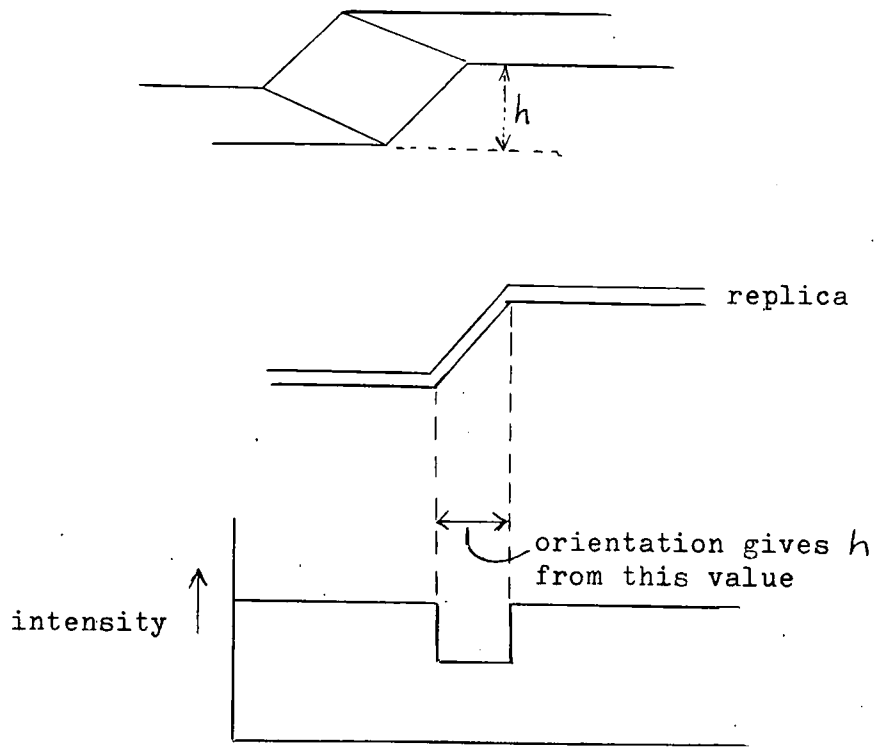

Fig. 81. Measurement of step height using replica.

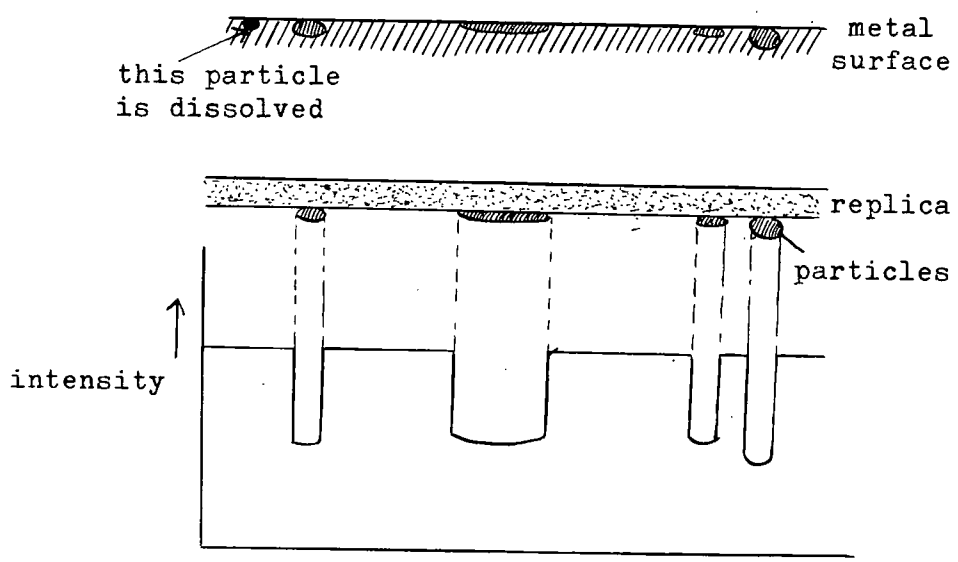

Fig. 82. Extraction replica for the examination of constituent particles.

9.5 APPLICATIONS OF THE REPLICA METHODS.

All metal specimens except thin films are opaque to the electron beam. Replicas are used to study surface features and provide information regarding slip bands, grain boundaries, fracture surfaces, and other features, see Fig. (81). They are very useful when used in conjunction with direct observation of the specimen, using the electron microscope. Correlation between surface features and internal structure may thus be observed.

Both carbon and oxide replica methods are useful as 'extraction replicas' to examine fine constituent, and precipitate particles. These are usually retained in place in the replica, permitting the determination of their size and shape, and of their distribution. Precipitate particles at grain boundaries, and within grains, can be shown.

An example of this is in the study of the aging of aluminium containing a small amount of copper. Copper particles in the surface are slow to oxidise and become attached to the oxide film with the result that differences in density of the image will be produced depending upon the opposition of the particular particles to the electron beam. As shown in Fig. (82) some particles may be completely dissolved.

Thomas and Nutting (1959) observed helical dislocations in aluminium 4% copper alloys quenched from the solid solution temperature. They studied thin foils using transmission electron microscopy, and took oxide replicas from samples of the alloy.

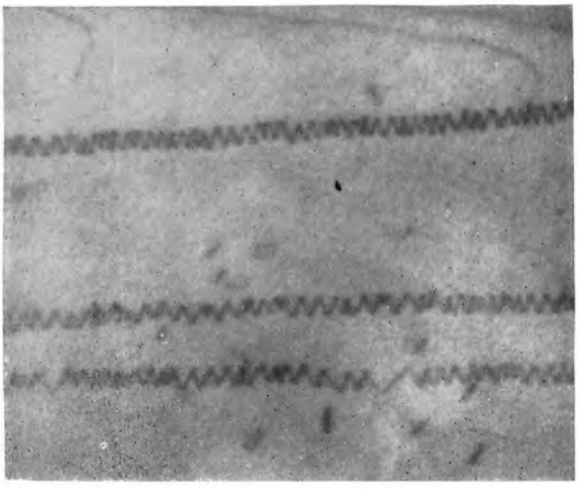

Plate 57. Thin foil of specimen quenched from 540 deg. C. (x 40,000) (After Thomas and Nutting, 1959).

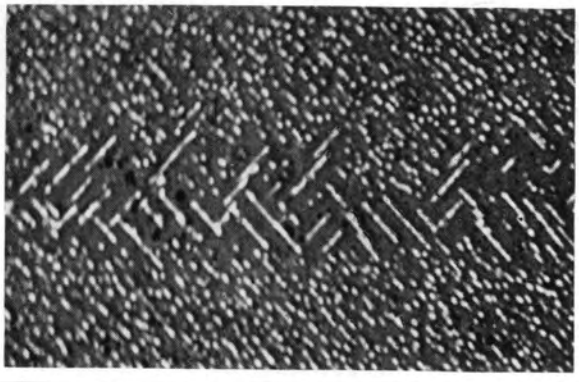

Plate 58. Oxide replica from specimen quenched from 540 deg. C. and aged 84 hours at 165 deg. C. (x 40,000) (After Thomas and Nutting, 1959).

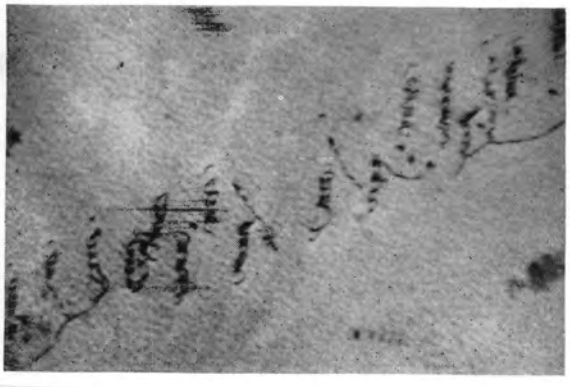

Plate 59. Thin foil of specimen quenched from 540 deg. C. (x 30,000) (After Thomas and Nutting, 1959).

They found the helices to have axes parallel to $[\bar{1}10]$ directions. Plate (57) shows the dislocations in a thin foil viewed along their length. Plate (58) shows an oxide replica with the preferential precipitation of copper atoms on the edge components of the helical dislocations. Plate (59) shows helices in a thin foil observed on inclined slip planes.

PART 10.

X-RAY METHODS.

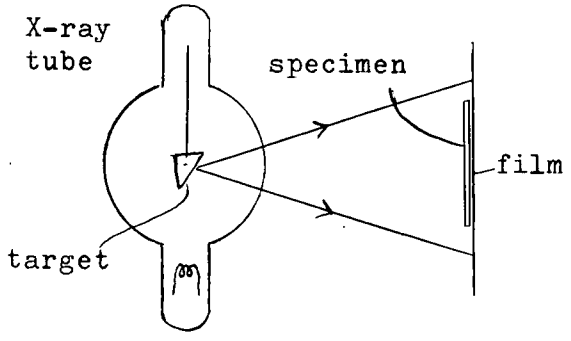

(i) Contact microradiography.

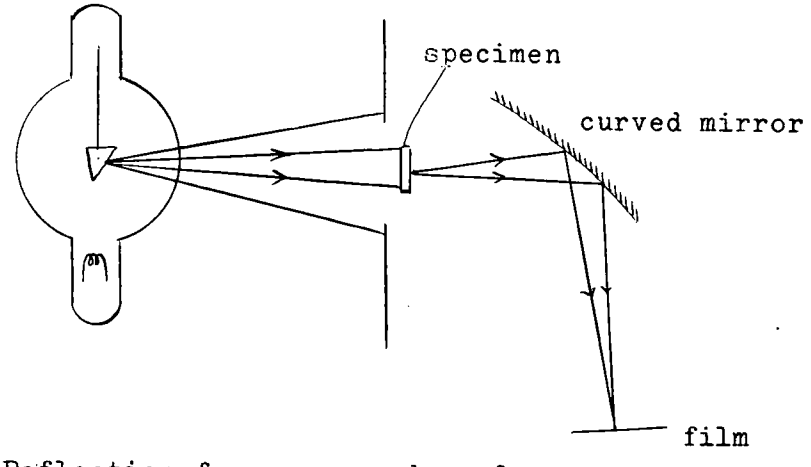

(ii) Reflection from a curved surface.

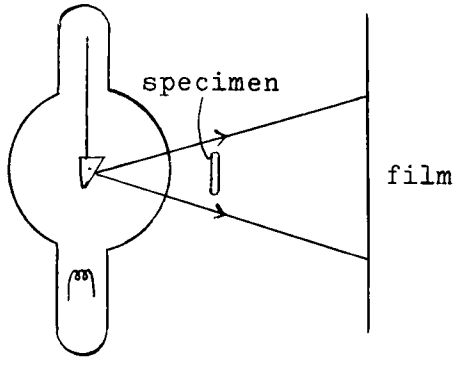

(iii) Projection by a source (low magnification).

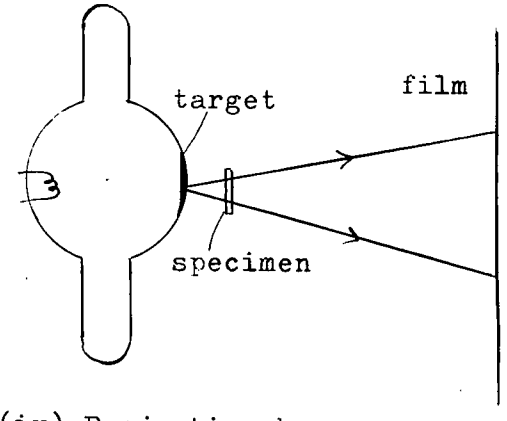

(iv) Projection by an ultra-fine focus (high direct magnification).

Fig. 83. The types of X-ray microscope. (After Cosslett, 1957).

10.1 INTRODUCTION.

X-rays have several properties which make them useful for microinvestigation. They have short wavelengths, in the order of 10^{-4} microns compared with 0.4 to 0.7 microns for visible light rays. This promises a high resolving power, comparable with that attained using the electron microscope, as the resolving power of an optical system is proportional to the wavelength used. X-rays also have great powers of penetration and may be passed through materials opaque to light.

A great advantage of X-rays, in common with the electron microscope, is that analysis may be combined with microscopy. Unfortunately, the refractive index of materials for X-rays is too close to unity for their use with lenses to be practicable. Reflection, contact, and shadow projection methods are used and descriptions of these, and their applications, may be found in the book edited by Cosslett, Engstrom, and Pattee (1957), and papers by Cosslett and Nixon (1953), and Nixon (1955). See Fig. (83).

The shadow projection method allows higher resolution and is simpler than the other methods. The principle of the microscope is shown in Fig. (84).

A point source of X-rays is used to project shadow images. The size of the electron spot on the target governs the size of the X-ray source, which in turn controls the sharpness of the image and the resolution attainable. As the source decreases in size, longer exposure times are required. Using sources of

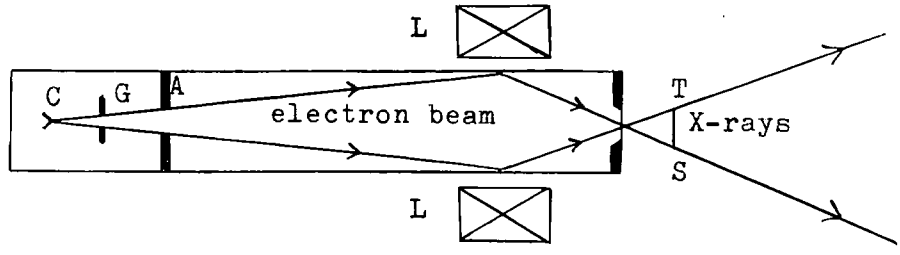

Fig. 84. Shadow projection microscope.
(After Cosslett, 1957).

C = cathode
G = grid
A = anode
T = target
S = specimen
L = magnetic lens to converge electron beam
P = photographic plate

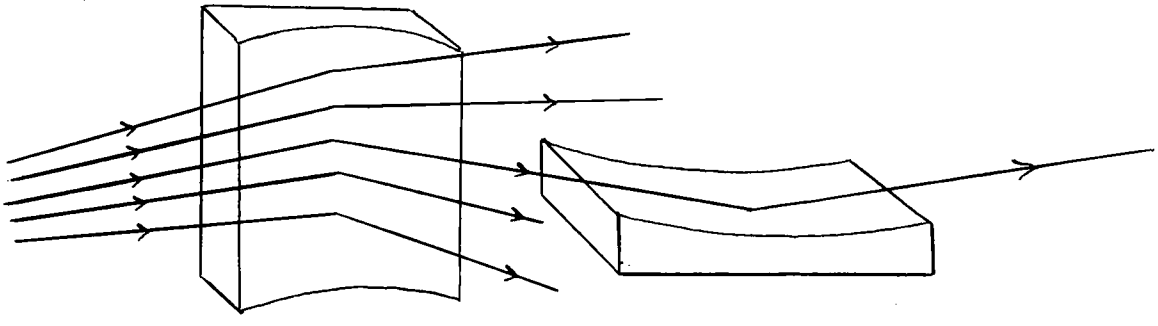

Fig. 85. Two-mirror focusing system of a reflecting microscope.

diameter about 0.1μ, a resolving power of 1μ, which is better than that of optical microscopes, has been achieved. Cosslett and Nixon (1953) consider the best possible practical resolving power to be in the region of 100 A. This is governed by the fineness of the electron beam, and with existing apparatus the exposure times would be of the order of hours. Correction of the spherical aberration of electron lenses will enable an increase in tube current, giving a more intense source. A cathode of higher specific emission would also help in improving resolution.

Reflection microscopes use mirror systems to focus the X-rays, see Fig. (83). The X-rays are totally reflected at an air-solid surface, and the critical glancing angle for X-rays of wavelengths of about 1 A is of the order of 0.1 deg. for aluminium, and 0.5 deg. for gold or platinum. Grazing incidence is necessary for efficient reflection, and focusing takes place only in the plane of incidence. Thus, to focus rays from a point object, a second mirror normal to the first must be used, as shown in Fig. (85). The practical resolving power is about 1μ, but with more perfect mirrors a resolution of 500 A is likely. The problem of Reflection Microscopy is treated by P. Kirkpatrick, (1957).

The availability of a plate (Gevaert Plates, 'Scientia' series, 9E 50 Lippmann emulsion type 400539) with a very fine grain size has enabled Votava, Berghezan, and Gillette (1957), using microradiography, to take high resolution stereomicro-radiographs. They studied aluminium containing 10% silver, and

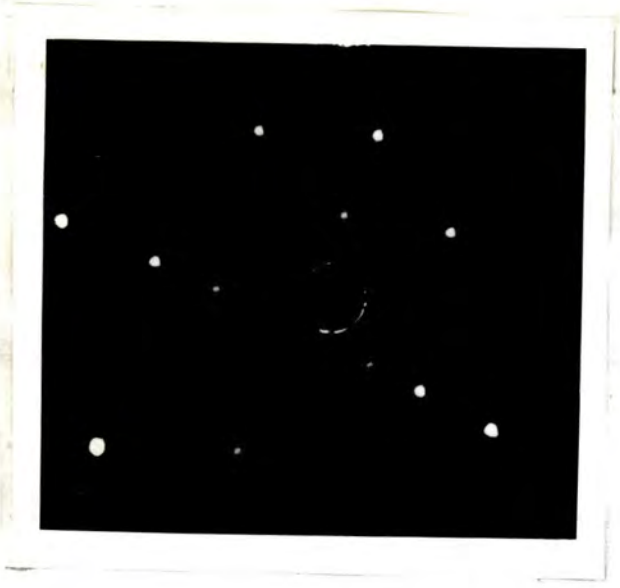

Plate 60. Laue back-reflection photograph of an unstretched silver single crystal. (After Andrade, 1950).

Plate 61. Laue back-reflection photographs of a highly stretched silver single crystal. (After Andrade, 1950).

the resolving power attained was about 0.5μ. Precipitation along grainboundaries, and precipitation in the matrix, may be clearly observed in a published photograph, page 608 of their article.

The thickness of the foils used is about 0.04 mm., and to take stereoradiomicrographs, the specimen and the film are tilted at 4 deg. to the X-ray beam.

The X-ray methods already described use the selective transmission depending upon the different absorption coefficients of the constituents. They reveal only differences in chemical composition, and thus cannot be applied to pure metals. Selective (Bragg) reflection may, however, be used with pure metals.

The effects of dislocation networks on diffraction will be considered, followed by a description of successful methods used to observe individual dislocations.

10.2 X-RAY DIFFRACTION.

Von Laue in 1912 realized that the ordered arrangement of atoms, or molecules, in crystals fulfilled the conditions essential for the diffraction of the short wave X-rays. The spacing between the atoms was known to be of the order of 10^{-8} cm. Unlike an ordinary grating, a crystal acts as a space grating rather than a plane grating.

On allowing a narrow pencil of X-rays to pass through a thin crystal and to fall on a photographic plate, the diffraction pattern obtained consists of a series of spots arranged in a

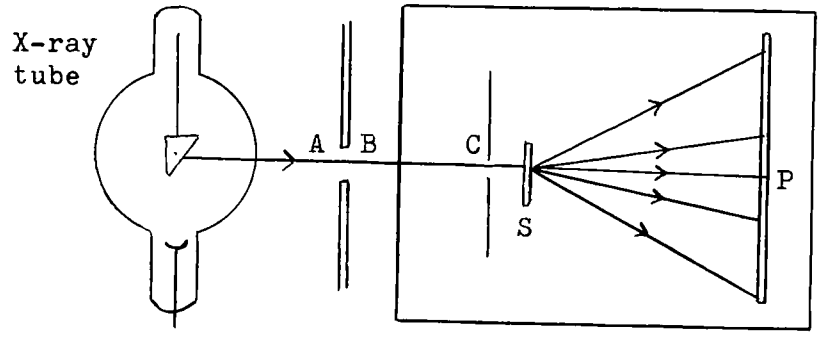

Fig. 86. Von Laue's apparatus.

A, B, and C = small apertures in lead screens.
S = specimen.
P = photographic plate.

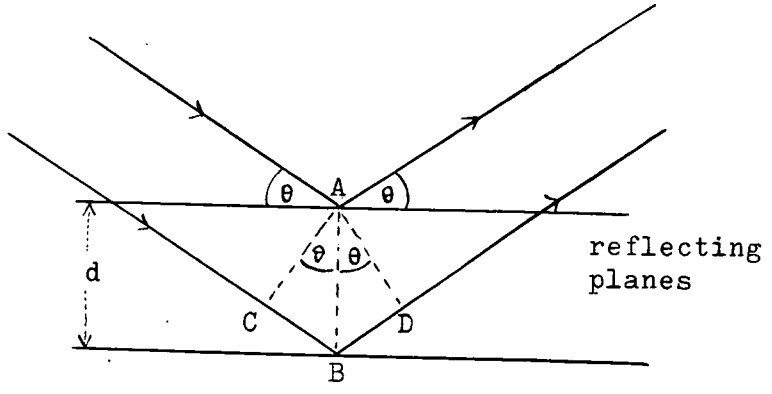

Fig. 87. Reflection of X-rays at close-packed planes. Reinforcement takes place when the path difference $CB + BD = n\lambda$
i.e. when $2d \sin\theta = n\lambda$.

definite pattern. Plate (62) is a photograph of the pattern produced by passing a fine beam of X-rays through a crystal of cubic structure. The general arrangement of the apparatus is shown in Fig. (86).

An interpretation of the diffraction pattern was given by Bragg. He assumed that the diffraction spots are produced by X-rays which are scattered from certain close-packed planes of atoms within the crystal. Bragg's equation $n\lambda = 2d\sin\theta$ gives the condition for reinforcement of X-rays reflected from a series of atomic planes, where n is the order of spectrum, λ the wavelength of the X-rays, d the separation of the planes, and θ the angle between the planes and the incident beam. The Laue method uses 'white' radiation so that the above condition may be fulfilled for several sets of planes at the same time. See Fig. (87). Comparatively few sets of parallel planes are sufficiently rich in atoms to produce intense diffraction spots, and the number of spots is usually small, see Plates (62), (63), and (64).

10.3 THE EFFECT OF DEFORMATION ON THE DIFFRACTION PATTERN.

An unstretched single crystal gives distinct Laue spots, see Plate (60). When the single crystal is stretched each of the spots becomes extended into a line as shown in Plate (61). This extension of spots is due to the existence in the crystal of planes rotated through small angles with respect to each other. The hardening of a single crystal is found to be proportional to

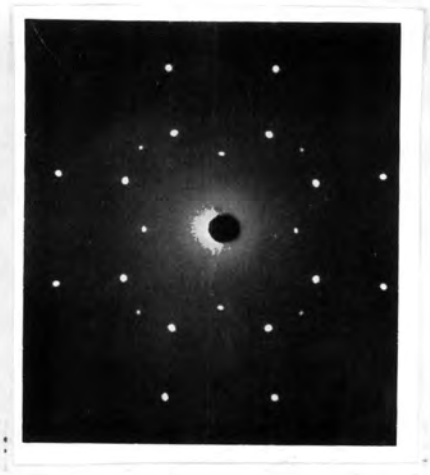

Plate 62. Fine beam of X-rays passing through a crystal of cubic structure.
(After Andrade, 1956).

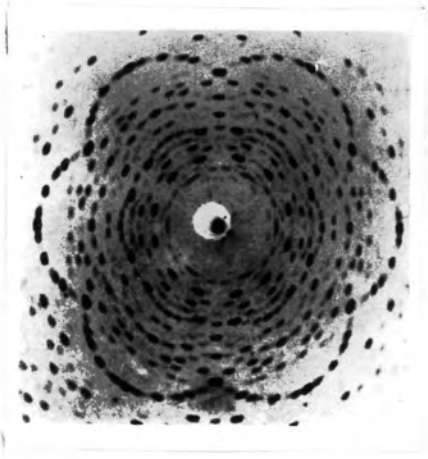

Plate 63. Fine beam of X-rays passing through a crystal of hexagonal structure.
(After Andrade, 1956).

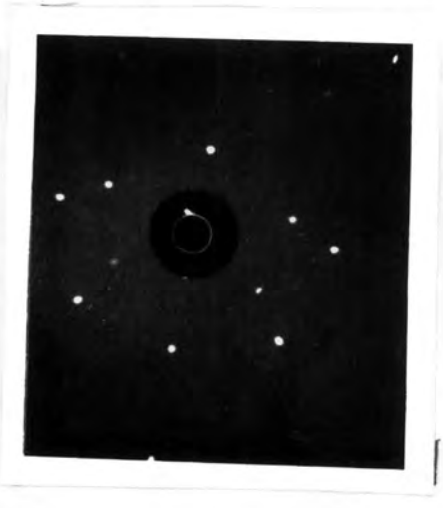

Plate 64. Fine beam of X-rays reflected back from a single crystal of gold.
(After Andrade, 1956).

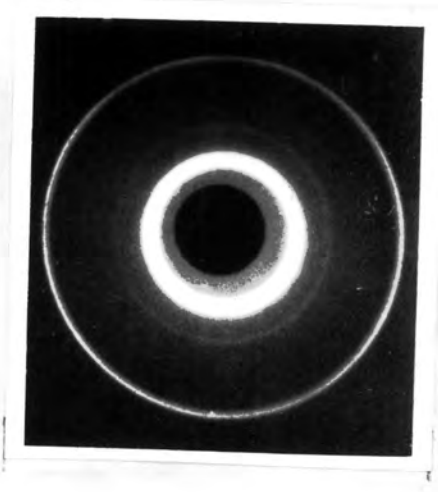

Plate 65. Fine beam of X-rays reflected back from a polycrystalline specimen of gold.
(After Andrade, 1956).

the spread of angle indicated by the extension of the spots, Andrade (1950).

In a polycrystalline specimen, consisting of many small crystals, all angles are represented, resulting in many spots which combine to give continuous clear circles as shown in Plate (65).

10.4 X-RAY SCATTERING BY DISLOCATIONS.

Scattering by single dislocations can be determined theoretically from expressions for the displacements associated with them, see Cottrell (1953), and Nabarro (1952).

The dynamical theory of X-ray diffraction applies to a large single crystal. The effects of multiple scattering and interference among waves reflected from all planes are taken into account. The theory indicates that the perfect crystal will be completely transparent to X-rays except in very small regions of reflection angle corresponding to the ordinary Bragg reflections, where total reflection occurs. The width of these regions is a few seconds of arc. Generally, in practice, this so called dynamical theory breaks down as local defects destroy the conditions necessary for the exacting phase relationships to hold.

The simpler kinematical theory of diffraction is more applicable to such a case. In this theory, multiple scattering is neglected, and the intensity of the multiple beam is assumed to be constant throughout the material. This gives a smoothed-out

intensity profile for each reflection, and not the total reflection of the dynamical theory. Nevertheless, in most nearly perfect crystals multiple scattering and interference take place, and are most conspicuous in the strong reflections. These are broad, their width depending upon the intensity.

For weak reflections the effect of multiple scattering may be neglected, and the kinematical theory applies. If the dynamical theory is to break down, the crystal must contain imperfections so close together that the regions of perfect crystal are too small for the theory to apply. Darwin (1914) proposed that natural crystals have perfect regions with widths of the order of up to 10^{-4} cm., and that the crystal has a mosaic structure. Bragg, James, and Bosanquet (1921) explained that secondary extinction is very important where there is a mosaic structure consisting of differently orientated blocks. The intensity incident on a particular block will not be equal to the intensity on the surface due to reflections above and below the block. Hall and Williamson (1951) found that in annealed and cold-worked metals only secondary extinction appears. They calculated the apparent particle size from the width of the lines, and found it to be of the order of 10^{-4} cm. in most annealed metals.

The 'apparent particle' has been identified with dislocation networks and it has proved possible to find the density of parallel dislocations necessary to give the secondary extinction. The 'apparent particle size' associated with dislocations is

rougly equal to their separation. Thus an apparent particle size of 10^{-4} cm. suggests a dislocation density of $10^{8}/cm.^{2}$ Seeger (1954) disagrees with this value on the grounds that the random distribution of dislocations is not realized, and this would lead to the above numbers being wrong by a factor of 10.

10.5 THE OBSERVATION OF INDIVIDUAL DISLOCATIONS BY X-RAY EXTINCTION CONTRAST.

10.5 (a) INTRODUCTION.

Newkirk (1958 a and b, and 1959) revealed individual undecorated dislocations in crystals of silicon and lithium fluoride. The positions of the dislocations can be seen with respect to the topography of the crystal, and also the direction, but not the sign, of their Burgers vector can be simply determined.

He used an X-ray diffraction method called the Berg-Barrett (B.B.) technique to observe subgrains, dislocation clusters, and individual dislocations. The technique is simple, and makes use of inexpensive apparatus. Barrett (1945) described the observation of subgrains in iron-silicon crystals and of defects within the subgrains. In some specimens slip bands were seen with respect to the topography of the rest of the specimen. Now, the actual sites of individual dislocations which emerge upon the crystal surface, and extend into the body of the crystal, have been located. The means of determining the directions of the Burgers vector was suggested by Wilson (1952).

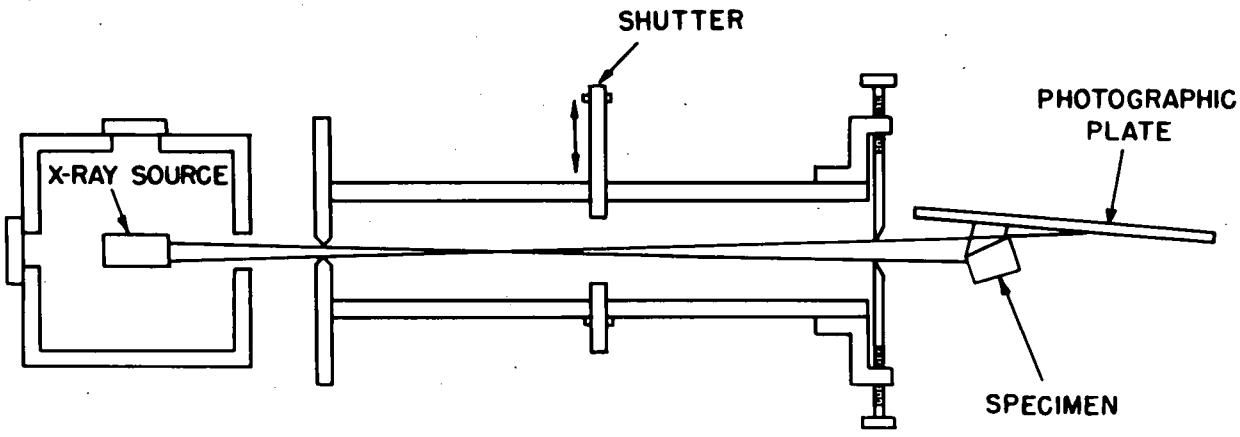

(a)

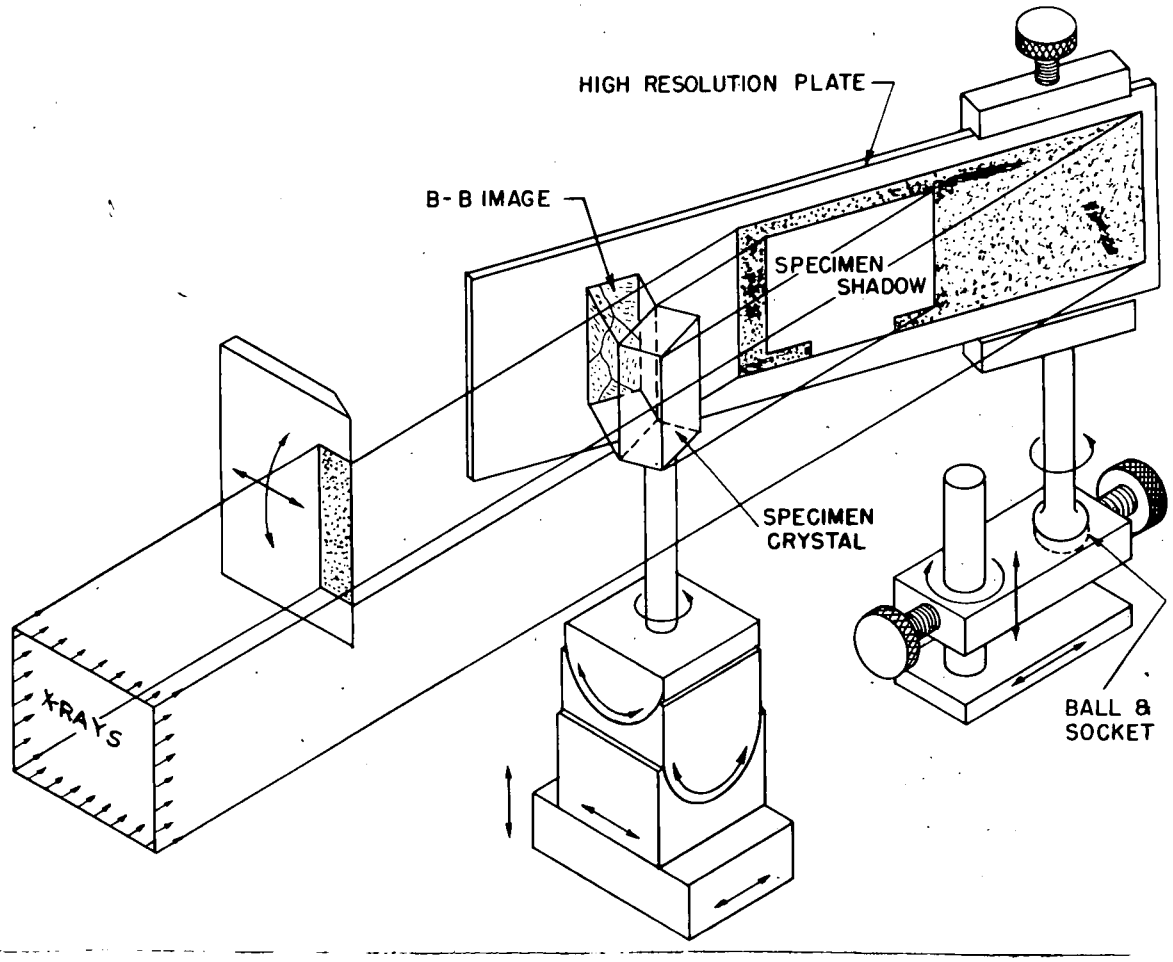

Fig. 88. The Camera.
(After Newkirk, 1959).

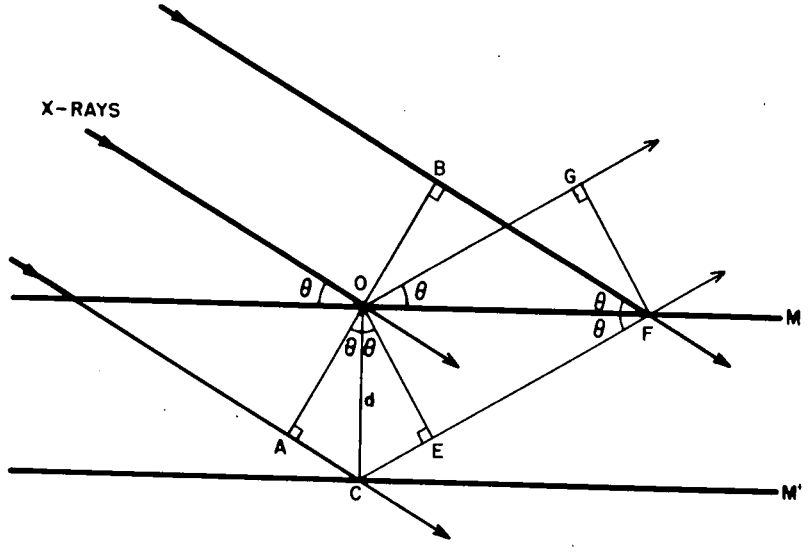

Fig. 89. Diffraction of X-rays.
(After Newkirk, 1959).

10.5 (b) EXPERIMENTAL METHOD.

1. The Camera.

The camera is shown diagramatically in Fig. (88). In practice the specimen is held much closer to the photographic plate than this diagram suggests. The distance between the X-ray source and the specimen is about 13 cm., and from the specimen to the plate about 0.1 mm. The resolution of micrographs depends upon the closeness of the plate to the specimen. The plate is held almost parallel to the incident beam so that the distance from the specimen to the plate is small for as large an area of the specimen as possible. The plate is shielded from the direct X-ray beam, and the primary beam permitted to fall only on the crystal. For his experiments Newkirk used one of the side ports of a standard CA-7 diffracting tube with the target on a line making an angle about 7 deg. with the target plane.

2. Formation of the Image.

The effects due to primary extinction are of most interest in this work. Conditions necessary to produce primary extinction are described by James (1950). Fig. (89) shows X-rays incident on a crystal lattice. The lattice planes will diffract coherently if the Bragg relationship is satisfied. Part of the energy of the diffracted ray CEF will be again diffracted at F into the direction of the originally incident beam. Due to a phase shift of $\frac{\pi}{2}$ at each reflection, the twice diffracted ray at F will be exactly out of phase with the primary ray giving destructive

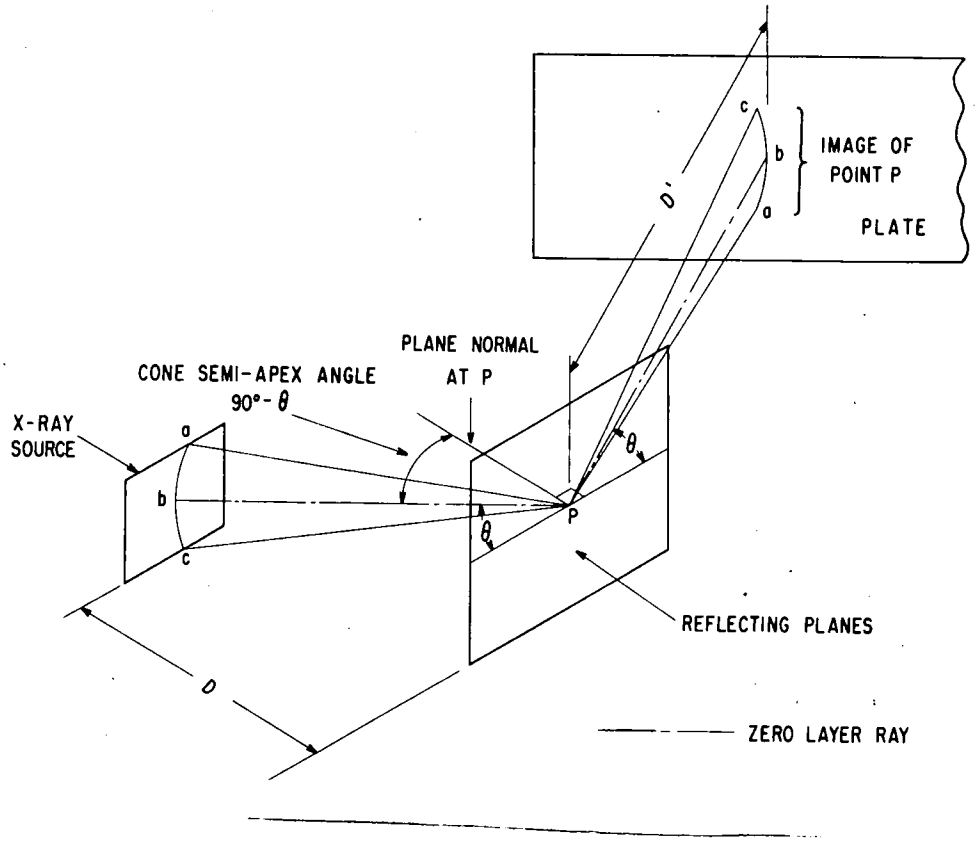

Fig. 90. Radiation permitting Bragg diffraction at a point P on the specimen can issue from an arc on the X-ray source area. Thus, the image of point P is an arc. Resolution is lost as the plate-to-specimen distance D′, is increased. (After Newkirk, 1959).

interference. The primary ray is thus rapidly extinguished as it passes through the crystal.

If, for any reason, the separation (d) of the lattice planes is reduced so that the Bragg conditions are not fulfilled, the emerging once diffracted rays will be more intense, and the primary rays suffering less attenuation, will penetrate further into the crystal giving more Bragg diffraction. Primary extinction is reduced by reduction of the periodicity, only if the latter is in the direction normal to the diffracting planes. Diffracted intensity may be increased as a result of local elastic strain, and the diffracting beam is of extra intensity where it emerges at dislocation sites. The effect is reversible, the diffracted intensity returning to its low value when the strain is removed.

If the extra diffracted intensity at a dislocation is caused by a local reduction of extinction, the extra intensity above background should depend upon the elastic strain component which is normal to the diffracting planes. Thus dislocations with their Burgers vector normal to the diffracting planes will give the greatest contrast, and those with their Burgers vectors parallel to the diffracting planes will give least contrast.

Preliminary results show that the longer the wavelength of the X-rays, the better the contrast obtained. Newkirk used a chromium target tube.

The vertical divergence of the incident radiation causes a reduction in resolution, as may be seen from Fig. (90). The

resolution could probably be improved by using horizontal slits. Improved resolution is obtained by making the distance between the plate and the specimen as small as possible compared with the distance from the specimen to the source. The ratio of these distances is in practice about 0.005. The greater the distance between the specimen and the source, the longer the exposure time must be, and so the best way to increase resolution is by having the specimen as close as possible to the plate. Exposure times, using Eastman High Resolution plates, were from four minutes to one and a half hours.

A small television camera tube, sensitive to X-rays, may be used instead of the photographic plate, enabling movement of dislocations to be followed.

10.5 (c) OBSERVATIONS OF DISLOCATIONS IN A SILICON CRYSTAL.

The crystal was grown by the Czochralski technique with its long direction parallel with $[111]$. From this was cut a specimen 25 mm. long, using a diamond saw. The specimen was in the form of a parallelopiped. Its sides were approximately parallel with (111), $(11\bar{2})$, and $(\bar{1}\bar{1}0)$.

Whilst maintained at 900 deg. C. for about five minutes, the specimen was chemically polished and twisted about its long axis. It was then etched using Dash's etch (1 hydrofluoric acid, 3 nitric acid, and 10 glacial acetic acid) and this produced straight rows of etch pits on the $(1\bar{1}0)$ and $(11\bar{2})$ surfaces. The specimen was cut into rods with their axis parallel with the $[111]$ axis. The

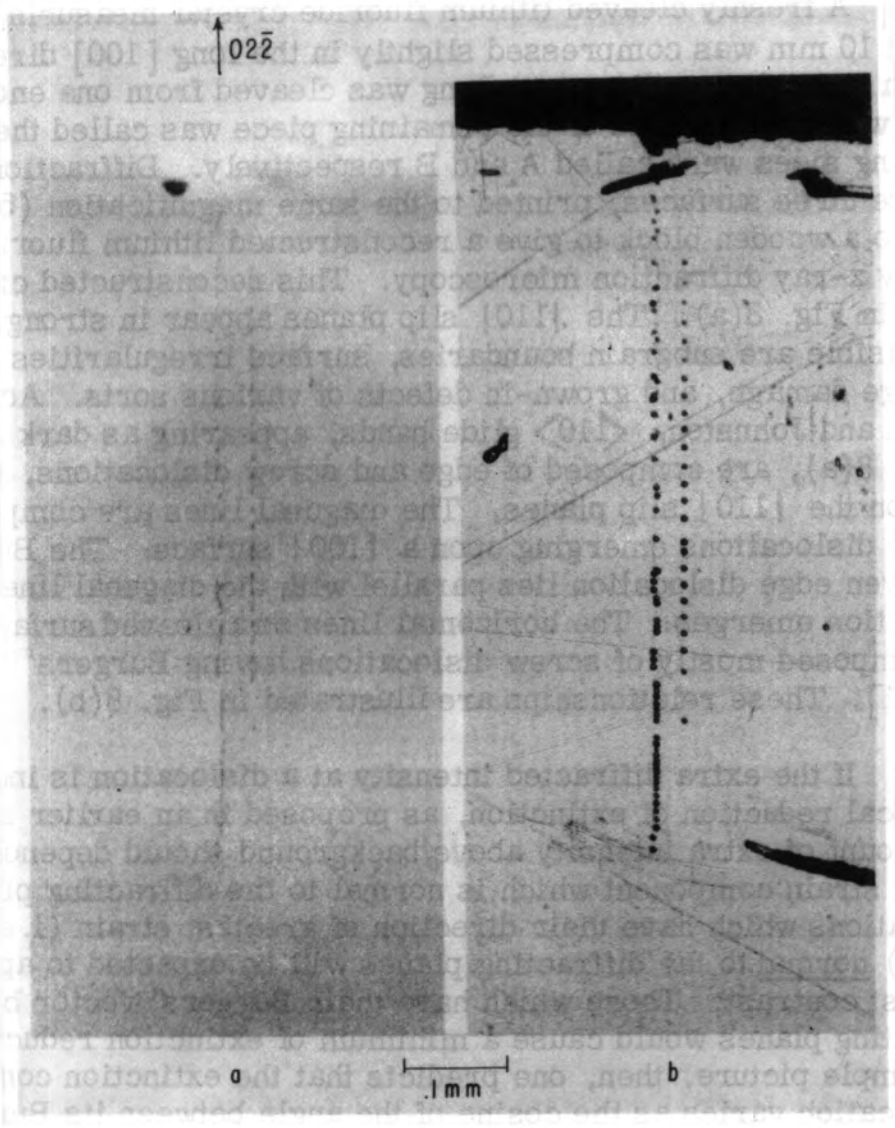

Plate 66. (a) Diffraction micrograph of unetched silicon crystal shown in Fig. 91c;
(b) light micrograph of same area, etched.

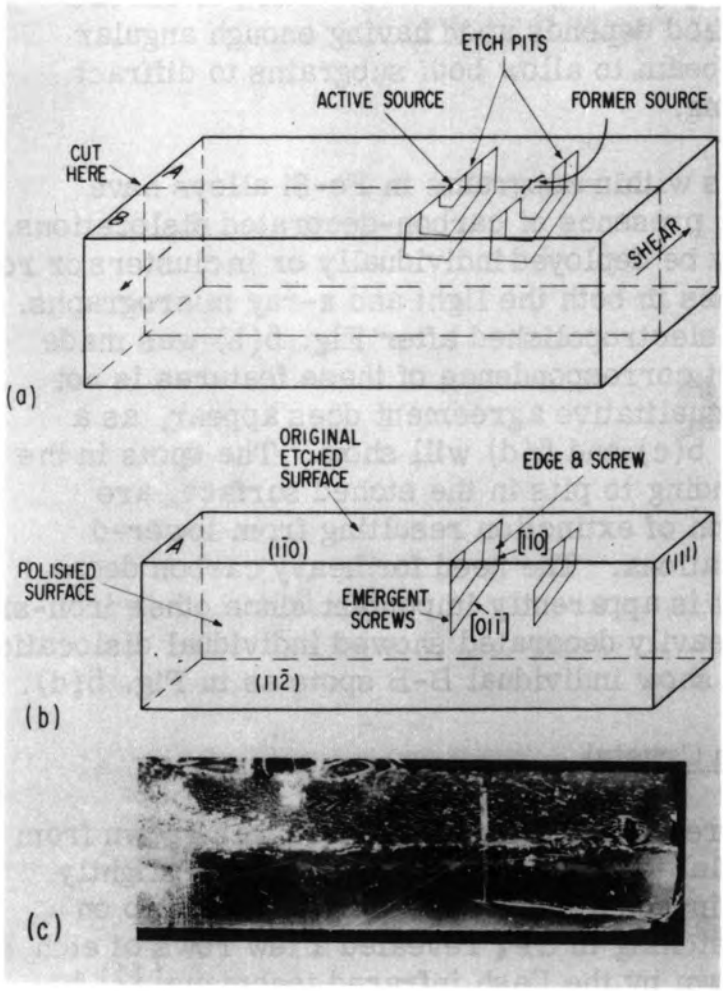

Fig. 91. A silicon crystal was cut through new dislocation loops as shown in (a) and (b). One of the new surfaces, containing two rows of emergent screw dislocations, was polished and etched to render the screws visible as pits, (c).
(After Newkirk, 1959).

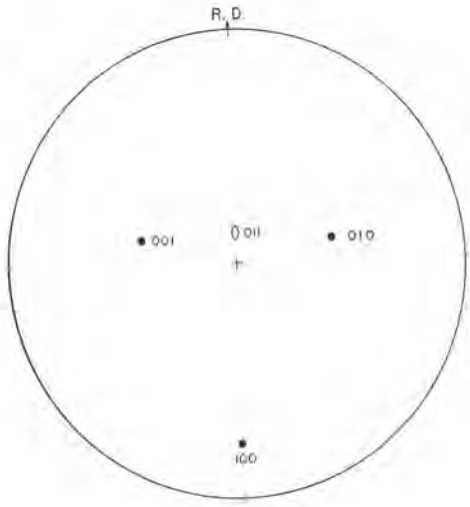

Fig. 92. The 011 reflection plane makes an angle of about 15 deg. with the surface of the specimen.
(After Newkirk, 1958b).

method used by Dash (see section 6.4) enabled Newkirk to observe the dislocations in the rod shown in Fig. (91). He then cut the rod as shown, and by polishing and treatment in Dash's etch, revealed rows of etch pits on the new $(11\bar{2})$ surface, see Fig. (91b). These etch pits were obviously associated with those on the $(1\bar{1}0)$ surface.

The etch pits on the $(11\bar{2})$ surface were photographed, and this surface was then carefully ground to completely remove the etch pits. An X-ray diffraction micrograph was then made from this surface. The image of the surface was formed on a high resolution spectrographic plate, by the $(02\bar{2})$ reflection of CrK_α radiation. The photograph showed spots corresponding to the etch pits on the previous photograph, see Plate (66).

By repeating the above procedure using the $(2\bar{2}0)$ reflections, which gave a less distinct pattern, Newkirk deduced that the best contrast is obtained when a reflection is used which has a large component of the dislocation's Burgers vector normal to the reflecting planes.

10.5 (d) OBSERVATION OF SUBGRAIN STRUCTURE IN AN IRON-SILICON CRYSTAL.

Newkirk (1958 b) used the B.B. technique on a single crystal of iron containing 3% silicon. Fig. (92) shows the orientation of the crystal, the basic circle representing the specimen surface.

After being in a carburizing atmosphere of low pressure acetylene, and at 980 deg. C. for half an hour, the crystal was

Plate 67. When etched with conventional reagents, the specimen shows no substructure; when etched by the Morris method this structure appears. (x 30) (After Newkirk, 1958b).

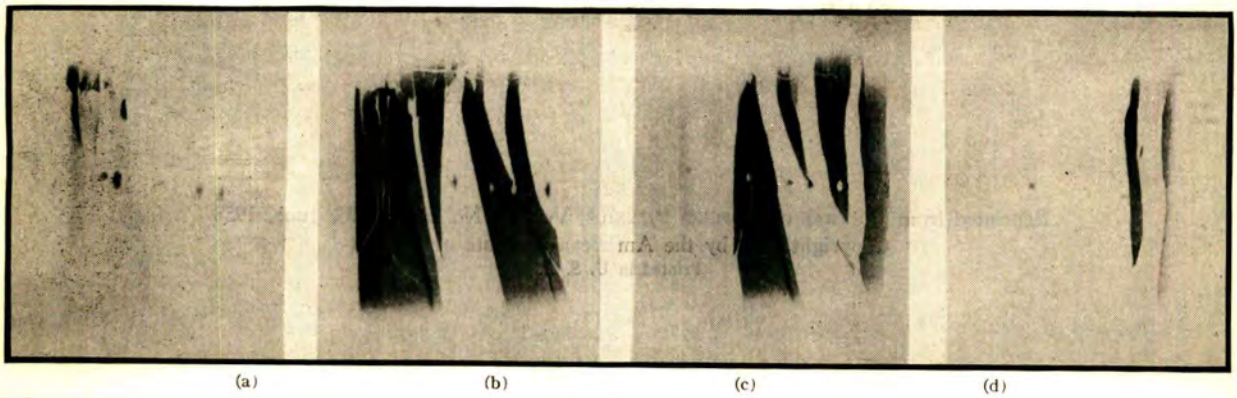

Plate 68. Berg-Barrett photographs made at ½ deg. intervals show that adjacent subgrains are misoriented by the order of ½ deg. Eastman V-O plates; image optically enlarged 12 x; positive print. (After Newkirk, 1958b).

(a)

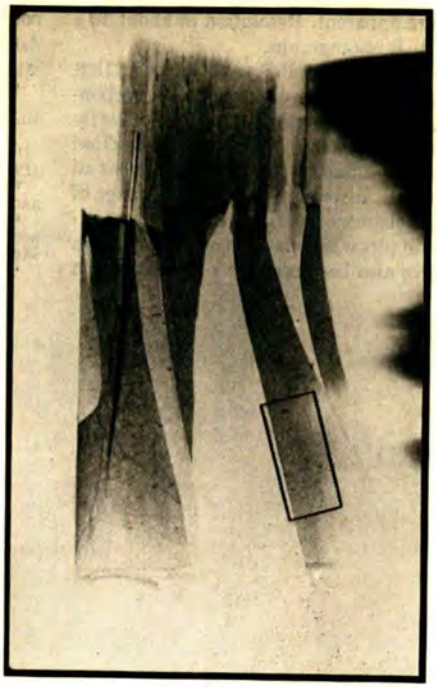

(b)

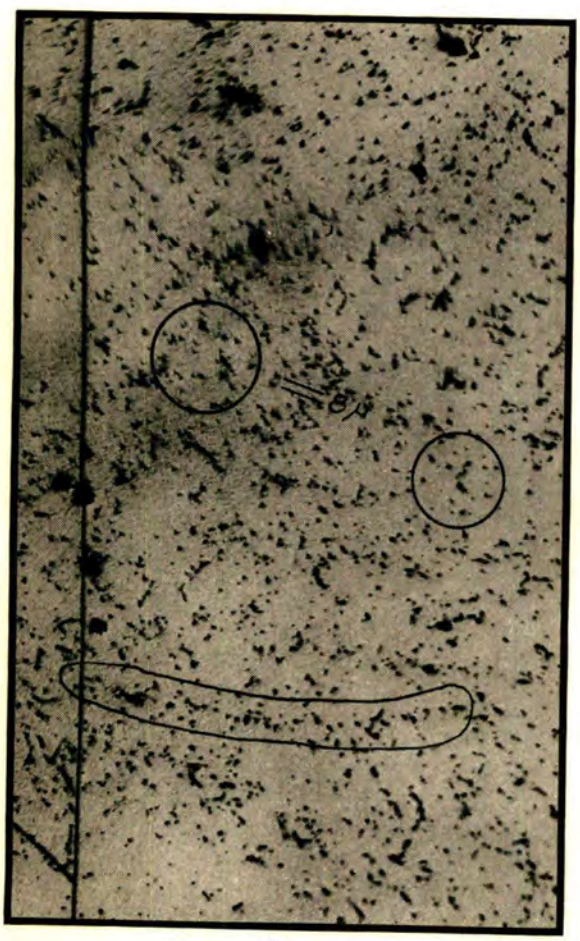

(c)

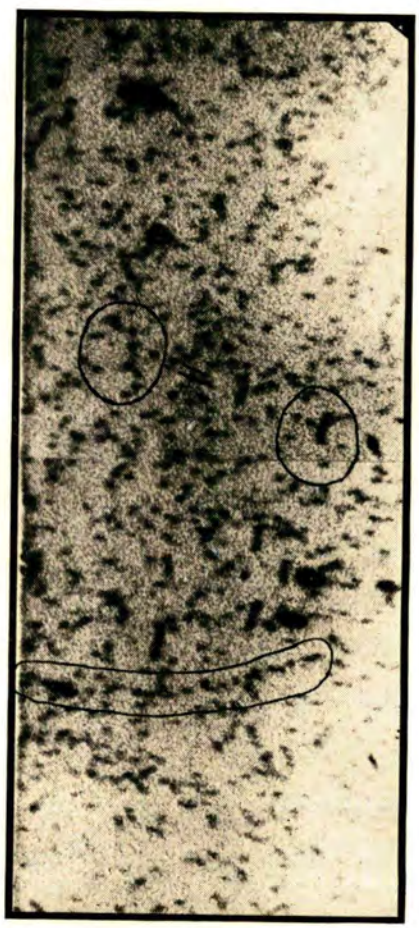

(d)

Plate 69. (a), (b), and (d) are X-ray reflection micrographs. (c) is a light micrograph of the same region after etching. (After Newkirk, 1958b).

cooled. Its surface was then mechanically abraided, electro-polished, and etched by the Morris (1949) method. The subgrains and low angled boundaries, and individual etch pits were clearly seen, as shown in Plate (67).

Newkirk used this specimen, still in the etched condition, to make a number of B.B. photographs with unfiltered Co-radiation. The distance apart of the target and the specimen was 11 cm., and between the specimen and the plate, 5 mm. Using this arrangement he took stationary photographs with the crystal rotated in ½ deg. steps about an axis in the surface plane, and normal to the rolling direction of the X-ray beam. The photographs are shown in Plate (68), and correspondence can clearly be seen with Plate (67). The subgrains reflecting on one photograph do not do so on the next, indicating the slightly different orientations of the subgrains, and showing that the tilt between adjacent grains must be of the order of ½ deg. The greatest possible resolution of about 10μ was obtained by holding the photographic plate 5 mm. from the specimen for one hour exposure.

Plate (69) shows the B.B. photograph (a) actual size and optically enlarged, (b) 20 x and (d) 190 x. These may be compared with a light micrograph of the etched specimen, Plate (69c). Considering that the etching was done after taking the B.B. photographs, correspondence is remarkably good. The correlation indicates that each B.B. spot marks one, or a cluster, of carbon decorated dislocations which emerge to give etch pits.

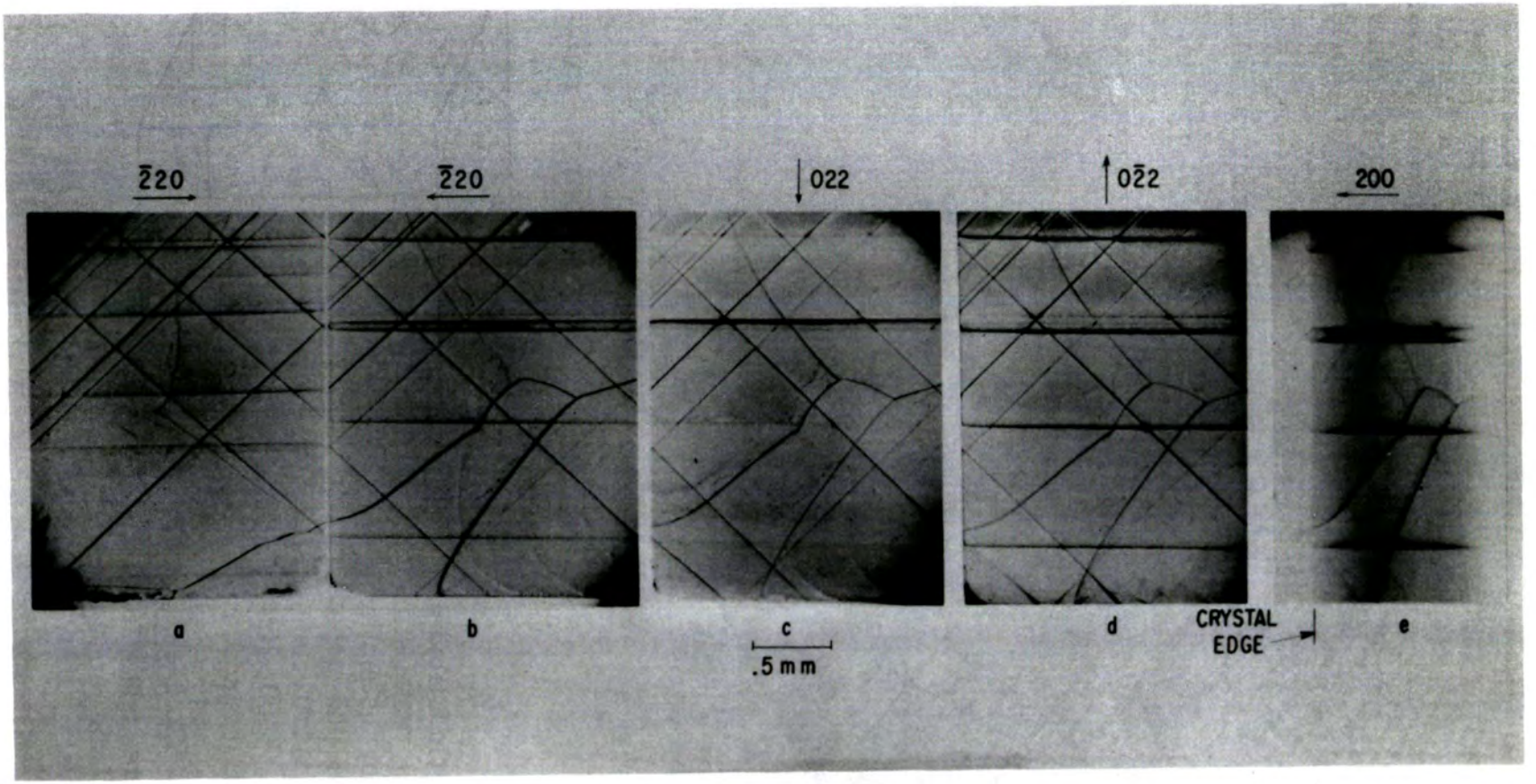

Plate 71
~~Fig. 9~~ Diffraction micrographs using {220} reflections (a-d) show both screw and edge dislocations. Using the 200 reflection, the screws and other crystalline features appear, but the edges do not. Notice the intensity reversal of the screws (horizontal lines) in c and d.

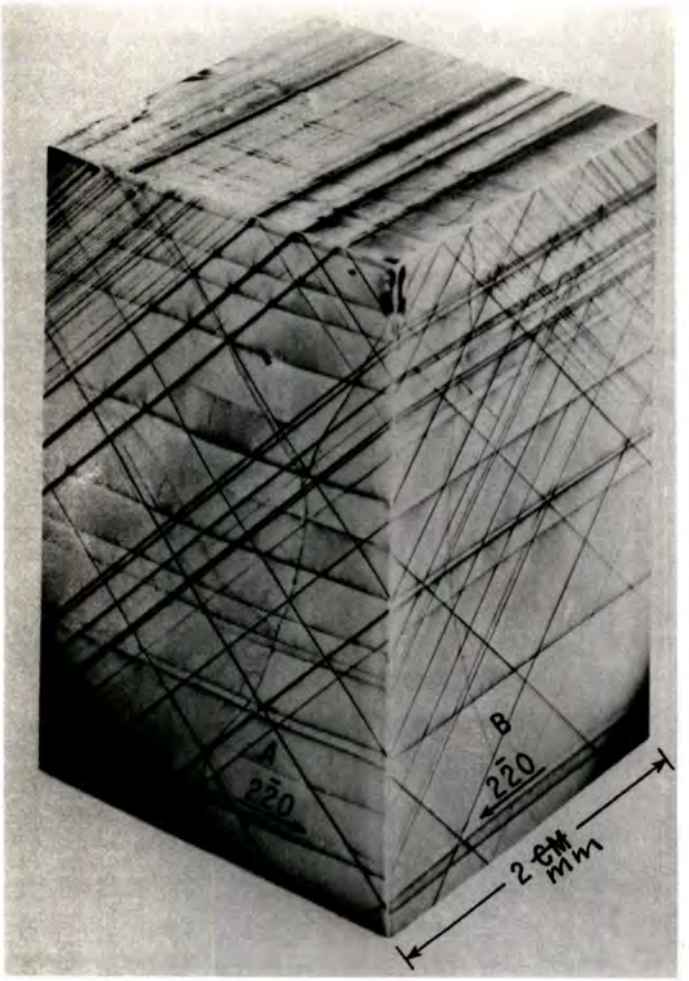

Plate 70

~~Fig. 8(a)~~ A reconstructed lithium fluoride crystal, as seen by x-ray microscopy, shows subgrain boundaries, slip planes, grown-in dislocations, and other structural details.

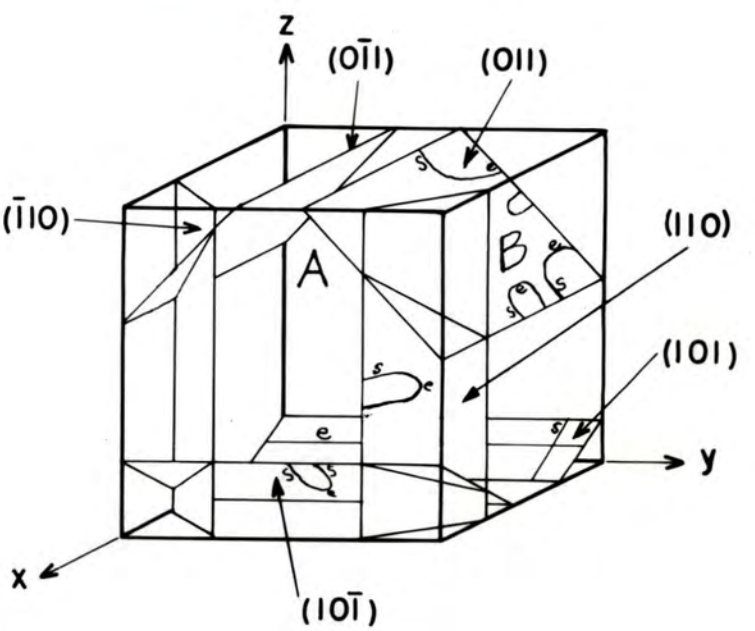

93

Fig. ~~8(b)~~ In a lithium fluoride crystal slip occurs by the motion of dislocation loops lying on {110} planes. Diagonal <100> lines on a {100} surface consist mostly of edge dislocations; horizontal and vertical <100> lines consist mostly of screws.

It is remarkable that although the above observation of dislocations was so successful, Newkirk found it extremely difficult to repeat the method with other similar crystals. He considers critical decoration to be necessary.

10.5 (e) STUDY OF LITHIUM FLUORIDE CRYSTALS.

Newkirk studied dislocations in a freshly cleaved lithium fluoride crystal with dimensions 2 x 2 x 10 mm. The crystal was compressed slightly in the long [100] direction. A portion about 4 mm. long was cleaved from one end. Diffraction micrographs were then taken of three surfaces, the end, and two adjoining sides of the crystal. The micrographs were printed to the same magnification and glued onto a wooden block. The reconstructed lithium fluoride crystal, as seen by X-ray microscopy, is shown in Plate (70), and subgrain boundaries, slip planes, and other structural details can be observed. (110) glide bands appear as dark straight lines. These are made up of edge and screw dislocations forming loops on the (110) slip planes. Slip in lithium fluoride occurs by motion of dislocation loops lying on the (110) planes. Diagonal [110] lines on (100) surface consist mostly of edge dislocations. The horizontal and vertical lines consist mostly of screws. The details are indicated in Fig. (93).

The diffraction micrographs in Plates (71 a,b,c,d, and e) show that dislocations with their Burgers vectors normal to the diffracting planes produce the greatest contrast, and those with their Burgers vectors in the diffracting planes give least

extinction reduction. The (220) reflection was used for Plates (71 a to d) and the (200) reflection for Plate (71e). The edge dislocations are seen as diagonal lines, and the screws as horizontal lines. The edge dislocations are clearly seen on all the (220) micrographs in Plates (71 a to d) as expected, as they have their Burgers vector at 60 degrees to the diffracting planes. In Plate (71e) the edge dislocations are not visible as their Burgers vectors are parallel with the diffracting planes. It is thus possible to determine the direction of the Burgers vectors from the different specific reflections used.

The depth to which observation is possible depends upon X-ray penetration, which varies with the density of the specimen. Using CrKα radiation structural detail in lithium fluoride can be seen to a depth of about 100μ. In denser materials penetration is much less. In silicon, for example, penetration is less than a micron.

10.5 (f) EXTENSIONS OF THE TECHNIQUE.

Pairs of diffraction micrographs have been used to give stereoscopic viewing of a particular region. The three dimensional effect can be used to find the depth of a defect below the crystal surface. Diffraction micrographs may be taken in transmission as well as reflection. The same general features are observed, but not nearly so clearly.

Newkirk has made diffraction micrographs of the metals zinc, iron, and tungsten. Subgrains and slip bands were observed, but

not the direction-dependent intensity effects seen in crystals of silicon and lithium fluoride.

10.6 THE STUDY OF INDIVIDUAL DISLOCATIONS IN CRYSTALS BY X-RAY DIFFRACTION MICRORADIOGRAPHY.

10.6 (a) INTRODUCTION.

Lang's early experiments (1957 and 1958) were made using the method of 'section topographs' to observe individual dislocations in silicon. Later he found the method of 'projection topographs' more convenient, and individual dislocations in single crystals of diamond, silicon, germanium, lithium fluoride, sodium chloride, silver chloride, magnesium oxide, calcite, quartz, and aluminium have been observed, (1959).

As described in section 10.5 (b), primary extinction causes attenuation of the direct X-ray beam as it passes through a perfect crystal. Destructive interference also tends to reduce the intensity of the integrated reflection. The integrated reflection may change by one or two orders of magnitude, depending upon the perfection of the crystal. The angular range of reflection from perfect crystals is limited to a few seconds of arc.

Any imperfections such as low angle boundaries, stacking faults, and the variations of lattice parameter around precipitates and dislocations, produce intensified reflecting power. Using (111) and (220) reflections of AgKα radiation from nearly perfect silicon, Lang found increased X-ray reflection to extend to about 10μ

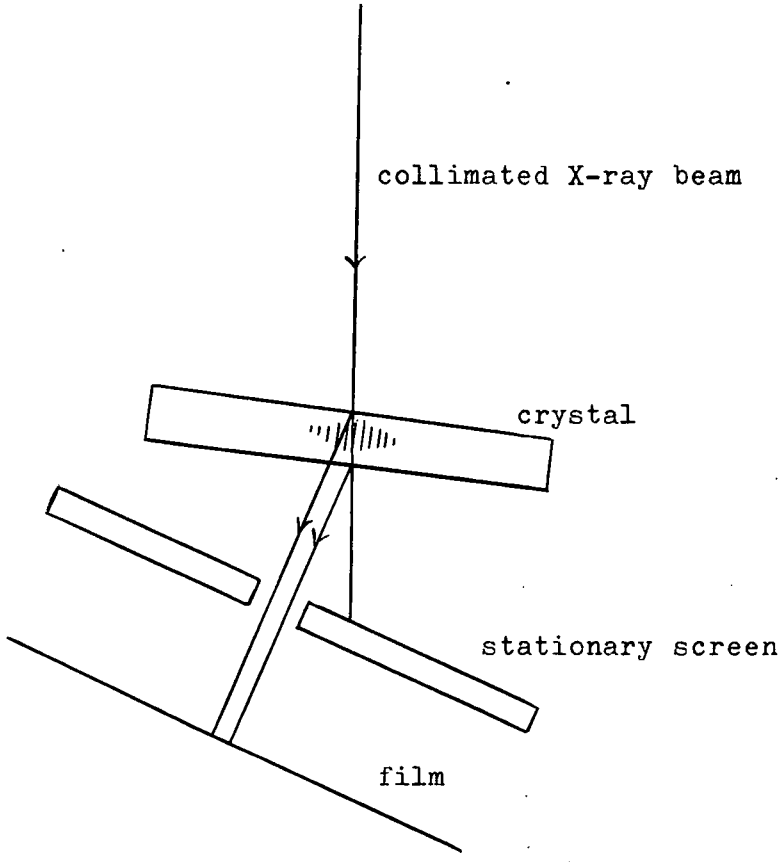

Fig. 95. Principle of projection topograph technique. (After Lang, 1959).

from the core of a dislocation. A dislocation may thus be regarded as a cylinder of diameter about 20μ at which increased reflection takes place. So long as the dislocation density is low, the large size of this cylinder enables individual dislocations to be made clearly visible. The size of the cylinder also limits the resolution in crystals where the dislocation density is greater. However, as the dislocation density increases, the size of the relatively imperfect region around a dislocation decreases, and it if found that the apparent width of the dislocation image decreases. At the limit of resolution of individual dislocations, the diameter of the cylinder reduces to about 5μ.

10.6 (b) EXPERIMENTAL METHOD.

Lang used the fluctuation in intensity on X-ray topographs to locate individual projection topograph dislocations. The principle of his projection topograph technique is shown in Fig. (95).

The collimated X-ray beam of MoKα , AgKα , or WKα radiation is incident upon the crystal, and reflection is taking place from the lattice planes roughly normal to the crystal faces of the specimen. The rays fall on a film placed close to the specimen. In order to scan an area, the crystal and the film are moved back and forth together during the exposure, the direction of motion being parallel to the crystal slice. The screen remains stationary to prevent the direct beam from reaching the film. An area of crystal about 1 inch square may be scanned at each operation.

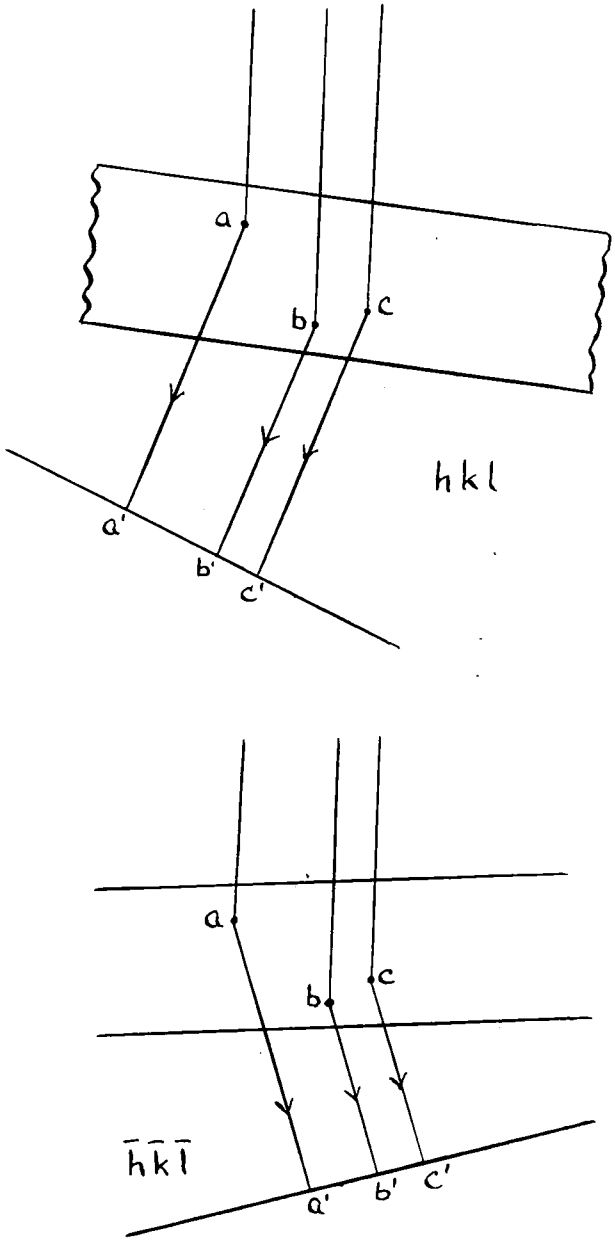

Fig. 96. Principle of diffraction stereomicroradiograph. (After Lang, 1959).

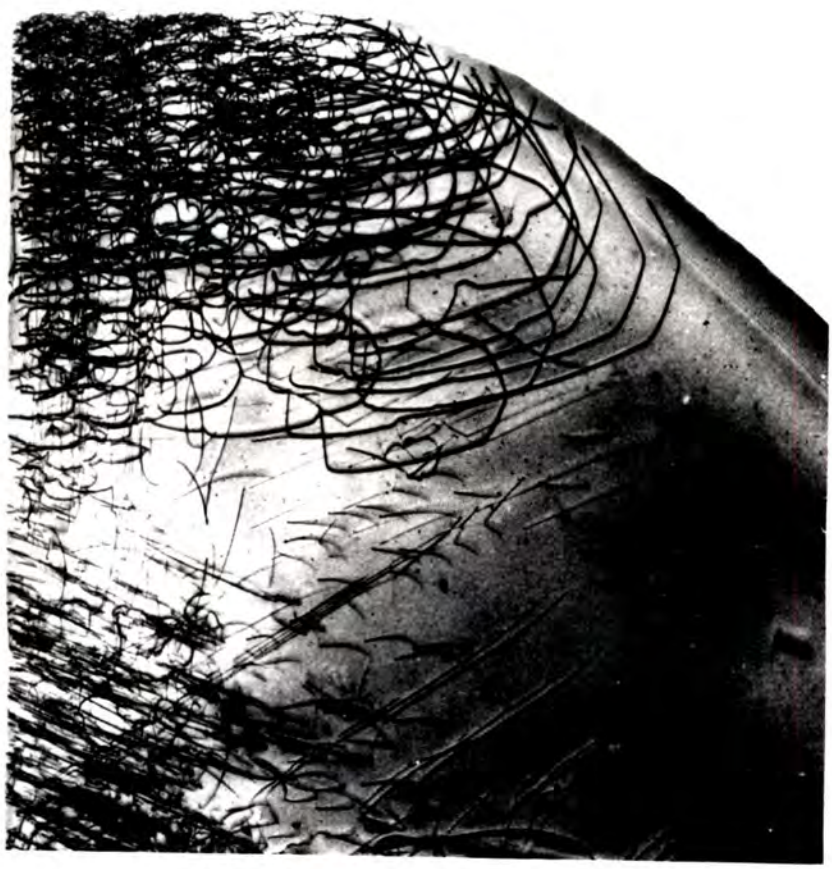

Plate 72a and b. Dislocations in silicon due to slip.
(a) 111 X-ray reflection,
(b) $2\bar{2}0$ X-ray reflection.
(After Lang, 1959).

The thickness of the slice used is limited by two factors. Firstly by the absorption of the radiation by the specimen, and secondly by the density of the dislocations. The higher the density of the dislocations, the thinner the specimen must be to enable resolution of individual dislocations. To study dislocations within subgrains, the thickness must be less than the average subgrain diameter.

Diffraction stereomicroradiographs have made it possible to determine the depth of dislocations below the surface of a specimen. The pairs of projection topographs are prepared from the pair of reflections hkl and $\bar{h}\bar{k}\bar{l}$ as shown in Fig. (96).

10.6 (c) OBSERVATIONS OF DISLOCATIONS IN SILICON AND ALUMINIUM.

Lang has observed dislocations in single crystals of several substances, see section 10.6 (a). His studies using silicon and aluminium will be considered briefly. Silicon is particularly suitable as its X-ray absorption is low, allowing relatively thick specimens to be used. Also verification of dislocation configurations seen by X-ray diffraction is possible by Dash's decoration technique. The two methods show absolute agreement. It is found that edge dislocations are most clearly visible when the Burgers vector makes a large angle with the net plane. It is thus possible to find the slip planes of dislocations if slip has taken place.

Plates (72a) and (72b) show dislocations in silicon due to slip. The topographs cover an area about ½ cm. square. The

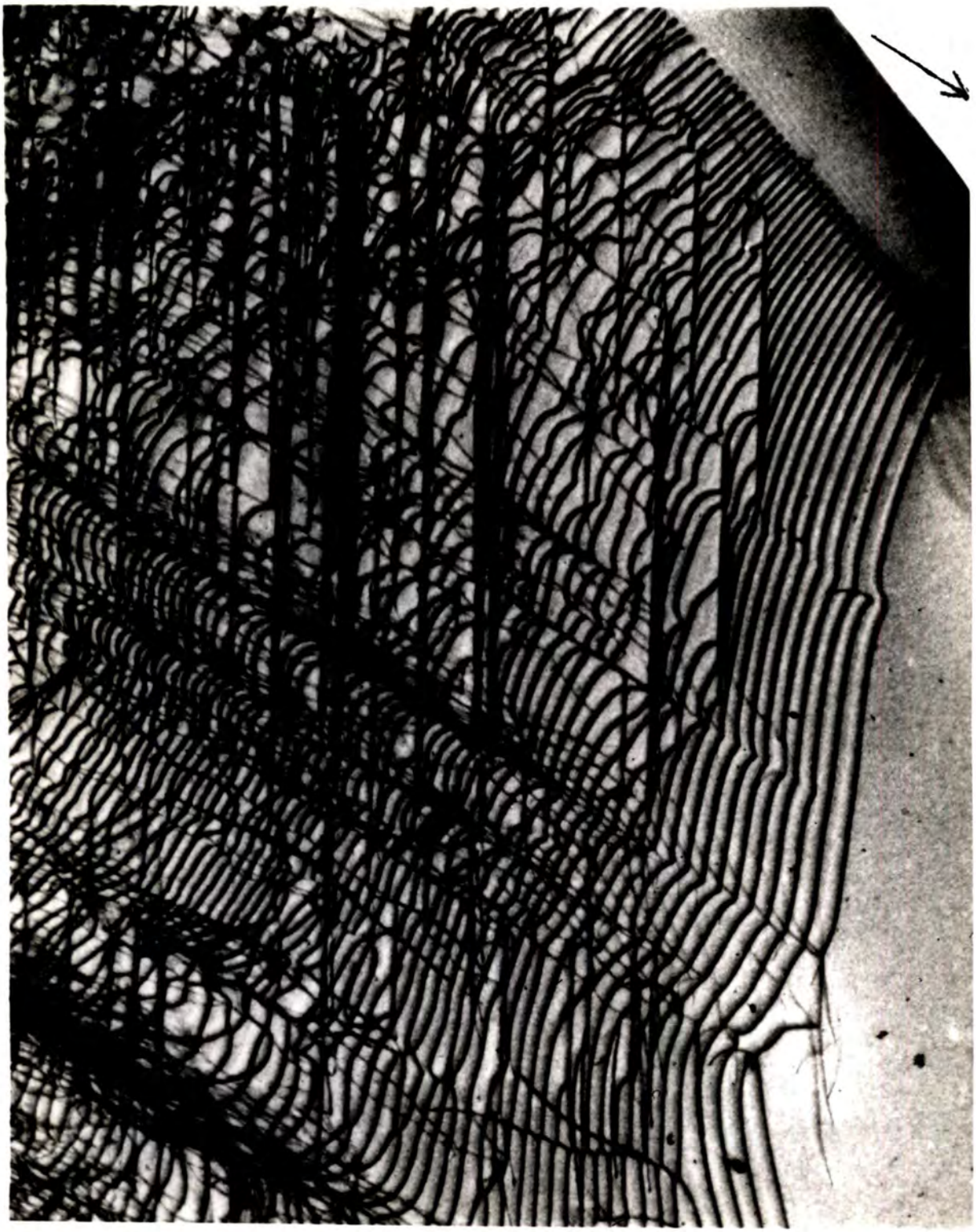

Plate 73. Dislocations in silicon due to slip, 111 reflection, AgKα radiation, field 12 x 8 mm. (After Lang, 1959).

crystal slice was cut parallel to a (111) plane which makes an angle 19½ deg. with the [111] direction, which is the growth direction. Slip, due to thermal stresses produced by cooling has taken place in the three (111) planes inclined to the growth axis.

Plate (72a) is due to the (111) reflection from the planes normal to the growth axis. Plate (72b) is the $(2\bar{2}0)$ reflection from the planes normal to the surface of the crystal slice, and containing the growth axis. The slice was 1¼ mm. thick and AgKα radiation was used. Some of the loops visible in Plate (72b) cannot be seen in (72a). Their Burgers vector is in the $[1\bar{1}0]$ direction and parallel to the reflecting planes used to give Plate (72a).

Plate (73) is a projection topograph of another part of the crystal slice used for Plate (72). It uses the (111) reflection. The Burgers vectors of the dislocations visible make an angle of 55 deg. with the (111) reflecting plane. The arrow shows the direction of the normal to the Bragg reflection plane.

Lang and Meyrick (1959) studied dislocation structures in high-purity recrystallized aluminium using the same X-ray diffraction method. The dislocation density was between 10^4 and 10^5 lines per cc. within the subgrains.

Portions from the purest region of zone refined originally 99.999% pure aluminium were taken and rolled into approximately 5 cm. x 1 cm. x 2 mm. strips. These were etched and washed, and, resting on a bed of alumina powder, allowed to anneal overnight in

air at 495 deg. C. They were then extended 2%, re-annealed overnight at 495 deg. C., and electropolished. The resulting grains had an area about 1 sq. cm.

111 and $\bar{1}\bar{1}\bar{1}$ reflections of AgKα radiation revealed interesting dislocation configurations. Many regular and irregular helical dislocations are seen, their pitch varying with about 50μ an average value. Also loops are visible. The configurations are similar to those described by Jones and Mitchell (1958), and Parasnis and Mitchell (1959). The smallest diameter of loop it is possible to resolve is 5μ. A variation from the mean lattice parameter of the order of 1 part in 10^6 causes a detectable increase in X-ray reflecting power.

10.7 CONCLUSION.

The methods used by Lang and Newkirk offer very promising means of observation of dislocations. Ultra thin specimens, as required for electron-microscope methods need not be used, and thus surface effects associated with thin films are avoided. The methods are not restricted to observation of dislocations close to the surface, but give information about the interior of the crystal. They do not require decoration, and are non-destructive. The efficiency of the method has been checked by older established methods. Repeated X-ray examinations of the same specimen can thus be made, and the movement of dislocations followed. The methods enable the directions of Burgers vectors to be determined.

The resolving power attained is not so good as that of the electron microscope, and the dislocation density must be correspondingly small if individual dislocations are to be distinguished. In order to observe individual dislocations, large single crystals must be used.

PART II.

THE STUDY OF METAL SURFACES USING THE FIELD ION MICROSCOPE.

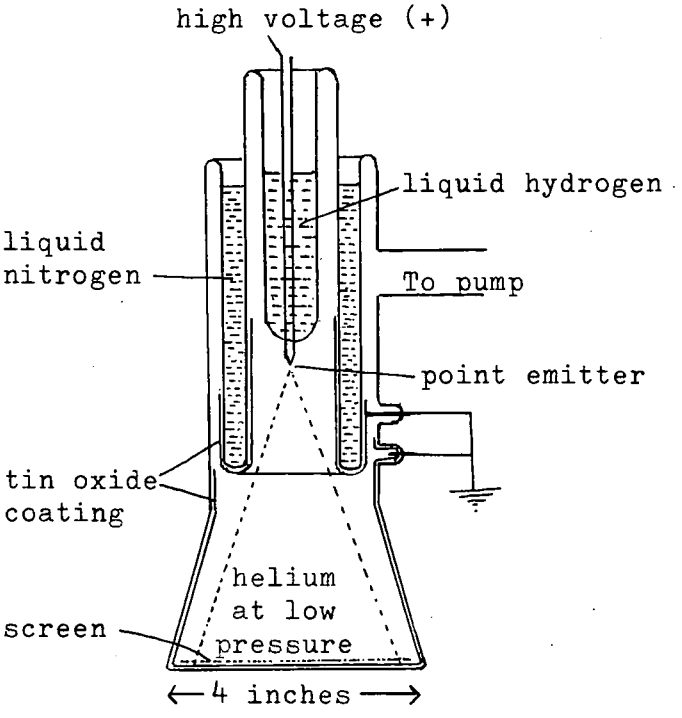

Fig. 97 Low temperature field-ion microscope. (After Müller, 1957).

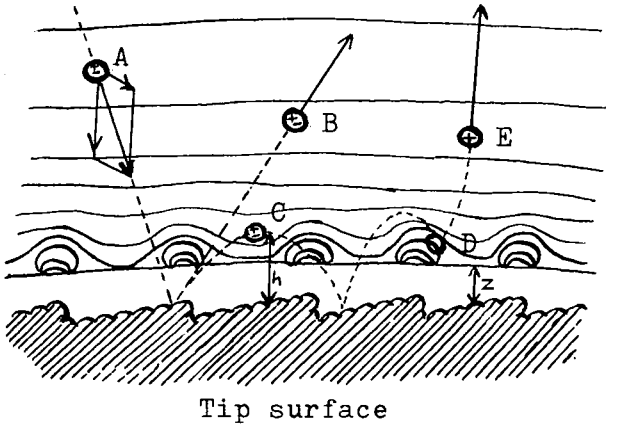

Fig. 98 Motion of atoms close to the tip surface.
At room temperature the polarized atom A will be elastically reflected (B).
At low surface temperature atom C hops through ionization zone until it is ionized at D, and then (E) accelerated by the field towards the screen.

11.1 INTRODUCTION.

The field ion microscope is a simple piece of apparatus, see Fig. (97), with a resolution of better than 3 A, which Müller (1957) has used to observe single atoms. He operated the microscope at low tip temperature, and with helium ions.

11.2 THE FORMATION OF THE IMAGE.

When a helium atom approaches a low temperature metal surface it encounters conditions shown in Fig. (98). The velocity of the atom is found by adding its velocity obtained using the kinetic theory of gases, and the attraction of the induced dipole.

$V = V_{gas} + V_{dip}.$

$$= \left(\frac{2kT}{m}\right)^{\frac{1}{2}} + F\left(\frac{\alpha}{m}\right)^{\frac{1}{2}}$$

Where k = Boltzmann constant T = gas temperature

m = mass of atoms F = field at the point considered

α = polarizability

As the atom approaches the surface there is an increase in the probability of autoionization due to increasing field and image force effect. The ionization probability, however, disappears when below a minimum distance $Z = \frac{(V_i - \phi)}{F}$, where V_i = the ionization potential of the atom and ϕ = work function of the surface. At this distance, the electron at the ground level of the helium atom sinks below the Fermi level. Using helium and tungsten, Z is about 5 A.

The ion image on the screen is produced by the variation in

ionization probability at different points at the surface. The ionization probability is highest above protruding atoms, or lattice steps, because of local field enhancement. This lateral probability is responsible for the formation of the ion image on the screen.

The field strength must be carefully adjusted, and the applied voltage must be within a range of 1% for best results. With a field in the region of 450 MV./cm., only a small percentage of the incident helium atoms will be ionized. At room temperature elastically rebounding atoms will have a large lateral velocity, and will pass through the ionization zone. The ions produced will retain lateral velocity and the image of a protrusion will be blurred. At lower temperatures the tip surface accommodates the helium atoms completely to tip temperature before evaporation, thus reducing the lateral velocity of the atoms and the ions to about $\left(\frac{2KTtip}{m}\right)^{\frac{1}{2}}$ At the temperature of liquid hydrogen this promises a resolving power greater than 1 A. The distance from the surface at which ionization takes place has an influence upon resolution. This is partly overcome by working at low temperatures. The atoms, instead of rebounding away from the surface, are attracted back to the surface by the induced dipole and, once an atom has touched the surface, it is restricted to small hops through the ionization zone until it becomes ionized and moves to the screen. For tips at liquid hydrogen temperatures, and a tip radius of 1000 A, the hopping height is a few angstrom units. This means that the ions

will originate very close to the surface, giving high resolution of surface details.

The temperature has a great effect upon the sharpness of the image, and 'focusing' may be carried out by adjusting the temperature. For a larger tip radius the temperature must be lower. Müller used tungsten and rhenium tips.

11.3 APPLICATIONS OF THE MICROSCOPE.

The most prominent detail is produced by protruding atoms where ionization prohibition is enhanced. On an otherwise atomically smooth surface this is provided by atoms which slightly protrude on the edges of low index net planes, such as the (011) and (112) planes in tungsten.

The field needed to ionize helium is as high as 450 MV/cm., and this limits the use of this ion microscope to the refractory metals. In the case of tungsten there is a wide margin between the image field and evaporation field. The evaporation rate is about one monolayer per second at 570 MV/cm. at 21 deg. K. Rhenium has a similar margin, but tantalum and molybdenum dissolve more readily. Long photographic exposures may be used successfully for tungsten and tantalum surfaces, and there is found to be very little change in arrangement of surface atoms over time intervals of about an hour.

Field evaporation is useful as by slowly increasing the field, single protruding atoms may be removed, giving the distribution of

(a)

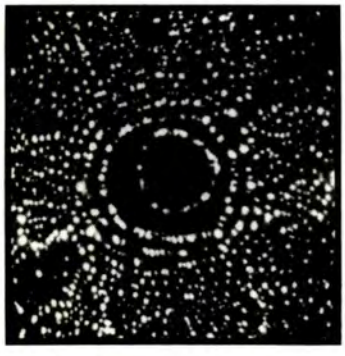

(b)

Plate 74. (a) Central part of tunsten tip of radius 700 A, 16,500 volts, after annealing at 2200 deg.K, with incomplete (011) net plane edge.

(b) Same tip after exposing tip to 18,000 volts for raising central net plane edge. (After Müller, 1957).

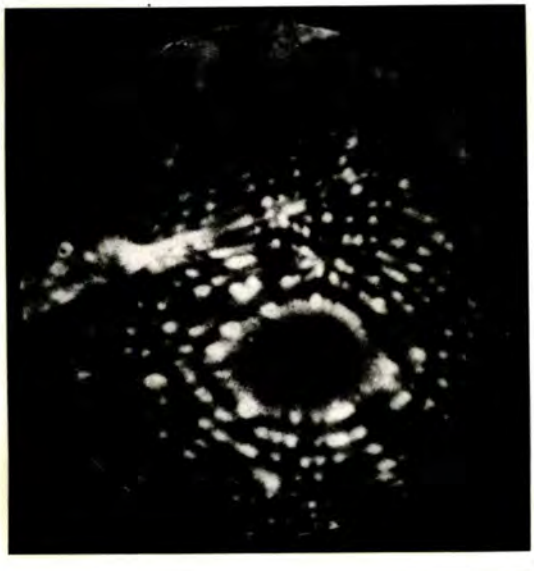

Plate 75. Dislocation near (011) plane on tungsten tip of radius 400 A, 11,300 volts, 15 microns helium pressure, tip temperature 60 deg.K. (After Müller, 1957).

binding forces over the metal surface. This works particularly well for tungsten. Plate (74a) shows the central part of a tungsten tip of radius 700 A, exposed to 16,500 volts after annealing at 2,200 deg. K. The horseshoe shaped edge of the (011) plane indicates a dislocation. The ends of the edge of the top plane presumably sink into the next lower plane. When a higher potential is applied the stress due to the field removes the dislocation, and the complete edge of the first plane is seen, as in Plate (74b).

Plate (75) shows a complex edge dislocation near the (011) plane on a tungsten tip at 60 deg. K. The radius of this tip is 400 A, the potential 11,300 volts, at 15 microns helium pressure.

Drechsler, Pankow, and Vanselow (1955) have observed screw dislocations on tungsten tips using hydrogen ions at room temperature. The resolving power of their instrument was about 6 A.

The field ion microscope has been used to study metal surfaces previously bombarded by ions. Müller observed a double spiral of 70 A diameter, produced when an ion impinged on the central (041) plane of a tungsten tip. By field desorption (i.e. evaporation) at 60 deg. K., he found the disturbance reached a depth of 10 planes of atoms.

11.4 CONCLUSION.

Any method capable of a resolving power of 3 A is useful to

study dislocations. Although confined to observation of the surface features of a very limited number of metals, the ability of high desorption to manipulate the surface and to remove a known number of layers of atoms, could yield valuable information about the nature and depth of deformation produced by impact of high energy ions with a top surface.

PART 12.

CONCLUSION.

When the theory of dislocations was introduced in order to account for the plastic behaviour of crystals there was no means of observing and studying dislocations. It was necessary first of all to establish the existence of dislocations and later to investigate the validity of the theoretical predictions. Until recently the properties of dislocations could only be inferred from the macroscopic behaviour of crystals. The methods now available for the study of individual dislocations have been described in detail, and their contribution towards an understanding of dislocations will be considered briefly.

The bubble raft was of value in showing that plastic deformation may be explained in terms of slip and movement of dislocations. The great assumption was that atoms in a three dimensional lattice behaved in a similar way to the bubbles, in their two-dimensional rafts. Not until methods of direct observation of actual dislocations were developed could the degree of similarity be confirmed. It is now realised that the bubble rafts provide a very much over-simplified picture.

Information gained from the study of crystal growth has been helpful in establishing some of the properties of dislocations. Dislocations were proved necessary to crystal growth, and the movement of dislocations was shown to be possible.

Observations of etch pits and of decorated dislocations entail the use of optical microscopes. Thus, these methods may be applied successfully only to crystals in which the dislocations

are sufficiently far apart to be resolved. The limit of resolution using ultra-violet light is about 1000 A. Decoration methods must utilize transparent crystals of simple structure, such as the silver halides and ionic salts. The improvement in the techniques of growing single crystals has greatly aided development in this field. Where decoration is effected by precipitation of large particles at dislocation lines, as in the case of the decoration of dislocations in sodium chloride with sodium, the dislocation arrangements must be interpreted bearing in mind that the decorating particles themselves could produce strains possibly giving rise to prismatic dislocations, and seriously affect the dislocation pattern. Certainly, in the case of lithium fluoride, excess lithium greatly increases the dislocation density. This method of decorating ionic crystals uses diffusion of the decorating medium to the imperfections at elevated temperatures, and at such temperatures considerable movement of dislocations will take place. When the specimen cools, the decorating particles will probably pin the dislocations and prevent them from attaining an equilibrium arrangement. The decoration of dislocations in the silver halides with photolytic silver does not suffer from these disadvantages, as the method does not depend upon the introduction of foreign particles, nor upon treatment at high temperatures. The depth to which decoration takes place below the surface of the crystals is, however, limited, and the method is restricted to the silver

halides.

The study of etch pits on crystals of lithium fluoride by Gilman and Johnson has made possible a critical evaluation of dislocation theory, but doubt has been cast upon some of their conclusions. Only dislocations reaching the surface can be etched, and a clear picture of arrangements below the surface is not provided. For example, the dislocation networks seen by transmission electron microscopy, and by decoration methods, could not be observed, nor inferred, from etch pits alone. A combination of the etch pit and decoration methods by Dash using silicon crystals, has proved successful, but here, as in similar decoration methods, the crystals must be transparent, in this case to infra-red rays, and of simple structure. In addition treatment at elevated temperatures is required.

An understanding of the plastic deformation of metals is of great practical importance, but the above methods only suggest what probably happens in metals. To observe dislocations in complex, opaque specimens such as metals, a different type of microscope with a higher resolution is necessary. This need has in part been satisfied by the electron and field-ion microscopes, and by X-ray diffraction. The electron microscope is a very powerful tool for observation, and it has enabled undecorated dislocation lines in thin foils to be seen, and their movements to be followed. The present resolving power using the transmission technique is about 5 A, and it is expected that with

existing lenses a resolving power of 2 to 3 A could be attained. The limiting factors are the displacement and contamination of the specimen due to the impact of the electron beam on the specimen. When the resolution of 2 A is attained, it should be possible to make visible all crystal lattices and individual atoms of high atomic number.

For use with the transmission electron microscope, the specimens must be very thin, and the electron beam causes considerable heating of the specimen. These two factors could modify the arrangements and lengths of the dislocation lines as compared with those in the bulk material. These possible effects have been carefully considered by Hirsch and his collaborators, and are not thought to be serious.

Higher resolving powers of up to 1 A have been attained using Moire patterns and the electron microscope, and again using the field-ion microscope, but their range of application is not so great as that of the transmission electron microscope. The use of Moire patterns makes it possible to detect and estimate the density of dislocations in thin films. The restriction to their application lies in the preparation and manipulation of the specimens. The two thin films, prepared in contact, must be in fairly well defined relative orientation, and consequently it is difficult to study polycrystalline foils. If a specimen is subjected to treatment then the interpretation of observations must allow for the fact that both the films are treated

simultaneously. The field-ion microscope has been used to study tungsten and rhenium surfaces. Surface atoms may be resolved and any displaced atoms detected.

It is likely that X-ray diffraction methods will be considerably developed in the near future, as these avoid some of the disadvantages of transmission electron microscopy. Thin foils are not necessary, and the beam does not cause heating of the specimen. Individual dislocation lines have been made clearly visible in large single crystals by Newkirk and Lang, and information obtained agrees with that gained by other methods of observation. Observations of dislocations in metals have not been so successful, and results as yet do not compare with those from electron microscopy. As with the electron microscope, continuous observation of moving dislocations is possible. It must be stressed, however, that the resolving power of the X-ray diffraction method is not as good as that of the electron microscope, and to observe single dislocations the use of large single crystals is necessary.

All methods described contribute towards a clearer understanding of dislocations, and provide experimental proof of dislocation theory. An example of this is given by considering experimental evidence that glide occurs. The dislocation loops produced by the presence of hysil glass spheres in crystals of silver chloride in experiments by Jones and Mitchell (1958), were due to glide movements. Gilman and Johnston, using the

multiple etching technique, were able to follow the movement of dislocations due to the application of high stresses. They were also able to measure the velocity of the dislocations. The cine camera used with bubble rafts, and with the transmission electron microscope has enabled the movement of dislocations to be studied, and sequence photographs of images produced by X-ray diffraction have provided information about dislocation movements.

Many of the predictions of dislocation theory have been verified. It has been shown, using the electron microscope, that extended dislocations clearly exist, and cross-slip and climb occur. Dislocations have been observed to cut each other. Attempts to predict processes with large numbers of dislocations involved, such as work hardening and fatigue, have been shown to be false. Progress in the understanding of plastic deformation is very rapid, and greatly assisted by observation methods. Undoubtedly, with the expected increase in resolving power of the transmission electron microscope perhaps to 2 A, and a cine camera taking 100 frames per second, to follow the more rapid dislocation movements in metals, much more valuable information will be forthcoming.

REFERENCES.

Abbe, E. (1937)	Arch. Mikr. Anat. 9, p.413.
Amelinckx, S. (1952)	Phil. Mag. 43, p.562.
(1956)	Phil. Mag. (8), 1, p.269.
(1957)	Dislocations and Mechanical Properties of Crystals, John Wiley, & Sons, Inc., New York. p.3.
Anderson, N. G. and Dawson, M. (1953)	Proc. Roy. Soc. A, 218, p.255.
Andrade, E. N. da C. (1950)	Endeavour lX, 36, p.165.
(1956)	Approach to Modern Physics, G. Bell & Sons, Ltd., London.
Bailey, J. E. (1958)	Cambridge Ph.D. Thesis.
Barrett, C. S. (1945)	AIME Trans. 161, p.15.
Bartlett, J. T. and Mitchell, J. W. (1958)	Phil. Mag. (3), 28, p.334.
Bassett, G. A., Menter, J.W., and Pashley, D. W. (1958)	Proc. Roy. Soc. A, 246, p.345.
Bennett, A. H., Jupnik, H., Osterburg, H., and Richards, O.W. (1951)	Phase Microscopy, John Wiley & Sons, Inc., New York.
Bollman, W. (1956)	Phys. Rev. 103, p.1588.
Bontinck, W., and Dekeyser, W. (1956)	Physica 22, p.595.
Bontinck, W. (1957)	Phil. Mag. (8), 2, p.561.
Bradley, D. E. (1954)	J. Appl. Phys. (5), p.165.
Bragg, W. L., James, R. W., and Bosanquet, C. H. (1921)	Phil. Mag. 42, p.1.
Bragg, W. L. and Nye, J. F. (1947)	Proc. Roy. Soc. A, 190, 474.
Bragg, W. L. and Lomer, W. M. (1949)	Proc. Roy. Soc. A, 196, 182.

Burgers, J. M. (1939)	Proc. Acad. Sci. Amst. 42, pp.293, 378.
Castaing, R. (1954)	Proc. 3rd. Int. Conf. on Electron Microscopy, London. p.379.
Clark, P. V. McD., and Mitchell, J. W. (1956)	J. Phot. Sci. 4, p.1.
Cottrell, A. H. (1953)	Dislocations and Plastic Flow in Crystals, Oxford University Press.
Cosslett, V. E., and Nixon, W.C. (1953)	J. Appl. Phys. 24, p.616.
Cosslett, V. E., Engström, A. and Pattee, H.H. Jr. (1957)	Proc. of Symp. on X-ray Microscopy and Microanalysis, Cambridge 1956. Academic Press, New York, 1957.
Cosslett, V. E. (1957)	Proc. of Symp. on X-ray Microscopy and Microanalysis, Cambridge 1956. Academic Press, New York, 1957.
Coulomb, P., and Friedel, J. (1957)	Dislocations and Mechanical Properties of Crystals, John Wiley, & Sons, Inc., New York. p.555.
Darwin, C. G. (1914)	Phil. Mag. 27, pp.315, 675.
(1922)	Phil. Mag. 43, p.800.
Dash, W. C. (1956)	J. Appl. Phys. 27, p.1153.
(1957)	Dislocations and Mechanical Properties of Crystals, John Wiley, & Sons, Inc., New York. p.57.
(1958)	J. Appl. Phys. 29, p.705.
Dawson, N. G. and Anderson, M. (1953)	Proc. Roy. Soc. A, 218, p.255.
Drechsler, Pankow, and Vanselow. (1955)	Z. Physik Chem. 4, p.249.
Edner, A. (1932)	Z. Physik 73, p.623.

Forty, A. J. (1952) Phil. Mag. 43, p.72.

Forty, A. J. and Frank, F.C. (1953) Proc. Roy. Soc. 217, p.262.

Frank, F. C. (1950a) Proc. Roy. Soc. A, 201, p.586.

(1950b) Phil. Mag. 41, p.200.

(1951a) Phil. Mag. 42, p.809.

(1951b) Phil. Mag. 42, p.1014.

(1951c) Acta. Cryst. 4, p.497.

(1951d) Proc. Phys. Soc. A, 64, p.941.

(1952) Adv. in Physics, 1, p.91.

(1955) Report of a Conference on Defects in Crystalline Solids, Phys. Soc. London. p.159.

(1955) Chemistry of the Solid State. Butterworths, London., p.1.

Friedel, J. (1956) Les Dislocations, Gauthier-Villars, Paris.

Gilman, J. J. and Johnston, W. G. (1956) Dislocations and Mechanical Properties of Crystal, John Wiley & Sons, Inc., New York.

(1959) J. Appl. Phys. 30, No.2, p.129.

Griffin, L. T. (1950) Phil. Mag. 41, p.196.

Gurney, amd Mott, N. F.(1939) Proc. Roy. Soc. A, 164, p.151.

Hall, W. H. and Williamson, G. K. (1951) Proc. Phys. Soc. Lond. 64B, pp937, 946.

Hausser and Scholtz. (1927) P. Wiss. Veroff. Siemens-Konzern, 5, p.144.

Hedges, J. M. and Mitchell, J. W. (1953a) Phil. Mag. (7), 44, p.223.

Heidenreich, R. D. (1949) — J. Appl. Phys. 20, p.993.

Heidenreich, R. D. and Shockley, W. (1948) — Report of Conference on Strengths of Solids, London Phys. Soc., p.57.

Hirsch, P. B., Horne, R. W., and Whelan, M. J. (1956) — Phil. Mag. 1, p.677.

Hirsch, P. B., Silcox, J., Smallman, R. E., and Westmacott, K. H. (1958) — Phil. Mag. 3, p.897.

Honess, A. P. (1927) — The Nature, Origin, and Interpretation of the Etch Figures of Crystals, John Wiley & Sons, Inc., New York.

Horn, F. H. (1952) — Phil. Mag. 43, p.210.

Horn, F. H., Kasper, J. S., and Fullam, E. F. (1952) — Nature, London. 169, p.927.

James, R. W. (1950) — The Optical Principles of the Diffraction of X-rays, Chap. VI. G. Bell & Sons, Ltd., London.

Johnston, W. G. (1957) — Dislocations and Mechanical Properties of Crystals, John Wiley & Sons, Inc., New York. p.52.

Jones, D. A. and Mitchell, J. W. (1957) — Phil. Mag. 2, p.1047.

Jones, D. A. and Mitchell, J. W. (1958) — Phil. Mag. (8), 3, p.1.

Keller, F. and Geisler, A. H. (1947) — Trans. A.I.M.E. 171, p.192.

Kirkpatrick, P. (1957) — Proc. of Symp. on X-ray Microscopy and Microanalysis, Cambridge. Acad. Press, New York. p.17.

Korndorffer, A., Rahbek, H., and Sultan, F. (1952) — Phil. Mag. 43, p.1301.

Lacombe, P., and Yannaquis, N. (1947) — Metaux et Corrosion, 22, p.35.

Lacombe, P., and Beaujard, L. (1948) — Rev. Met. 45, p.317.

Lang, A. R. (1957) Acta. Met. 5, p.358.

(1958) J. Appl. Phys. 29, p.597.

(1959) J. Appl. Phys. (30), 11. p.1748.

Lang, A. R. and Meyrick, G. (1959) Phil. Mag. (4), 43, p.878.

Machlin, E. S. (1957) Dislocations and Mechanical Properties of Crystals, John Wiley & Sons, Inc., New York. p.164.

Mitchell, J. W. (1957) J. Phot. Sci. 5, p.49.

Mitchell, J. W. and Mott, N. F. (1957) Phil. Mag. (8), 2, p.1149.

Morris, C. E. (1949) Metal Progr. 56, p.696.

Mott, N. F. (1951) Proc. Phys. Soc. London. B64, p.729.

Müller, E. W. (1957) J. Appl. Phys. 28, p.1.

Nabarro, F. R. N. (1947) Proc. Phys. Soc. 59, p.256.

(1952) Advances in Physics, 1, p.269.

Newkirk, J. B. (1958a) Phys. Rev. 110, p.1465.

(1958b) J. Appl. Phys. (29) 6, p.995.

(1959) Trans. of Metallurgical Soc. of AIME, 215, p.483.

Nixon, W. C. (1955) Proc. Roy. Soc. A, 232, p.475.

Nutting, J. and Smith, E. (1956) Brit. J. Appl. Phys. 7, p.214.

Nye, J. F., Spence, R. D., and Sprackling, M. T. (1957) Phil. Mag. (8) 2, p.772.

Obinemov, I. W. and Schekinkoo, L. W. (1927) Z. Physik, 41, p.907.

Orowan, E. (1934) Z. Phys. 89, p.634.

Parasnis, A. S. and Mitchell, J. W. (1959)	Phil. Mag. (8) 4, p.171.
Pashley, D. W., Menter, J.W., and Bassett, G. A. (1957)	Nature, 179, p.752.
Patel, J. R. (1958)	J. Appl. Phys. (29) 1, p.170.
Patel, J. R. and Alexander, B. H. (1956)	Acta Met. 4, p.385.
Peirls, R. (1940)	Proc. Phys. Soc. 52, p.34.
Polanyi, M. (1934)	Z. Physik. 89, p.660.
Read, W. T. (1953)	Dislocations in Crystals, McGraw-Hill, New York.
Read, W. T. and Shockley, W. (1950)	Phys. Rev. 78, p.275.
Rexer, E. (1931)	Z. Physik. 70, p.159.
(1932a)	Z. Physik. 75, p.777.
(1932b)	Z. Physik. 76, p.735.
(1932c)	Z. Physik. 78, p.538.
Schmid, E. and Boas, W. (1935)	Kristallplastizitat, Julius Springer, Berlin. p.271.
Seeger, A. (1954)	Naturforsch, 9a, pp.758, 856, 870.
(1957)	Dislocations and Mechanical Properties of Crystals, John Wiley & Sons, Inc., New York. p.243.
Seitz, F. (1950)	Phys. Rev. 79, p.723.
Siedentopf, H. (1905)	Phys. Z. 6, p.855.
Silcox, J. and Hirsch, P. B. (1959)	Phil. Mag. 4, p.72.
Smekel, A. (1929)	Z. Physik. 55, p.289.
(1933)	Handbuch der Physik. Sec. Edit. Springer, Berlin. 24/2, p.795.

Taylor, G. I. (1934) — Proc. Roy. Soc. A, 145, p.362.

Teague, D. M. (1953) — Symp. on Techniques for Electron Metallography, A.S.T.M. Spec. Publ. No.155.

Thomas, G. and Whelan, M. J. (1959) — Phil. Mag. 4, p.511.

Thomas, G. and Nutting, J. (1959) — Acta. Met. 7, p.515.

Tolansky, S. (1948) — Multiple Beam Interferometry of Surfaces and Films, Oxford University Press, London.

(1953) — Vacuum, I. p.127.

Turnbull, D.T. and Belk, J. A. (1952) — Laboratory Practice, 1. p.403.

Van Bueren, H. G. (1957) — Philips Research Reports, 12, pp.1-45, 190-239.

Van der Vorst, W. and Dekeyser, W. (1956) — Phil. Mag. (8) 1, p.882.

Verma, A. R. (1951) — Phil. Mag. 42, p.1005.

(1953) — Crystal Growth and Dislocations, Butterworths Scientific Publications, London.

Vogel, F. L., Pfann, W. G., Corey, H.E. and Thomas, E. E. (1953) — Proc. of Symp. on X-ray Microscopy and Microanalysis, Cambridge. Acad. Press, New York. p.603.

Votava, E., Berghezan, A., and Gillette, R. H. (1957) — Proc. of Symp. on X-ray Microscopy and Microanalysis, Cambridge. Acad. Press, New York, p.603.

Whelan, M. J., Hirsch, P. B., Horne, R. W., and Bollman, W. (1957) — Proc. Roy. Soc. A, 240, p.524.

Wilson, A. J. C. (1952) — Acta. Cryst. 5, p.318.

Young, F. W. (1958) — J. Appl. Phys. 29, p.760.